Climatology and large-scale Dynamics of Derechos in Germany

Inaugural-Dissertation

zur

Erlangung des Doktorgrades

der Mathematisch-Naturwissenschaftlichen Fakultät

der Universität zu Köln

vorgelegt von

Christoph Gatzen

aus Düsseldorf

Köln, 2018

Berichterstatter (Gutachter):	**Prof. Dr. Joaquim Pinto**
	Prof. Dr. Yaping Shao
	Prof. Dr. Andreas Fink

Tag der Disputation: 16. Mai 2018

Abstract

This thesis introduces a German climatology of wide-spread convective wind events so-called “derechos”. In a period of 18 years between 1997 and 2014, 40 derechos have been classified based on wind gust measurements and radar data. Although this leads to a significant lower derecho density compared to large regions in the United States, a high potential threat associated with these storms is indicated. Two seasonal peaks of derecho occurrence and typical large-scale flow patterns were identified. Whereas this is similar to the United States climatology, a contrast is that German derechos form with less instability. This corresponds to the greater importance of low-instability derechos that mostly form in the cold season.

Low-instability derechos form in thermodynamic conditions similar to high-shear, low-CAPE environments introduced in the United States. High resolution model analysis of eight events with the COSMO model shows the development of conditional instability very close to derechos. This explains that proximity soundings sometimes do not indicate any CAPE. Furthermore, observations and model simulations of the eight events indicate that instability forms close to the ground. It is hypothesized that the combination of a level of free convection close to the ground and strong low-level flow can favor mesovortices that are associated with the highest winds in derechos. As mesovortices form in weak-instability environments as well as in high-instability environments, it is proposed to keep the term derecho for low-instability events and distinguish between warm-season and cold-season derechos.

To investigate processes that cause the development of CAPE close to low-instability derechos, the focus is set on local lapse rate changes. These are analyzed in the model fields using calculations of the local lapse rate tendency equation. According to the findings, local lapse rate increase is not only determined by horizontal lapse rate advection, but to a comparable degree by stretching of low-level air masses. Other processes like differential latent heat release in potential unstable layers that are lifted were not found to be important. Stretching occurred especially downstream of moving PV intrusions. Therefore, the findings of this thesis can contribute to the conceptional understanding of convective initiation close to PV intrusions. An example is the “split-front” concept that is modified since our concept explains why cold-season derechos can form in the absence of well-developed surface fronts.

Kurzzusammenfassung

Diese Arbeit stellt eine Klimatologie für großflächige Gewitterorkane, sogenannte "Derechos", für Deutschland vor. Mit Hilfe von Böenmeldungen und Radarbildern konnten im 18-jährigen Zeitraum von 1997 bis 2014 insgesamt 40 Derechos klassifiziert werden. Damit wird ein hohes Gefahrenpotential verdeutlicht. Die resultierende Ereignisdichte zeigt, dass Derechos in weiten Teilen der Vereinigten Staaten häufiger auftreten. Beide Klimatologien zeigen zwei jahreszeitliche Häufigkeitsschwerpunkte und vergleichbare Wetterlagen, in denen Derechos auftreten. Im Gegensatz zu diesen Gemeinsamkeiten entstehen Derechos in Deutschland häufiger in Situationen mit geringer Instabilität. Damit verbunden ist auch die im Vergleich zu den Vereinigten Staaten relativ hohe Bedeutung von winterlichen Derechos in Deutschland.

In der amerikanischen Literatur wurde für entsprechende Wettersituationen der Begriff "high-shear, low-CAPE environments" eingeführt. Für acht Fallbeispiele zeigt die Analyse hochaufgelöster COSMO-Simulationen, dass sich erst im direkten Derechoumfeld CAPE bildet, was erklärt, warum in der Nähe aufgestiegene Radiosonden bisweilen keine Instabilität zeigen. Darüber hinaus zeigen Beobachtungen und Modellfelder dieser acht Fälle bereits in tiefen Atmosphärenschichten Labilisierung. Dies könnte in Verbindung mit starker Strömung in Bodennähe die Entwicklung von kleinräumigen Wirbeln, sogenannten "Mesovortices" begünstigen, welche nach bisherigem Kenntnisstand mit den stärksten Windböen in Derechos in Verbindung gebracht werden. Damit ähneln Winterderechos den Sommerderechos, was dafür spricht, auch Winterderechos als solche zu bezeichnen.

Um zu untersuchen, durch welche Prozesse es im direkten Derechoumfeld zu CAPE kommt, wurde ein besonderes Augenmerk auf die Entwicklung des vertikalen Temperaturgradienten gelegt. Die lokale Tendenzgleichung des vertikalen Temperaturgradienten wurde für COSMO-Simulationen auf Druckflächen berechnet. Die Ergebnisse legen nahe, dass neben der Advektion des vertikalen Temperaturgradienten durch den Horizontalwind vor allem Streckung bodennaher Luftschichten wesentlich zur lokalen Labilisierung beiträgt. Die Streckung fand dabei vor allem stromab von positiven Anomalien der Potentiellen Vorticity statt. Die präsentierten Ergebnisse ergänzen somit das bisherige konzeptionelle Verständnis, warum im Bereich von positiven PV-Anomalien häufig Gewitter entstehen. So kann beispielsweise im Unterschied zum "Split-Front"-Konzept verstanden

werden, warum winterliche Derechos auch ohne ausgeprägten Bodenfronten entstanden. Auch spielte bei Hebung einer potentiell instabilen Luftmasse mit der Höhe abnehmende latente Wärmefreisetzung bei der Labilisierung keine wesentliche Rolle.

Contents

1 Introduction and Motivation

Severe wind events are among the main natural hazards on Earth (e.g. MunichRe, 2018). Large-scale winter storms play a dominant role in Europe (e.g. MunichRe, 2012; Ulbrich et al., 2001), but convective events pose a high threat of severe wind gusts as well (Groenemeijer et al., 2017). These downbursts are typically limited to the convective scale (Dotzek and Friedrich, 2009), but sometimes, convective wind events affect a large area and can have a comparable impact as other large-scale storm systems (Ashley and Mote, 2005).

Such a convective wind event observed together with a group of graduate students in meteorology of the Free University of Berlin (Fig. 1) has been my first impulse to focus on a phenomenon named "derecho". This event in the summer of 2002 was special because of several reasons: Its local intensity at the observation site where numerous trees have been destroyed, the destructive impact on the urban infrastructure of Berlin and the size of the affected area. The analysis of this and comparable severe weather events across Germany set the fundament of this work (e.g. Gatzen, 2004; Gatzen et al., 2011).

The severe storm system that initiated this work hit Germany's capital Berlin on 10 July 2002, and was accompanied by extremely high wind gusts (Gatzen, 2004). It has been one of the city's worst hazardous weather events in the past 50 years, killing 4 and injuring 35 (Berliner Zeitung, 2012). Berlin was not the only region affected. Wind gust measurements and damage reports document a 700 km long and 100 km wide path extending across all of eastern Germany, parts of the Baltic Sea and eastern Denmark including capital Copenhagen (European Severe Weather Database (ESWD); Dotzek et al., 2009). Eighteen locations reported wind gusts of 33 m/s or more, with a maximum wind gust of 50 m/s close to the Baltic Sea (Fig. 2 and Fig. 3).

The impact of this storm that caused eight fatalities and fifty injured across the complete path was large: Highways, streets, and railway tracks were blocked by trees. Damage to the electricity infrastructure caused power outages for 150.000 people; on the Baltic Sea, 59 persons were rescued from dangerous or life-threatening situations on the waters (Frankfurter Allgemeine Zeitung, 2002). Imprecise weather forecasts were made responsible for a couple of incidents. The fire department of Berlin criticized the warnings of the German weather service (DWD) as inade-

quate and stated that a youth camp would have been evacuated in the case of extreme wind warnings (Fokus, 2002). Two boys died at that camp during the storm. The German Federal Bureau of Aircraft Accident Investigation (BFU) concluded that insufficient weather forecasts caused the incident of a scheduled Swissair flight. The airplane was severely damaged during an emergency landing after the crew failed to avoid the storm system (Avherald, 2010; Bundesstelle für Flugunfalluntersuchung, 2010; Wikipedia, 2015c). Fortunately, none of the passengers was killed. Media articles remarked that the public was not well prepared as warnings had not indicated an extreme event (Fokus, 2002; n-tv, 2002).

The "Berlin Storm" evolved across central eastern Germany during the afternoon. Wind measurements recorded a chronological progression of widespread severe winds including extreme gusts along a bow-shaped front that moved from south to north at a speed of 25 m/s (Fig. 2). Radar images indicated rapidly developing, intense thunderstorms ahead of this front (Gatzen, 2004). Gatzen (2004) showed that this storm met the criteria for long-lived, convectively induced storms known as derechos (after Hinrichs, 1888; Johns and Hirt, 1987). The case study illustrates that the intensity, size, and rapid development of these events can have a high impact on the society and its infrastructure. Derechos are known especially from the United States, but can also form in other regions including Europe, e.g. the Baltic Sea region (Punkka et al., 2006; Toll et al., 2015), Spain (López, 2007), Central Europe (e.g. Gatzen, 2004; Gatzen et al., 2011; Púčik et al., 2011; Simon et al., 2011; Celiński-Mysław and Matuszko, 2014), western Europe (Hamid, 2012), and eastern Europe (Gospodinov et al., 2015). Little is known about German dere-

Figure 1: *Left: Leading gust front of the severe storm system of July 2002, observed to the north of Berlin after it affected the city. Looking to the east, the gust front is moving from right to left. Right: Johannes Dahl, Steffen Dietz, Friedrich Föst, Jan Hoffmann, and Sebastian Unger observing the storm.*

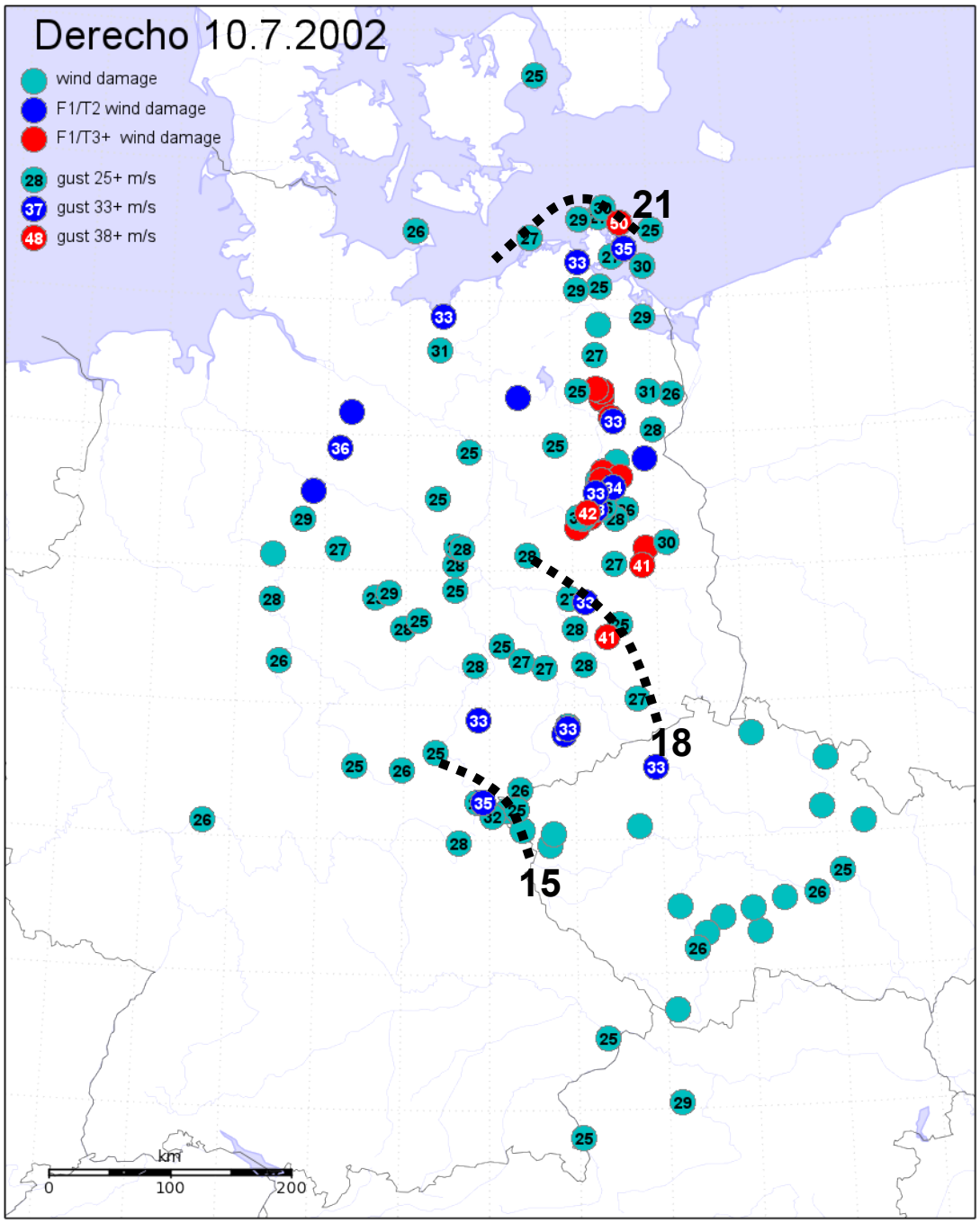

Figure 2: *The "Berlin storm": Wind reports on 10 July 2002 across Germany (bullets with numbers of measured maximum wind gusts in m/s) and damage reports (bullets without numbers, colored according to the rating on the Fujita and TORRO scale (Dotzek, 2009): F1/T2 wind intensity corresponds to 33 – 42 m/s, T3 to more than 42 m/s). Gust front positions, approximated by radar reflectivity images, are indicated by black dotted lines. UTC time is labeled at the end of each line.*

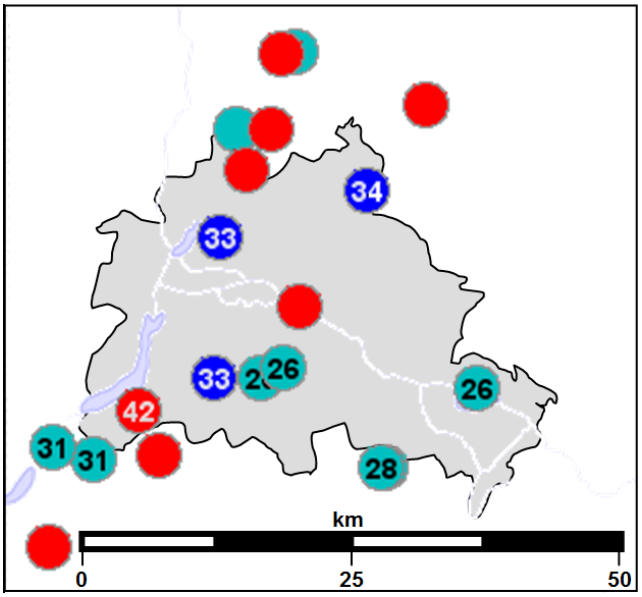

Figure 3: *The "Berlin storm": Wind measurements and damage reports on 10 July 2002 focused on the Berlin area. The symbols are the same as in Fig. 2.*

chos, although scientists have documented similar events across Germany in the past, e.g. Köppen (1882, 1896), Faust (1948), Kurz (1993), Haase-Straub et al. (1997), and Kaltenböck (2004). But potential derechos were treated as unique phenomena and not compared to similar events as stated in Kaltenböck (2004) and Faust (1948). Other publications mention that widespread severe winds were observed but skip an analysis of the path length of wind damage (e.g. Haase-Straub et al., 1997; Kurz, 1993). As a consequence, a climatology that could reflect the potential hazard of German derechos does not exist. In a first attempt, Gatzen (2013) analyzed German severe wind events in ten warm seasons. 14 derechos were found, and they accounted for 38 percent of wind gusts exceeding 25 m/s and for 90 percent of extreme wind gusts exceeding 40 m/s. It is this significant role of derechos in producing severe wind gusts in Germany together with their potential impact on modern society that motivates this work. The main scope is to increase the awareness of such storms in Germany, especially by showing how many derechos have occured in the past to calculate the derecho risk across the country. Moreover, the thesis is addressed to operational weather forecasters to improve their conceptional understanding of derechos to support derecho forecasts. For example, we introduce large-scale flow patterns in German derecho situations.

The aims of this thesis are the following:

- Build a German derecho climatology that indicates the derecho risk as well as derecho characteristics like track length and wind intensity, spatial and seasonal occurrence, moreover the local thermodynamic conditions as indicated by vertical profiles, and large-scale weather conditions supportive for derechos. Compare the results to the derecho climatology of the United States as a reference.

- Use simulations of the non-hydrostatic COSMO-DE model to analyze the development of low-instability derechos in the context of an ingredients-based forecasting approach.

- Work out a conceptual model of processes that are important to forecast low-instability derechos.

This thesis is structured as follows: In chapter 2, an overview of derecho research is presented, including a section dedicated to German derecho publications. Furthermore, the lapse rate tendency equation will be introduced as theoretical basis of the following analysis. Chapter 3 describes the data and the methods used to classify and analyze German derechos. Moreover, it is explained how we use the COSMO-DE model to estimate the terms of the lapse rates tendency equation. Chapter 4 presents a derecho climatology for Germany and gives typical large-scale flow situations and associated thermodynamic characteristics. A focus is set on low-instability events, especially on processes that allow for CAPE in initially stable environments. We use simulations with the COSMO model and calculate the different terms of the local lapse rate tendency equation to analyze such processes. Chapter 5 concludes this work with a conceptual image of a process that causes lapse rate increase in cold-season derecho events.

2 State of the art

2.1 The definition of a derecho

A derecho is defined as intense deep moist convection that is organized on the mesoscale and that produces a swath of widespread severe wind gusts (Johns and Hirt, 1987). Tropical storms are excluded from the derecho definition (Evans and Doswell, 2001). On plan-view radar images, derechos are typically structured as bands of convection that form one or multiple bow-shaped reflectivity echoes that travel rapidly. Directly associated with these bow echoes, wind reports indicate chronological, concentrated occurrence of severe wind gusts over a region whose major length axis exceeds 400 km. This length axis is perpendicular to the convective gust front, aligned with the motion vector of the convective system. A threshold for the width of derechos is not required.

According to Johns and Hirt (1987) the derecho definition refers to families of downburst clusters as defined by Fujita and Wakimoto (1981). They found that damaging straight-line wind events associated with deep moist convection can affect regions of various sizes. Fujita and Wakimoto (1981) defined five different classes based on the path lengths: Wind events with a major length axis of 400 m or less were defined as burst swaths, followed by microbursts (400 m - 4 km), downbursts (4 km - 40 km), downburst clusters (40 km - 400 km) and families of downbursts clusters (400 km or more). It follows that a derecho is a family of downburst clusters.

According to its definition the classification of derecho events is based on reports of severe wind gusts and radar images. The threshold of a wind report to be regarded as severe differs slightly, depending on the wind speed units that are used. The United States Storm Prediction Center (SPC) includes straight-line (i.e. non-tornadic) wind reports, based on measurements or analyzed wind damage, that exceed 57 miles per hour (about 25.48 m/s). The original derecho definition by Johns and Hirt (1987) refers to 50 knots (about 25.72 m/s), whereas other publications refer to 25 m/s (Evans and Doswell, 2001) what is about Beaufort 10 or T1 on the TORRO wind speed scale (Meaden, 1976). Wind reports within the derecho path have to indicate concentrated wind gust occurrence. In practice, this requires a maximum distance that is allowed between successive wind reports. This distance also differs slightly in the literature. Johns and Hirt (1987) allow

up to 3 hours for gaps between successive wind reports to be included in the same derecho event, Coniglio and Stensrud (2004) 2.5 hours, and Evans and Doswell (2001) as well as Bentley and Mote (1998) 2 hours. An additional spatial distance between successive wind reports is limited to 200 km in Coniglio and Stensrud (2004), meaning that each wind report of the derecho event occurs within a distance of 200 km of the other wind reports, Bentley and Mote (1998) use a distance of 2° of latitude and longitude, Evans and Doswell (2001) use a threshold of 167 km (100 miles). Finally, for all wind reports that are included in a derecho event it has to be possible to follow their occurrence chronologically together with bowing radar structures that indicate spatial and temporal continuity of the convective system.

Some authors include one more criterion to define a derecho. Johns and Hirt (1987) require three reports of "significant" wind gusts of at least 65 kt (33 m/s) or wind damage related to at least F1 wind speed (at least 32.5 m/s), separated by 64 km (40 miles) or more, to occur within the derecho's path. The SPC refers to a threshold of 75 mph (33 m/s). Other authors classify derechos without this criterion (Evans and Doswell, 2001; Bentley and Mote, 1998). Coniglio and Stensrud (2004) combine different classification schemes into their definition of low-end and high-end derechos. Events that include three wind gusts as required by Johns and Hirt (1987) are classified moderate derechos, others low-end derechos. Furthermore, events that indicate at least three wind reports exceeding 38 m/s, two of them occurring during the mature phase of the associated convective system, are classified high-end derechos.

The appearance of the derecho's radar structure on plan-view radar displays has also been used to characterize derecho sub-classes. Progressive derechos consist of just one single bowing structure at least for some time during their lifetime, whereas serial derechos are composed by several bowing elements that may develop along a larger squall line they are embedded in (Johns and Hirt, 1987, Fig. 4). Furthermore, characteristics of the synoptic-scale flow have been used to define derechos. For example, Evans and Doswell (2001) introduced weakly forced, strongly forced, and hybrid derechos, depending on the magnitude of synoptic-scale forcing for ascent. Finally, Corfidi et al. (2016) propose a revised definition of derechos. They increase the path length to 650 km, introduce a minimum path width (100 km along most of the path), and also propose that a derecho is "a family of damaging downburst clusters associated with a forward-propagating,

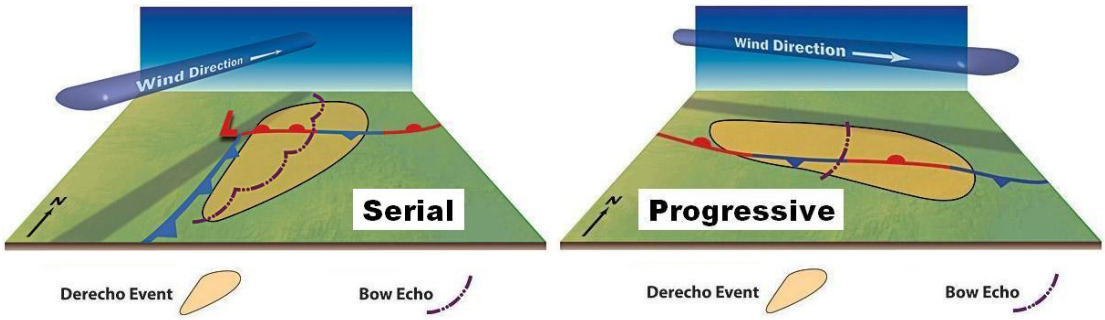

Figure 4: *Conceptual overview of serial and progressive derechos. The left figure displays a typical frontal system associated with bowing segments of a serial derecho. The right image gives a typical situation associated with a progressive derecho. Fronts are displayed with conventional symbols, the position of the gust fronts of bow echoes are indicated by partly dotted lines. Regions with high wind occurrence are highlighted. Image courtesy: Dennis Cain (NOAA/NWS).*

mesoscale convective system that, during part of its existence, displays evidence of one or more sustained bow echoes with mesoscale vortices and/or rear-inflow jets." Additionally, only damage reports that occurred with the mature convective system, i.e. after initial convective storms have merged to a cold-pool driven system, have to be included to classify the event.

The denotation of derechos is relatively young compared to that of other meteorological phenomena. The term derecho was first introduced by Hinrichs (1888) who described convective windstorms similar to Fujita's and Wakimoto's families of downburst clusters. Hinrichs named these events derechos to avoid mixing of tornadic and non-tornadic wind events. The word "derecho" is of Spanish origin and can be translated with "direct" or "straight ahead" (Johns and Hirt, 1987). However, there had been no further research based on this first proposal. Due to a tendency "to discourage research on severe local storms in the United States during the next 50 years" (Johns, 2007; Galway, 1992), the term derecho was not used for nearly a century, until Johns and Hirt (1987) revived the term derecho to draw the forecaster's attention on the large convective wind events that frequently caused fatalities and widespread damage across the eastern parts of the United States.

The derecho definition of Johns and Hirt (1987) initialized extensive research on derechos in the United States. In the following sections, results of this research concerning climatology and life-cycle will be summarized.

2.2 Derecho climatology of the United States

Derechos are known especially from the United States, where research on these phenomena looks back to a history of more than 30 years (e.g. Johns and Hirt, 1983). The climatology has been studied by various authors, e.g. Johns and Hirt (1987), Bentley and Mote (1998), Bentley and Sparks (2003), and Coniglio and Stensrud (2004). According to their findings, derechos tend to occur to the east of the Rocky Mountains, and only a few events have been classified farther west (Fig. 5). The maximum of the regional frequency is located to the south-west of the Great Lakes during the warm season (May to August), whereas it shifts southward to the lower Mississippi valley in the cold season (September to April). The spatio-temporal derecho density is about more than one event per year for quadratic grid boxes with a side length of 200 km in the most affected area as found by Coniglio and Stensrud (2004), using only moderate and high-end events according to their definition. Derechos tend to occur in clusters that have been described as derecho "families" (Ashley et al., 2004), meaning that two or more events follow each other within a few days associated with the same, repeating weather patterns, especially heat waves. United States derechos indicate a dis-

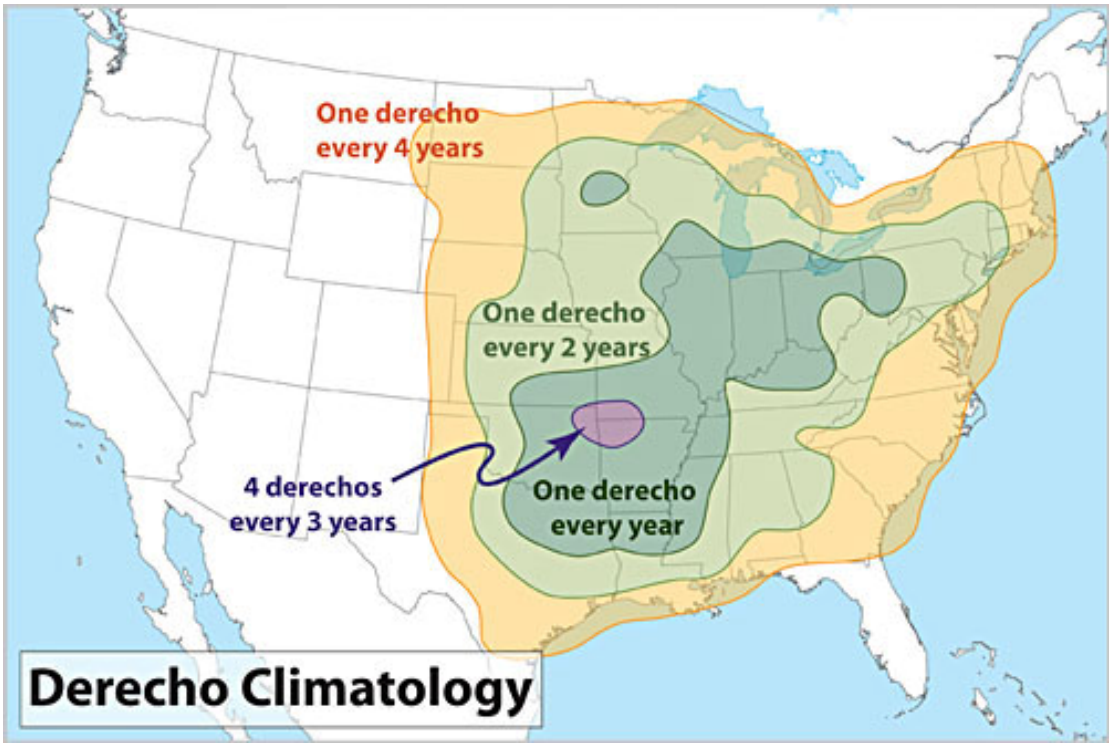

Figure 5: *Overview of the derecho frequency across the United States. Image courtesy: Dennis Cain (NOAA/NWS). Available at http://www.spc.noaa.gov/misc/AbtDerechos/. Accessed: 2016-11-28*

tinct annual cycle with a prominent warm-season maximum. About 60 percent develop in May, June, and July, and more than 75 % between April and August for an investigation based on 377 events between 1986 and 2003 (Ashley and Mote, 2005). Analysis of the exact time of derecho occurrence indicates a clear dependence of diurnal heating with a maximum late in the day (e.g. Johns and Hirt, 1987; Bentley and Mote, 1998).

The warm-season maximum points to the convective origin of derechos. Analysis of the organization and structure of derecho-related deep moist convection has been based especially on radar imagery. Johns and Hirt (1987) found that derechos are accompanied with bowing structures on plan-view radar reflectivity displays. These bowing structures are known as bow echoes (Fujita, 1978) and are frequently associated with long swaths of damaging surface winds (e.g. Fujita, 1978; Przybylinski, 1995). A derecho-producing mesoscale convective system (MCS) can consist of a single bow echo or several bow echoes at the same time that may be embedded in a large squall line (progressive and serial derecho, respectively, according to Johns and Hirt, 1987) (Fig. 4).

2.3 Bow echoes

Fig. 6 illustrates the structure and evolution of bow echoes from the initial to the mature stage. Bow echoes evolve from intense convective storms, either single cells or groups of cells, or along a squall line, and their size varies between tens to a few hundred kilometers (e.g. Klimowski et al., 2003). At the flanks of the bow echo, counter rotating vortices have been specified in previous literature, e.g. by Fujita (1978) and Weisman (1993) who introduced the term “bookend vortices”. Between the bookend vortices forms a remarkable feature that is observed with bow echoes, the rear-inflow jet (RIJ) (e.g. Smull and Houze Jr, 1987; Przybylinski, 1995). This is a system-relative elevated low-level jet that points from the rear to the front of the convective system and drives the bowing process of the leading gust front (e.g. Fujita, 1978; Jorgensen and Smull, 1993). At low levels, bow echoes are accompanied by a pool of cold air masses (Evans and Doswell, 2001). Strong cold pools can be identified on surface pressure maps and are called mesohighs (e.g. Adams-Selin and Johnson, 2010). Mesohighs together with bowing radar structures have been first identified by Hamilton (1970). The pressure gradient force at the flanks of the mesohigh causes the cold pool to spread out horizontally.

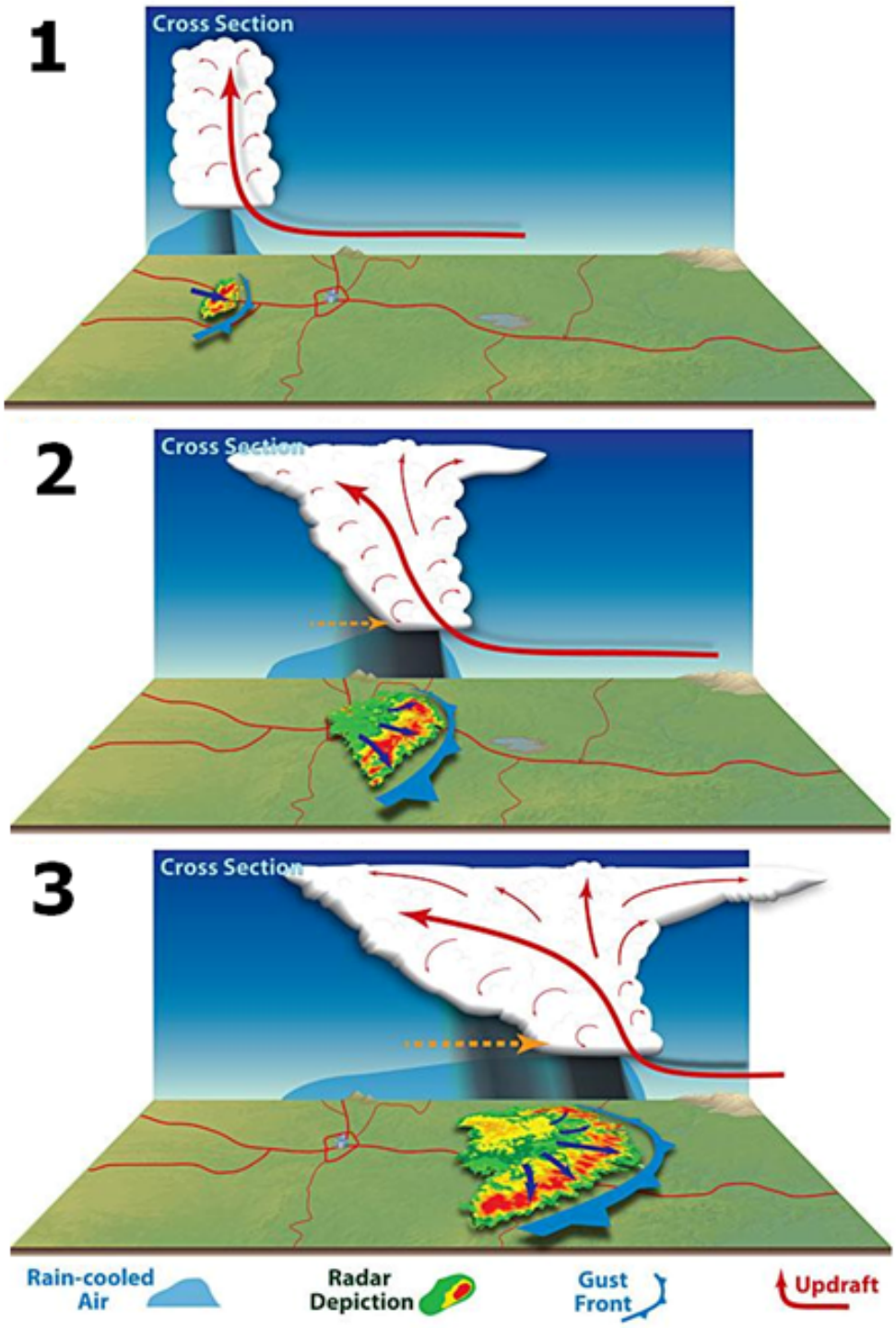

Figure 6: *Conceptual overview of bow echo formation from the initial stage (1) to the mature stage (3). The dashed arrow in dark yellow depicts the rear inflow jet. The blue arrows illustrate the flow close to the ground within the cold pool. Image courtesy: Dennis Cain (NOAA/NWS). Available at http://www.spc.noaa.gov/misc/AbtDerechos/. Accessed: 2016-11-28*

Its speed can be partly approximated by the theoretical speed c of a density current: Both cold pool depth h and intensity given by the density perturbation $\Delta\rho$ relative to the environmental density ρ_0 contribute to the cold pool speed c according to

$$c = \sqrt{2gh\frac{\Delta\rho}{\rho_0}} \tag{1}$$

Here, g denotes Earth's gravitation constant. Taking into account the environmental flow, the cold pool gradually expands preferentially in the direction of the main flow (Corfidi, 2003). New initiation, e.g. along the cold pool's gust front, allows the convective system to become persistent (Corfidi, 2003). On horizontal radar displays, a large bowing line eventually forms when the convective system undergoes this upscale growth and matures (Fig. 6).

A better approximation of the movement of derechos is the combination of (i) the advection by the flow and (ii) the propagation due to the development of new convection that merges to the convective system (Corfidi, 2003). Corfidi et al. (1996) approximate the advective component of the system's movement by the mean cloud-layer wind. The propagation component is determined by development of new convection at the flanks of the convective cold pool. Corfidi et al. (1996) recommends to take the negative of the flow vector of the low-level jet to estimate the propagation: Especially low-level air is forced upwards when it flows against the cold pool. Therefore, new initiation is favored at the flank of the convective system that points towards the low-level jet (upper illustration in Fig. 7). The stronger the low-level flow, the faster new cells form, what increases the propagation speed. When the low-level jet is strong compared to the mean cloud-layer wind, new initiation in the opposite direction of cell advection can cause a slow moving or quasi-stationary gust front. Here, the motion vectors of propagation and advection cancel themselves. A flash flood event may result at this quasi-stationary gust front ("echo training"; upper illustration in Fig. 7).

New cell development can be additionally supported by vertical pressure perturbations that result from convective updraft interaction with the vertical wind shear of the environmental flow (i.e. linear dynamic pressure perturbations, e.g. Markowski and Richardson, 2011): Vorticity and deformation of the environmental flow interfere with those of the buoyant updraft to result in pressure perturbations that support or work against new initiation (Fig. 8). New cell development is favored

at the downshear flank of a cold pool (bottom illustration in Fig. 7). In some situations, advection and propagation of a convective system can be positively superimposed, e.g. when the wind speed increases with height while its direction is constant (i.e. pure speed shear), so that the upshear and downshear flanks are co-located with the upwind and downwind flanks of the MCS, respectively. This supports fast forward moving gust fronts and a derecho may form at the downwind flank of the system.

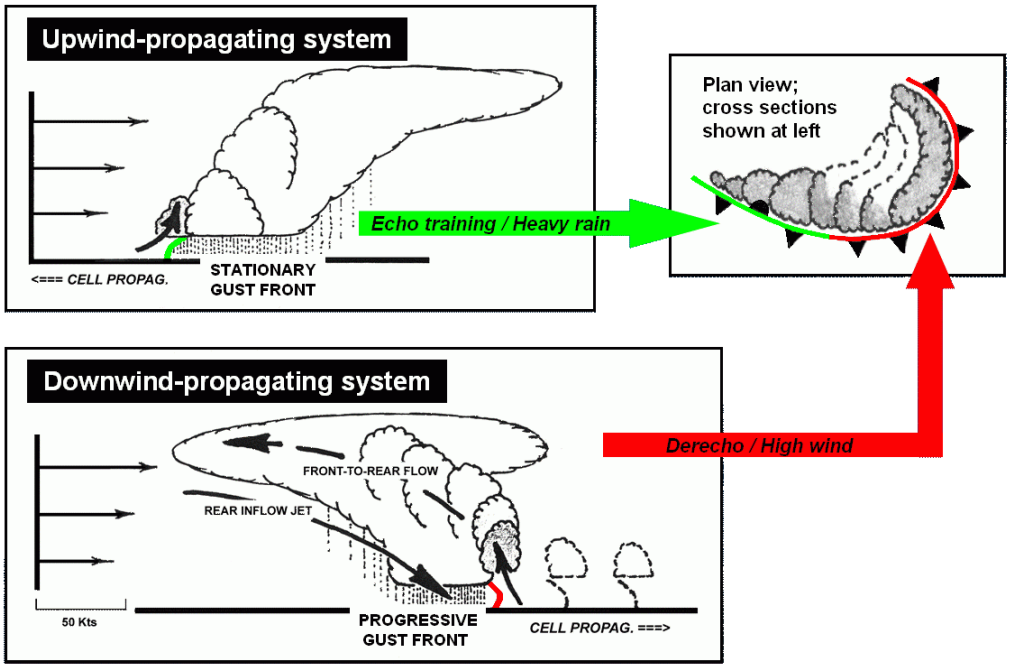

Figure 7: *Concept of a bow echo with training storms at the upwind flank (vertical cross section upper left) and a fast forward moving gust front at the downwind flank (vertical cross section bottom) of the system. The upwind (green) and downwind (red) gust front are indicated in the horizontal illustration in the upper right corner. Image taken from Corfidi (2003, their Fig. 3), ©American Meteorological Society. Used with permission.*

During the intensification and evolution of the convective system, the system-generated movement can change. For example, the convective system's propagation will be influenced by the environmental conditions to initiate new convection at the gust front, e.g. spatial variations of instability or low-level convergence. Also the speed at which the gust front travels typically changes during the life-cycle of the MCS. When MCSs mature, the speed of their gust fronts frequently

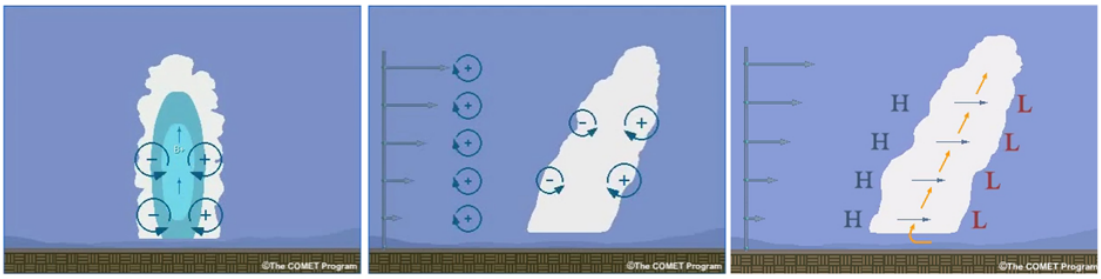

Figure 8: *Illustration of vorticity generated by a buoyant updraft (B+) (left) and its superposition with the vorticity generated by the environmental vertical wind shear (center; arrows to the left indicate the flow vector at different heights). The right image indicates the location of perturbation pressure in this situation. Downshear, positively superimposed vorticity will cause low perturbation pressure. At the upshear flank, high perturbation pressure is caused by the positive superposition of the deformation associated with the updraft and vertical wind shear. "The source of this material is the COMET © Website at http://meted.ucar.edu/ of the University Corporation for Atmospheric Research (UCAR), sponsored in part through cooperative agreement(s) with the National Oceanic and Atmospheric Administration (NOAA), U.S. Department of Commerce (DOC). ©1997-2016 University Corporation for Atmospheric Research. All Rights Reserved."*

accelerates. Using numerical simulations, Mahoney et al. (2009) showed that successive momentum transport of the system-generated rear-inflow jet and the environmental flow into the surface based cold pool is responsible for increasing speed of the cold pool, its gust front, and of the convective system itself.

As the derecho-producing MCS lives on, Coriolis force becomes increasingly important. The front-to-rear flow turns, so that the stratiform precipitation region shifts to the left of the center line (looking with the derecho movement). The flow within the cold pool also turns and causes an outflow boundary along the right flank of the system, sometimes named arrow (upper right illustration in Fig. 7). Furthermore, the anticyclonic vortex of bow echoes will weaken with time, whereas the development of the cyclonic vortices is favored, both effects caused by convergence of Coriolis rotation. Initially symmetric bow echoes transform to comma shaped radar echoes (Fujita, 1978). Eventually, convective systems lead to intense, cyclonically rotating mesoscale convective vortices (MCV; Gamache and Houze Jr, 1982) when continuous system-scale stretching further affects the comma-shaped echo (e.g. Conzemius and Montgomery, 2009). Derechos that undergo this transition to form a warm-core, cyclonically rotating mesoscale storm system are sometimes referred to "super–derechos" (e.g. Evans et al., 2014), although no clear definition exists for this term.

2.4 Initiation of bow echoes

Recent studies point out how deep moist convection organizes into bow echoes. Findings from observational and numerical studies (e.g. a storm-scale simulation by James et al. (2006)) tend to focus on the interaction of convective updrafts with the convectively generated cold pool. Convective updrafts have a tendency to lean rearward onto the cold pool in response to the circulation driven by the cold pool (cf. Fig. 9). This circulation evolves from baroclinic horizontal vorticity between the different air masses of cold pool and pre-storm environment [1]. The tilting of the updrafts onto the cold pool increases the extension of the convection and the region where precipitation penetrates the cold pool, adding to the cooling due to evaporation and melting (e.g. Rasmussen and Rutledge, 1993). The increased cooling causes a strengthening of the mesohigh within the cold pool, corresponding to low thicknesses between pressure levels close to the ground. On the other hand, relatively high thicknesses evolve within the convective region due to latent heat release and due to warm air advection by the front-to-rear flow. As a quasi-hydrostatic response a mid-level mesolow forms at the leading flank of

[1] Baroclinic vorticity is generated by the buoyancy torque between air masses of different density, e.g. Doswell (2001): Dense air has a tendency to sink relative to light air, resulting in vorticity along the interface of the different air masses

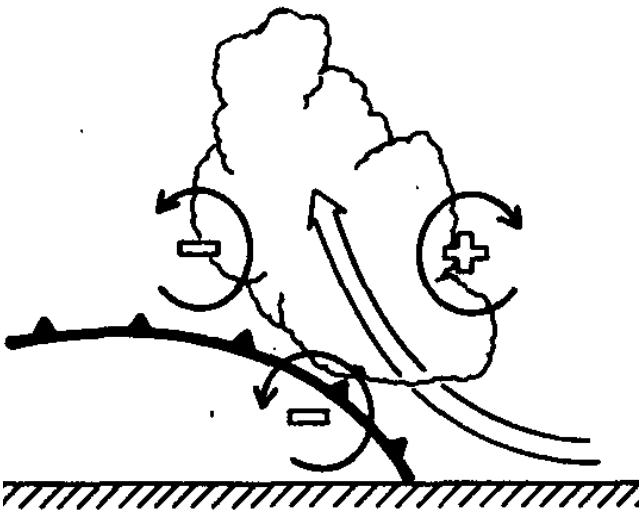

Figure 9: *Concept of convection leaning backward over the cold pool in response to the circulation between the cold pool and the environment. Image taken from Rotunno et al. (1988, their Fig. 18 b), ©American Meteorological Society. Used with permission.*

the convective system (e.g. Fujita, 1978; Mahoney et al., 2009). The horizontal perturbation pressure gradient force between the mesohigh and the mesolow accelerates the rear-to-front flow within the cold pool and increases the advection of cooled air towards the leading gust front. This further intensifies the cold pool and its circulation, initiating a positive feedback between deep moist convection, cold pool, and rear inflow jet. As the rear inflow jet is accelerated by the perturbation pressure gradient forces, it will evolve at the location where these are maximized.

When the cold pool is not homogenous, a local maximum in cold pool intensity or its vertical extension (i.e. the cold pool depth) is favored for bow echo development (James et al., 2006). But one can also think of the dependency of the mid-level mesolow to inhomogeneities of diabatic heating and warm air advection above the cold pool's leading edge that results in a local maximum of the rear inflow jet and bow echo formation.

Inhomogeneities within the cold pool can initiate bow echoes in an additional way: Analysis of a case during the BAMEX field campaign (Davis et al., 2004) indicated bookend vortices with a diameter of 70-80 km that appeared at the flanks of convective lines already prior to bow echo formation (Wakimoto et al., 2006b). An explanation is that horizontal vorticity of the baroclinic circulation of the gust front is tilted to the vertical due to variations of the local cold pool depth. This has been suggested by Wakimoto et al. (2015) based on an observational study of a squall line bow echo using radar data. Tilting of the horizontal, system-generated baroclinic vorticity can also occur at the flanks of updrafts to form a pair of counter rotating vortices that intensify due to stretching (Weisman and Davis, 1998) (Fig. 10). The pair of vortices is thought to focus and strengthen the rear-inflow jet to initiate a bow echo (Weisman, 2001). Updrafts that interact with the cold pool's gust front do not necessarily have to initiate along the gust front but can also form in the pre-system environment and merge with the convective system. Such cell mergers have been described prior to bow echo formation (Klimowski et al., 2004; Burke and Schultz, 2004).

2.5 Generation of severe wind gusts

The generation of severe wind gusts at the ground is subject of ongoing research. High wind generation in association with mesoscale convective systems has been

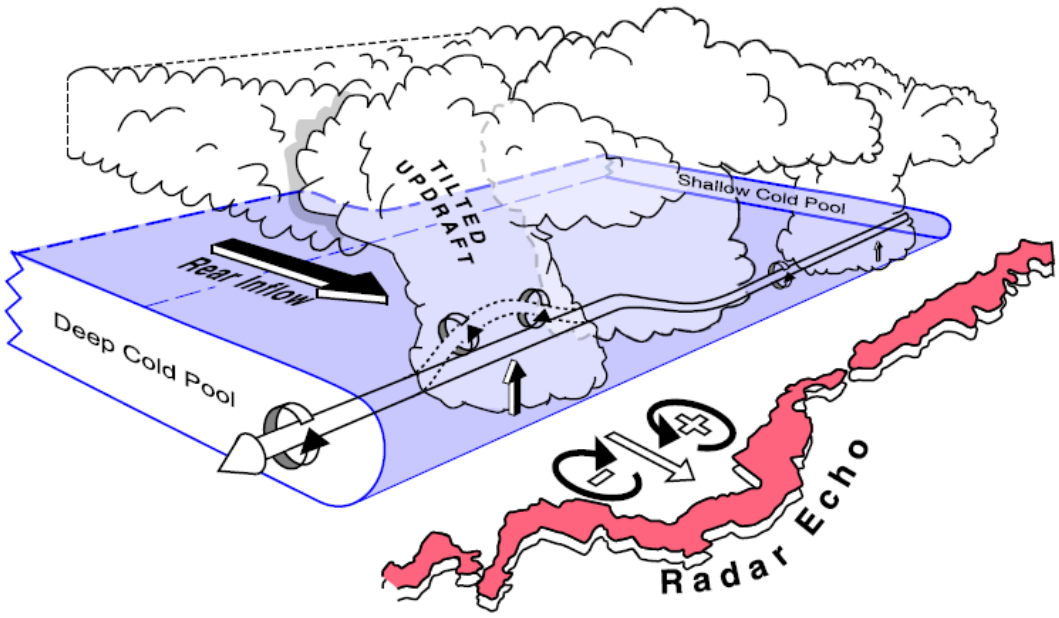

Figure 10: *Illustration of tilting of baroclinic vorticity (illustrated by the rotating vortex tube) by new updrafts in the vicinity of inhomogeneous cold pools. Image taken from Wakimoto et al. (2015, their Fig. 17), ©American Meteorological Society. Used with permission.*

found to be complex compared to pure parcel theory that describes the downward acceleration of undiluted air parcels in microbursts. Microbursts spread out horizontally when hitting the ground to produce straight line winds. The three contributions to downdraft acceleration are given by:

$$\frac{dw}{dt} = -\frac{1}{\bar{\rho}}\frac{\partial p'}{\partial z} + g\frac{\partial T_v' - \overline{T}_v}{\overline{T}_v} - gl \tag{2}$$

Here, the acceleration of the vertical wind component w is due to vertical pressure perturbations (first term on the rhs) with the density of the environmental air $\bar{\rho}$ and the perturbation pressure p', the buoyancy (second term on the rhs) with the gravitational acceleration g and the virtual temperatures of the downdraft and the environmental air, T_v' and $\overline{T}_v$, respectively, and the water loading (third term on the rhs) with the water mixing ratio l. The second term is related to the concept of environmental downdraft CAPE (DCAPE; Emanuel, 1994). DCAPE is a parameter that is based on the negative buoyancy of the downdraft air that evolves due to evaporative cooling in relatively dry environmental air. While DCAPE can be used to approximate the severe potential of some microbursts [2],

[2]Similar to CAPE, DCAPE can be calculated by vertical integration between the level of

it seems to be not a good forecast parameter for derechos (Evans and Doswell, 2001). Strong evaporation due to dry air masses at mid levels may even limit the intensity of mesoscale convective systems as indicated by model simulations (James and Markowski, 2010). Instead, early studies suggested that a combination of greater cold pool speed and embedded downbursts yields high winds and also explains the observed heterogeneous damage patterns of convective wind events (Fujita and Wakimoto, 1981). Furthermore, the high momentum of the elevated rear inflow jet could be transported to the surface by convective downdrafts.

Recent high resolution radar data and numerical simulations indicate that severe wind gusts are the result of the descending rear-inflow jet indeed, however, the reason for this descent is its interaction with small-scale vortices embedded in the cold pool and centered close to the ground (Wakimoto et al., 2006b,a; Wheatley et al., 2006; Xu et al., 2015). These small-scale vortices were observed in

free sink to the ground of the temperature difference between the environment and the adiabatic sinking curve of downdraft air parcels. The maximum speed c_{max} of the downdraft is

$$c_{max} = \sqrt{2DCAPE} \tag{3}$$

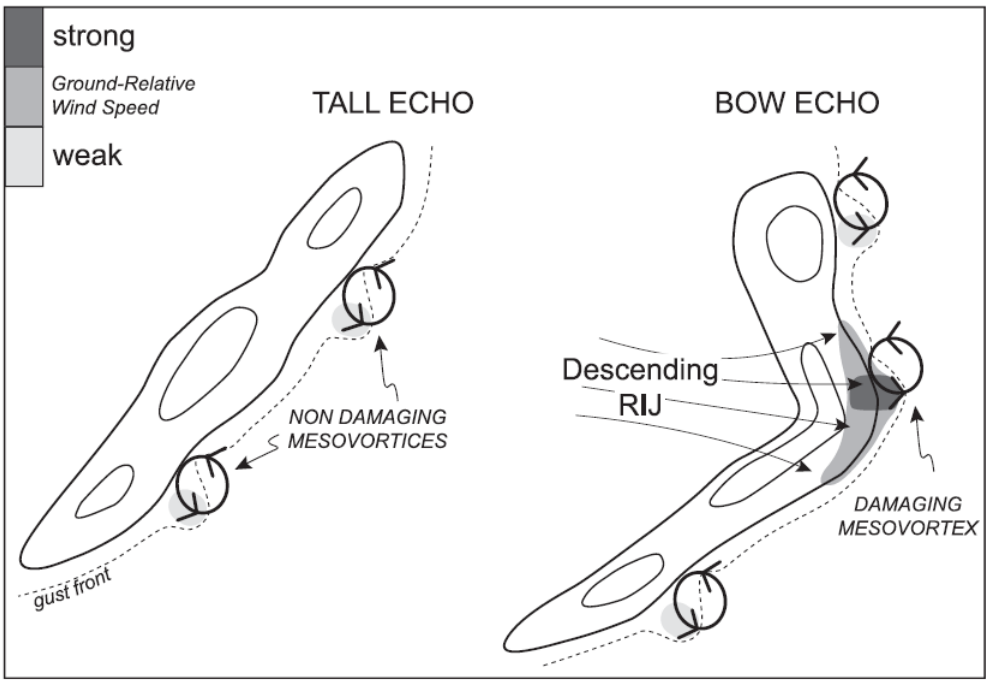

Figure 11: *Concept of high-wind production as a consequence of mesovortex and rear inflow jet interaction. Image taken from Atkins and St. Laurent (2009b, their Fig. 14),* ©*American Meteorological Society. Used with permission.*

Doppler radar data and have been introduced as "mesovortices" by Przybylinski (1995). They can also produce tornadoes that have been documented in association with bow echoes (e.g. Forbes and Wakimoto, 1983; Atkins et al., 2005). Observational studies (e.g. Wheatley et al., 2006; Wakimoto et al., 2006b,a) and model studies (Trapp and Weisman, 2003; Weisman and Trapp, 2003) agreed that the strongest surface winds are associated with mesovortices. According to the analysis by Wakimoto et al. (2006a) the high winds can be regarded as the result of a superposition of the rear-inflow jet and the rotational flow of the vortex (Fig. 11). In the model simulation (Trapp and Weisman, 2003; Weisman and Trapp, 2003), the rear-inflow jet accelerated when entering a mesovortex. This acceleration is driven by strong horizontal pressure gradients at the flanks of the vortex core due to its intense negative pressure perturbation. At the same time, the rear-inflow jet is gradually descending towards the ground. Trapp and Weisman (2003) point out that this descent is not related to downbursts that would cause much faster descent. Instead, vertical perturbation pressure gradients associated with the mesovortex cause the downward displacement. As mesovortices are centered close to the ground (e.g. Funk et al., 1999), the resulting perturbation pressure minimum is also at low levels, bringing the rear-inflow jet to the surface where it can produce severe gusts.

The genesis of mesovortices is subject of ongoing research (Schenkman and Xue, 2016), and the origin of the needed vertical vorticity close to the ground is not completely understood. Typically, gust fronts are associated with strong deformation along their leading edge what is not supportive for vorticity concentration and can even shear vortices apart. On the other hand, gust fronts can create high values of horizontal shear vorticity between the rising, warm air and the sinking, cold air. A process that tilts this horizontal vorticity into the vertical and brings it close to the ground where it can be stretched to form a vortex is thought to be crucial for mesovortex evolution.

One possibility is tilting of horizontal vorticity by convective up- or downdrafts observed in model simulations and observational studies (Trapp and Weisman, 2003; Wakimoto et al., 2006a; Atkins and St. Laurent, 2009a; Schenkman et al., 2012). At the flanks of up- or downdrafts, the vortex tubes are tilted and form pairs of counter rotating vortices. For example, based on radar data, Wakimoto et al. (2006a) suggests that between new updrafts along the gust front, dry downdrafts that compensate the upward mass transport can tilt vortex tubes (Fig. 12).

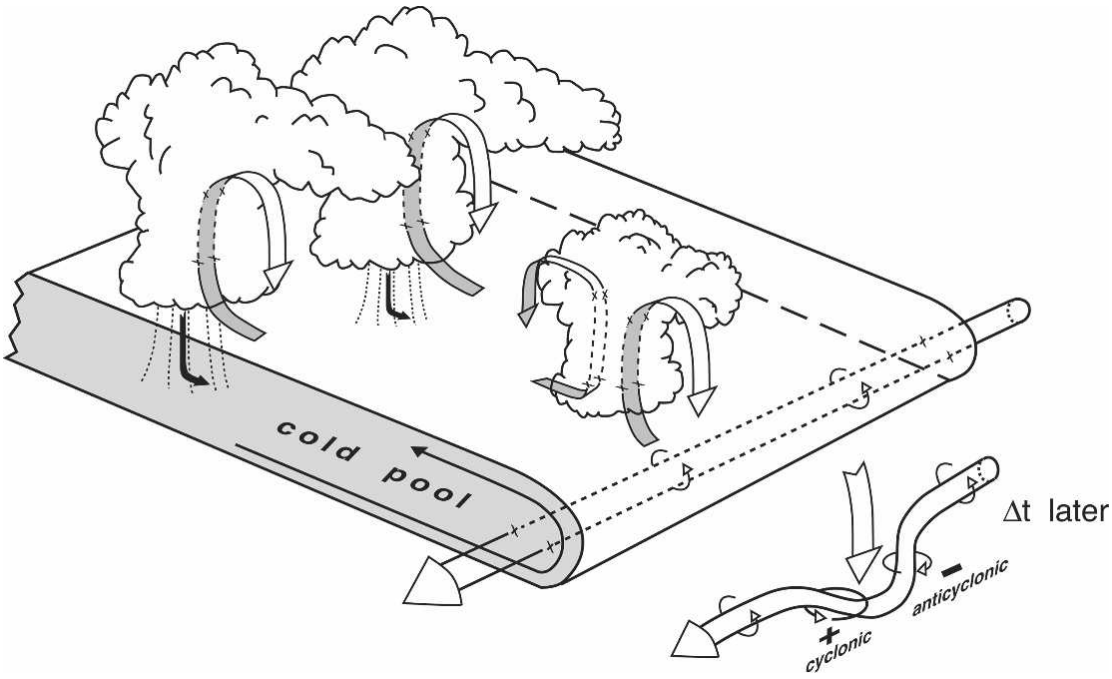

Figure 12: *Tilting of a gust front's horizontal vorticity by subsidence in the vicinity of new convective storms to form mesovortices. Image taken from Wakimoto et al. (2006b, their Fig. 12), ©American Meteorological Society. Used with permission.*

In model simulations, also other possible mechanisms have been analyzed. Atkins and St. Laurent (2009a) described how cyclonic mesovortices formed due to the tilt of baroclinic horizontal streamwise vorticity that evolves when air moves along the gust front, equivalent to the process that leads to low-level rotation of mesocyclones (Rotunno and Klemp, 1985; Davies-Jones and Brooks, 1993). Streamwise vorticity means that the vorticity vector of the flow is parallel to the mean wind vector. In contrast, pure crosswise vorticity has the vorticity vector perpendicular to the flow vector. Recently, simulations of the flow in supercell downdrafts have shown that horizontal streamwise vorticity increases close to the updraft and tilts to result in positive vertical vorticity near the ground (Rotunno et al., 2017; Dahl et al., 2014; Parker and Dahl, 2015). It can be suggested that similar processes allow cyclonic mesovortices in derechos when updrafts interact with the gust front. These updrafts may by forced by the gust front itself or initiate ahead of the cold pool and merge with the system later on. This model can explain why cyclonic mesovortices are much more often observed then anticyclonic ones.

Furthermore, frictional generated vorticity has been discussed to be important for mesovortex formation (Xu et al., 2015). Also vertical vorticity that is linked to

inhomogeneities in the low-level horizontal flow could be stretched by new updrafts similar to non-mesocyclonic tornadogenesis. Independent of the original source of low-level vertical vorticity, convective updrafts can support mesovortex development. When intense updrafts are present above the genesis region of vertical vorticity, the vortex lines can be concentrated and stretched to form intense, persistent vortices. This might be the explanation why severe wind gusts are frequently associated with convective storms that merge. Mesovortices within the cold pool of one convective cell could be stretched by the other convective updraft. Gatzen (2013) found such cell mergers indicated by radar images in 75% of 252 severe convective wind events analyzed in the warm seasons of 1997 to 2011 across Germany.

2.6 Environmental conditions associated with derechos

In summary, derechos can evolve when persistent, intense deep moist convection forms a cold pool and rear-inflow jet. The associated baroclinic vorticity and convective updrafts along the gust front may cause mesovortices that are related to the strongest winds. It is therefore important to have repeating initiation ahead of the moving cold pool. Initiation of convective storms requires an overlap of necessary "ingredients" in the environment (Doswell et al., 1996): A combination of low-level moisture and a large temperature decrease with height (hereafter steep lapse rates) to obtain positive buoyancy for ascending air parcels plus a source of upward vertical motion to lift air parcels to their level of free convection. All of the three ingredients are essential and cannot be replaced by large values of the other two. High moisture and strong lift will not lead to deep moist convection when there are not steep lapse rates, for example.

Especially large conditional instability has been described in association with derechos. Conditional instability is a combined view of two of the three ingredients and becomes positive when rich low-level moisture and steep lapse rates overlap. Johns and Hirt (1987) found extremely unstable air masses indicated by an average 500 hPa Lifted Index of -9 when examining atmospheric soundings in derecho paths. Here, the Lifted Index is calculated by the difference between the environmental temperature and the temperature of a surface-based parcel that follows pseudoa-

diabatic ascent. Johns et al. (1990) again observed high instability as indicated by convective available potential energy (CAPE) ranging between 2600 and 6300 J/kg for a set of long-lived derechos, with an average maximum of 4500 J/kg along the derecho path. CAPE is the amount of kinetic energy that positively buoyant parcels obtain during buoyant ascent, here calculated for surface-based parcels by integrating vertically the buoyancy between the level of free convection (LFC) and the equilibrium level (EL) (e.g. Doswell and Rasmussen, 1994):

$$\text{CAPE} = \int_{LFC}^{EL} g \frac{T_{v,p} - T_{v,env}}{T_{v,env}} \, \mathrm{d}z \tag{4}$$

where $T_{v,p}$, $T_{v,env}$ are the virtual temperatures of the ascending air parcel and the environment, and z is the height, respectively. Large CAPE can favor strong upward acceleration within convective updrafts, associated with stronger stretching of bookend vortices and also mesovortices (e.g. Wakimoto et al., 2006a). Additionally, intense updrafts can support a stronger mesolow and perturbation pressure gradient force that accelerates the rear-inflow jet (Mahoney et al., 2009).

However, CAPE has to overlap with sufficiently strong lift according to the ingredients-based approach before a convective storm can develop (Doswell et al., 1996), e.g. when air is forced upwards due to the solenoidal circulation at the edge of the cold pool's gravity current. But there may be also other sources of lift: Adams-Selin and Johnson (2010) analyzed high-resolution observational data and describe an interaction of the cold pool, the associated mesohigh, and bow echoes. They found prior to bow echo development a replacement of the mesohigh to the region ahead of the convective line, what they call the "pressure surge – new bowing" cycle. One of their hypothesizes is that this pressure surge evolves in response to non-hydrostatic convergence ahead of the approaching cold pool. This can be regarded like a ship's bow wave and becomes especially important when the convective system matures and increases its speed. The faster system's speed can also support the convection in another way. Faster system movement increases the system-relative inflow of moist, buoyant air masses as well as the low-level convergence ahead of the cold pool (Evans and Doswell, 2001).

Many studies have addressed the effects of environmental vertical wind shear on the intensity and maintenance of convective systems (e.g. Rotunno et al., 1988; Corfidi, 2003; Klimowski et al., 2003). Based on results of idealized model studies, this has been explained with the interaction of the cold pool and the vertical wind

shear especially at lower levels (Weisman, 2001). In weak-shear simulations, the cold pool's gust front was mainly affected by the circulations that evolve between the cool air of the cold pool and the warm air of the environment. This lead to a lesser cold pool depth at the gust front with cool air spreading outward in a rather shallow layer. The lift of pre-system warm air will therefore be limited in vertical extent and maybe insufficient to lift parcels to their LFC. When the environmental vertical shear was strong, this tendency was compensated locally. Instead, the cold pools leading edge looks like a tidal wave on the downshear flank of modeled convective systems. Fig. 13 illustrates this concept in the x,z-plane. The convective outflow is cold and has a higher density compared to the environmental air. It spreads out horizontally at the ground. At the intersection of cold and warm air, vertical shear evolves and a ring of horizontal vorticity continues to support the outward movement of cold air close to the ground. When there is no vertical wind shear, a symmetric vorticity ring will move outward (Fig. 13, left). In a situation with vertical wind shear (Fig. 13, right), there is horizontal vorticity in the environmental flow. It would cause downshear (i.e. to the right in Fig. 13, right) tilting of the convective cloud in the absence of cold pools. When a cold pool develops, both vorticity of the environment and along the cold pool intersection will be superimposed. At the downshear flank of the storm, the vorticity of the environment is opposed to the cold pool circulation. This weakens the cold pool circulation and supports lift to initiate new storms. Rotunno et al. (1988) described an "optimal" balance between the vorticity of the environment that is dependent on the magnitude of the vertical wind shear, and the cold pool-generated circulation. In this situation, the vorticity associated with the shear of the environment, $\mathbf{\Delta u}$ over a certain depth, is balanced by the vorticity associated with the shear of the gust front, that is controlled by the gust front speed c (eq. 1; a high gust front speed causes high vertical wind shear across the gust front and hence shear vorticity). Between the opposed circulations at the flanks of the cold pool, a vertical jet provides deep lifting to initiate intense, upright storms with strong updrafts (Rasmussen and Rutledge, 1993) that are supportive for the longevity of modeled convective systems (Weisman, 2001). In this respect, vertical wind shear can compensate for weaker CAPE as it allows more intense updrafts to form derechos, e.g. by increased stretching of mesovortices (Weisman and Trapp, 2003). Weisman (1993) found that CAPE down to 2200 J/kg favored bow echo development in his model simulations. This famous theory for strong, long-lived squall lines is also known as Rotunno-Klemp-Weisman (RKW) theory.

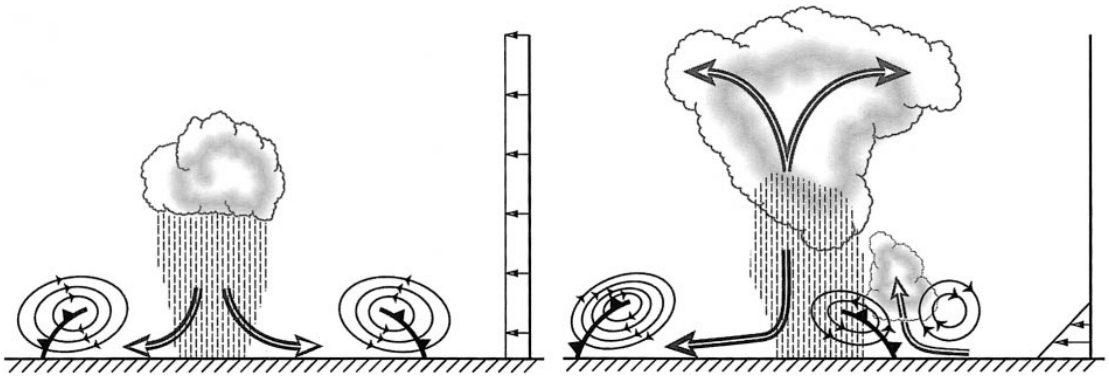

Figure 13: *Conceptual model for deeper lift on the downshear flank of convective cold pools in presence of vertical wind shear. Storm-relative vertical wind profile is given by arrows to the right of each figure. The cold pool's gust front is marked as a cold front. Circulations at the cold pool intersection and within the environmental flow are given by closed rings with arrows indicating the sense of rotation. Left: Cold pool circulation in a situation with no environmental vertical wind shear. Right: Cold pool circulation and initiation of new storms in a situation with environmental vertical wind shear. Image taken from Weisman and Rotunno (2004, their Fig. 1), ©American Meteorological Society. Used with permission.*

Johns (1993) remarked that RKW theory cannot explain the large variance of the observed thermodynamic environments for derechos occurring throughout the year, especially in the cold season with limited CAPE. Additionally, severe bow echoes occurred in association with weak cold pools due to stable nocturnal boundary layers (Weisman, 2001) and widespread convective wind storms that may meet derecho criteria were observed in regions with limited environmental vertical wind shear as in the tropics (Negrón-Juárez et al., 2010). Evans and Doswell (2001) examined 51 derechos, using the surface equivalent potential temperature difference between the cold pool and the environment to estimate cold pool strength, and proximity soundings to analyze the vertical wind shear. They found a large variability for analyzed combinations of cold pool strength and vertical wind shear and concluded that an optimal balanced state between the cold pool intensity and environmental vertical wind shear was not indicated in their data set, what is confirmed by recent results (Bryan et al., 2006; Coniglio et al., 2012). While RKW cannot explain the whole range of thermodynamic environments observed with derechos, there are similarities in observational studies. Processes on the synoptic scale were analyzed for derecho data sets by Johns and Hirt (1987), Johns et al. (1990), Bentley et al. (2000), Evans and Doswell (2001), Coniglio and Stensrud (2004), Burke and Schultz (2004), and Cohen et al. (2007). A combination of their findings reflects similarities for a majority of events:

1. All derecho examinations documented strong low-level warm air advection along the path of derechos, e.g. close to frontal boundaries (e.g. Davis et al., 2001).

2. Together with this warm air advection, Johns and Hirt (1987) and Johns et al. (1990) observed strong low-level jets pointing towards the center line of the derecho.

3. Divergence at upper levels (250 hPa) (Johns and Hirt, 1987; Johns et al., 1990; Coniglio and Stensrud, 2004) was also found for almost all cases. Prior to derecho formation, Coniglio et al. (2012) documented inertial instability at upper levels that increases the potential of upscale growth due to divergence and ventilation in the anvil layer (Blanchard et al., 1998).

Both synoptic-scale processes at the upper and lower boundary of the troposphere interact with deep moist convection in derecho events and may allow for upscale growth and longevity. However, RKW theory indicates that the combination of rich low-level moisture and steep lapse rates, associated with high CAPE, and strong low-level vertical wind shear can result in derecho development without further synoptic-scale forcing. The source of strong forcing for ascent is the interaction of the cold pool with the environmental vertical wind shear in underlying idealized simulations (Weisman, 1993). Observational studies showed that indeed some derechos form in situations characterized by high CAPE values in combination with weak synoptic-scale forcing (Johns et al., 1990).

In situations when CAPE is significantly weaker and even close to zero, Evans and Doswell (2001) found strong synoptic-scale forcing at mid levels. It is not completely understood how CAPE is generated in these situations, and which role synoptic-scale processes play (Sherburn and Parker, 2014). Since proximity soundings sometimes do not show CAPE at all, one possibility is that CAPE is only available over a limited area that is unlikely to be represented by the sounding network, an aspect that was also raised by Potvin et al. (2010). It is interesting to analyze these situations with respect to the overlap of low-level moisture and steep lapse rates, and how large-scale processes influence this overlap.

Corfidi et al. (2016) propose to name low-instability events "squall-line windstorm" to distinguish them from "internally driven" derechos. Internally driven means that the wind event evolves as a response to repeating, intense deep moist convection, e.g. the rear inflow jet is mainly accelerated by the perturbation pressure gradients produced by the convection. Externally driven storms do much more depend on the large-scale environment, e.g. very strong flow that can support the generation of severe wind gusts or cold fronts that provide strong lift. However, despite their different generation, some low-instability derechos show similar features comparable to high-instability derechos such as long-lived bow echoes (though typically embedded in a squall line; e.g. Gatzen et al. (2011)) and mesovortices have been documented with low-instability convective lines (e.g. Clark, 2009).

2.7 Derechos forming with low environmental instability

Soundings indicate that the environmental thermodynamic profile is very variable in derecho situations (e.g. Evans and Doswell, 2001). In weak CAPE environments, there is at least a tendency for rich low-level moisture (e.g. Burke and Schultz, 2004) and strong low-level vertical wind shear reasoning the term "high-shear, low-CAPE environments" in recent publications (e.g. Evans, 2010; King and Parker, 2014). However, Corfidi et al. (2006) also document cases with relatively weak low-level moisture and only modest low-level vertical wind shear.

Evans and Doswell (2001) analyzed a data set of derechos that includes events with low environmental instability as sampled by proximity soundings, i.e. soundings that were taken in or near the damage path and that were launched within 2 hours and 167 km from the derecho as indicated e.g. by radar images. They found that these events were accompanied by strong synoptic-scale forcing at mid levels based on a subjective analysis of 500 hPa and surface pressure charts. Strong synoptic-scale forcing was suggested to be present with high-amplitude mid-level troughs and strong surface cyclones. Evans and Doswell (2001) introduced the term "strongly-forced derechos" for these events. Comparable flow situations were also described by other authors, e.g. Johns (1993) (their dynamic pattern in serial derecho events), Bentley and Mote (2000), and Burke and Schultz (2004) (for long-lived cold-season bow echoes).

Further observational studies of strongly-forced derechos indicated frontogenetic processes at upper and mid levels (Sherburn and Parker, 2014). The synoptic-scale weather patterns described by Evans and Doswell (2001) are frequently associated with intense mid-level jet streaks that can lead to frontogenesis. Following a review of upper-level frontogenesis by Lackmann (2011), upper-level fronts can form e.g. in response to upper-level confluence together with cold air advection (e.g. Rotunno et al., 1994). The origin of upper-tropospheric cold air advection is not completely understood (e.g. Lang and Martin, 2010; Schultz, 2013). Schultz and Doswell (1999) showed that upper-level cold air advection can evolve within both south-westerly and north-westerly flow, e.g. due to rotational frontogenesis that increases the angle between isentropes and isohypses.

Once cold air advection and confluence have evolved, a maximum of cold air advection can be expected at the axis of jet streams due to the wind speed maximum that partly controls the along-flow cold air advection. At mid levels, quasi-geostrophic vertical motions would balance the cold air advection and cancel the cold air advection maximum. At upper levels, the large stability at the tropopause limits the quasi-geostrophic vertical motion that cannot balance the cold air advection maximum within the upper-level jet (e.g. Hoskins and Bretherton, 1972). As a consequence, ongoing quasi-geostrophic sinking with the along-flow cold air advection maximum gradually expands downward to mid levels. Below the jet streak core with its cold air advection maximum, mid levels will warm in response to quasi-geostrophic descent. Given weaker sinking or even rising motions at the flanks of the jet streak core, the isentropes below the jet will tilt correspondingly. This tilting frontogenesis is illustrated in Fig. 14 where the jet maximum would be located in the center of the images with the flow moving into the page. The result is that the tilt of isentropic surfaces becomes large especially between the jet streak axis and the cyclonically sheared flank of the jet, leading to the formation of an upper-level front. The tilting effect increases the frontal gradients and concentrates them below the jet streak. Additionally, the warm flank of the jet shifts to the jet core, where sinking and adiabatic warming is present. The frontal circulation is therefore a thermally indirect one, with sinking at the warm side (right part of Fig. 15) and weaker sinking or even rising air motions at the cold flank of the front (left part of Fig. 15).

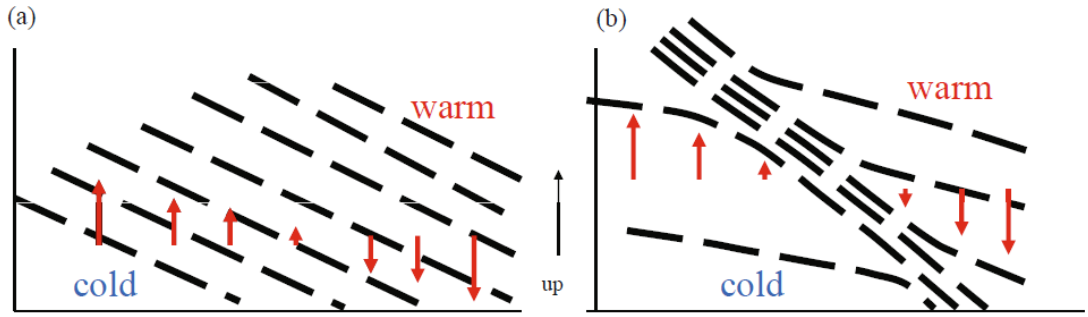

Figure 14: *Concept of an earlier (a) and a later (b) stage during tilting frontogenesis. Dashed lines represent isentropes, arrows indicate vertical motion. Image taken from Lackmann (2011, his Fig. 6.6),* ©*American Meteorological Society. Used with permission.*

In response to continuing descent, high potential vorticity of the tropopause region penetrates the troposphere. The dynamic tropopause will therefore move downward and eventually forms a tropopause fold along the upper front visible as high PV values extending downward in Fig. 16. PV is the parameter of choice to indicate the position of upper-level fronts, and they are sometimes called PV intrusions or stratospheric intrusions. The term cold front aloft has also been used (Hobbs et al., 1990). Since upper-level fronts are not only indicated by high values of potential vorticity compared to the environment, but also by very low relative humidity, they become visible on water vapor channel satellite images, so that they are sometimes called dark stripes.

The connection of strongly-forced derechos and upper-level fronts is supported by observational studies. Corfidi et al. (2006) give a detailed overview of strongly-forced synoptic-scale situations which they found for high wind producing mesoscale convective systems associated with limited low-level moisture. According to their findings, derechos formed at the cyclonically sheared flank of intense jet streak exits. This has also been frequently documented in derecho case studies, e.g. Van Den Broeke et al. (2005); Fink et al. (2009); Pistotnik et al. (2011); Gatzen et al. (2011). Cold-season narrow cold-frontal rain bands (e.g. Browning and Reynolds, 1994) tend to become more intense and severe at the cyclonically-sheared flank of upper-level jet streaks as indicated by a 10-year climatology in Germany (Gatzen, 2011). Convective initiation has been linked to dark stripes in the water vapor channel satellite image (e.g. Pajek et al., 2007) and studies documented stratospheric intrusions that co-exist with low-instability severe convective storms (e.g. Johns, 1993; Lane et al., 2006; Wasula et al., 2008; Clark, 2009;

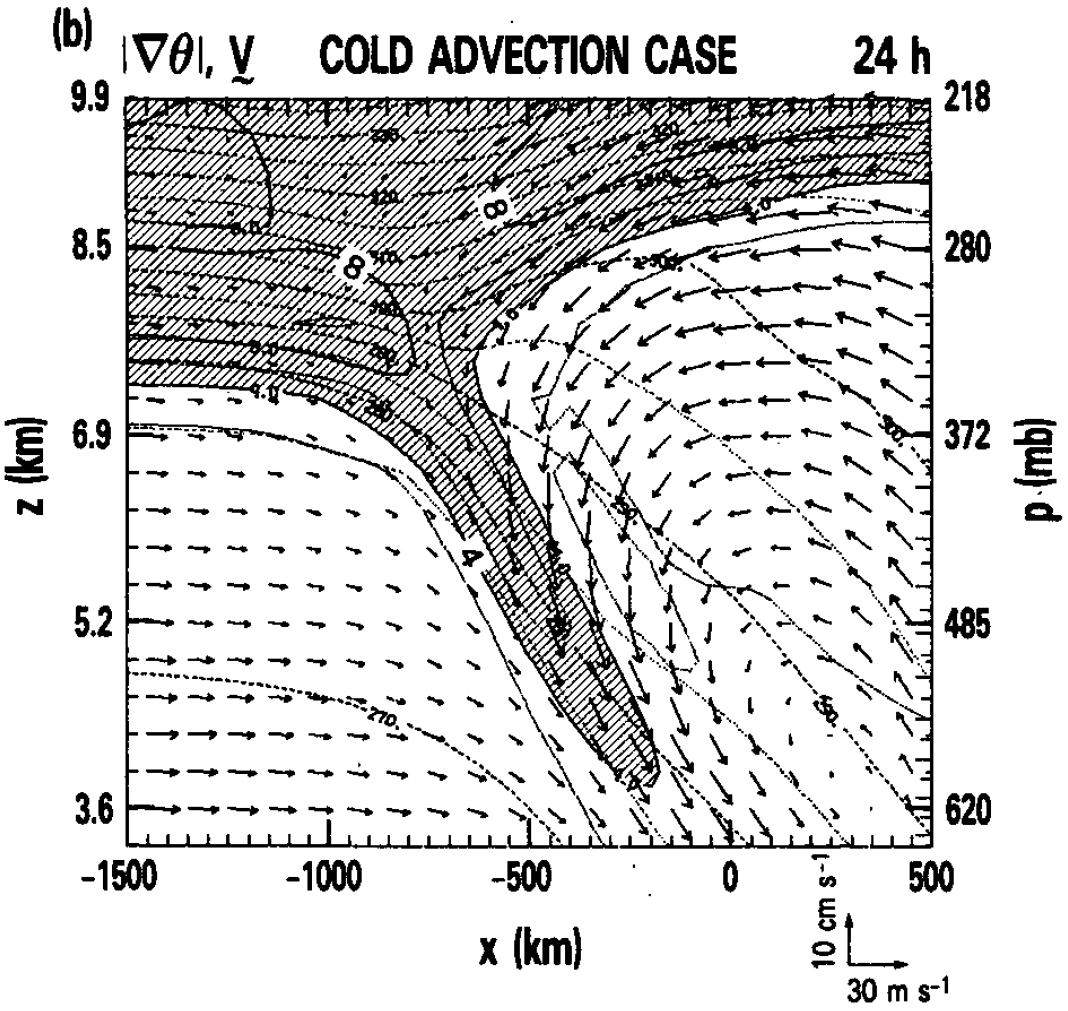

Figure 15: *Vertical cross section from a simulated upper-level front that evolves due to horizontal shear and cold air advection. The shaded region indicates stable air masses (potential temperature gradient greater than* $4 \cdot 10^{-5}$ *K/m), the vectors display the winds in the cross section. Image taken from Keyser et al. (1986, their Fig. 4),* ©*American Meteorological Society. Used with permission.*

Evans, 2010; Pistotnik et al., 2011; Clark, 2013; King and Parker, 2014). Based on current findings about high-shear, low-CAPE convective storms Sherburn and Parker (2014) summarize that upper-level fronts could play a role in these situations. From observations of upper-level fronts in Germany, low levels may also become unstable as convective clouds are frequently observed below tropopause folds (Fig. 17).

Overlooking the range of observed environmental conditions in which derechos formed, those associated with typical cold-season mid-latitude cyclones are least

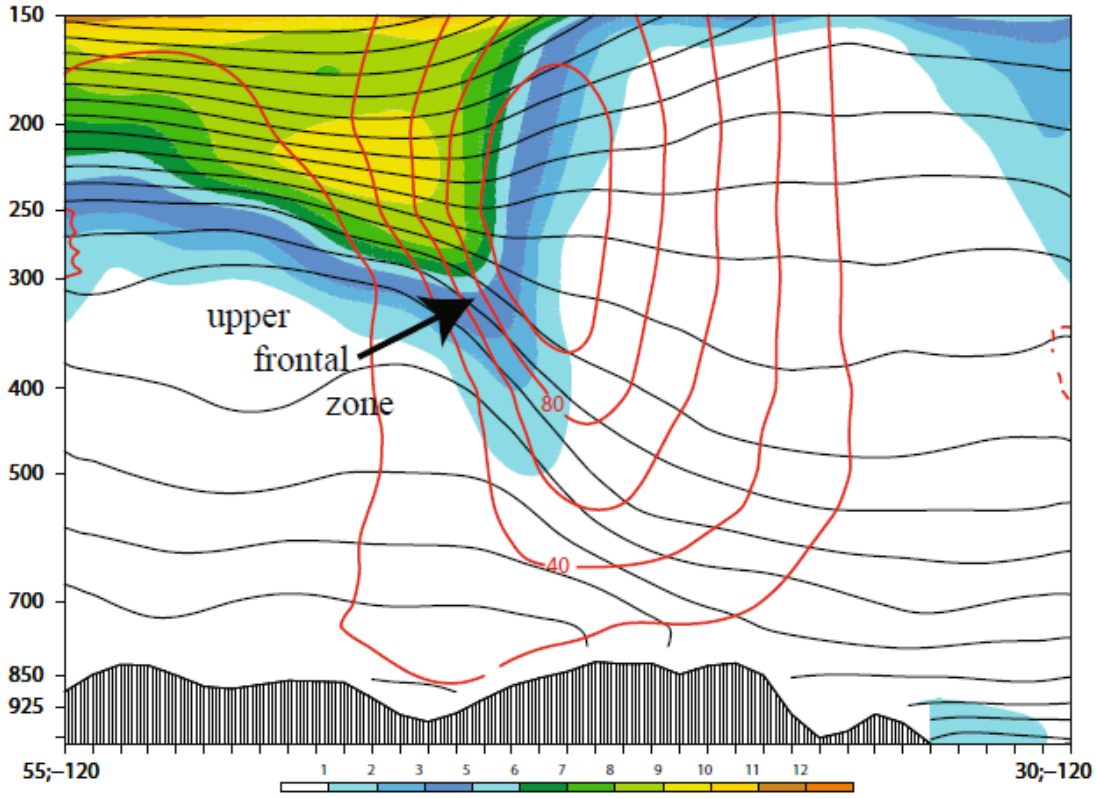

Figure 16: *Example of a cross section (from north (left) to south) that displays an upper level front. The PV [in PVU] is given by the color bar at the bottom, isentropes are given every 5K (black solid contours) and isotachs are given in red contours [in m/s]. Image taken from Lackmann (2011, his Fig. 6.36), ©American Meteorological Society. Used with permission.*

understood with respect to the ingredients-based approach. Whereas low-level moisture (e.g. Burke and Schultz, 2004) and large-scale forcing (e.g. Evans and Doswell, 2001) are typically in place, there is a lack of steep lapse rates according to proximity soundings (e.g. Potvin et al., 2010). This is clear as in the cold-season, the warm conveyor belt of mid-latitude cyclones tends to evolve stable lapse rates due to low-level cooling especially over the continents. This means that the lapse rate is below the moist adiabatic lapse rate and therefore does not allow for positive buoyancy. Consequently, the necessary conditions for deep moist convection are not fulfilled according to the ingredients-based approach.

It has been argued that in some situations, convective storms may form in the absence of steep lapse rates. One popular concept of how convective storms can form in association with stable lapse rates was introduced by Browning and Roberts (1996). This concept is based on the suggestion that in some situations potential instability may be a sufficient condition for convective storms, even when

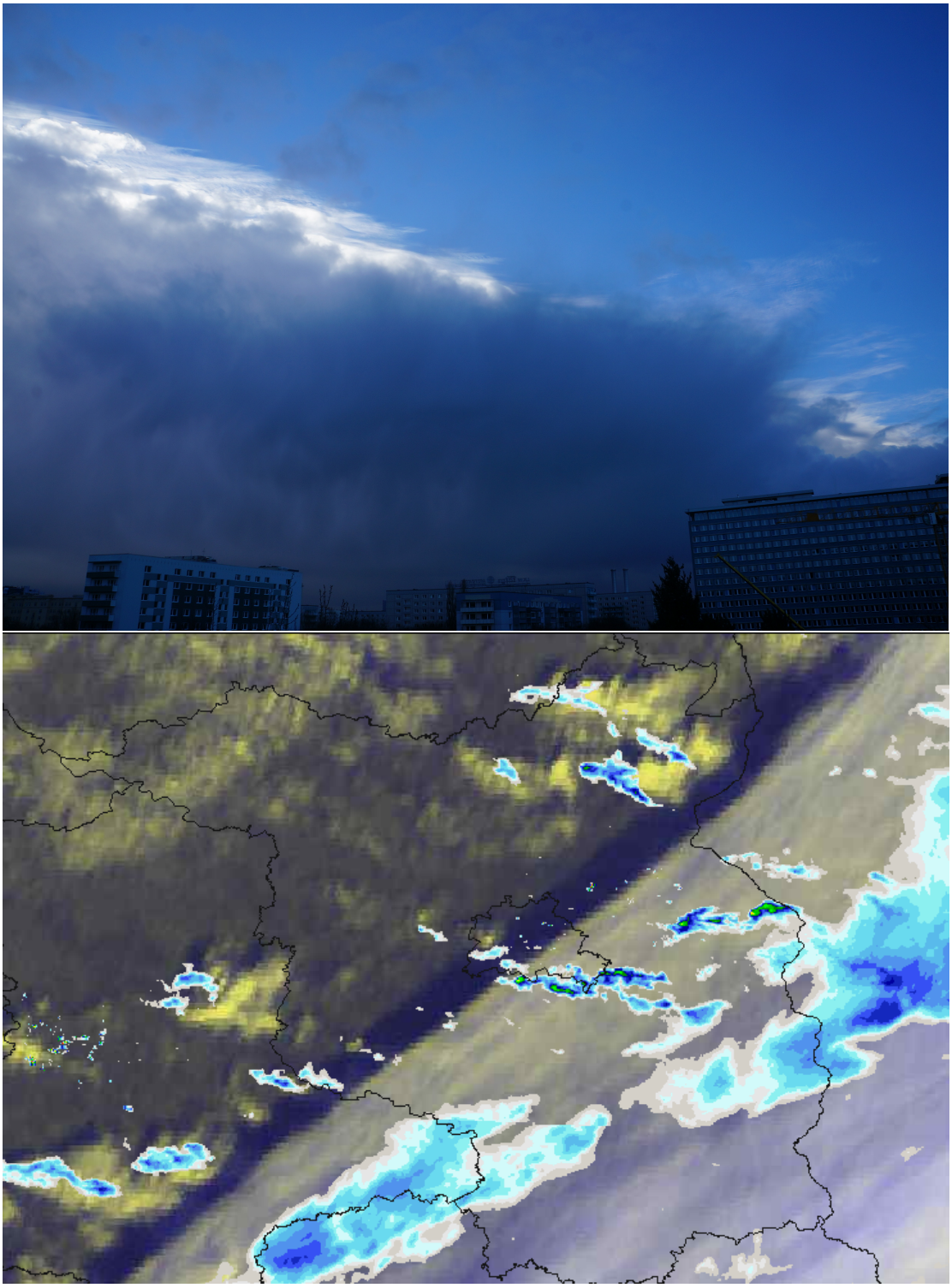

Figure 17: *View of an upper level front that crossed Berlin on 28 January 2016. Top: Photo from the city center of Berlin, looking to the south, at 09:14 UTC (photo: Christoph Gatzen). Bottom: Satellite (MSG) and radar composite on the same day at 09:00 UTC. Note the showers below the detaching upper-level cloud shield of the front captured in the photo and indicated in the radar display. Data source: EUMETSAT and Deutscher Wetterdienst / Image courtesy of MeteoGroup.*

conditional instability is not present. This means that the pseudo-potential temperature decreases with height while the lapse rate is stable at the same time. This is not an exceptionally rare condition and is possible for large vertical changes of relative humidity with dry air masses atop of moist air masses. An air mass that descends from the tropopause level to mid-levels (a dry intrusion) and overrides the warm conveyor belt later on can result in potential instability in this way. According to Browning and Roberts (1996), strong lift affecting such a vertical air column leads to condensation in the low, moist levels first, while the dry air at higher levels is still unsaturated. Stratiform low-level clouds would form, and with ongoing ascent, the low level air mass would cool slowly according to the latent heat release, whereas a larger cooling rate according to the dry adiabatic cooling rate can be expected in the unsaturated air mass aloft. As a consequence, the lapse rate will increase between the cloudy air at low levels and the clear air aloft. At some point, the moist warm conveyor belt becomes positively buoyant with respect to the dry air mass aloft. Deep moist convection could develop although there has been no conditional instability before.

Observations of cold-season convective storms do not support this conceptual model. Typically, stratiform clouds are not observed prior to convective initiation (Markowski and Richardson, 2011). Latent heat release prior to convective initiation is therefore not indicated. It is also argued that potential instability is released and consumed instantly within a strongly-forced precipitating line. This could be the case when an upper-level cold front "overruns" a surface cold front ("split front" concept). Potential instability evolves ahead of the surface cold front that also acts as a source of strong lift (e.g. Browning and Roberts, 1996). A superposition of the upper front with the surface cold front can assist in deep lifting (see Fig. 18, after Shapiro, 1982).

Some more thoughts about this concept give rise to critical questions. Potential instability is especially needed to explain convective initiation in the cold season when environmental CAPE is weak or absent. However, potential instability is much more common in the warm season when rich moisture is available and latent heat release is higher. Nonetheless, in the warm season there are no indications that potential instability release is important in convective storms forecasting that can be based on the ingredients-based approach only.

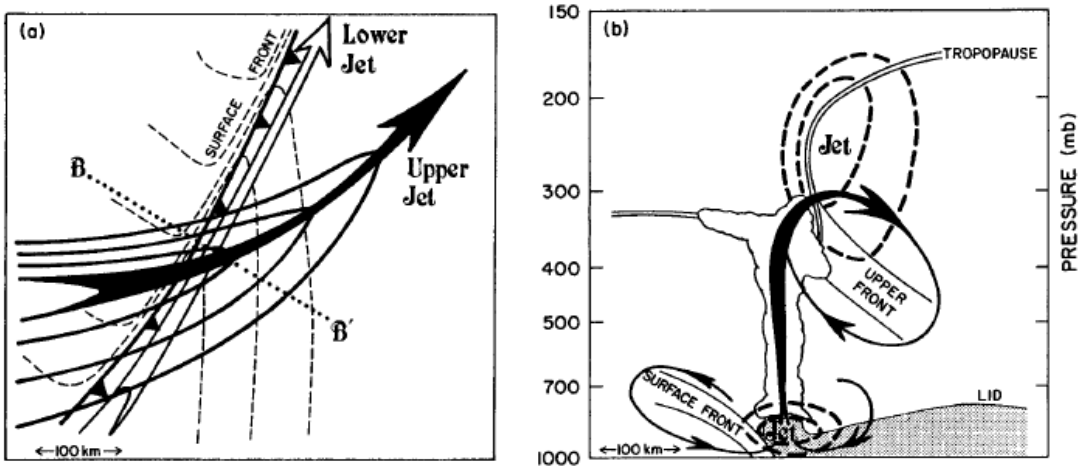

Figure 18: *Illustration of the superposition of the frontal circulations of upper level front and surface front. (a) Position of the vertical cross section (B–B') relative to the position of surface front and the upper-level jet. (b) Vertical cross section from B–B'. Pressure is given to the left [hPa], positions of surface and upper-level front are marked. The thermally direct circulation of the surface front and the thermally indirect circulation of the upper-level front are given by closed lines with arrows pointing to the direction of the circulations. Furthermore, the tropopause (double line) and regions with high wind speed (dashed isotachs) are included. Image taken from Shapiro (1982),* ©*American Meteorological Society. Used with permission.*

There is another argument with respect to the potential instability concept: Positive buoyancy would develop at a height where the dry air mass is lifted, that is typically at mid levels. Here, the difference of moist and dry adiabatic lapse rates is small, so only weak positive buoyancy can be achieved in the cold season at mid-levels even for strong lifting. In contrast, CAPE may form at low levels: Model simulations (McCaul Jr and Weisman, 2001) point out the importance of low-level buoyancy for severe convective storms forming in low environmental instability (e.g. Sherburn and Parker, 2014; Sherburn et al., 2016; King et al., 2017). The release of potential instability is questionable as CAPE forms close to the ground where lift is limited and large differences in pseudo-potential temperature are not present.

Finally, the derecho data set this thesis is based on contains events that formed in the absence of well-defined surface fronts. In these events, frontal lift seems to be not needed to initiate storms. It is therefore questionable that potential instability is released directly in these situations. Summarized, there are some indications that dry mid-level air and associated potential instability at mid levels may be not a dominant factor in the formation of low-instability derechos.

Rapid destabilization of a profile with lapse rates that exceed at least the moist adiabate can be also obtained by moisture increase. Sherburn et al. (2016) found that low-instability derechos formed close to a moisture ridge with low-level moisture advection and warm air advection.

Besides the concept that steep lapse rates are not needed in cold season convection events, there are also concepts that focus on rapid lapse rate increase in the vicinity of upper-level fronts. One is the concept of an upper-level cold front that leads to strong cooling at mid-levels and weaker cooling at low-levels (Colson, 1960), causing lapse rate increase due to differential temperature advection (Banacos and Ekster, 2010). One could even think of situations, in which a cold front aloft leads to cold air advection at mid-levels, whereas at the same time, warm air advection is present at low-levels. However, strong cold air advection and associated isentropic descent would counteract the lift needed to initiate convective storms (e.g. House, 1958). Additionally, mid-level sinking would lead to dry-adiabatic warming of the descending air what can result in stronger inversions between the ascending low-level air mass and the upper-level air. Although differential cyclonic vorticity advection could compensate the isentropic descent, it is at least questionable that strong cold air advection can support deep moist convection in these situations.

Increased diabatic heating of low-level air masses due to the clearing and associated sunshine below dry intrusions has been discussed (Wasula et al., 2008; Pistotnik et al., 2011). As this heating would be concentrated near the ground, it increases the lapse rate by the differential diabatic heating (Banacos and Ekster, 2010). This concept would not explain events that occur during the night or over the sea. Insolation is also pretty limited in the cold season and does likely have a minor impact on the lapse rate evolution.

Finally, differential vertical motion can result in changes of the lapse rate due to stretching (Banacos and Ekster, 2010). With increasing upward vertical motion with height, a positive lapse rate tendency results. This concept can be expected to be important especially at low levels and near inversions where lift is suppressed what allows large vertical changes of vertical motion. One possible situation would be rapid changes of lapse rates related to the strong low-level forcing in response to an upper-level front. Quite strong lift can be expected ahead of a progressing PV intrusion due to strong differential cyclonic vorticity advection. Additionally,

relatively weak stability is located within and directly below cyclonic PV anomalies (Hoskins et al., 1985; Thorpe, 1985). When a PV intrusion moves towards a location, the isentropes are lifted (Figs. 16 and 19). Especially close to the ground, this lift will likely increase with height, corresponding to stretching. Even in the case of cold air advection, when the flow on isentropic surfaces is "downslope", lift results when the effect of the PV intrusion is larger than this downslope flow since the vertical velocity is a combination of isentropic displacement and isentropic upglide (Hoskins et al., 2003). For example, this is the case when the PV intrusion moves faster than the speed of the low-level flow. In that case, the local upward displacement of the isentrope is faster than the downward displacement of air parcels moving downslope on this isentrope.

If the PV intrusion comes close to the ground, the stretching could lead to steepening lapse rates: In Figs. 16 and 19, the thickness between the isentropes increases below the PV intrusion that corresponds to stretching. This stretching can eventually lead to the rapid evolution of CAPE in the close vicinity of derechos, so that proximity soundings and even low-resolution model data may not be repre-

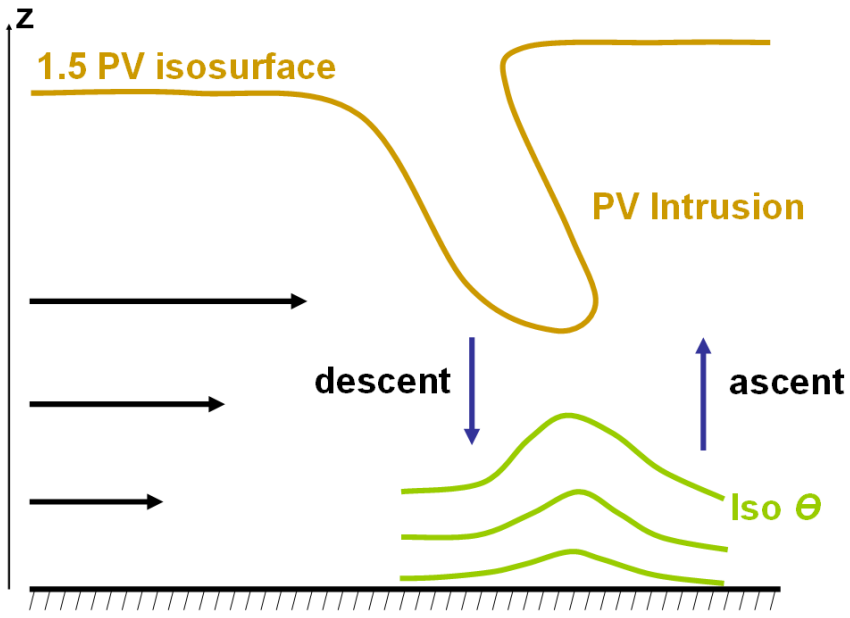

Figure 19: *Schematic overview of a PV intrusion. Wind vectors at different heights are given in black to the left, a PV isosurface is given by the solid brown contour line. Ahead of the moving PV intrusion, ascending motions are present, whereas subsidence can be expected in its wake. This can also be seen from the thickness between isentropes at low levels (green contour lines). Modified illustration from EUMeTrain; http://www.eumetrain.org/data/2/28/Content/pv.htm*

sentative (Potvin et al., 2010; King et al., 2017). Shallow cumulus clouds that are sometimes observed together with upper-level fronts (Fig. 17) may indicate that low-level instability evolves in these situations. One important restriction has to be mentioned, this is that this process leads to steep lapse rates just for unsaturated air. In saturated air, stretching can only result in a moist adiabatic lapse rate. Latent heat release that sets in will disable further lapse rate increase until the moisture is removed from the air mass.

Although the cited literature offers some indications that the strong synoptic-scale forcing in low-instability derecho events is associated with upper-level fronts, there is no consensus about the processes that allow for intense, persistent deep moist convection. This topic could be addressed using the ingredients-based approach to forecast convective storms. The advantage is that these ingredients can be analyzed and followed separately to the point where they overlap to initiate convective storms (Doswell et al., 1996). In practice, a forecaster analyzes the low-level moisture field using ground-based weather observations and rawinsonde data. Once the moisture field is constructed, it is analyzed where and when rich low-level moisture overlaps with steep lapse rates to obtain CAPE, i.e. the necessary thermodynamic conditions to enable deep moist convection (Doswell, 1987). This is done by calculating the lapse rate between different pressure levels as given by sounding data. The observed lapse rate can be compared to model-derived lapse rates on pressure levels to get indications on the model's forecast confidence. Furthermore, operational forecast model data can be routinely plotted to show the fields of low-level moisture (e.g. the mixing ratio of the lowest 50 hPa mixed layer) and a lapse rate field (e.g. between 800 and 600 hPa) together.

Low-instability derechos do not seem to match the ingredients-based approach as an overlap of rich low-level moisture and sufficiently steep lapse rates may not be indicated by available data. One reason could be that small-scale local changes are not resolved by observational data. Low-level moisture is typically available with high horizontal and temporal resolution due to the ground observation network. To analyze lapse rate changes, we will use high resolution data of German cold-season derechos. The lapse rate tendency equation will therefore be analyzed in the model fields with respect to the underlying thermodynamic processes that change the lapse rate. It will be introduced in the following chapter. Based on this analysis, a conceptual model can be derived for these situations.

2.8 The lapse rate tendency equation

The lapse rate γ expresses the temperature change with height:

$$\gamma := -\frac{\partial T}{\partial z} \tag{5}$$

where γ is positive for decreasing temperature T with height z and negative for increasing temperature with height. The change of the lapse rate γ over a given location can be expressed by the local lapse rate tendency equation (e.g. Banacos and Ekster, 2010). Since changes of the lapse rate are associated with changes of the internal energy of the air in a vertical column, the lapse rate tendency can be derived from the first law of thermodynamics. The mass-specific first law of thermodynamics states that the change of internal energy e of an isolated system can be expressed by the sum of the heating rate per unit mass Q and the work done by volume changes of the system:

$$\frac{de}{dt} = Q - p\frac{d\alpha}{dt} \tag{6}$$

where p is the pressure and $\alpha = \rho^{-1}$ is the mass-specific volume or the reciprocal of the density ρ. The equation of state of ideal gases reads $p\alpha = RT$ with T as absolute temperature and $R = 287\,\mathrm{J/(kgK)}$ as specific gas constant for dry air. With help of the total derivative $d(p\alpha) = pd\alpha + \alpha dp = RdT$, the first law of thermodynamics (6) can be rewritten in the following form

$$\frac{de}{dt} = Q - R\frac{dT}{dt} + \alpha\frac{dp}{dt} \tag{7}$$

Since $de = c_v dT$ and $c_p = c_v + R$ with $c_v = 717\,\mathrm{J/(kgK)}$ and $c_p = 1004\,\mathrm{J/(kgK)}$ being the specific heat at constant volume, and pressure, respectively, it follows that the first law of thermodynamics can also be expressed as[3]

$$Q = c_p\frac{dT}{dt} - \alpha\frac{dp}{dt}\ . \tag{8}$$

Following Markowski and Richardson (2011) and Banacos and Ekster (2010), the material time derivative of T is expressed as

$$\frac{dT}{dt} = \frac{\partial T}{\partial t} + \mathbf{V}\cdot\nabla_h T + w\frac{\partial T}{\partial z} \tag{9}$$

with the horizontal wind vector $\mathbf{V}$ and the vertical wind component w. Given

[3]The derivation of (8) is similar to the way Holton (2004, chapters 2.6, 2.7) presents it.

hydrostatic conditions, i.e. $dp = -g\alpha^{-1}dz$ one obtains

$$Q = c_p \left(\frac{\partial T}{\partial t} + \mathbf{V} \cdot \nabla_h T + w \frac{\partial T}{\partial z} \right) + gw \tag{10}$$

Derivation with respect to z and multiplying by -1 yields

$$\begin{aligned} -\frac{\partial Q}{\partial z} = c_p \Bigg[& \frac{\partial}{\partial t} \left(-\frac{\partial T}{\partial z} \right) + \mathbf{V} \cdot \nabla_h \left(-\frac{\partial T}{\partial z} \right) + w \frac{\partial}{\partial z} \left(-\frac{\partial T}{\partial z} \right) \\ & - \frac{\partial \mathbf{V}}{\partial z} \cdot \nabla_h T - \frac{\partial w}{\partial z} \frac{\partial T}{\partial z} \Bigg] - g \frac{\partial w}{\partial z} \ . \end{aligned} \tag{11}$$

Using the lapse rate definition (5) and introducing the dry adiabatic lapse rate $\Gamma_d := g c_p^{-1}$ leads to:

$$-\frac{1}{c_p} \frac{\partial Q}{\partial z} = \left[\frac{\partial \gamma}{\partial t} + \mathbf{V} \cdot \nabla_h \gamma + w \frac{\partial \gamma}{\partial z} - \frac{\partial \mathbf{V}}{\partial z} \cdot \nabla_h T - \frac{\partial w}{\partial z} (\Gamma_d - \gamma) \right] \ . \tag{12}$$

This equation can be solved for the local lapse rate tendency $\partial\gamma/\partial t$:

$$\underbrace{\frac{\partial \gamma}{\partial t}}_{\text{LRT}} = \underbrace{-\mathbf{V} \cdot \nabla_h \gamma}_{\text{I}} \underbrace{- w \frac{\partial \gamma}{\partial z}}_{\text{II}} + \underbrace{\frac{\partial \mathbf{V}}{\partial z} \cdot \nabla_h T}_{\text{III}} + \underbrace{\frac{\partial w}{\partial z} (\Gamma_d - \gamma)}_{\text{IV}} \underbrace{- \frac{1}{c_p} \frac{\partial Q}{\partial z}}_{\text{V}} \ . \tag{13}$$

From $\gamma = -\partial T/\partial z$ it follows that the temporal change of the local lapse rate γ is positive for increasing lapse rates, corresponding to destabilization, and negative for decreasing lapse rates, corresponding to stabilization within an observed layer over a given location.

$$\begin{aligned} \frac{\partial \gamma}{\partial t} &> 0 \ : \text{ lapse rate increase} \quad \longleftrightarrow \quad \text{destabilization} \\ \frac{\partial \gamma}{\partial t} &< 0 \ : \text{ lapse rate decrease} \quad \longleftrightarrow \quad \text{stabilization} \end{aligned}$$

The lapse rate tendency, i.e. the temporal change of the lapse rate, can be dependent on various processes. One of these processes is the advection of environmental lapse rates. This includes both: the advection of horizontal lapse rate gradients by the horizontal flow (term I, Fig. 20 b) as well as the advection of vertical lapse rate gradients by the vertical flow (term II, Fig. 20 c).

Another process denoted as term III in the lapse rate tendency equation (13) is

the differential thermal advection (Fig. 20 d). This term describes the effects of vertical different horizontal temperature advection on the lapse rate tendency. Due to the fact that in a geostrophic flow the thermal wind is directed parallel to the thickness field between two pressure levels, $\partial \mathbf{V}_g / \partial z \cdot \nabla_h T = 0$, the lapse rate change is provided by the vertical shear of the ageostrophic component of the flow (Banacos and Ekster, 2010; Markowski and Richardson, 2011). This can be either a thermally indirect flow (and corresponding lapse rate increase) or a thermally direct flow (lapse rate decrease). The combined effect of term I and term III describes changes of the local lapse rate due to differential temperature advection (Markowski and Richardson, 2011):

$$-\mathbf{V} \cdot \nabla_h \gamma + \frac{\partial \mathbf{V}}{\partial z} \cdot \nabla_h T = -\frac{\partial}{\partial z}(-\mathbf{V} \cdot \nabla_h T) \tag{14}$$

Term VI in (13) is the effect of vertical stretching on the lapse rate (Fig. 20 e). When vertical motion differs in the vertical, adiabatic temperature changes will be also different in the vertical in the same time period: Increasing ascent with height will cause the upper levels to cool more rapidly compared to the lower levels, leading to a lapse rate increase (and hence, destabilization). When lift decreases with height, stabilization occurs. If upper level sinking is stronger compared to low-level sinking, upper-level diabatic warming will exceed low-level warming, leading to stabilization. If upper-level sinking is weak compared to low-level sinking, the lapse rate between the two layers will increase. According to Banacos and Ekster (2010) and Markowski and Richardson (2011), the lapse rate increases for $\partial w / \partial z$ as long as the local lapse rate is smaller than the dry-adiabatic lapse rate ($\Gamma_d - \gamma$ is positive). It can be added, that, when the affected air mass is saturated, lift will result in latent heat release that influences further lapse rate increase due to differential diabatic heating. When lift acts on saturated air masses, a moist adiabatic lapse rate is the steepest possible lapse rate that can evolve due to the combined effects of stretching and differential diabatic heat release.

Processes associated with diabatic heating are combined in term V (Fig. 20 a). When diabatic heating changes in the vertical, it can change the lapse rate. For example, increasing diabatic heating with height (as would be the case for lift of saturated air increasing with height) would lead to stabilization. Generally, destabilization can be expected above a maximum of diabatic heating, whereas stabilization occurs below a maximum of diabatic heating. Fig. 20 illustrates the influence of the individual processes addressed by the lapse rate tendency equation.

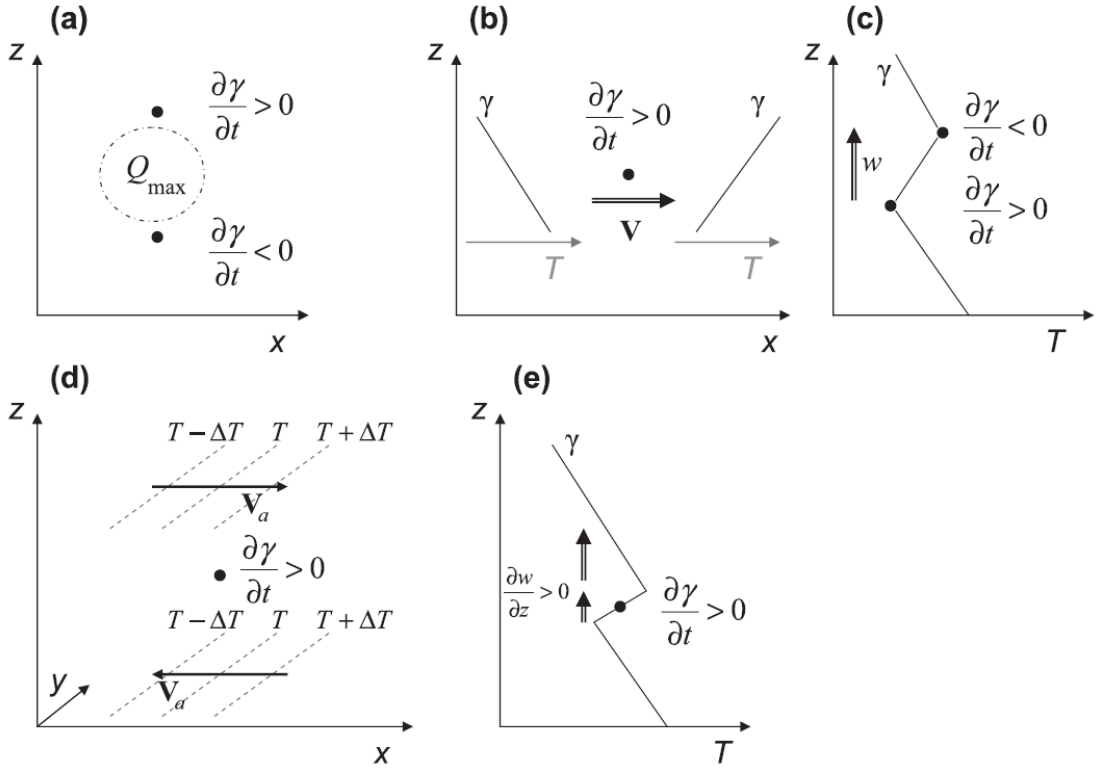

Figure 20: *Illustration of the terms in the local lapse rate tendency equation. a) Diabatic heating term, here for a local maximum Qmax of diabatic heating; b) horizontal advection term; c) vertical advection term; d) differential temperature advection term by the ageostrophic flow Va; e) stretching term. Image taken from Banacos and Ekster (2010, their Fig. 2),* ©*American Meteorological Society. Used with permission.*

Under geostrophic conditions, the lapse rate is conserved following the flow, what explains that horizontal advection plays a dominant role on the synoptic scale. It is this property that is practically used in ingredients-based forecasting. Banacos and Ekster (2010) and Markowski and Richardson (2011) give a scale analysis of the different terms of the lapse rate tendency equation (13) for synoptic-scale flow and estimate the magnitude of the horizontal advection term (I) at $10^{-7}\mathrm{Km}^{-1}\mathrm{s}^{-1}$. This is about 1-2 orders greater than the other terms in the lapse rate tendency equation. The vertical advection term (II) and the differential thermal advection term (III) have a magnitude of $10^{-8}\mathrm{Km}^{-1}\mathrm{s}^{-1}$, whereas the stretching term (IV) and the diabatic heating term (V) are about $10^{-9}\mathrm{Km}^{-1}\mathrm{s}^{-1}$. On the mesoscale, as in the presence of fronts, jets, and deep moist convection, the individual terms can become much larger (Markowski and Richardson, 2011).

2.9 Derechos in Germany – a literature review

Only a few derechos have been classified across Germany so far. In the scientific literature, six analyzed events can be found. The Berlin derecho (Gatzen, 2004) has been the first documented derecho and also the first published derecho that occurred outside of North America (Punkka et al., 2006). In the years 2007 to 2010, five further events occurred according to peer-reviewed publications (Gatzen et al., 2011; Pistotnik et al., 2011; Púčik et al., 2011; Simon et al., 2011; Hamid, 2012; Celiński-Mysław and Matuszko, 2014), indicating that derechos are not uncommon in Germany:

The Berlin derecho of 10 July 2002 affected eastern and northern Germany along a 600 km long path according to Gatzen (2004). It hit the German capital Berlin. Its high death toll and impact on the infrastructure made it one of the most remarkable weather events in Germany over the past decades. The derecho evolved ahead of a large squall line and moved in an along-front direction. Radar images showed repeating cell mergers and associated multiple bowing structures at the leading gust front (cf. section 2.4). This appearance on the radar image has been named a bow echo complex that is defined as a mesoscale convective system in which bow echoes are "the primary, but not the only, organized convective structure" (Klimowski et al., 2004).

The "Kyrill"-derecho of 18 January 2007 produced a 1500 km long and about 200 km wide swath of severe wind gusts that extends across northern Germany and reached moderate intensity (Gatzen et al., 2007; Fink et al., 2009; Gatzen et al., 2011; Celiński-Mysław and Matuszko, 2014). It formed along a surface cold front and included a few prominent, 100 km wide bow echoes that were embedded in the cold-frontal precipitation band, known as squall-line bow echoes (Klimowski et al., 2004), also matching the definition of a serial derecho (Johns and Hirt, 1987). Together with the derecho, tornadoes hit eastern Germany and parts of Poland and the Czech Republic, including three F3 and four F2 tornadoes which caused high damage and injured four people (European Severe Weather Database (ESWD); Dotzek et al., 2009). The "Kyrill" storm killed 47 people and produced losses of several billion dollars across Europe (Wikipedia, 2015b).

On 1 March 2008, the very strong "Emma"-Derecho affected most of Germany (Gatzen et al., 2011; Pistotnik et al., 2011; Celiński-Mysław and Matuszko, 2014).

The derecho formed along a cold-frontal rain band. The path of this derecho was 1500 km long; its width reached 500 km across Germany. Wind measurements and damage reports justify it to be a high-end derecho according to the definition by Coniglio and Stensrud (2004). As for the "Kyrill"-event, radar images reflect a serial derecho with a few dominant squall-line bow echoes. Furthermore, Pistotnik et al. (2011) documented very strong downbursts along the derechos' path with intensity estimations as high as F3.

Three publications refer to the derecho of central Europe on 25 June 2008 (Púčik et al., 2011; Simon et al., 2011; Celiński-Mysław and Matuszko, 2014). It initiated over south-east Germany, producing one wind gust exceeding 25 m/s and then moved into the Czech Republic, Slovakia, northern Austria, and northern Hungary (Púčik et al., 2011). The path was about 600 km with a width of 150 km (Celiński-Mysław and Matuszko, 2014), and damage surveys point out at least moderate intensity (Púčik et al., 2011; Simon et al., 2011). Most damage was associated with two bow echoes that belonged to the same MCS (Púčik et al., 2011; Celiński-Mysław and Matuszko, 2014).

Celiński-Mysław and Matuszko (2014) document another derecho that affected Poland on 23 July 2009 and initiated across the border between the Czech Republic and eastern Germany. Damage and severe wind gust measurements were reported within a 550 km long and 150 km wide path. Based on wind measurements, the intensity of this derecho was at least moderate. The authors mention that isolated cells formed ahead of the derecho that merged to the MCS.

Hamid (2012) published an analysis of a west-European derecho that affected eastern France and the Benelux countries on 14 July 2010. The derecho moved into north-western Germany where it dissipated. According to Hamid (2012), the damage path across Belgium and the Netherlands was 300 km long and extended farther into France[1]. A damage survey included reports of winds in excess of 29-37 m/s (corresponding to EF0 on the enhanced Fujita scale, Doswell et al. (2009)) and embedded regions with wind-related damage of EF1 (38-49 m/s) or even EF2 (greater than 50 m/s). As shown by radar images, a few bowing elements formed at the leading edge of an extensive mesoscale convective system. Hamid (2012) investigated a couple of mesovortices embedded in the leading gust front and demonstrated their relation to the damage pattern.

[1] Analysis of this event for this work indicates a path length of 500 km.

Although the number of analyzed derechos is small, some similarities can be found. Focusing on the environmental conditions of derechos as described above, the derechos indicated several of these:

- Indications for upper-level divergence: For the Berlin derecho, the 300 hPa analysis given in Gatzen (2004) shows a coupled jet configuration[2], a strong anticyclonically jet streak entrance can be found for the west-European derecho, and upper-level divergence is also mentioned for the Central European derecho (Púčik et al., 2011).

- Indications of low-level forcing: Strong warm air advection is mentioned for all events except for the Kyrill and Emma derechos (Gatzen, 2004; Púčik et al., 2011; Simon et al., 2011; Celiński-Mysław and Matuszko, 2014; Hamid, 2012). Additionally, convergence lines and pre-frontal boundaries were analyzed for three events (Gatzen, 2004; Celiński-Mysław and Matuszko, 2014; Hamid, 2012).

- Rich low-level moisture: Seasonably rich low-level moisture has been documented for all derechos except for the west-European event with modest low-level moisture (surface dewpoints around 15°C according to Hamid, 2012).

- Steep lapse rates / high CAPE: Gatzen (2004),Púčik et al. (2011),Celiński-Mysław and Matuszko (2014), and Hamid (2012) document high CAPE between 1000 and 2500 J/kg based on proximity soundings and model data. Indications for steep lapse rates are given in Gatzen (2004) and Hamid (2012), the latter mentioning the presence of a so-called "Spanish Plume"[3].

- Strong vertical wind shear: All publications mention strong vertical wind shear at low levels.

- Strong mid-level forcing: Strong mid-level forcing is mentioned by some pub-

[2]A coupled-jet configuration is a situation in which upper-level divergence at the anticyclonically sheared entry of a jet streak overlaps with the upper-level divergence at the cyclonically sheared exit of another jet streak, providing strong quasi-geostrophic forcing (e.g. Uccellini and Kocin, 1987; Hakim and Uccellini, 1992)

[3]A "Spanish Plume" (Morris, 1986) is an elevated mixed layer advected north across the Iberian Peninsula. It is characterized by high temperatures at 850 hPa and deep mixing in response of strong diurnal heating over the Iberian plateau or the North African Atlas mountains.

lications, i.e. due to intense, negatively tilted short-wave troughs[4] (Gatzen, 2004; Hamid, 2012) or at the cyclonically-sheared exit of strong jet streaks (Gatzen et al., 2011; Pistotnik et al., 2011). Fink et al. (2009), Pistotnik et al. (2011), and Celiński-Mysław and Matuszko (2014) document dry intrusions and strong mid-level flow what could also result in strong mid-level forcing.

The small sample size of German derechos does not allow for detailed climatological conclusions. For example, regional differences of derecho occurrence in Germany are not identifiable. However, most events took place in the warm season, and CAPE was rather high for European relations: For three of six derechos, 2000 J/kg as given in the publications by Púčik et al. (2011), Hamid (2012), and Celiński-Mysław and Matuszko (2014) exceeds the 90 % percentile of the most unstable CAPE distribution for severe convective wind environments in Central Europe as investigated by proximity soundings (Púčik et al., 2015). On the other hand, two of six derechos formed in the cold season and were associated with marginal CAPE values (Gatzen et al., 2011; Pistotnik et al., 2011). Furthermore, synoptic- and mesoscale features known from United States derechos have been also frequently documented across Germany. This is divergence at upper levels and warm air advection and convergence lines ahead of the derecho path at low levels. Additionally, strong low-level vertical wind shear that can support low-level upward lift according to RKW theory was described in most publications (Gatzen, 2004; Gatzen et al., 2011; Pistotnik et al., 2011; Púčik et al., 2011; Celiński-Mysław and Matuszko, 2014; Hamid, 2012). Overlooking subjective conclusions by the authors on the strength of mid-level forcing, all events indicated the presence of strong mid-level flow due to jet streaks close to the derecho events. Most events were clearly strongly-forced as indicated by mid-level flow charts presented in the publications. For confirmation of these results, as a next step further derecho events have to be analyzed. The following section will give an overview over the used methods to classify and analyze derecho events from observed and simulated data sources.

[4]Negatively-tilted troughs are oriented from north-west to south-east on the northern hemisphere and are frequently associated with strong differential cyclonic vorticity advection and initiation of convective storms (e.g. Macdonald, 1976)

3 Data and Methodology

The previous section showed that derechos have occurred in the past across Germany and neighboring countries. Since there is little known about German derechos so far, research from the United States was presented in order to support forecasts and warnings. There are two further objectives of this thesis. One is to present a more substantial climatology of German derechos to adjust the presented conceptual forecast models of large-scale dynamics to German derecho situations, but also to raise the awareness for these storms, e.g. among forecasters. Second, we will address open questions on low-instability derechos that frequently occur in Germany, and refer in particular to large-scale processes that are supportive. This chapter describes data and methods we use to classify and analyze German derechos.

In section 3.1 we give an overview of the data sources. This section also describes how these data are utilized and combined. Section 3.2 informs about the COSMO model used to analyze German derechos, while sections 3.3 and 3.4 explain which cases are simulated and how favorable processes for derecho development are found. We describe how we analyze cross sections of the model simulations in section 3.5 and the statistical analysis of the lapse rate tendency equation in section 3.6.

3.1 Classification and analysis of German derecho events

The classification of derechos following Johns and Hirt (1987) is based on severe weather reports. These are wind gust measurements on the one hand and damage reports that are rated with respect to the wind speed on the other hand. A systematic analysis of damage reports has not been done in Germany except for the recent decade that is well-represented in the European Severe Weather Data Base (ESWD; Dotzek et al., 2009). Therefore, the search for derechos was based on Germany's observation network operated by the German weather service (online available at www.dwd.de). This network is relatively dense and allows for a high detection rate of large-scale wind events moving across the country. For every day, stations reporting at least 25 m/s were counted. Days with five or more of such records were selected as potential derecho dates. The wind records in this

data set go back to the 1940s (Fig. 21), however, the density of this network increased strongly, especially in the 1970s, so that the detection rate also decreases when going backward in time. A lower detection rate can also be expected along the borders of Germany due to limited data available in the neighboring countries.

A different approach was used in the cold seasons (October to March) that have a much higher frequency of severe wind gusts than the warm season. In the cold season, radar data was analyzed with respect to convective radar structures to detect potential derecho events. For the years 1998 to 2009, such analysis had been already prepared for a work about cold-season narrow cold-frontal rain bands (Gatzen, 2011) and was used in this work. Lightning data was also monitored to support the subjective analysis of radar images, although lightning was not required to classify deep moist convection as there may be convective storms without lightning (Van Den Broeke et al., 2005).

Potential derechos were analyzed with respect to convectively induced severe wind gusts. Here, convectively induced means that the severe wind events are associated with deep moist convection. Deep moist convection is defined similar to Doswell (2001) as convection that leads to the transport of low-level water vapor and heat to the upper levels of the troposphere and in exchange, dry and cold air masses from upper levels down to the low levels. To indicate deep moist convection, radar and lightning data were analyzed. Lightning data of the Siemens Blids lightning network (Wikipedia, 2015a) available back to the year 2000 have been consulted. For dates before the year 2000, data from the Arrival Time Difference (ATD) system operated by the UKMO (Lee, 1986) were used from wetterzentrale.de (2016). Lightning was supposed to be always associated with deep moist convection.

As deep moist convection does not need to produce lightning (Van Den Broeke et al., 2005), radar data was analyzed with respect to deep moist convection. Indications of deep moist convection can be high reflectivity or tight reflectivity gradients described by Burke and Schultz (2004) for their analysis of radar data with respect to bow echoes. These radar characteristics were searched in quarter-hourly plan-view radar images of the German radar composite. The composite is an interpolation of the data from the German radar network. The reflectivity of the lowest elevation scans is interpolated on a Cartesian grid with a horizontal resolution of 2 km, a vertical resolution of 1 km, and seven intensity thresholds

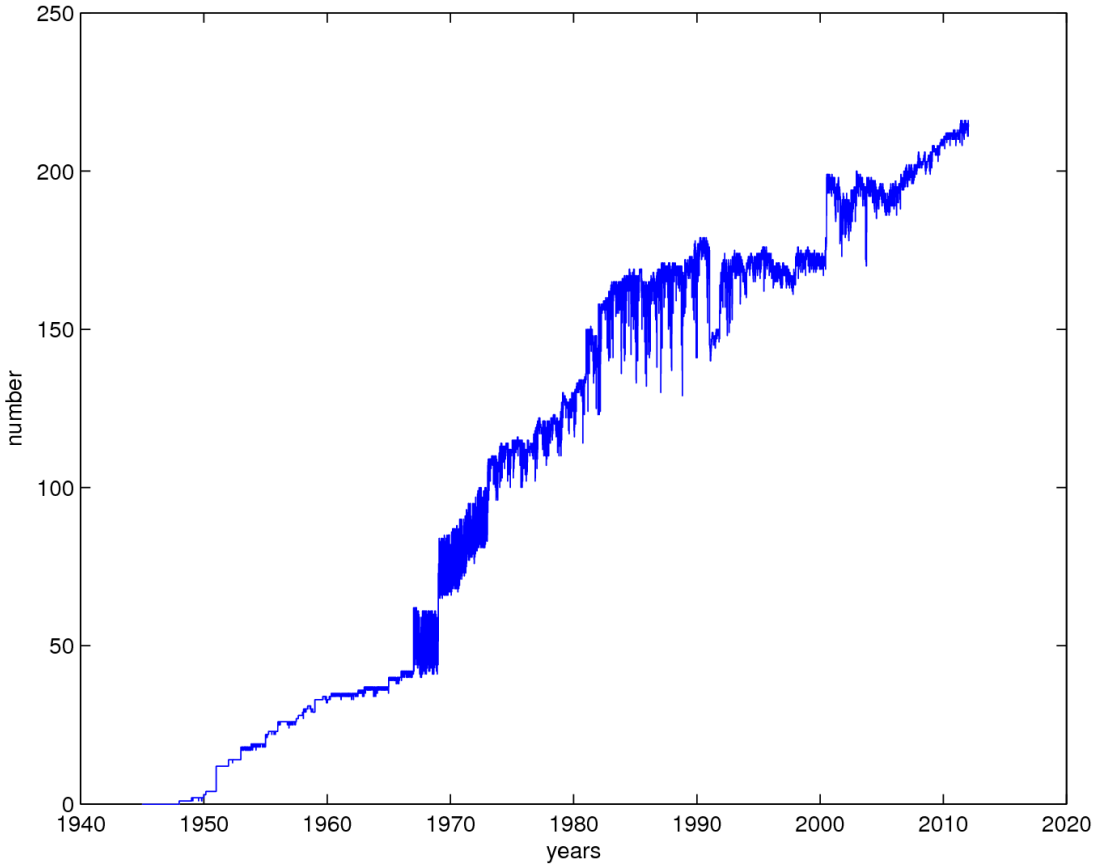

Figure 21: *Total number of observation sites that report daily maximum wind gusts across Germany as of the German Weather Service network.*

(Schreiber, 2000). High resolution data of the German weather service (Deutscher Wetterdienst, DWD, 1997) could be included in the analysis for years since 2009. A spatial resolution of 1 km x 1° azimuth angle, images in 5-minutes intervals, and intensity classes in 2-dBZ steps were available at MeteoGroup. Since radar images were available back to 1996, dates before 1997 were not included in the derecho climatology.

To increase the number of wind measurements, also data of the Meteomedia / MeteoGroup network have been used. While the number of measurement sites of the DWD increased relatively slowly since the 1980s (see Fig. 21), the network of Meteomedia grew rapidly. The combined data set contained 260 measurement sites with hourly wind records for the first derecho in 1997 and increased to more than 1000 sites in total for derecho dates around the year 2011, corresponding to a density across Germany's area (approximately 360,000 km^2) between 0.7 and nearly 3 measurement points per 1000 km^2 (Fig. 22). Beyond the borders of Ger-

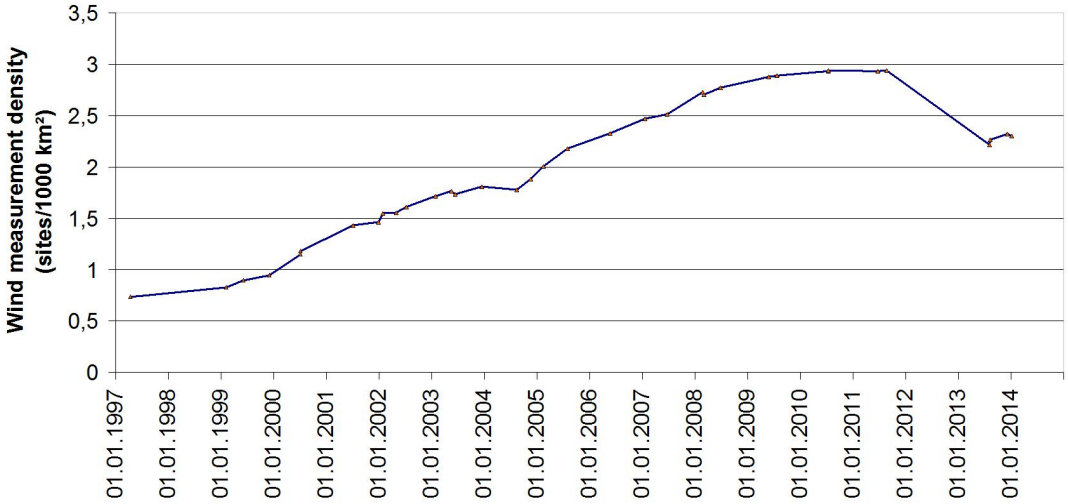

Figure 22: *Data density (number of wind measurement sites per 1000 km^2) across Germany for derecho dates between 1997 and 2014 using the combined networks of DWD and MeteoGroup. To obtain the measurement site coverage, the German territory was divided by the number of measurement sites available at each of the derecho dates.*

many, the density of available wind measurement sites was low and was limited to internationally distributed wind gust reports from SYNOP and METAR data also available at MeteoGroup, so that the chance to detect high wind events decreased. In recent years, increased reporting to the ESWD allowed for a better detection rate. Additionally, radar data was frequently not available, so that derechos moving across the borders of Germany had to be followed using wind measurements and lightning data only.

Wind data and archived plan-view radar displays were analyzed together to compare the wind intensity before and after a radar structure related to the convective event crossed the measurement site. If severe winds were just recorded in the hour of the passage of the convective line, these reports were classified as convective wind events. When wind gusts exceeded 25 m/s in the hour prior to and in the hour of the passage of a convective line, it was checked if the wind speed increased by at least 3 m/s with the line's passage. Otherwise, the wind report was not used for the wind event analysis. This was done to find out if, in the limits of the data resolution, the wind gusts were primarily caused by deep moist convection.

Figs. 23 and 24 illustrate the procedure using two case study examples: In the first example, six severe wind reports occur in the hour before the line's passage (white circles in Fig. 23a) of which four do not indicate a significant increase an

hour later (red circles in Fig. 23b). The remaining two of these stations had a significant increase in wind speed (white circles in Fig. 23b). Three more stations exceeded the threshold of 25 m/s (white circles in Fig. 23b), whereas at many other locations, this threshold was not reached with the convective line's passage. Given this weak increase of wind gusts, the wind event was not decided to be primarily caused by convection. In the second case, 36 severe wind records were reported in the hour of the line's passage (white circles Fig. 24b). Comparison to Fig. 24a shows that although 11 of these locations already reported severe winds in the hour before, only three of these did not indicate a significant increase in wind speed (red circles Fig. 24b). This event was decided to be a convective wind event.

Selected events were analyzed following the definitions by Johns and Hirt (1987) including some of the modifications done by Evans and Doswell (2001): No gaps of more than 2 hours between wind reports were allowed inside a derecho path. The reports had to indicate a chronological progression as well as their association to a convective storm, e.g. a squall line or convective cluster. Multiple swaths of wind gusts had to be a part of the same convective system showing a linear or bow shaped radar signature. Randomly distributed reports were not taken into account. The path length of a wind event was roughly determined by the shortest distance (linear distance) between the first and the last severe wind report. For some derechos that follow a curved path, this can lead to shorter distances as following the center points of the derecho. More important, cold frontal rain bands that produce severe wind gusts along a very wide path may be overestimated with respect to their path length when the derecho start and end points are separated by a large along-front distance. For these events, the center line of subjectively analyzed bowing structures was followed instead. The path length of the derecho of 28 January 2003 was reduced from 800 to 440 km for this reason. In general, wind events with a path length shorter than 400 km were sorted out.

For all derechos found, location and time of initiation and dissipation, path length, duration, and the number of available wind reports of the date in question across Germany were listed. The initiation and dissipation time was approximated by the hour of the first and last wind gust measurement within the derecho path; damage reports were not taken into account. The time span between the first and the last wind gust measurement was used as derecho duration. Derecho events were classified with respect to the measured wind intensity. Moderate derecho events met the requirement by Johns and Hirt (1987) to involve at least three wind reports of

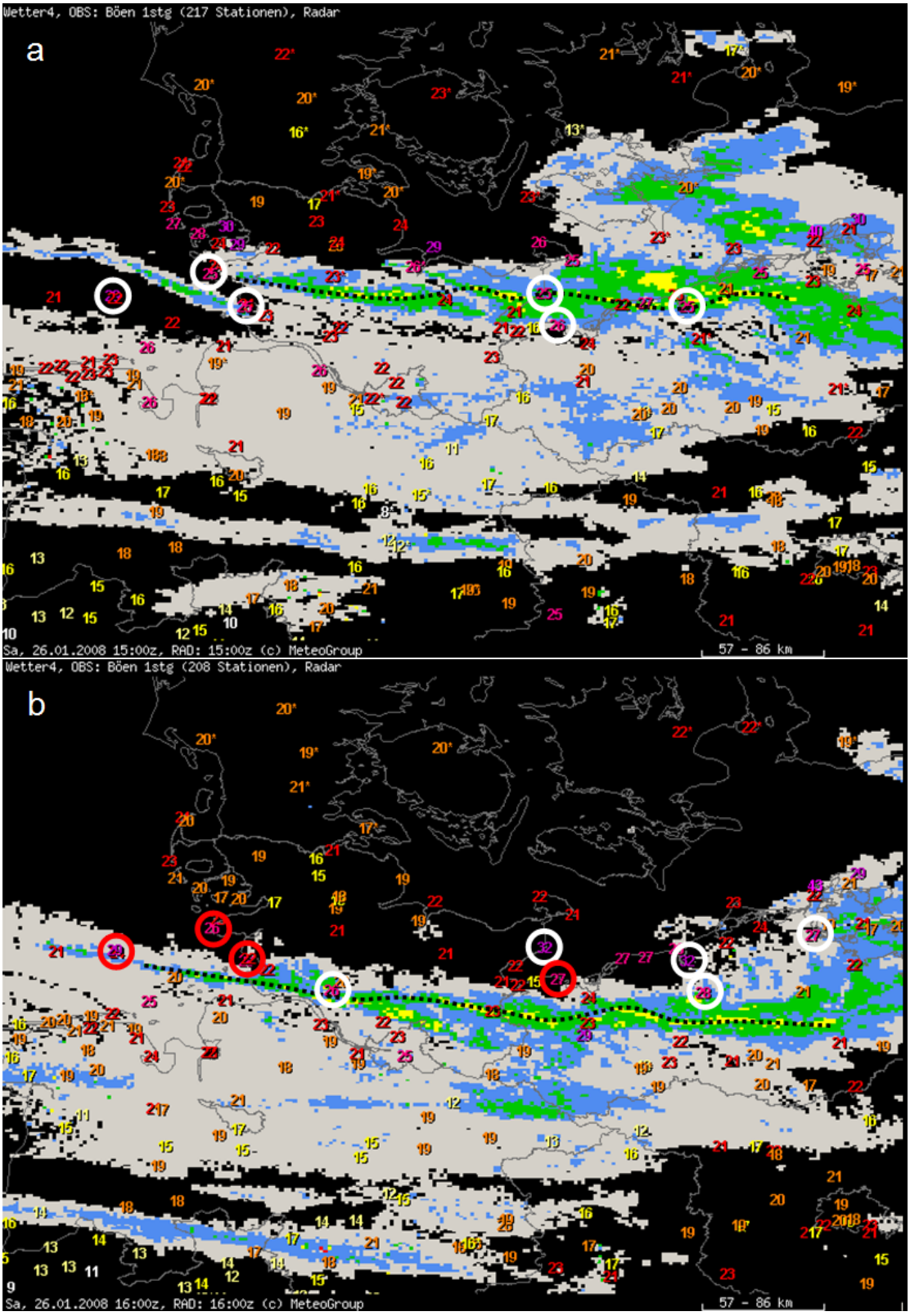

Figure 23: *Radar display and hourly maximum gusts (m/s) on 26 Jan 2008, 15 UTC (a) and 16 UTC (b). White circles highlight gusts > 25 m/s close to the convective line, red circles in b) those not used for classification. Radar reflectivity thresholds are given in light blue (below 19 dBZ), dark blue (19–28 dBZ), green (28–37 dBZ), yellow (37–46 dBZ) and orange (above 46 dBZ). Data source: Deutscher Wetterdienst / MeteoGroup. Image courtesy: MeteoGroup.*

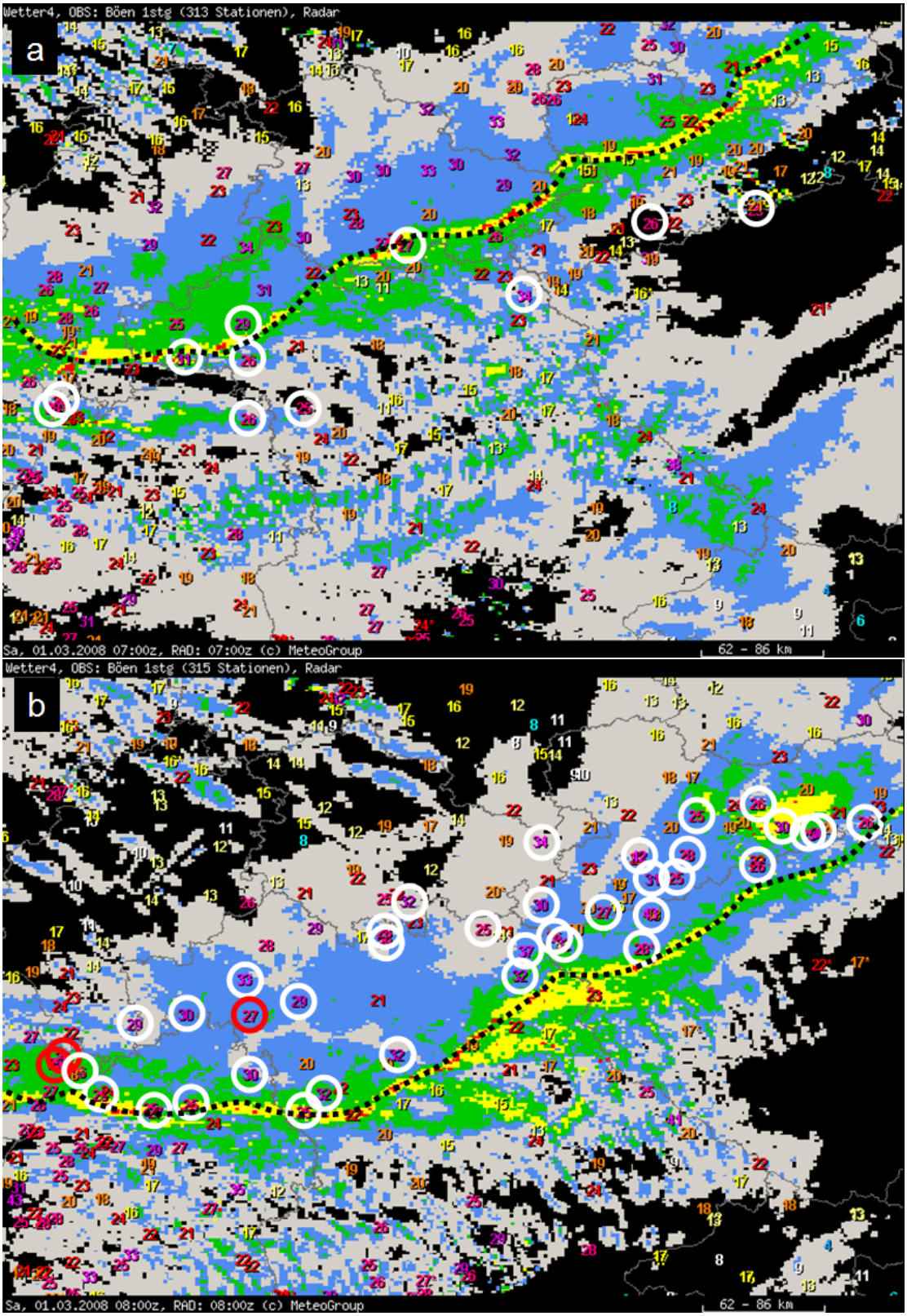

Figure 24: *Radar display and hourly maximum gusts (m/s) on 1 March 2008, 07 UTC (a) and 08 UTC (b). White circles highlight gusts > 25 m/s close to the convective line, red circles in b) those not used for classification. Radar reflectivity thresholds are given in light blue (below 19 dBZ), dark blue (19–28 dBZ), green (28–37 dBZ), yellow (37–46 dBZ) and orange (above 46 dBZ). Data source: Deutscher Wetterdienst / MeteoGroup. Image courtesy: MeteoGroup.*

33 m/s or greater separated by 64 km or more. High-end derechos had to include at least three wind measurements of 38 m/s or higher, whereas low-end derechos had no more than two gust measurements exceeding 33 m/s. These criteria are comparable to those defined by Coniglio and Stensrud (2004) to distinguish the intensity of derechos. Damage reports were not used in the classification. The regional distribution of derecho frequency was calculated for quadratic grid boxes of 200 km x 200 km across Germany. For each box, every event was counted that at least caused one convectively induced wind gust within it. The total number of derechos per grid box was divided by the number of years of the period in consideration, i.e. 18 years, to get the derecho density in events per year and grid box.

For every classified derecho event, environmental conditions were documented and analyzed with respect to similarities within the data set. This is, on the one hand, the meso- and synoptic-scale flow, focusing on features often described in derecho situations, e.g. the mid-level flow pattern. To find similarities, reanalysis data (ERA-Interim; Simmons et al., 2007) was displayed together with the derecho path using the wetter4 analysis tool available at MeteoGroup. A similar procedure was used to describe the 850 hPa flow, focusing on temperature advection. Archived GFS charts available at wetter3.de (http://www1.wetter3.de/Archiv/) were consulted to analyze the fields of 300 hPa divergence and potential vorticity (PV) on the 320 K isentropic surface, the latter to detect PV intrusions indicated by sharp PV gradients and PV exceeding 1.5 PV–Units (PVU; 1 PVU $= 10^{-6}\mathrm{Kkg}^{-1}\mathrm{m}^{2}\mathrm{s}^{-1}$). PV was only available back to 1999. SYNOP data were analyzed subjectively with respect to frontal boundaries and convergence zones, using temperature, dewpoint, and wind records. To get an overview of the different flow patterns, dates with similar 500 hPa flow according to (e.g. Coniglio and Stensrud, 2004; Burke and Schultz, 2004) (section 2.6) were grouped together to build composite charts. This was done using the compositing web site by the National Oceanographic and Atmospheric Administration (NOAA) Earth System Research Laboratory (ESRL, Earth System Research Laboratory, 2015). NCEP model data was available for the years 1997 to 2010, so that 32 out of 40 derechos were included in the cluster calculation. The reanalysis run (available at 00, 06, 12, and 18 UTC) closest before the initiation time of the derecho was used.

To analyze the environmental lapse rates, proximity soundings were searched using adopted criteria from Evans and Doswell (2001). Soundings had to be taken

within 150 km and 2 hours of the derecho path to be included in the analysis[5]. For every sounding, it was checked if it was launched ahead of the derecho gust front, e.g. by radar data and surface observations like wind direction and temperature. Sounding displays and computed parameters were taken from the sounding website of the University of Wyoming (University Wyoming, 2015). Sounding derived parameters used are based on the lifting curve of the lowest 500 m mixed layer parcel, i.e. low-level mixing ratio, lifted condensation level (LCL), mixed layer CAPE (MLCAPE), and equilibrium level temperature (ELT). For CAPE, LCL, and ELT, the virtual temperature of the mixed layer parcel has been used. For ELT, only soundings with a level of free convection (LFC) calculated at the website of the University of Wyoming were used. In addition to the parameters provided by the University of Wyoming, the vertical wind shear in the lowest kilometer (low-level vertical wind shear) and the lowest 6 km (deep layer vertical wind shear) was calculated by the vector difference of the wind vectors of the lowest level and the wind vectors at 1 km and 6 km above ground level, respectively. Wind vectors at 1 km and 6 km above ground level were calculated by linear interpolation between the closest wind measurements above and below these heights.

3.2 COSMO 4.8-CLM: model configuration

Some of the German derecho situations with low environmental instability were selected for high-resolution model analysis. Simulations with the COSMO model (http://www.cosmo-model.org), Climate Limited-area Model version 4.8, subversion 17 (Rockel et al., 2008) were provided by the University of Cologne. This model is used for operational weather forecasts at the German Weather Service and was also chosen to simulate European severe wind events at the Meteorological Institute of the University of Cologne (Ludwig et al., 2014; Born et al., 2012). As boundary conditions, interpolated coarse-grid data of the driving model ERA-Interim were used. The grid spacing of the convection permitting COSMO model simulation was set to 0.025 degree, corresponding to approximately 2.8 kilometer grid size and a time step of 25 seconds for the Runge-Kutta scheme integration. Furthermore, the model includes 35 vertical layers.

[5]To increase the number of soundings for the digging trough pattern, a few soundings were included that do not match the criteria by Evans and Doswell exactly: These were chosen although the derecho crossed the sounding site after three hours instead of two (see table 3).

Table 1: *Date, start and end time, and model domain of performed COSMO simulations. N, E, W stand for north, east, and west, respectively.*

Date	Time (UTC)	Latitude	Longitude
28 12 2001	09 – 21 UTC	47° – 56° N	6° E – 18° E
28 01 2002	12 – 23 UTC	47° – 56° N	6° E – 18° E
28 01 2002	13 – 18 UTC	47° – 56° N	6° E – 18° E
18 01 2007	12 – 00 UTC	47° – 56° N	6° E – 18° E
22 02 2008	15 – 22 UTC	50° – 56° N	6° E – 25° E
01 03 2008	02 – 18 UTC	45° – 53° N	0° E – 22° E
03 01 2014	14 – 21 UTC	48° – 53° N	5° W – 13° E
21 10 2014	13 – 04 UTC	45° – 52° N	5° W – 18° E

The output data of the simulations were interpolated on 31 pressure levels, with pressure intervals of 25 hPa between 1000 and 450 hPa and further pressure levels at 400, 350, 325, 300, 275, 250, 200, and 150 hPa. The output time interval was set to 15 minutes. Dependent on the derecho event, the model domain and simulation period has been adjusted across central Europe. The simulations were started before the derechos developed according to the derecho analysis, and stopped during or even after the dissipation phase of the derecho events. Eight cold-season events associated with weak environmental CAPE have been simulated (Table 1).

3.3 Lapse rate analysis in simulations

To analyze the different terms of the lapse rate tendency equation, it is needed to fix pressure levels of the model output between which these values are relevant. Depending on the simulated event or even on different locations and times during the same event, convection can vary in depth, so that the upper pressure level for the lapse rate calculation is variable as well. However, if lightning occurs, one can at least suggest a requirement for the equilibrium level temperature according to Van Den Broeke et al. (2005): Especially at temperatures below $-10°C$ there are supercooled rain droplets co-existing with ice particles what supports charge separation when upward vertical motion is strong enough (Saunders, 2008). The convective equilibrium level can be suggested to be at least some distance above

this level so that sufficient lift occurs, and Van Den Broeke et al. (2005) estimate an equilibrium level temperature below $-15°C$ for thunderstorm development. As a lower boundary for the lapse rate tendency calculation, the Lifted Condensation Level (LCL) was chosen: Below this level, ascending parcels cool dry adiabatically, but above, they follow the weaker moist adiabate so that steepening environmental lapse rates may result in positive buoyancy at some point along the ascending curve. When the LCL is fixed, the moist adiabatic lapse rate of the ascending curve starting at the LCL can be followed until it reaches a temperature of $-15°C$. Between these two points, the moist adiabatic lapse rate can be estimated based on sounding data. It can be regarded as a lower limit for the lapse rate to allow for thunderstorms when sufficient lift occurs.

Proximity soundings within the pre-derecho environment of low-instability events were searched. The pre-derecho environment was defined as the area of the derecho path that has not been crossed by its gust front so far and was broadly estimated using the analyzed derecho positions and paths together with the gust front position identified in the model fields. To guarantee that these soundings represent the thermodynamic environment of the considered event, hourly dewpoint observations at the sounding site were not allowed to change by more than $1\,K$ from the sounding launch time to the arrival time of the derecho. The arrival time was estimated using SYNOP readings like wind shift, temperature jump, or thunder observation. Furthermore, lightning should be detected along the derecho at the time it crossed the location. In the next step, the ascending curve for moist adiabatic ascent and the LCL had to be found. Both were directly taken from the sounding website provided by the University of Wyoming (University Wyoming, 2015). Additionally, the pressure level at which the lifting curve reaches a temperature of $-15°C$ was estimated by graphical analysis of the sounding image provided at the web page of the University of Wyoming. An illustration of the method is given in Fig. 25.

Box-and-Whisker diagrams of the pressure of these two points were analyzed to decide which model output pressure levels represent the majority of events. This was done for simplicity reasons, although some derecho environments may vary from these average values. The moist adiabatic lapse rate was calculated using the temperature and geopotential height of the LCL and $-15°C$ temperature point of the lifting curve. While the temperature of the LCL is directly taken from the web page of the University of Wyoming, the geopotential height was estimated

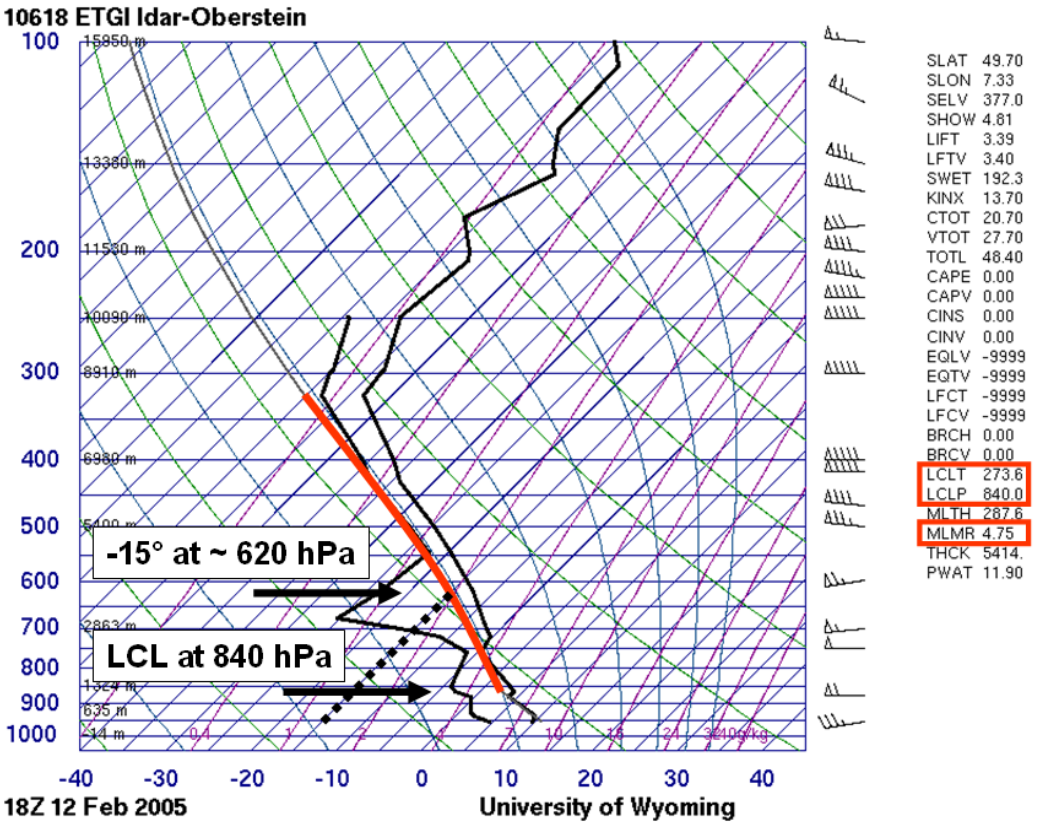

Figure 25: *Illustration of the method to search for the nearest pressure levels for the lifted condensation level and the pressure level at which the ascending curve of low-level parcels reaches a temperature of* $-15°C$*. In the list of computed sounding indices, the values of LCL pressure and temperature as well as the lowest 500 m mixed layer parcel mixing ratio are highlighted. Sounding display courtesy of the University of Wyoming (University Wyoming, 2015).*

using the height values of neighboring measurement points of the sounding. The resulting lapse rate was rounded to the first decimal place as it is only a broad reference value for the analysis of the lapse rate fields. In the last step, again a Box-and-Whisker diagram was analyzed to estimate lapse rate values plotted routinely for all events that were simulated.

A limitation of this method is that the simulated low-level moisture can differ from the observed moisture, so that the ascending curves of the simulations differ from reality. Furthermore, the pressure level at which low-level ascending parcels reach -15°C can vary from case to case, meaning that the regarded pressure level might not be adequate for individual events. The same is true for the estimated LCL pressure. Therefore, further pressure levels were tested for the lapse rate analysis and compared to the layer here defined.

3.4 Numerical calculation of the lapse rate tendency equation

The individual terms of the local lapse rate tendency equation (Eq. 13) were calculated using COSMO data on pressure levels. The calculation is based on the resolution of the model output grid size, i.e. approximately 2.8 km horizontal resolution, a vertical resolution of pressure levels every 25 hPa, and a temporal resolution of 15 minutes. Since the lapse rate tendency equation is given in Cartesian coordinates, its evaluation on pressure levels is rather an approximation since these layers are not necessarily horizontal. As a consequence, the height distance over which the lapse rate tendency is computed is not constant in space and time. However, the results of the approach presented here are directly applicable to operational analysis, monitoring, and forecasting of deep moist convection as forecasters typically work with pressure maps[6]. To obtain further details of the lapse rate and its tendency, cross sections are analyzed that cut through the strongest lapse rate tendency between the defined pressure levels ahead of and in the path of the derechos.

The different terms of the lapse rate tendency equation were calculated at every grid point. The lapse rate γ at a given grid point with the horizontal coordinates (x_0, y_0) on a pressure level p at output time t, $\gamma_p(x_0, y_0, \phi(x_0, y_0, p, t), t)$ and the geopotential $\phi = gz$ with gravitational acceleration $g = 9.81\,\mathrm{ms}^{-2}$ and height z was interpolated using central differences, i.e. the next upper and lower grid points, $(x_0, y_0, \phi(x_0, y_0, p+1, t), t)$ and $(x_0, y_0, \phi(x, y, p-1, t), t)$, respectively (Fig. 26a):

$$\gamma_p = \left.\frac{\partial T}{\partial z}\right|_{(x_0,y_0,p,t)} \approx g \left.\frac{T_{p-1} - T_{p+1}}{\phi_{p-1} - \phi_{p+1}}\right|_{(x_0,y_0,t)} \tag{15}$$

where the indices here and hereafter indicate the specific point in space and time.

[6]For example, a typical display of model data would be the lapse rate between 700 and 500 hPa overlaid to the lowest 500 m mixed layer mixing ratio to analyze the overlap of low-level moisture and mid-level lapse rates.

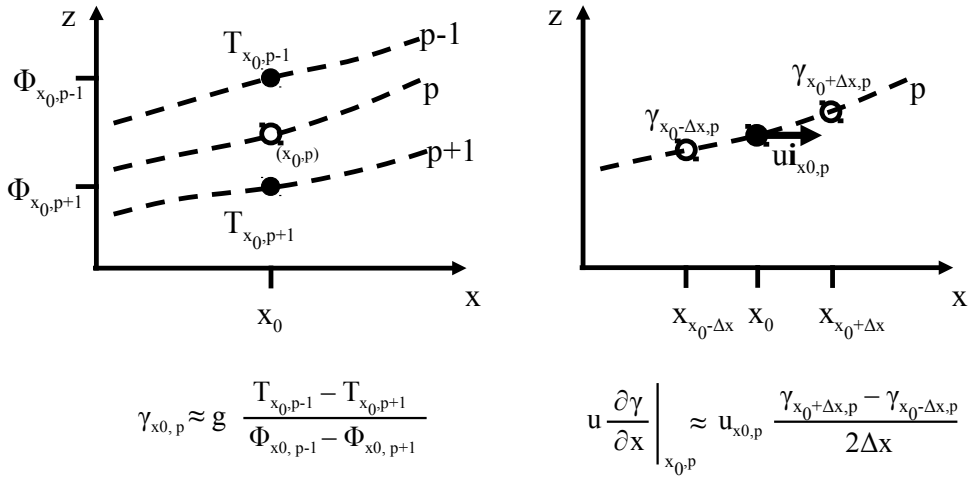

(a) Local lapse rate (b) Horizontal advection of the lapse rate

Figure 26: *Illustration of how (a) the local lapse rate and (b) the horizontal lapse rate advection term are calculated in the (x,z)-plane. In (a) temperature T and geopotential ϕ are taken from the neighboring grid points above and below the pressure level in question. In (b) lapse rate γ is taken from the neighboring grid points in x-direction to obtain the lapse rate gradient, the wind vector $u\mathbf{i}$ with horizontal unit vector in x-direction $\mathbf{i} = (1,0,0)$ is taken at the grid point where the lapse rate advection is calculated.*

The difference field of the temperature between the two pressure levels $p+1$ and $p-1$ was divided by the thickness field between the pressure levels. The lapse rate tendency on a pressure level p was then determined using the calculated lapse rate field one model output step in the future ($t+15$ minutes), and one in the past ($t-15$ minutes), divided by the temporal distance between them (i.e., 30 minutes). In this respect, the lapse rate tendency at a given grid point with coordinates (x_0, y_0, p) at time t was calculated by centered differences in both space and time, using the neighboring grid points:

$$\left.\frac{\partial \gamma_{p,t}}{\partial t}\right|_{(x_0,y_0,p,t)} \approx \left.\frac{\gamma_{p,t+\Delta t} - \gamma_{p,t-\Delta t}}{2\Delta t}\right|_{(x_0,y_0,p)} \tag{16}$$

where Δt is the temporal spacing between two time steps, i.e. here $\Delta t = 15\,\mathrm{min}$.

To obtain the local lapse rate advection by the horizontal flow, the gradients of the lapse rate in direction of x and y had to be calculated, taking into account that the grid points are placed on a spherical surface. While the distance in y-direction

Δy is 111 km between every degree in latitude, it changes slightly across the model domain in x-direction between the longitudes: The distance between longitudes is a function of the latitude; the largest distance is at the equator, the smallest at the poles. The Euclidian distance between longitudes Δx can be calculated using the circumference at a given latitude θ:

$$\Delta x = \frac{2\pi R_E \cos(\theta)}{360^\circ} \cdot \Delta lon \tag{17}$$

$$\Delta y = 111km \cdot \frac{\Delta lat}{1^\circ} \tag{18}$$

with R_E for the Earth's radius and for Δlon and Δlat given in degree [°]. In the same way, the derivatives in x- and y-direction had to be written as a function of latitudes and longitudes. Since the COSMO equator and poles have been shifted so that the model domain is at low latitudes, only small corrections have to be made.

The horizontal advection was then computed as the scalar product of the horizontal wind vector $\mathbf{V} = (u, v)$ and the horizontal gradient of the lapse rate $\nabla_h \gamma$. Centered differences of the lapse rate in x- and y-direction were used to obtain the horizontal lapse rate gradient around a location (x_0, y_0, p) at time t

$$\begin{aligned} \mathbf{V} \cdot \nabla_h \gamma \Big|_{(x_0,y_0,p,t)} &= \left(u \frac{\partial \gamma}{\partial x} + v \frac{\partial \gamma}{\partial y} \right)_{(x_0,y_0,p,t)} \\ &\approx u_{x_0} \frac{\gamma_{x_0+\Delta x} - \gamma_{x_0-\Delta x}}{2\Delta x} \Bigg|_{(y_0,p,t)} + v_{y_0} \frac{\gamma_{y_0+\Delta y} - \gamma_{y_0-\Delta y}}{2\Delta y} \Bigg|_{(x_0,p,t)} \end{aligned} \tag{19}$$

where Δx, Δy represent the horizontal spacing in x-, and y-direction, respectively. Horizontal changes of ϕ between the pressure levels around a grid point, i.e. the slope of the pressure levels, were not taken into account (Fig. 26b).

For the lapse rate advection by upward and downward motions, the vertical lapse rate gradient had to be calculated. It was approximated by the lapse rates on the next pressure level above and below the pressure level in question, keeping the x

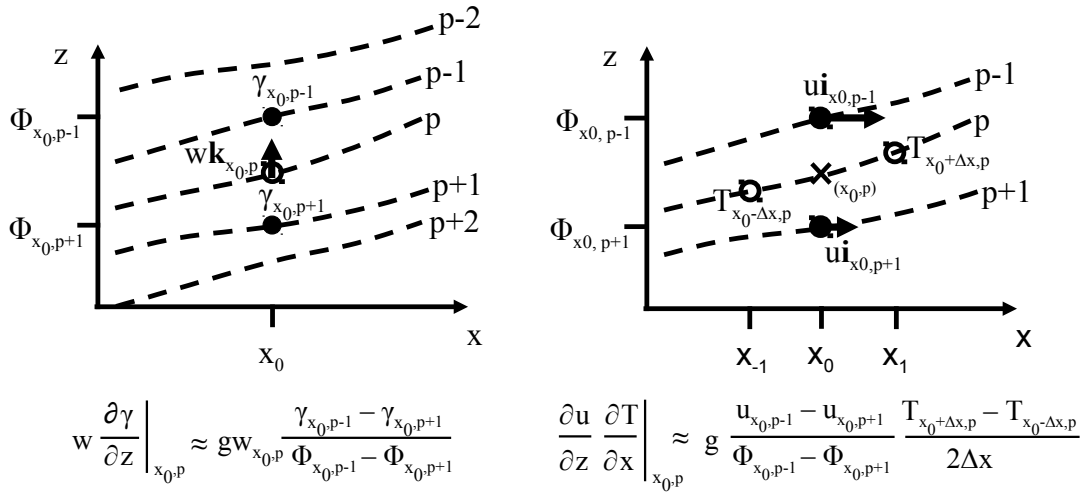

(a) Vertical advection of lapse rate (b) Differential temperature advection

Figure 27: *Illustration how (a) the vertical lapse rate advection and (b) the differential temperature advection term are calculated in the (x,z)-plane. In (a) lapse rate γ is calculated from the neighboring grid points in p-direction to obtain the vertical lapse rate gradient, the vertical motion $w\mathbf{k}$ with vertical unit vector $\mathbf{k} = (0,0,1)$ is taken at the grid point where the lapse rate advection is calculated. In (b) temperature T is taken from the neighboring grid points in x-direction to obtain the horizontal temperature gradient, the wind vector $u\mathbf{i}$ is taken at the neighboring grid points in p-direction to get the vertical wind shear where $\mathbf{i} = (1,0,0)$ is the unit vector in x-direction.*

and y coordinates fixed. Similar to the determination of the lapse rate given in the passage above, the temperature and geopotential of the neighboring pressure levels, i.e. $p-2$ and p on the one hand, p and $p+2$ on the other hand, had to be taken into account. The vertical lapse rate gradient was then multiplied with the vertical wind speed w at the grid point located at (x_0, y_0) on pressure level p at time t (Fig. 27a):

$$w\frac{\partial\gamma}{\partial z}\Big|_{(x_0,y_0,p,t)} \approx g w_p \frac{\gamma_{p-1} - \gamma_{p+1}}{\phi_{p-1} - \phi_{p+1}}\Big|_{(x_0,y_0,t)} = g w_p \frac{T_{p-2} - 2T_p + T_{p+2}}{\phi_{p-2} - 2\phi_p + \phi_{p+2}}\Big|_{(x_0,y_0,t)} \tag{20}$$

Similar to the calculation of the horizontal lapse rate gradients as described above, the horizontal gradients of the temperature field around a grid point (x_0, y_0, p) at time t were received to yield the differential thermal advection term. The

vertical shear of the flow was calculated using the difference of the horizontal wind vectors $\mathbf{V} = (u, v)$ in the (x, y)-plane between the upper $(p-1)$ and lower $(p+1)$ pressure levels (Fig. 27b):

$$\begin{aligned}\left.\frac{\partial \mathbf{V}}{\partial z} \cdot \nabla_h T\right|_{(x_0,y_0,p,t)} &= \left(\frac{\partial u}{\partial z}\frac{\partial T}{\partial x} + \frac{\partial v}{\partial z}\frac{\partial T}{\partial y}\right)_{(x_0,y_0,p,t)} \\ &\approx g\left(\frac{u_{x_0,p-1} - u_{x_0,p+1}}{\phi_{x_0,p-1} - \phi_{x_0,p+1}}\right)\left(\frac{T_{x_0+\Delta x,p} - T_{x_0-\Delta x,p}}{2\Delta x}\right)\Bigg|_{(y_0,t)} \\ &+ g\left(\frac{v_{y_0,p-1} - u_{y_0,p+1}}{\phi_{y_0,p-1} - \phi_{y_0,p+1}}\right)\left(\frac{T_{y_0+\Delta y,p} - T_{y_0-\Delta y,p}}{2\Delta y}\right)\Bigg|_{(x_0,t)}\end{aligned} \tag{21}$$

For the stretching term calculated at a grid point with the coordinates (x_0, y_0, p) at time t, the differential vertical wind speed is approximated using vertical wind speed w and geopotential ϕ of the next upper $(p-1)$ and lower $(p+1)$ pressure levels and the lapse rate as described above (Fig. 28a):

$$\left(\Gamma_d - \gamma\right)\frac{\partial w}{\partial z}\Bigg|_{(x_0,y_o,p,t)} \approx g\left(\Gamma_d - \gamma_p\right)\frac{w_{p-1} - w_{p+1}}{\phi_{p-1} - \phi_{p+1}}\Bigg|_{(x_0,y_o,t)} \tag{22}$$

And finally, the differential diabatic heating was directly obtained from the model output. In the COSMO model, diabatic tendencies due to latent heat release, radiation, and turbulence are not routinely given as model output variables, however, they are summed up during a model time step, yielding a combined diabatic heating provided as a temperature tendency ΔT that was used in this calculation. The diabatic tendencies of all the model time steps were summed up, leading to the temperature tendency due to diabatic heating during an output interval Δt (i.e., 15 minutes). To achieve the differential heating at a grid point at output time t, the temperature tendency at output time t that refers to the prior output was added to the temperature tendency of the following output interval. This sum was divided by the time of the two output intervals $2\Delta t$, i.e. 30 minutes. The vertical differential of these diabatic heating terms was then obtained by the cen-

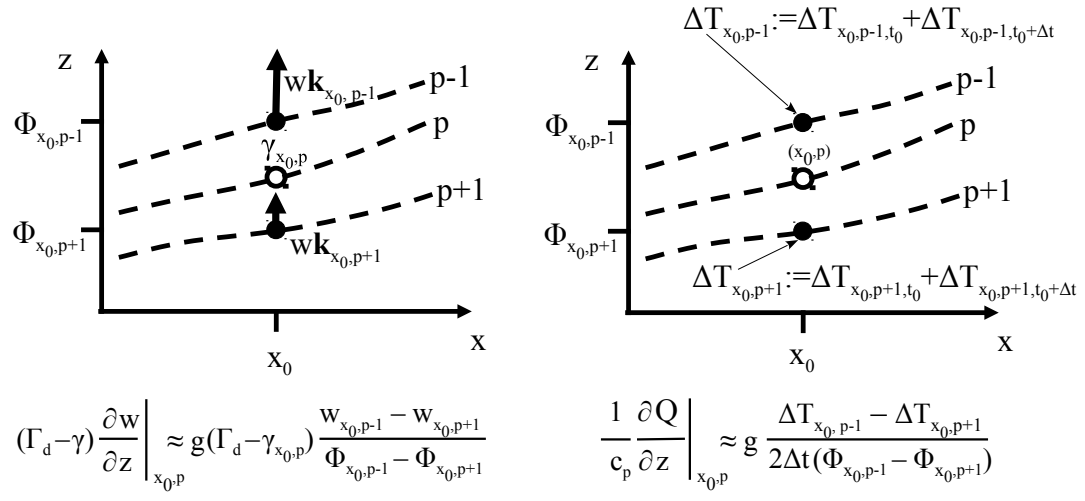

(a) Stretching term (b) Differential diabatic heating term

Figure 28: *Illustration how (a) the stretching term and (b) the diabatic heating term are calculated in the (x,z)-plane. In (a) lapse rate γ is taken at the grid point in question, the shear of the vertical wind is calculated using the vertical flow $\mathbf{w} = w\mathbf{k}$ with vertical unit vector $\mathbf{k} = (0,0,1)$ of the neighboring pressure levels. In (b) the diabatic heating is calculated at the levels above and below the location at which the lapse rate tendency is analyzed. The temperature difference ΔT_{x_0} due to diabatic heating at location x_0 within one output time interval backward (given at time t) is summed to that of the output interval forward (given at time $t + \Delta t$ with $\Delta t = 15\,min$). This sum is divided by the total time interval, i.e. $2\Delta t = 30\,min$.*

tral difference of the neighboring upper $(p+1)$ and lower $(p-1)$ output pressure levels (Fig. 28b). The differential diabatic heating term at a grid point with the coordinates (x_0, y_0, p) at time step t is calculated as:

$$\frac{1}{cp}\frac{\partial Q}{\partial z}\bigg|_{(x_0,y_0,p,t)} \approx g\frac{\left(\Delta T_{p-1,t}+\Delta T_{p-1,t+\Delta t}\right)-\left(\Delta T_{p+1,t}+\Delta T_{p+1,t+\Delta t}\right)}{2\Delta t\left(\phi_{p-1,t}-\phi_{p+1,t}\right)}\bigg|_{(x_0,y_0)} \tag{23}$$

To get the values for chosen pressure levels, e.g. 900 to 600 hPa, all tendencies on the related output pressure levels were summed up and weighted by the thickness fields between them.

A residual was calculated as the difference of the lapse rate tendency as directly obtained from the lapse rate fields and the sum of all terms on the rhs of the

lapse rate tendency equation (Eq. 24). For a positive local lapse rate tendency it follows: Where the sum of the individual terms is smaller than the lapse rate tendency, the residual is positive. Where the sum is larger, the residual is negative.

$$Residual = \frac{\Delta\gamma}{\Delta t} + \mathbf{V} \cdot \nabla_h \gamma + w\frac{\Delta\gamma}{\Delta z} - \frac{\Delta \mathbf{V}}{\Delta z} \cdot \nabla_h T - \frac{\Delta w}{\Delta z}(\Gamma_d - \gamma) + \frac{1}{c_p}\frac{\Delta Q}{\Delta z} \quad (24)$$

Limitations of this approach have to be taken into account. First, the output resolution differs from the exact model resolution. In particular, this holds for the vertical resolution given that 35 terrain following sigma levels from the COSMO model that are interpolated on 31 pressure levels every 25 hPa of the model output. This can lead to significant interpolation errors especially where the slope of sigma and pressure levels is large, e.g. near steep topographic gradients. But also the time intervals of the output, i.e. 15 minutes, differ strongly from the model time steps, i.e. 25 seconds, so that calculations of temporal derivatives are not exact. To completely match the model tendencies with the integrated lapse rate tendency equation, the use of exactly the same numerics, e.g. 5th order advection and diffusion, and of the model resolution (e.g., output time intervals of 25 seconds) is required. For this reason, the model's lapse rate tendency at a grid point (the left hand side of the local lapse rate tendency equation 13) cannot exactly be equalized by the terms on the rhs, that are calculated with the output data.

The choice to use pressure levels instead of sigma levels increases the inaccuracy of this calculation further. The lapse rate tendency equation in its presented form is only valid on a Cartesian grid. Using pressure as vertical coordinate, horizontal derivations contain errors that increase with the tilt of the pressure levels relative to the horizontal. Horizontal advection is then calculated with the horizontal wind vector at a grid point, whereas the horizontal gradients are calculated on pressure levels that deviate from the horizontal, especially near frontal boundaries where the tilt of pressure levels is large. All terms calculated in this work are affected by one or even a combination of some of these deficiencies. For the lapse rate tendency on the left hand side, it is the time derivative of the vertical derivatives of the temperature and geopotential, all based on the output resolution. For the horizontal lapse rate advection, it is the horizontal gradient of the vertical gradients of the temperature and geopotential. The vertical lapse rate advection is based upon vertical gradients of vertical temperature and geopotential gradients using grid points far above and below the grid point in question (i.e. two pressure

levels above and below). The calculation of the differential temperature advection uses horizontal gradients of the temperature combined with vertical gradients of the horizontal flow vector. The stretching term is based on the vertical gradients of the vertical wind speed combined with the vertical gradients of the temperature and geopotential. An finally, the diabatic heating uses the time derivative of the vertical gradient of diabatic heating.

All these inaccuracies can be expected to yield large deviations between the lhs and right hand side of the lapse rate tendency equation as calculated in this work. The residual term has been added to the right hand side of eq. 13 to account for the deviations that follow from this approach. The magnitude of this residual term was used to assume the accuracy of the calculation. However, from a small residual term it does not follow necessarily that the calculation errors of the different terms are small, given the large degree of inaccuracies that could cancel themselves. The horizontal and vertical distribution of the residual may at least indicate where calculation errors could be large. In this respect, results of this calculation were interpreted with care especially when the residual was large.

To get an idea of the magnitude of inaccuracy, possible deviations of the exact calculation of the terms can be approximated. For example, the influence of strongly tilted pressure levels or the output grid spacing can be estimated, using assumptions for parameters as wind speed and temperature gradients. The influence of the large time interval of the model output was tested. Results of the original model output data were compared to the same model run with an output interval of 25 seconds, i.e. the exact integration time step. In this particular test, only minor changes concerning the horizontal fields were observed.

An additional test was done to analyze the calculation of the stretching term. As can be seen from equation 13, the dry adiabatic lapse rate γ_d is included in the stretching term. This can be regarded as "reference" lapse rate using parcel theory: The parcels within a vertical column of air will follow dry adiabatic lapse rates with different speed what results in increasing lapse rate between them. The adjustment of the lapse rate is proportional to the differential vertical motion (the stretching) and the actual deviation of the lapse rate from the dry adiabatic lapse rate. The lapse rate increase stops when the dry adiabatic lapse rate is reached. In a moist air mass, vertical stretching through ascent will lead to saturation that influences the lapse rate tendency due to the differential diabatic heating. This

diabatic heating does not allow for dry adiabatic lapse rates and the thermodynamic profile will approach the moist adiabate until the moisture is precipitated. In theory, the lapse rate tendency equation includes this process in the diabatic heating term. In practice, however, the combined effects of stretching and differential diabatic heating may be not reproduced in the calculation. The reason is that the calculation of the stretching term and the differential diabatic heating term are not based on the same time: The stretching is based on the actual values of vertical motion and lapse rates, whereas the differential diabatic heating relies on the diabatic heating of prior and later output times. In case of stretching by ascent, this can lead to an overestimation of the stretching term since the dry adiabatic lapse rate no longer represents the correct "reference" lapse rate, because the combination of the stretching term and diabatic heating term cannot be regarded in the calculation. Given high relative humidity close to saturation, the effect of the stretching term is too large as diabatic heating has not started yet. Consequently, the calculation does not include the effect of saturation. One can address this problem by using the moist adiabatic lapse rate at this point, according to parcel theory (Peter Banacos, personal communication). The same problem can be expected for vertical lapse rate advection due to ascent of moist air masses. In both cases, the terms in the lapse rate tendency equation can be too large and were tested using moist adiabatic lapse rates in case of high relative humidity. The test did only show relatively small changes of the stretching term. One reason is that the difference between dry and moist adiabatic lapse rates is relatively small for the moisture values associated with the regarded derechos.

3.5 Analysis of the lapse rate tendency

In order to identify similarities of derecho events, the different terms of the lapse rate tendency equation were compared along horizontal maps in hourly time steps. Again, the focus was set to the region of the derecho path ahead of the gust front and in particular to the area where the lapse rate tendency was positive in the considered layer between 900 and 650 hPa. Therefore, not only high PV at 600 hPa and the derecho gust front as analyzed by radar were included in the maps, but also the area where the lapse rate tendency was large and exceeded $0.5\mathrm{Kkm^{-1}h^{-1}}$.

To complement the horizontal maps, cross sections of the individual terms in the lapse rate tendency equation were analyzed. These cross sections were chosen sub-

jectively so that they cut through the PV intrusions as well as the derecho path. In the cross sections, PV exceeding 1.5 PVU was displayed together with the lapse rate tendency and the individual terms of the lapse rate tendency equation. The focus of the analysis was set to the regions of positive lapse rate tendency and its visual correlation with the PV field. Here, the cross sections of individual terms were compared to find similarities, taking into account that the analyzed fields cannot be interpreted independent of each other. For example, flow across complex terrain can easily result in large horizontal variations of the lapse rate with weaker lapse rates over mountains and steeper lapse rates over valleys. While the local lapse rate tendency is zero, both lapse rate advection and stretching are large and cancel each other.

3.6 Area definition for statistical analysis of the lapse rate tendency terms

Based on the subjective analysis of PV and lapse rate tendency described in section 3.5, areas on model maps were defined with respect to the distribution and temporal evolution of the PV field. Such areas with large temporal PV tendencies were approximated by large local horizontal PV advection: Assuming that PV is approximately conserved on pressure levels, its local tendency can be expressed by PV advection according to the material derivative:

$$\frac{dPV}{dt} = \frac{\partial PV}{\partial t} + \mathbf{V} \cdot \nabla PV \approx 0 \tag{25}$$

Taking horizontal flow and PV at 600 hPa, the local PV tendency was approximated by its horizontal advection. As for horizontal lapse rate advection, horizontal PV advection was calculated using centered differences based on the model output grid. Areas with PV advection greater than 2 PVU/h were taken for further calculations of the lapse rate tendency. In these areas, the lapse rate terms of all output grid points were calculated and displayed in Box-and-Whisker diagrams to find a more objective confirmation of the results. To analyze also areas farther downstream of current PV changes, PV advection has also been calculated for later time steps up to 5 output times ahead (+15 min to +75 min). This means that we looked for areas with large PV changes in the next 5 time steps, i.e. with future local PV changes greater 2 PVU/h. In these areas, the current lapse rate tendency and the individual terms in the lapse rate tendency equation were then

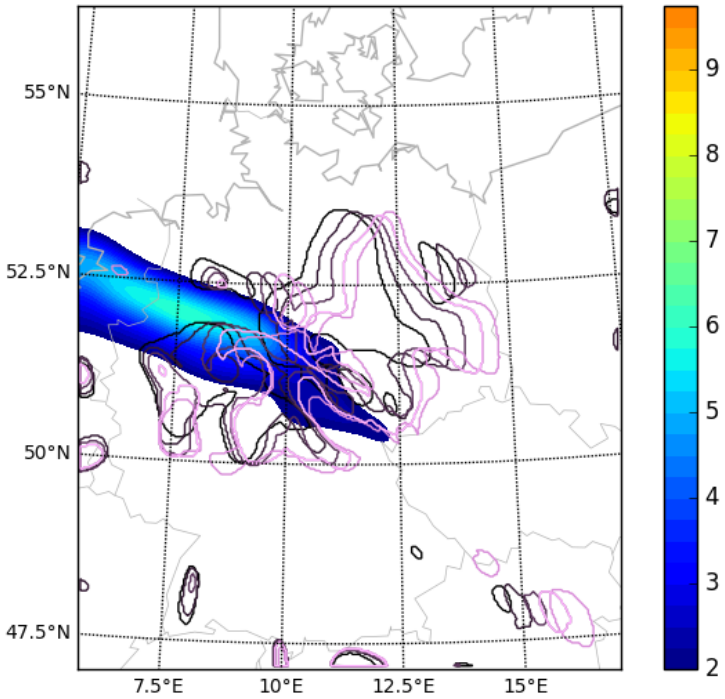

Figure 29: *Illustration of the areas chosen for the calculation of the terms of the lapse rate tendency equation on 28 December 2001, 12 UTC. PV at 600 hPa is shaded for values exceeding 2 PVU as given by the color bar to the right. The threshold of 1.5 PVU did also show some local PV maxima not associated with the PV intrusion and is not displayed in this figure for this reason. Areas of horizontal lapse rate advection greater than 2 PVU/h are surrounded by black contours. Contours gradually changing from black to pink show these areas as well, but for advection within the next 15, 30, 45, 60, 75 minutes, respectively.*

analyzed. In particular, the lapse rate tendency terms at time t were calculated in an area of large PV increase at $t+0$ minutes, $t+15$ minutes, $t+30$ minutes, $t+45$ minutes, $t+60$ minutes, and $t+75$ minutes. In (Fig. 29), these different areas are plotted together with the PV field at 600 hPa. It can be seen that future local PV changes are located on both flanks of the PV intrusion (i.e., to the north and south). This indicates that the axis of the PV intrusion rotates counterclockwise in the next 5 output time steps. We will analyze the terms of the lapse rate tendency equation in these areas and compare the results with the remaining area of the model domain in order to find out how PV changes influence processes associated with local lapse rate changes.

4 Results and Discussion

4.1 German derecho climatology

This section presents the collection of classified German derechos. Next to the general derecho occurrence, the focus is on large-scale dynamics and to distinguish between weather patterns in which derechos form. The main contrasting characteristics of these weather patterns are emphasized and it is shown that nonetheless the potential impact of associated derechos is not different.

During the research period between 1997 and 2014, 40 derechos have been classified, of which 24 events reached moderate or high-end intensity (Table 2). This corresponds to an average frequency of 2.2 derechos per year over Germany. German derechos have been found to produce extreme wind gusts (Gatzen, 2013). Considering the high vulnerability of urban concentrations to severe wind gusts as wind damage is especially related to the maximum wind intensity (Dotzek and Friedrich, 2009), a relatively high potential risk of fatalities and losses infers from

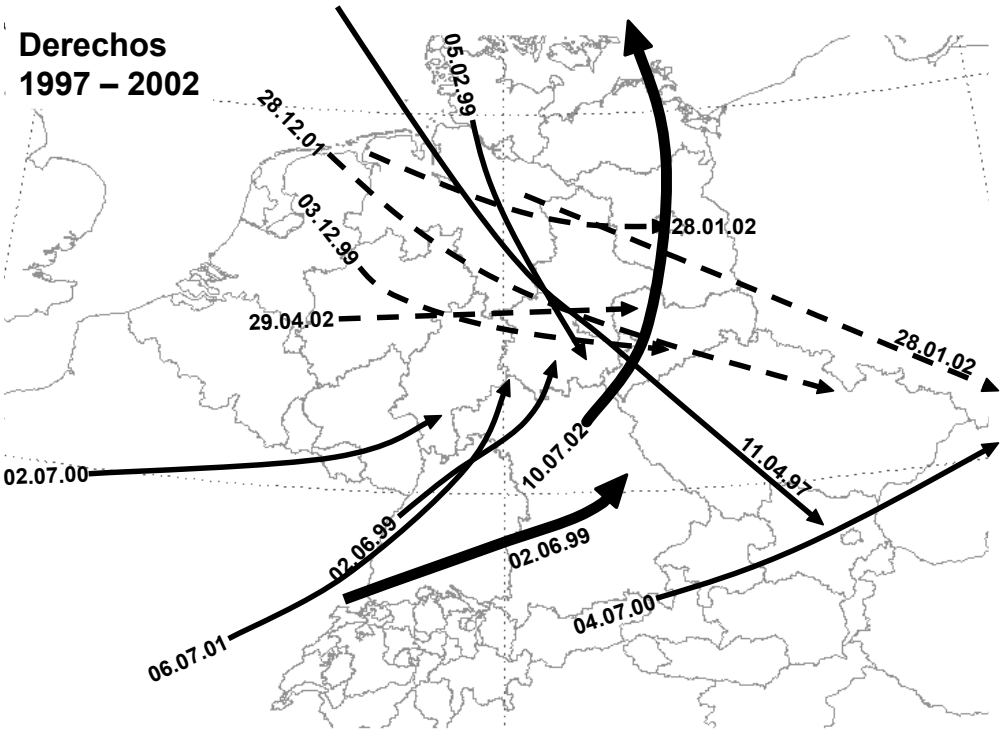

Figure 30: *Tracks of derechos found for 1997 to 2002. Thick lines, thin lines, and broken lines relate to high-end, moderate, and low-end intensity derechos. Dates are given at the start or ending point of each track.*

Table 2: *Derecho events found between 1997 and 2014. Initiation time is given in dd.mm.yyyy hh, countries of start and end points are abbreviated as GER (Germany), AUT (Austria), FRA (France), SVK (Slovakia), CZE (Czech Republic), POL (Poland), DEN (Denmark), SUI (Switzerland), BEL (Belgium), NED (Netherlands), SRB (Serbia), SCO (Scotland), ENG (England), CRO (Croatia).*

Initiation time (UTC)	Path length (km)	Duration (h)	Intensity	Path
11.04.1997 02	1620	16	moderate	NW GER - E AUT
05.02.1999 00	660	10	moderate	N GER - Centr GER
02.06.1999 14	420	6	moderate	SW GER - Centr GER
02.06.1999 15	600	7	**high**	E FRA - SE GER
03.12.1999 15	560	6	low	NW GER - E GER
02.07.2000 14	550	7	moderate	N FRA - W GER
04.07.2000 11	630	7	moderate	SE GER - N SVK
06.07.2001 17	450	6	moderate	E FRA - Centr GER
28.12.2001 09	750	12	low	NW GER - N CZE
28.01.2002 12	930	12	low	N GER - SE POL
28.01.2002 13	430	5	low	NW GER - E GER
29.04.2002 12	410	6	low	W GER - E GER
10.07.2002 16	600	7	**high**	SE GER - E DEN
28.01.2003 06	440	6	low	W GER - SE GER
19.05.2003 15	620	6	low	N SUI - Centr CZE
14.06.2003 06	1000	15	moderate	N FRA - SE AUT
15.12.2003 21	700	6	low	N GER - E CZE
12.08.2004 15	590	9	low	N SUI - E AUT
19.11.2004 06	850	12	moderate	S GER - SE POL
12.02.2005 15	610	7	low	S BEL - SE GER
29.07.2005 14	740	11	**high**	NW SUI - E GER
20.05.2006 12	600	8	moderate	W GER - NW CZE
18.01.2007 13	1100	11	moderate	N NED - SE POL
21.06.2007 06	1020	15	moderate	W SUI - N SVK
22.02.2008 15	1150	13	moderate	NW DEN - E POL
01.03.2008 02	1520	16	**high**	W NED - Centr SRB
25.06.2008 16	570	6	low	E GER - Centr SVK
26.05.2009 12	570	8	moderate	SW SUI - SW CZE
23.07.2009 17	520	7	moderate	SE GER - N SVK
23.07.2009 15	670	7	low	E GER - Centr POL
12.07.2010 09	650	6	moderate	S BEL - SW DEN
14.07.2010 12	500	5	moderate	Centr FRA - Centr NED
22.06.2011 12	450	6	low	SW GER - E GER
22.06.2011 13	550	5.5	moderate	E FRA - SE GER
24.08.2011 16	440	6	low	W GER - E GER
04.08.2013 10	790	10	low	N SUI - W SVK
06.08.2013 12	750	10	moderate	SW GER - E GER
05.12.2013 05	1160	13	**high**	N SCO - NW GER
03.01.2014 14	680	7	low	N FRA - N GER
21.10.2014 13	1600	15	moderate	S ENG - E CRO

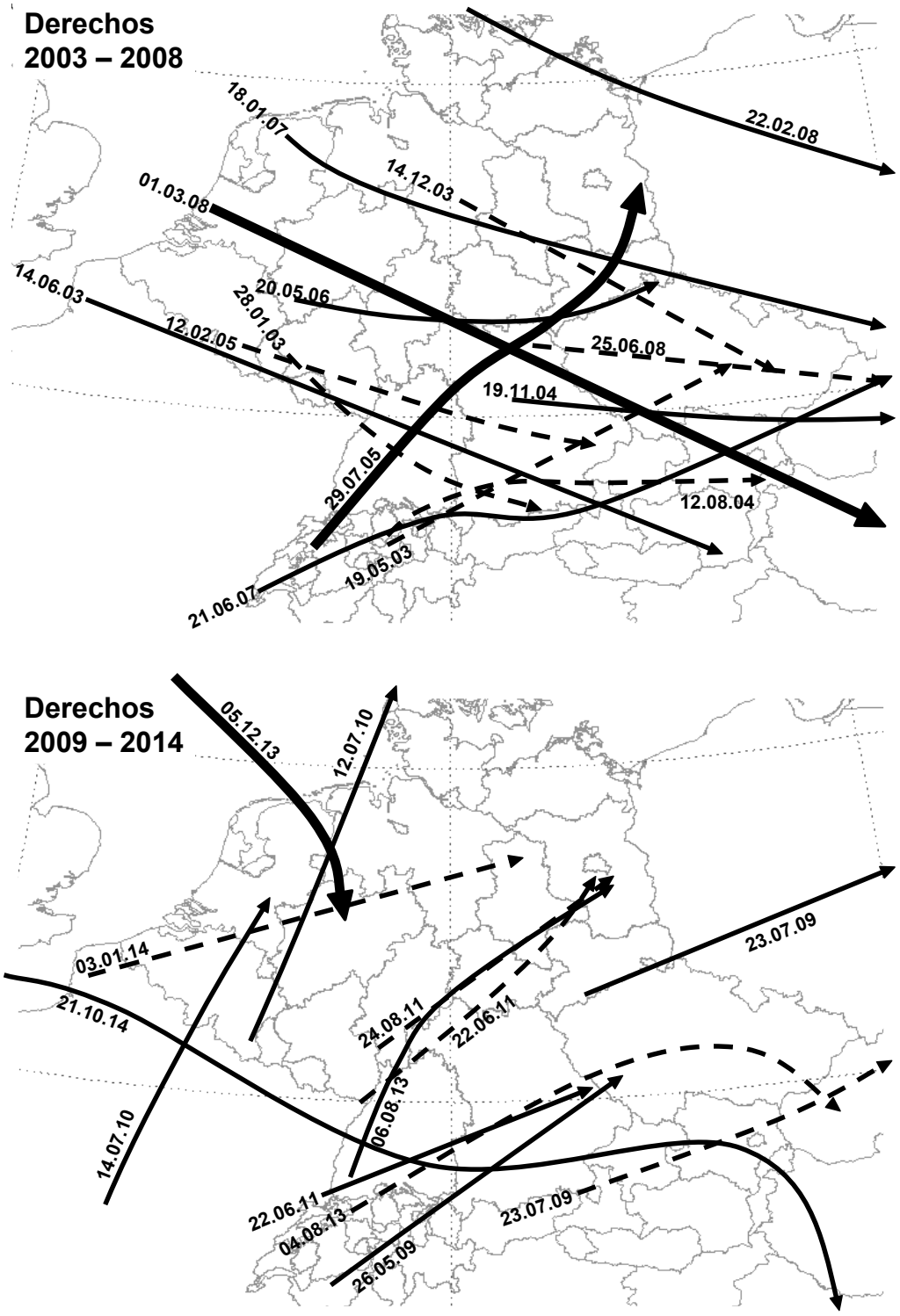

Figure 31: *Tracks of derechos found for the periods of (top) 2003 to 2008 and (bottom) 2009 to 2014, following the center line of the elongated fields of related wind reports. Thick lines, thin lines, and broken lines relate to high-end, moderate, and low-end intensity derechos. Dates are given next to each track.*

this number. There are examples of derechos and comparable events that hit urban areas in the past and caused many fatalities. This is partly due to downed trees (12 fatalities in the derecho of 6 July 2001, 8 during the Berlin derecho, and 6 fatalities during the Pentecost storm, a bow echo that produced a 300 km long damage path in 2014; Dotzek et al. (2009)), a risk that has increased since the maturation of trees planted in the cities about 50 year ago what has been described in the United States as well (Corfidi et al., 2017). But there can be also many fatalities and injuries at numerous open air events that take place every summer across Germany. An example is the Pukkelpop festival in Hasselt with 5 fatalities and 140 injured during the 18 August 2011 bow echo event. The urban infrastructure has been found to be vulnerable to derechos as well. High losses occurred after the Pentecost storm in western Germany due to structural damage to the railway network. Again, maturation of trees causes the railway network prone to long-lasting disruption. And although widespread power outages have not occurred so far with German derechos, high winds have been found to destroy even large pylons constructed to sustain winds in excess of 200 km/h during the Emma derecho (Pistotnik et al., 2011). Electric power transformation substations might be destroyed by mesovortices as well. Due to the relatively high derecho density across Germany found in this work, it might be worth to improve emergency plans in case of derecho warnings issued by the German Weather Service, e.g. for open air festivals, and invest in precaution to avoid derecho impacts, e.g. vegetation care at sensible locations.

The relatively high number of German derechos allows to investigate some of their characteristics. The path length was about 740 km on average and ranged between 410 and 1620 km, and the duration was about 8 hours and 50 minutes on average, with 5 hours at minimum and 16 hours at maximum. German derechos frequently crossed the borders and it was possible to follow their continued path back and forwards in all the direct neighboring countries. Some events were tracked even farther to Scotland, England, Croatia, Hungary, Serbia, Slovakia, and the Ukraine. For all derechos, the end location is east of the initiation point (Figs. 30 and 31). Aside from this zonal motion component, the meridional component of the derecho paths indicates basically two groups of derechos: Derechos in one group move to the south, in the other to the north. It is possible to relate both groups to different seasons of the year, a cold-season group (October – March) that moves southward, and a warm-season group (April – September) that moves northward, with an exception of just three events, 16 June 2003, 3

January 2014, and 21 October 2014. With respect to the derecho intensity, about half of the cold-season events are of weak intensity (8 out of 15), compared to a majority of moderate and high-end intensity events in the warm season (17 out of 25; table 2). Apart from these discrepancies, the track length of the derechos is quite similar for both groups.

The spatio-temporal density of derechos indicates a south – north decline across Germany with a derecho density per 200 km × 200 km of almost one event per year over southern and central Germany and one event in two years in the northern portions (Fig. 32). To compare the derecho density to Coniglio and Stensrud (2004), only moderate and high-end intensity derechos were taken into account. For southern central Germany, this leads to 13 events per grid box during the 18-year period, corresponding to a derecho density of 0.72 (Fig. 32). This is about three derechos every four years and comparable to the derecho density around the Appalachian mountains in the north-eastern United States. According to Coniglio and Stensrud (2004), most of the eastern United States have a significantly higher derecho density, reaching 1.36 or four derechos every three years per grid box from Minnesota and Iowa to Pennsylvania and from the eastern parts of the southern Plains to the lower Mississippi Valley. It has to be noted that the small spatial extent of the investigated region in Germany leads to a lower detection rate especially near the German borders.

The data set of German derechos was further analyzed with respect to the synoptic-scale forcing in association with derechos. In general, high CAPE is relatively rare across Central Europe even in the vicinity of severe deep moist convection (Brooks, 2009) and especially for severe convective wind events (Púčik et al., 2015). As summarized in sections 2.6 and 2.7, mid-level forcing is likely important for derecho development in low-instability situations. To receive indications of the synoptic-scale forcing, the data set was analyzed with respect to the large-scale mid-level flow (500 hPa). Similar flow characteristics adopted from Coniglio and Stensrud (2004) and Burke and Schultz (2004) were grouped to clusters of five weather patterns altogether averaged in Fig. 33. Strong mid-level flow in the vicinity of intense troughs is evident for almost all events. South-east moving derechos preferentially evolve at the western periphery of intense, amplifying long-wave troughs quite similar to north-west flow patterns (Burke and Schultz, 2004), hereafter digging trough pattern (Fig. 33e), or with eastward racing short-wave troughs (zonal pattern, Fig. 33d). Furthermore, strong south-westerly mid-level winds are fre-

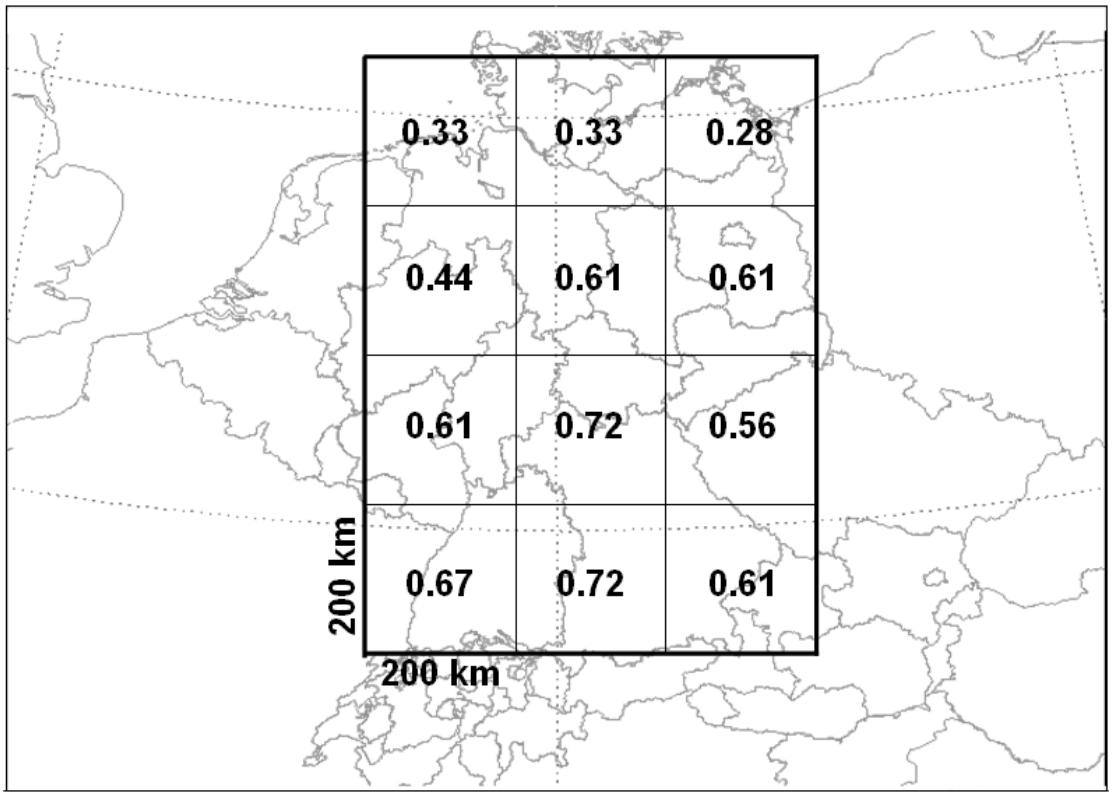

Figure 32: *Derecho density (1997 – 2014) given in derechos per year that at least partly affected the displayed quadratic grid boxes with a side length of 200 km. The calculation is based on moderate and high-end intensity derechos only.*

quently observed, with the derecho moving along the eastern periphery of intense troughs (upstream trough pattern, Fig. 33a) or farther east entering a downstream mid-level ridge (trough/ridge pattern, Fig. 33b). Both situations are quite similar, but they can mean a difference to forecasters: Trough/ridge derechos can form like upstream trough events in the area with favorable forcing close to the upstream trough, but they outpace this trough after some time and move well into the "calm" downstream ridge. Here, there is a tendency to develop into the most unstable air mass and in the direction of the downshear flank of the cold pool. This behavior caused by the propagation of the convective system is especially important in trough/ridge situations due to frequently weaker flow close to the ridge that is associated with a smaller advective movement component. The derecho movement will then attain a larger angle to the mid-level flow vector compared to most other derecho situations in Germany that are characterized by strong mid-level flow in which the downshear flank of the cold pool does not differ much from the downwind flank. Caution with respect to the derecho movement is also important for the last derecho cluster, characterized by relatively weak

north-westerly flow at the northern flank of a subtropical ridge (upstream ridge pattern, Fig. 33c). Only one derecho developed in this situation.

The large-scale flow in most European derecho situations does not differ much from the flow characteristics described in the United States, e.g. upper-level divergence was indicated for all events. Many of the weather patterns are quite similar to those introduced in the United States, e.g. in the publication by Coniglio et al. (2004): The zonal pattern (their Fig. 8), the upstream trough pattern (their Fig. 6), the trough/ridge pattern (their Fig. 7, ridge pattern cluster 1) and the upstream ridge pattern (their Fig. 7, ridge pattern cluster 3). The digging trough pattern seems to be not typical for derecho formation in the United States, though, and is displayed in Fig. 34 for four examples. These show similarities with the Northwest-Flow severe weather outbreaks described in the warm season Johns (1982) and also for cold-season bow echoes Burke and Schultz (2004). All derechos classified in digging trough patterns formed close to strong mid-level jets, typically at the cyclonically sheared flank. Moreover, as indicated by the two different times for each derecho in Fig. 34, the derechos stayed close to the jet streak axes where PV intrusions can form (cf. chapter 2.7). Therefore, the analysis of derechos in digging trough patterns will also include PV in the mid-troposphere to test this relationship (section 4.3).

Further investigation reveals large differences for the five derecho clusters. One example is that low-level warm air advection was evident in almost all upstream trough, trough/ridge, and upstream ridge events (21 of 23), whereas most of the zonal and digging trough events indicated cold air advection at 850 hPa (15 of 17). This is an important contrast to low-level warm air advection typically described in derecho situations (section 2.6) and indicates that dependent on the weather pattern different processes may support derechos. This hypothesis is further suggested by PV analysis on the 320 K isentrope (analysis for events back to 1999). PV intrusions were found for all zonal and digging trough situations, but only for 5 of 21 derechos occurring with the other clusters. Based on this finding, it could be possible that PV intrusions have an impact on the development of derechos.

The differences between the weather patterns are also visible in their thermodynamic characteristics. Proximity soundings (summarized in table 3) were used to analyze the distribution of CAPE for each weather pattern (Fig. 35). For upstream trough, trough/ridge, and upstream ridge patterns, the medians of the

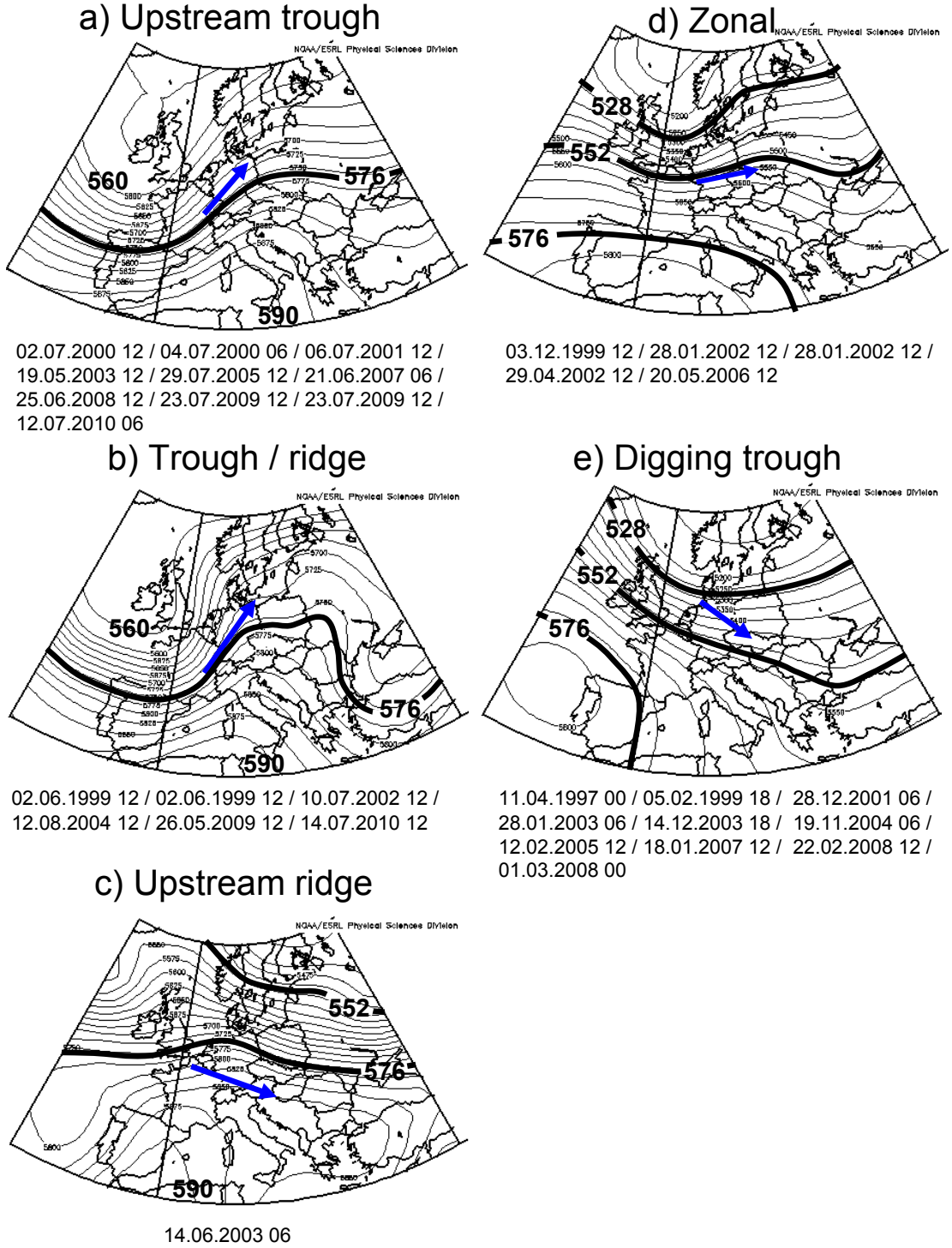

Figure 33: *Cluster overview of 500 hPa geopotential height for derecho events found in the years 1997 to 2010 based on NCAR/NCEP reanalysis (Kalnay et al., 1996) of derecho dates. Geopotential is given by black lines with contours every 25 gpm (clusters on the left) and 50 gpm (clusters on the right). 528, 552, 576 gpdm isolines are highlighted (thick lines). Derecho paths are displayed by blue arrows. Dates used for the clustering are given below the charts. Images were produced using the compositing web site by the National Oceanographic and Atmospheric Administration (NOAA) Earth System Research Laboratory (ESRL, Earth System Research Laboratory, 2015).*

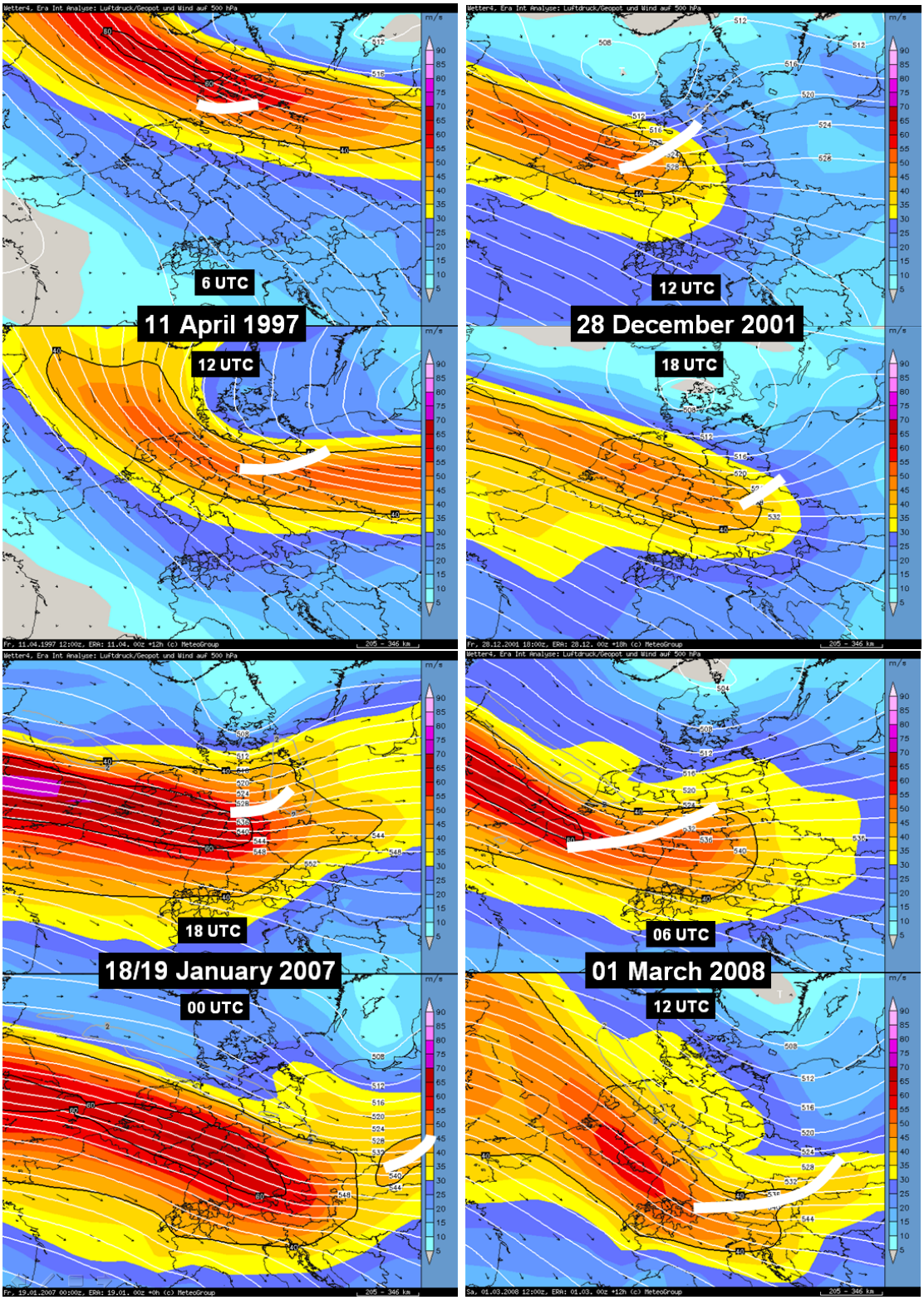

Figure 34: *500 hPa geopotential height (in gpdm; white solid lines) and wind speed (in m/s) displayed together with derecho positions (solid thick white lines) for four different derechos at two times each (dates and times are given in the center of each box). Data source: ERA-Interim, ECMWF / Image courtesy: MeteoGroup*

Table 3: *Proximity soundings grouped for each derecho weather pattern between 1997 and 2014. Sounding sites are given by their WMO synop code. Sounding codes marked with a * are chosen although the derecho crossed the sounding site after three hours instead of two. For the sounding marked with ** is was not clearly evident form the SYNOP data that it was crossed by the derecho before or after the launch time.*

Date / Time (UTC)	Sounding #	Weather pattern	Date / Time (UTC)	Sounding #	Weather pattern
11.04.1997 12	12425**	digging trough	02.06.1999 12	10618	trough/ridge
05.02.1999 00	10035	digging trough	02.06.1999 12	10739	trough/ridge
05.02.1999 06	10393	digging trough	10.07.2002 18	10393	trough/ridge
05.02.1999 12	11520*	digging trough	26.05.2009 18	10771	trough/ridge
05.02.1999 12	10771	digging trough	26.05.2009 18	11520	trough/ridge
28.12.2001 12	10238	digging trough	14.06.2003 12	10739	upstream ridge
28.12.2001 12	10410	digging trough	02.07.2000 12	07145	upstream trough
28.12.2001 18	11520	digging trough	04.07.2000 12	10868	upstream trough
28.01.2003 12	11035	digging trough	04.07.2000 12	11035	upstream trough
28.01.2003 12	06610	digging trough	07.07.2001 12	10868	upstream trough
15.12.2003 00	11520	digging trough	19.05.2003 18	11520	upstream trough
15.12.2003 00	10548	digging trough	29.07.2005 12	06610	upstream trough
19.11.2004 06	10771	digging trough	30.07.2005 00	12425	upstream trough
19.11.2004 12	11952*	digging trough	21.06.2007 12	10739	upstream trough
12.02.2005 18	10618	digging trough	23.07.2009 12	11520	upstream trough
18.01.2007 18	10393	digging trough	22.06.2011 12	10618	upstream trough
23.02.2008 00	10393	digging trough	22.06.2011 12	10739	upstream trough
23.02.2008 00	12425*	digging trough	22.06.2011 18	10771	upstream trough
01.03.2008 00	06260*	digging trough	22.06.2011 18	10393	upstream trough
01.03.2008 06	10618	digging trough	24.08.2011 18	10548	upstream trough
05.12.2013 12	10035*	digging trough	04.08.2013 12	10739	upstream trough
21.10.2014 12	07145	digging trough	06.08.2013 12	10739	upstream trough
21.10.2014 18	10771	digging trough	06.08.2013 12	06610	upstream trough
28.01.2002 12	10410	zonal			
28.01.2002 18	10393	zonal			
29.04.2002 12	10410	zonal			
29.04.2002 12	06260	zonal			
20.05.2006 12	10410	zonal			
20.05.2006 12	07145	zonal			
20.05.2006 12	06260	zonal			
20.05.2006 18	10771	zonal			

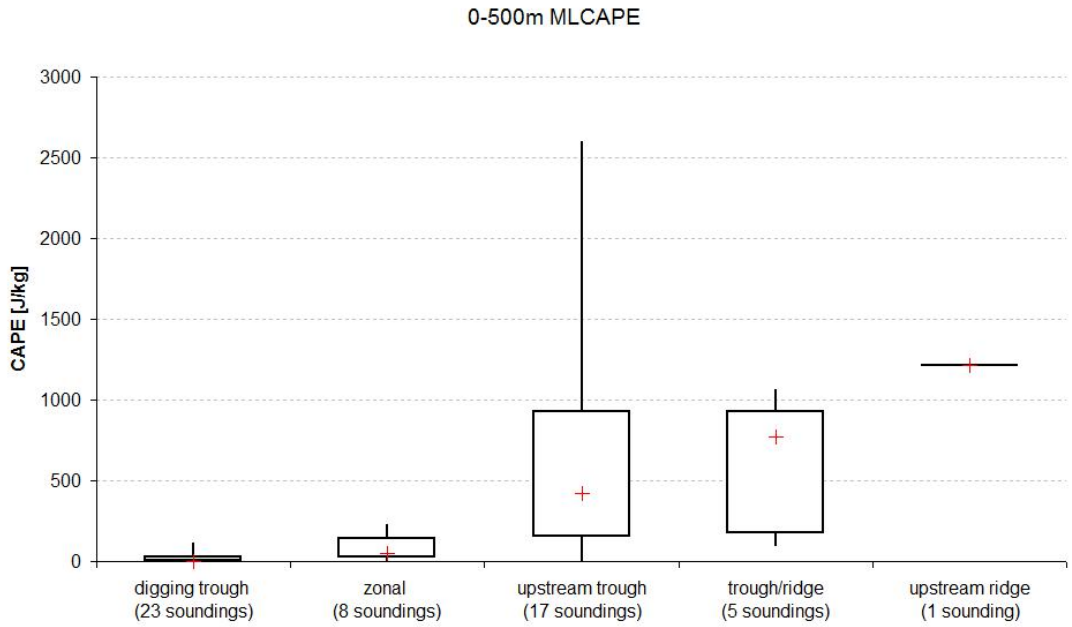

Figure 35: *Box-Whisker diagram of 500 m mixed layer CAPE [J/kg] based on proximity soundings for each classified derecho weather pattern. The crosses mark the median, boxes are plotted for the 25 and 75 percentile, and thin lines for the minimum and maximum, respectively. The number of soundings of each weather pattern is given together with the name of each weather pattern (after Fig. 33).*

CAPE distribution are 419.3, 771.6, and 1211 J/kg, respectively. Compared to the United States, instability is relatively weak for derecho cases, though, as CAPE is below 1000 J/kg for the majority of events and only three soundings have CAPE exceeding 1500 J/kg. However, much more obvious are very low CAPE values for the digging trough and zonal clusters that have a median of 0 and 50.37 J/kg, respectively. 13 of 31 proximity soundings of the digging trough and zonal pattern did not indicate any CAPE at all. This conflicts the presence of convective storms as identified in radar images and further confirmed by detected lightning for all derechos presented in this study.

Following the ingredients-based approach (section 2.6), at least some of the soundings chosen for this investigation do not represent the environment of the derechos, even though they were launched in their proximity as defined in section 3.1. Rapid changes of CAPE close to the derecho can be expected for these cases like in a model simulation of the great UK tornado outbreak in November 1981 that displays a narrow, just 50–100 km wide zone ahead of a cold front with positive CAPE of about 100 J/kg (Apsley et al., 2016). Changes of CAPE can be attributed to changes of low-level moisture on the one hand and the lapse rate on

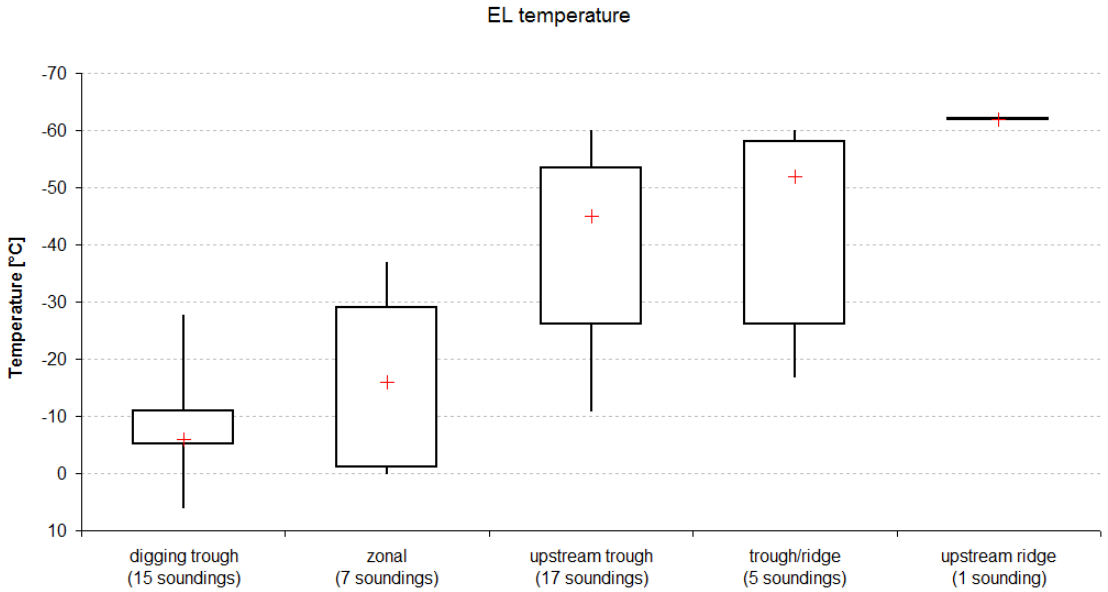

Figure 36: *Box-Whisker diagram of the equilibrium level temperature based on 500 m mixed layer virtual temperature of proximity soundings for each classified derecho weather pattern. The crosses mark the median, boxes are plotted for the 25 and 75 percentile, and thin lines for the minimum and maximum, respectively. The number of soundings of each weather pattern is given together with the name of each weather pattern. Only soundings with a level of free convection (LFC) were used.*

the other hand. For low-instability derechos in the south-eastern United States, strong low-level moisture advection is currently discussed to cause rapid CAPE changes that are not represented by the sounding network (King et al., 2017; Sherburn et al., 2016). In addition to zero CAPE in some proximity soundings, we found that even soundings with CAPE may not represent the derecho environment. This is indicated by equilibrium level temperatures that are too warm to explain the occurrence of thunderstorms. For the digging trough pattern soundings that have CAPE, the median of the equilibrium level temperature is about -6°C (Fig. 36). According to Van Den Broeke et al. (2005), lightning becomes unlikely for warm equilibrium levels with temperatures above -15°C (section 3.3).

The sounding statistics show that the digging trough and zonal cluster are characterized by cold but relatively moist air masses: They have both weaker boundary-layer moisture and a lower level of free convection (LFC) compared to the other clusters (Fig. 37, middle). For the digging trough and zonal clusters, only 3 out of 22 computed LFCs had a lower pressure than 800 hPa, whereas 7 had a higher pressure than 900 hPa. The lifted condensation level (LCL, not shown) was about 600 m on average, while no proximity sounding had a higher LCL than 1000 m.

Some soundings have LCL heights of less than 400 m, indicating that the air is already close to saturation. Abundant low-level moisture found for long-lived, severe cold-season bow echoes in the United States (Burke and Schultz, 2004) with a low-level mixing ratio of at least 9 g/kg cannot be confirmed for German events that sometimes show remarkable low moisture of just 4 g/kg (Fig. 37, top). However, this is not necessarily a conflict. A mixing ratio of 4 g/kg for the lowest 500 meter mixed parcels means average dewpoints about 0°C, what is not a low value for the German winter season. From this it still follows that derechos form in relatively moist environments.

Another aspect that lead to large differences between the clusters were the kinematics: Vertical wind shear and flow intensity change strongly between the clusters. This is in particular obvious for the distribution of 1 km wind speed (Fig. 37, bottom). The medians are 58 and 47 knots for the digging trough and zonal pattern, compared to 16, 14, and 6 knots for the upstream trough, trough/ridge, and upstream ridge pattern, respectively. The digging trough and zonal flow patterns therefore form in situations associated with low instability and very strong vertical wind shear (median of 0-1 km bulk shear is about 41.3 and 35.7 knots, respectively). Extreme low-level shear could be important for derecho development. It has been described for low-CAPE derechos in the United States, too: Here, such situations are known as "high-shear, low-CAPE environments" (e.g. Evans, 2010; King and Parker, 2014).

Strong flow may support low-instability derechos in various ways. First, it will affect the movement of the convective system relative to the ground due to advection and due to successive momentum transport of the environmental flow into the surface based cold pool (section 2.3). Second, linear pressure perturbations will support new initiation of storms at the downshear flank of the convective gust front (section 2.3) what sustains the convective system and further increases the system's speed due to propagation. Third, the ability of derechos to produce severe wind gusts is related to mesovortices that form in response to stretching of low-level vorticity. High low-level vertical wind shear contains large horizontal vorticity that can be a reservoir of vertical vorticity converted by tilting (section 2.5). Strong environmental flow may compensate less acceleration of the rear inflow jet between meso-low and and meso-high compared to high-instability derechos (section 2.4). Low-instability derechos are dependent on an "external" contribution and are less "internally-driven" (section 2.6, Corfidi et al., 2016).

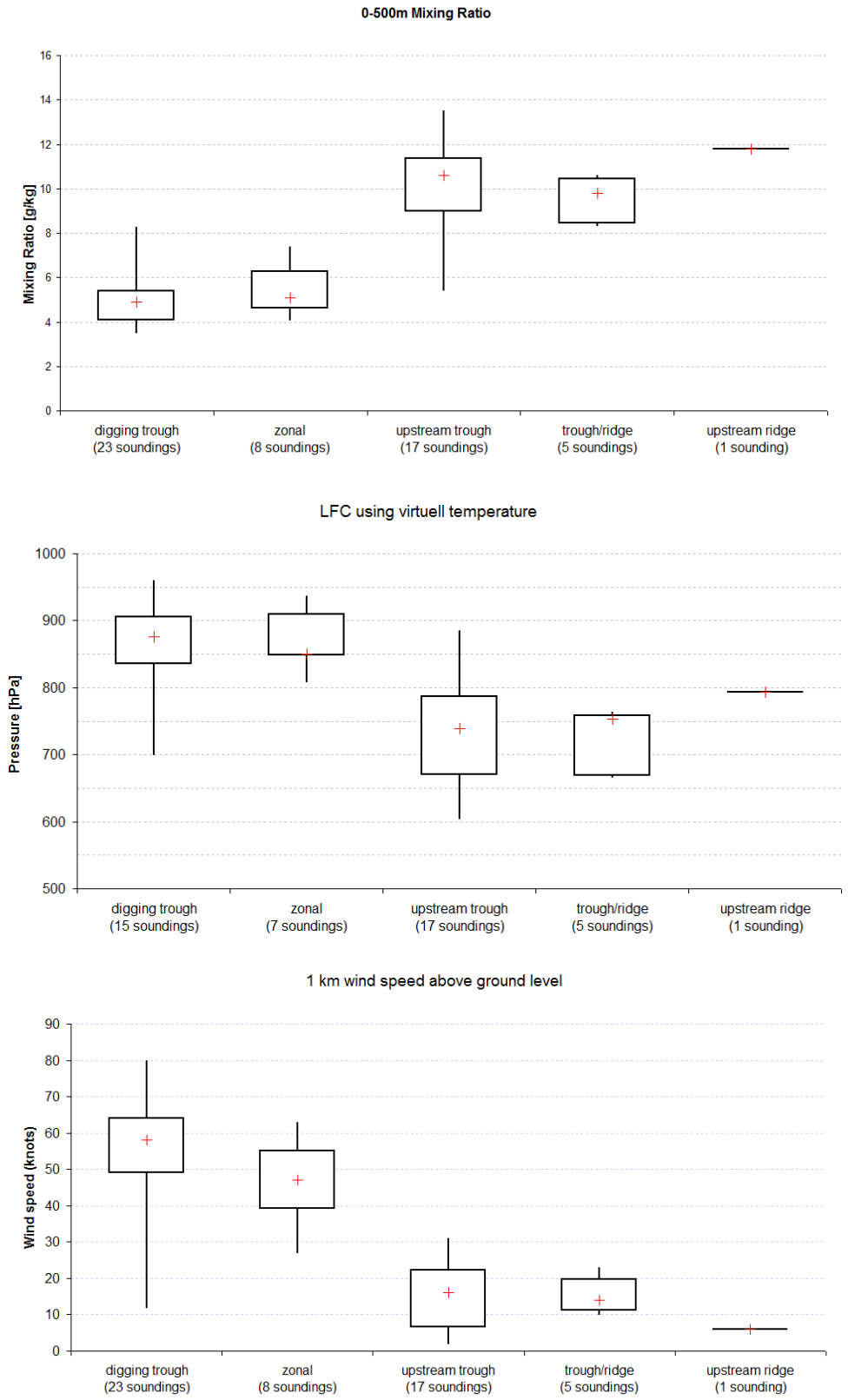

Figure 37: *Box-Whisker diagram of the average mixing ratio [g/kg] in the lowest 500 m above ground (top), pressure at the level of free convection [hPa] using virtual temperature (center) and horizontal wind speed [knots] at 1 km above ground (bottom) based on proximity soundings (number given below the graph) for each classified derecho weather pattern. Median (crosses), 25 and 75 percentile (boxes), and minimum and maximum (thin lines) are plotted.*

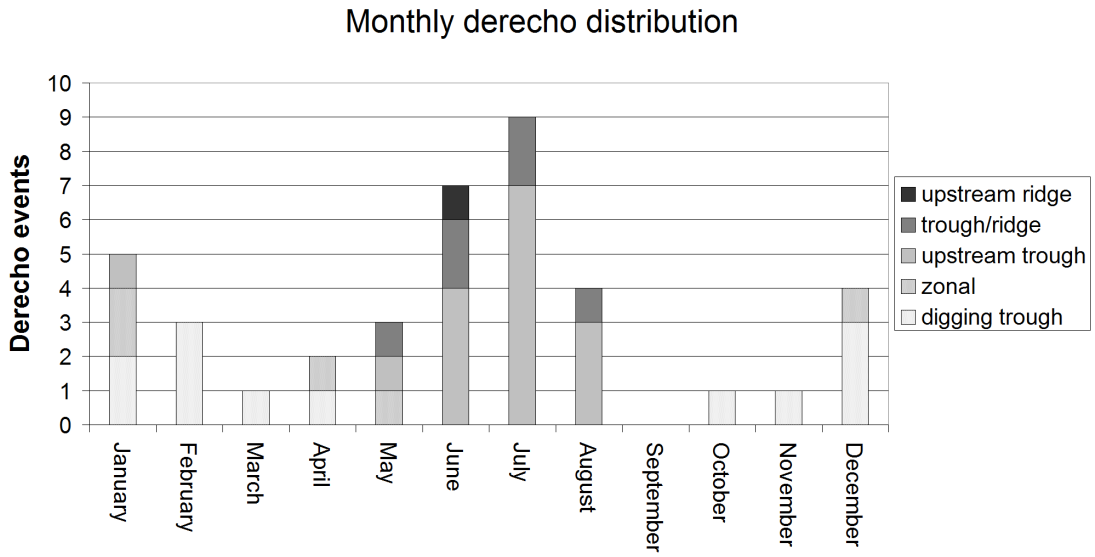

Figure 38: *Monthly numbers of derechos in Germany in the period 1997-2014. Grey shades correspond to different derecho clusters as defined in the figure.*

The influence of external and internal processes is also reflected by the seasonal distribution of derechos. German derechos indicate a warm-season maximum with 16 events in the investigated period (18 years from 1997 to 2014) or 40 % occurring in June and July (Fig. 38). This can be expected since derechos are convective storms that form especially during the seasonal solar heating maximum which favors both rich low-level moisture and steep lapse rates. The maximum peaks at the end of June when the average derecho frequency is one derecho every three years for the 30-day running mean (not shown). A warm season maximum is also evident for the derecho distribution across the United States (e.g. Bentley and Mote, 1998). In Germany, a further, but weaker maximum can be identified in the cold season: Five events occurring in January make it the month with the third highest derecho frequency in the investigated period. This indicates the importance of external factors for derechos. These factors can be related to dynamic forcing as discussed by Evans and Doswell (2001). They may be more dominant in German derecho situations compared to the United States: The cold-season, including the months from October to March, accounts for 15 out of 40 derechos (or 38 %). This is a contrast to the climatology of the United States where the cold-season contributes much less to the derecho number, e.g. less than 25 % according to the publication by Ashley and Mote (2005). The different German climate, e.g. the higher latitude and maritime influence, are likely the main reason.

Considering the seasonal frequency of the different derecho clusters, the summer season is dominated by the weather patterns upstream trough and trough/ridge, whereas cold-season derechos mostly occur with the mid-level flow classes digging trough and zonal (Fig. 38). Vice versa, the seasonal distribution of the derecho clusters can explain differences found for the environmental air mass like CAPE, shear, and low-level mixing ratio: In the cold-season, weaker low-level moisture and stronger vertical wind shear are typically observed across Germany in comparison to the warm season.

Despite the differences of the large-scale flow and environmental parameters, German cold-season derechos do not indicate a weaker intensity or track length as warm-season derechos (Fig. 39). Especially the digging trough cluster does neither indicate that derechos tend to be weaker nor that the track length is shorter compared to both upstream trough and trough/ridge cluster. The track length average of the digging trough cluster is even greater than that of all other clusters. As a consequence, the general statements of this section do not change if the thresholds for derechos are changed, e.g. if only moderate and high-end intensity derechos are taken into account. It follows that the impact of derechos is comparable in low- and high-instability situations.

The presented German derecho climatology offers an opportunity to study processes that support intense deep moist convection in situations with low instability. It differs from the United States climatology in the way that it not only contains a large relative number of cold-season events; most of these events even develop in an environment that does not support thunderstorms due to very warm equilibrium levels. As thunderstorms develop nonetheless atmospheric processes cause rapid changes with respect to the equilibrium level in the close vicinity of these derechos. The cluster analysis shows that these events are most frequently associated with distinct synoptic-scale flow, the digging trough and zonal pattern. Events classified as such patterns could reflect the processes that allow for colder equilibrium levels needed to develop thunderstorms in cold-season derechos. Changes of the equilibrium level are dependent on both low-level moisture changes and lapse rate changes. These parameters will be displayed on pressure levels that we define in the following section.

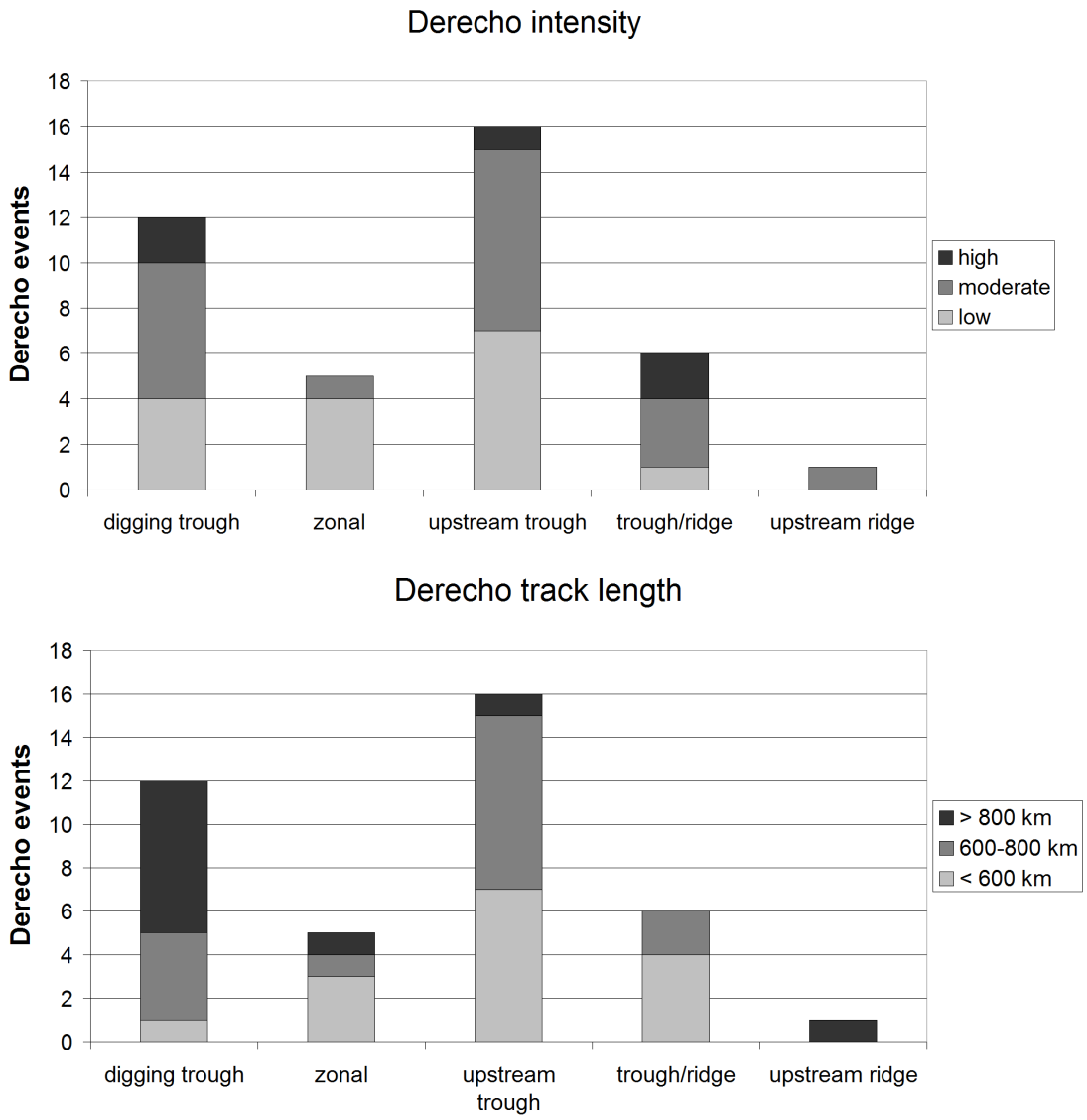

Figure 39: *Intensity (top) and track length (bottom) of the German derechos. Cluster names are given below the graphs. Intensity and track length are given by gray shades as defined in the figure.*

4.2 Pressure level definition for moisture and lapse rate analysis

To test the hypothesis that instability rapidly changes close to derechos, we interpret combined horizontal charts of lapse rates and low-level moisture calculated from high-resolution model fields. Pressure levels need to be fixed for each parameter displayed in the charts. An argumentation how we define pressure levels will be given in the following.

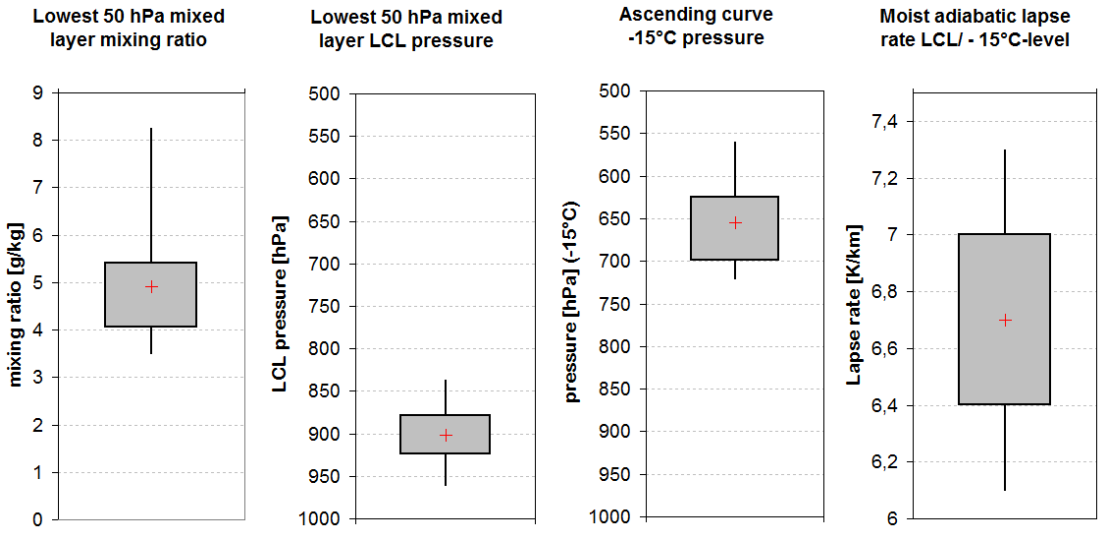

Figure 40: *Box-and-Whisker plots of numbers obtained from a group of 23 proximity soundings (using the lowest 500 m mixed layer parcel and its lifting curve) for the digging trough weather pattern listed in table 3. The crosses mark the median, boxes are plotted for the 25 and 75 percentile, and thin lines for the minimum and maximum, respectively. a) lowest 500 m mixed layer mixing ratio; b) LCL pressure; c) estimated pressure where the lifting curve reaches a temperature of -15° C; d) estimated average lapse rate for moist adiabatic ascent from the LCL until a temperature of -15° C is reached.*

To represent the horizontal field of low-level moisture, the mixing ratio at 975 hPa was chosen. A better approximation would be the lowest 500 m mixed moisture, however, the taken value can give a good overview as well. Two pressure levels are needed to calculate the lapse rate. To find these pressure levels, proximity soundings of the digging trough pattern (listed in table 3) were evaluated according to the method described in section 3.3. First, the average pressure of the lifted condensation level (LCL) was calculated for these soundings. The average LCL pressure was then used to choose a model output pressure level for further calculations. The same was done for the pressure at which a temperature of -15°C is reached along the lifting curve of low-level mixed parcels. The distribution of these values are plotted together with the lowest 500 m mixed parcel mixing ratio and the associated average moist adiabatic lapse rate between LCL and the level of -15°C temperature in Fig. 40. Since the median of the LCL pressure is 901.9 hPa, 900 hPa was chosen as the lower level for the lapse rate calculation in the model. For the upper level with a temperature of -15°C, the median is 655 hPa, and as nearest model pressure level 650 hPa was chosen. Both pressure levels are very close to the ground. For example, classic charts display 700 to 500 hPa lapse rates combined with low-level moisture. But these are values that represent warm-season convective environments rather than cold-season situations and are

therefore not useful to interpret instability in the presented cases. Charts adjusted to the cold season that display lapse rates on lower pressure levels could support forecasters much more. Finally, the median of the estimated moist adiabatic lapse rates between these two levels is 6.7 K/km, with the first and third quartiles of 6.4 and 7.0 K/km, and minimum and maximum values of 6.1 and 7.3 K/km. For further investigation values exceeding 6.0 K/km were highlighted in the model charts.

4.3 Low-instability derechos in observations and simulations

Eight events classified as digging trough and zonal flow patterns were chosen for high-resolution simulations. In this section, observations and COSMO simulations of these derechos are analyzed with respect to the ingredients-based methodology. To estimate the accuracy of the model simulation, the three ingredients were compared to observations. The first ingredient, low-level moisture, was analyzed with respect to zones of relatively rich moisture. A fixed threshold was not used. To identify zones of high low-level moisture in the model simulation, the 975 hPa mixing ratio was taken. This pressure level is close to the ground and can be expected to be representative. The model map of low-level mixing ratio was then compared to observations. We used charts of interpolated dewpoint readings at the ground. A comparison of both fields allows to detect and compare zones of rich moisture, in particular the position of fronts or cold pools. For the lapse rate, only a few proximity soundings were available for comparison. However, much more soundings were analyzed to characterize the thermodynamic environment of derechos, most are listed in table 3. One common result of the sounding analysis was that all presented derechos formed in low instability. The only exception is the event of 21 October 2014 that moved into a zone with higher instability during the mature and dissipation phase. For the third ingredient, lift, we distinguished between situations characterized by well-developed cold fronts (indicated by narrow cold-frontal rain bands) and situations where such fronts were not observed prior to derecho development. On the one hand, intense frontal lift has been supposed to allow direct release of potential instability (Browning and Roberts, 1996). On the other hand, well-developed fronts are a source of external forcing (section 2.6) used to distinguish between high- and low-instability derechos (Corfidi et al., 2016). Once derechos developed gust fronts we expect that lift is strong enough

to sustain deep moist convection as long as there is CAPE. The position of the gust front was compared between model and observations as well. It turned out that model-derived maximum wind gusts or wind direction were not good indicators of the gust front position since the strong background flow overlaid the gust front. Instead, the simulated gust front's position was much better visible by the decrease of 975 hPa mixing ratio that was compared to the radar image and the surface dewpoint analysis.

In the following we will give an overview over each of the eight low-instability derecho cases separately.

28 December 2001

On 28 December 2001 a convective wind event matching the derecho criteria crossed parts of Germany. The derecho approached the North Sea coasts of the Netherlands and Germany at about 9 UTC (Fig. 41). Given severe wind reports from offshore platforms, ships and over parts of east England, the derecho started farther to the north-west as actually analyzed, especially since lightning was detected in that area (not shown). Along the coasts of Germany and the Netherlands wind gusts exceeded 25 m/s at many locations, with a peak wind gust of 33 m/s at Hörnum on the island of Sylt (Fig. 41, top). Farther onshore, gusts were weaker on average, but locally, severe gusts still occurred as indicated by a damage reports in north-west Germany (F1/T2 damage[4] in the city Leer and downed trees in Coesfeld; European Severe Weather Database (ESWD); Dotzek et al., 2009). Until the evening hours, the gust front moved south-east into the Czech Republic. Along its path across central and eastern Germany wind measurements exceeded 25 m/s, but only mountain stations reported more than 32 m/s (Fig. 41, top). Therefore, the illustrated event is of low-end intensity. The strongest wind gust of 50 m/s was observed on top of the mountain Fichtelberg at 18 UTC and can be attributed to the passage of the convective line since winds were significantly less in the hour before (42 m/s) and after (36 m/s) the event. At 12 UTC the radar composite image (Fig. 41, bottom) shows a bow-shaped cold-frontal rain band that extends from the lower Rhine valley to Hanover and farther to Hamburg. The rain band is embedded in stratiform precipitation except for its south-western end where there is just a weak, thin line. Here, shallow, linear convection can be assumed. Lightning is detected from south of Hamburg to north of Essen. At two

[4]F1/T2 wind intensity on the Fujita / TORRO scale corresponds to 33 – 42 m/s (Dotzek, 2009).

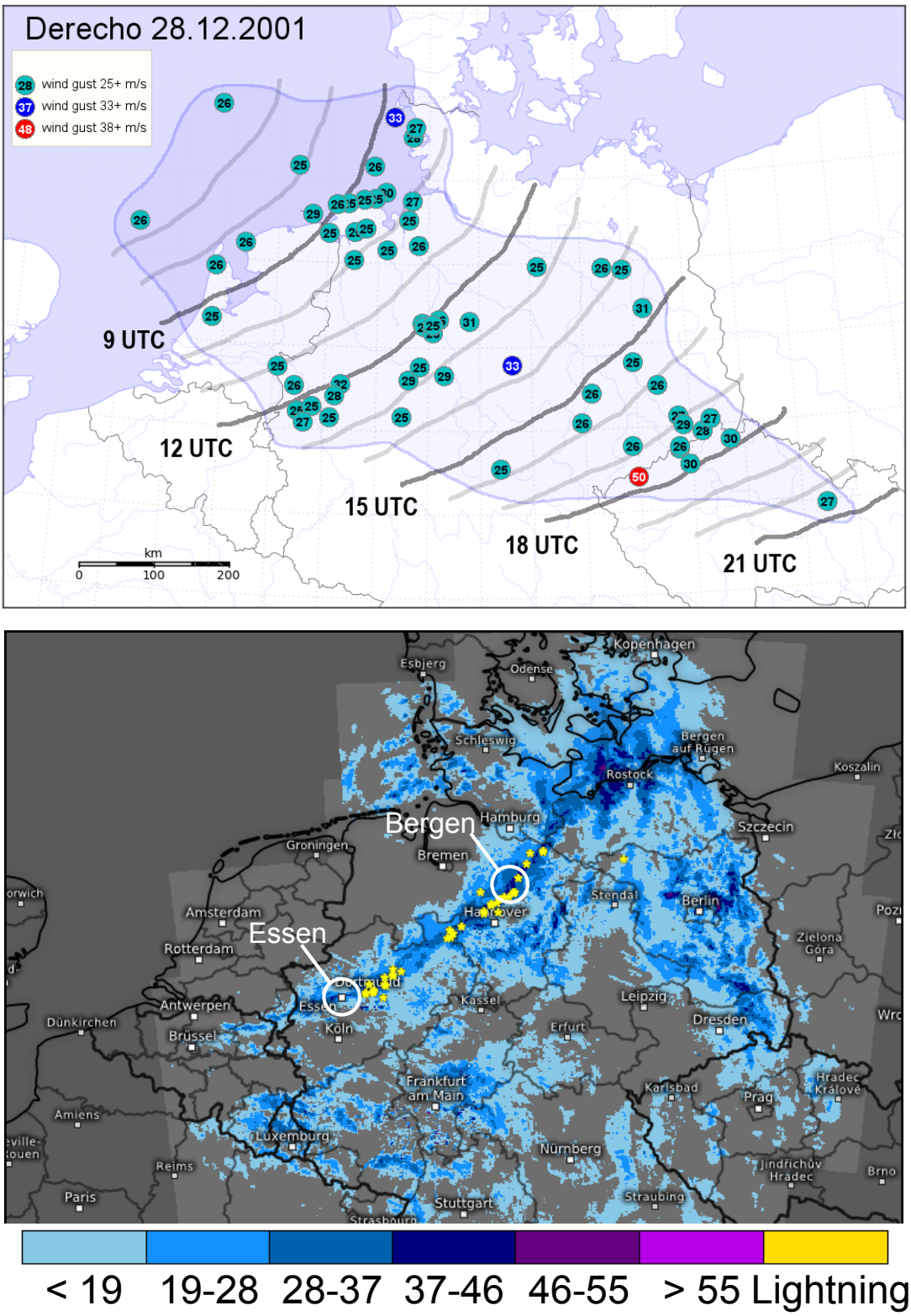

Figure 41: *Top: Wind measurements (dots, given in m/s) and hourly derecho position (thick lines, labeled every third line) on 28 December 2001. The affected area is highlighted in blue. Bottom: Radar composite image of 28 December 2001, 12 UTC and lightning detection (yellow stars) between 11:45 and 12 UTC. Locations of proximity soundings are indicated by white circles. Radar reflectivity is given in dBZ according to the color bar. Data source: Deutscher Wetterdienst / Image courtesy: Kachelmann GmbH (bottom).*

locations (Bergen and Essen) along the rain band, soundings had been launched for the 12 UTC ascents. The sounding locations are marked in Fig. 41, bottom. Both soundings match the definition by Evans and Doswell (2001) to be regarded as proximity soundings for this particular derecho event.

The Bergen sounding (Fig. 42, top) had been launched at 10:47 UTC, one hour before the observation site reported a thunderstorm with graupel and a 39 knots gust for the 12 UTC weather observation. The sounding indicates strong vertical wind shear and stable lapse rates especially below 700 hPa. As a consequence, CAPE is not calculated although the air mass is close to saturation. It can be interpreted as a profile through clouds atop of a stable low-level air mass. Hourly observation data from Bergen do not indicate a change of the wind direction, temperature or dewpoint from 11 to 12 UTC. This is also indicated by ground observations ahead of the derecho (Fig. 43). There are no indications of a moisture increase. Dewpoint readings of neighboring locations are also lower compared to the sounding site (Fig. 43).

At Essen there is strong vertical wind shear as well. However, in contrast to the Bergen sounding, steep lapse rates are visible ahead of the cold-frontal rain band (Fig. 42, bottom) which at this time produced lightning to the north-east of the location. It is interesting to see such steep lapse rates close to the ground given the weak diurnal heating. Other processes may be responsible for the steep lapse rates that formed especially at low levels with a level of free convection just 600 m above the ground. Weak CAPE of 50 J/kg is calculated with an equilibrium level slightly below 700 hPa. The equilibrium level temperature is -12°C. A comparison with the Bergen sounding shows much drier air between 750 and 550 hPa and inversions that are not observed in Bergen. This dry air might be associated with an upper-level front or tropopause fold indicated by reanalysis data (not shown). Since the temperature lapse rate between 570 and 750 hPa is much less than the dry adiabatic lapse rate, the temperature profile could reflect lift in this layer. Below 850 hPa, both soundings show a moist air mass close to saturation. Lift constant with height would cause more instability due to moist adiabatic cooling in the saturated air at low levels and dry adiabatic cooling at mid levels. In this respect, the sounding could reflect the process of potential instability release. CAPE forms between the saturated air masses with diabatic heat release at 900 hPa and dry adiabatic cooling at mid levels. But also other processes can be thought to cause this vertical profile, like differential temper-

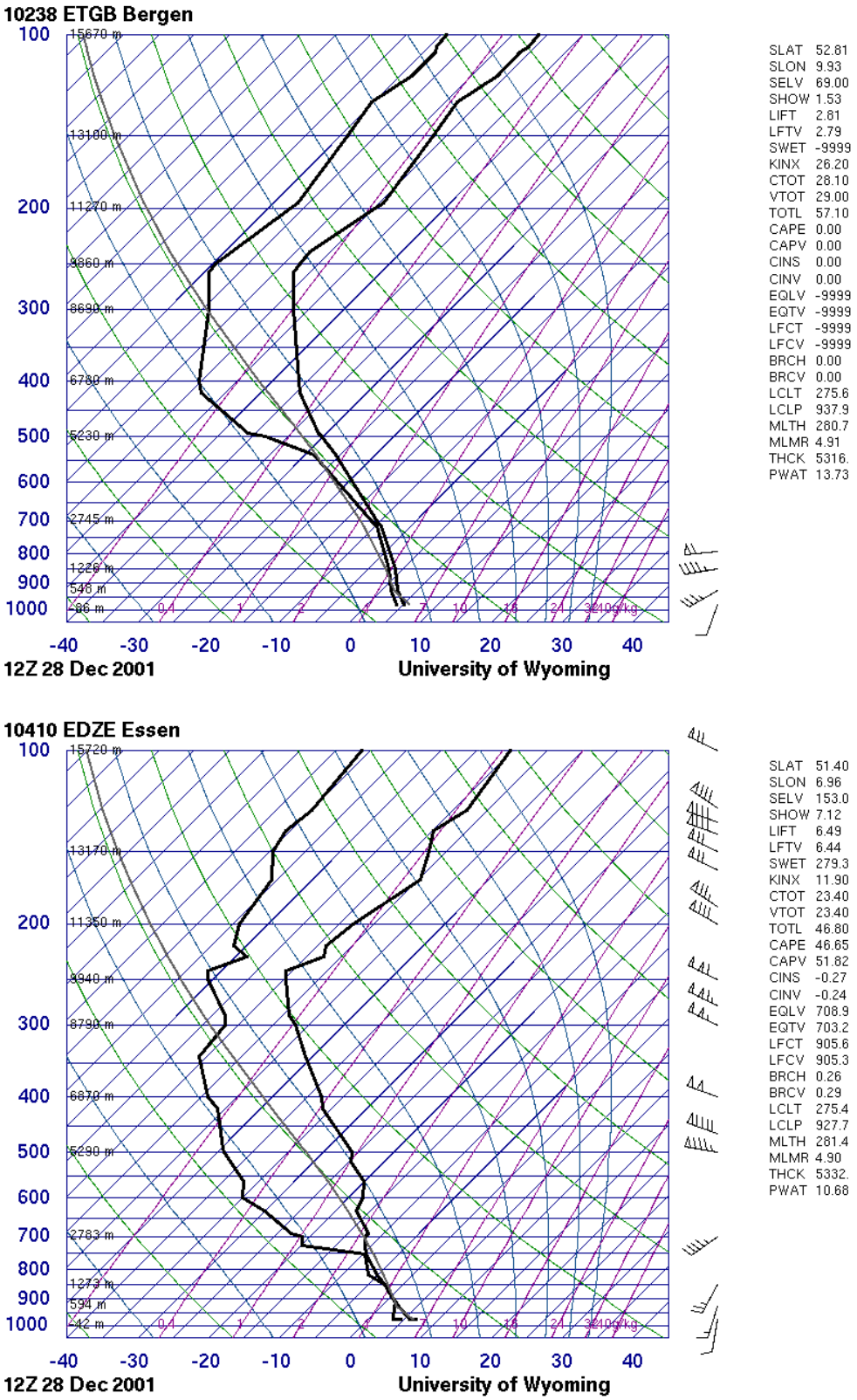

Figure 42: *Skew-T/log p diagram at Bergen (top) and Essen (bottom). Image courtesy: University of Wyoming.*

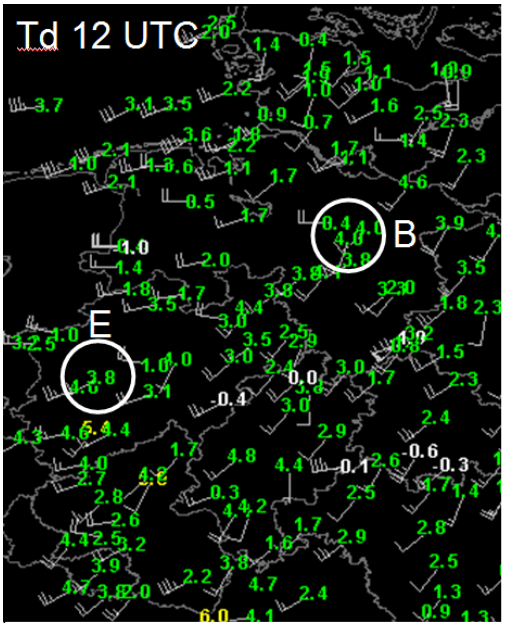

Time (UTC)	dd (°)	ff (kts)	T (°C)	Td (°C)	WW
10:00	180	08	4.9	4.9	61
11:00	200	12	5.3	4.2	63
12:00	200	16	5.2	4.0	96
13:00	210	08	1.6	1.0	29

dd: Wind direction
ff: Wind speed
T: Temperature
Td: Dewpoint
WW: Weather code (61=light rain, 63=moderate rain, 96=thunderstorm with hail or graupel, 29=thunder in the last hour)

Figure 43: *Ground observations of 28 December 2001. Left: 12 UTC dewpoint ground readings (°C) and wind barbs (kts) across north-western Germany. Locations of Bergen (B) and Essen (E) are in the center of the white circles. Right: Time series of ground observations at Bergen. Data source: Deutscher Wetterdienst / Image courtesy: MeteoGroup.*

ature advection or stretching. The low-level mixing ratio does not significantly differ between Bergen and Essen, indicating a rather homogenous distribution of low-level moisture ahead of the derecho. The main difference of both soundings with respect to CAPE is therefore the different lapse rate.

The proximity sounding in Bergen cannot represent the observed thunderstorms following the ingredients-based approach. For the Bergen profile a lapse rate increase is more likely the reason to yield CAPE and sufficiently cold equilibrium level temperatures, given that the moisture increase is weak or even zero. Furthermore, the comparison with the sounding at Essen leads to the assumption that lapse rate changes at relatively low levels occur prior to the approach of the derecho. Such lapse rate changes can be assumed from the lapse rate field in the COSMO model maps (purple lines in Fig. 44, top). Large horizontal gradients can be seen over northern Germany, where the lapse rate increases from about 6.5 to 7.5 K/km along 52.5°N between 12.5 and 9°E. Even larger gradients are indicated close to Essen at 52°N / 7.5°E.

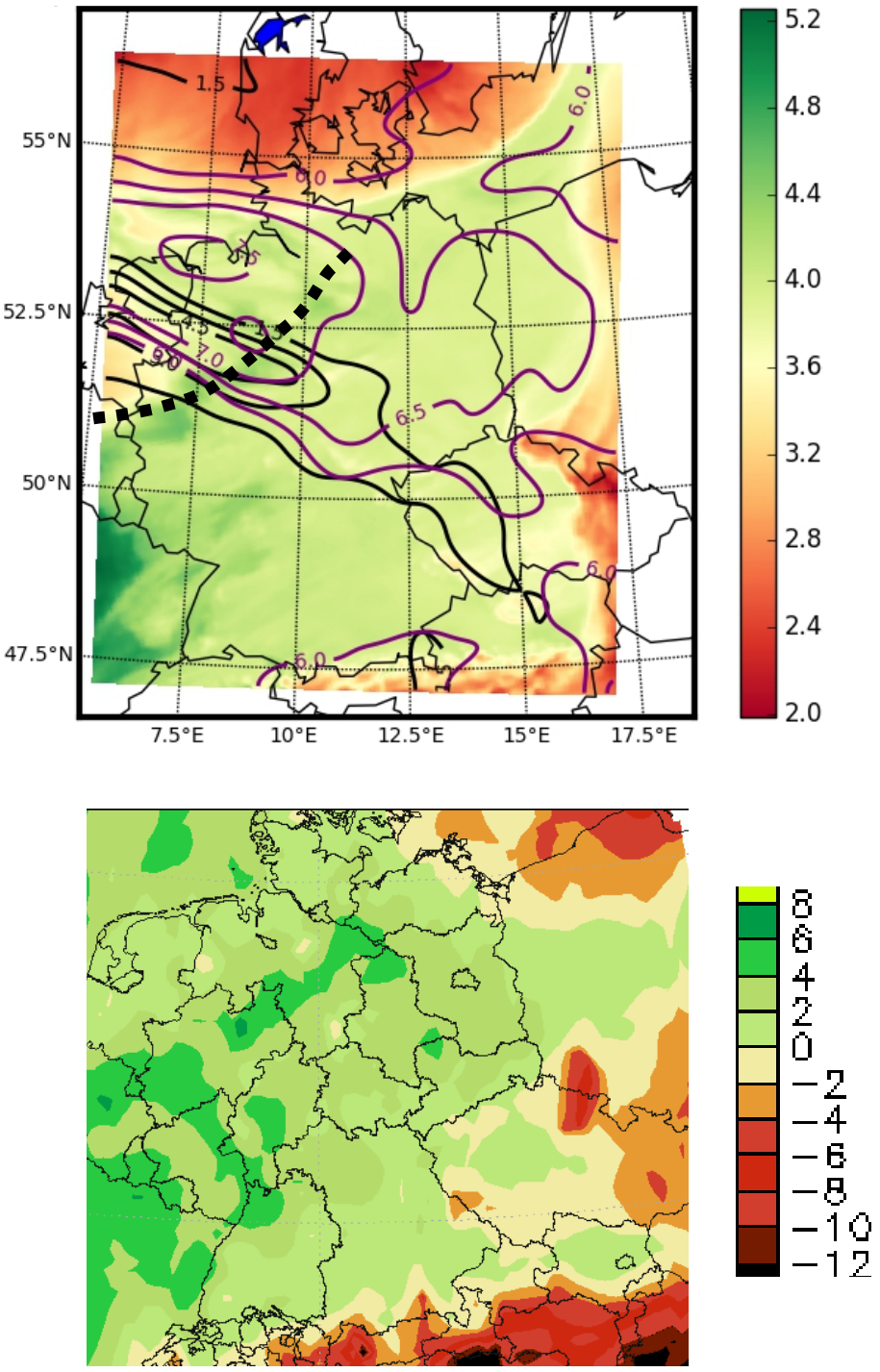

Figure 44: *28 December 2001, 12 UTC. Top: Derecho position, based on diagnostic data (dotted line) and simulated fields of low-level moisture (975 hPa, shaded, in g/kg), lapse rates (thin purple lines every 0.5 K/km, starting at 6 K/km) and PV (black lines every 1.5 PVU, starting at 1.5 PVU). Bottom: Interpolated surface dewpoint field derived from SYNOP data. Dewpoint is given in °C according to the color bar to the right. Data source: Deutscher Wetterdienst / Image courtesy: MeteoGroup.*

The model simulation is rather accurate with respect to the derecho gust front: Just south-east of the derecho the COSMO model map indicates a band of rich low-level moisture that is also visible in the surface dewpoint chart (Fig. 44, bottom). This band of rich moisture overlaps with steep lapse rates in the northern portions whereas weak lapse rates are located in the south according to the COSMO simulation. However, comparison with the soundings at Bergen and Essen shows some differences with respect to the observed lapse rate: In Bergen, the lapse rate from the sounding is less steep by about 0.3 K/km compared to the model. At Essen, the lapse rate from the sounding is steeper by more than 1.3 K/km (7.3 K/km in the sounding, less than 6 K/km on the model map). One reason can be that due to the strong flow the balloons are advected downstream so that they measured a slantwise lapse rate. Additionally, given the large gradients of the lapse rate, even small model inaccuracies can cause large local deviations between model and observation. The model simulation reflects the measured lapse rate at least close to the sounding location with more than 7 K/kg less than 100 km away. Comparing the model lapse rate field with the lightning occurrence (Fig. 41, bottom), lightning occurred where steep lapse rates exceeding 7 K/km overlap with the band of rich moisture. Overlaid to the area of the largest horizontal lapse rate gradient, the COSMO model shows high PV values that reflect a PV intrusion. The PV intrusion is oriented nearly perpendicular to the narrow cold-frontal rain band. The close relationship of low-instability derechos and PV intrusions as summarized from the literature review (section 2.7) is therefore confirmed for this event.

28 January 2002 (first derecho)

On 28 January 2002, two derechos have been classified across Germany. The first one (Fig. 45) looks quite similar to the derecho of 28 December 2001 (Fig. 41): Both events are of low-end intensity with a wide and long path. On the radar display, a narrow cold-frontal rain band embedded in stratiform precipitation can be seen that thins out at its south-western end. COSMO maps show PV intrusions nearly perpendicular to the rain band and lapse rates exceeding 7 K/km north-east of the PV intrusion (Figs. 46, top and 44, top). However, there are also differences. The derecho path of 28 January 2002 is oriented from west to east whereas the derecho of 2001 was moving south-eastwards. This is interesting because the associated rain bands have the same orientation for both events. It is

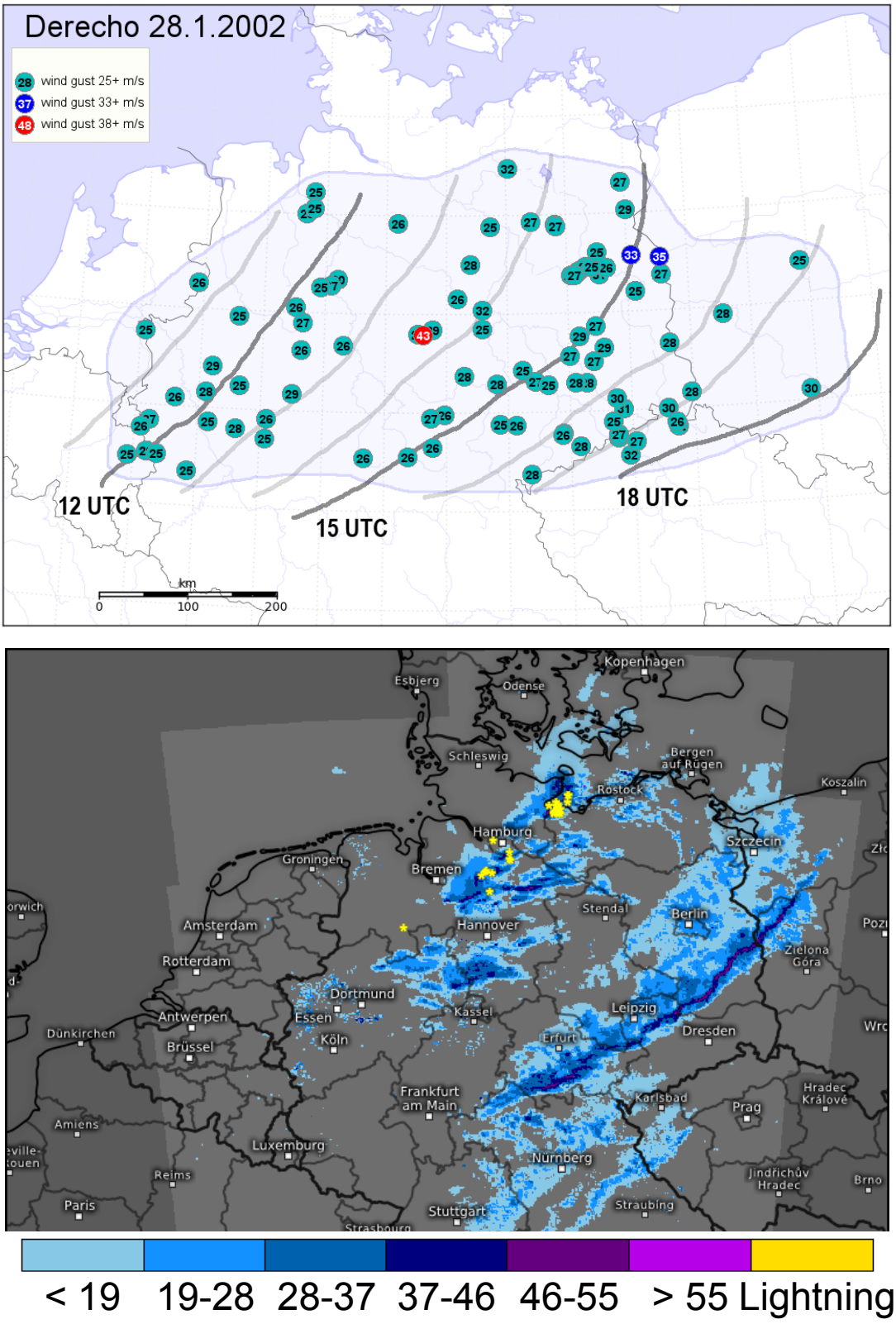

Figure 45: *Top: Wind measurements (dots, in m/s) and hourly derecho position (thick lines, labeled every third line) of the first derecho on 28 January 2002. The affected area is highlighted in blue. Bottom: Radar composite image of 28 January 2002, 15 UTC and lightning detection (yellow starts) between 14:45 and 15 UTC. Radar reflectivity is given in dBZ by the color bar. Data source: Deutscher Wetterdienst / Image courtesy: Kachelmann GmbH (bottom).*

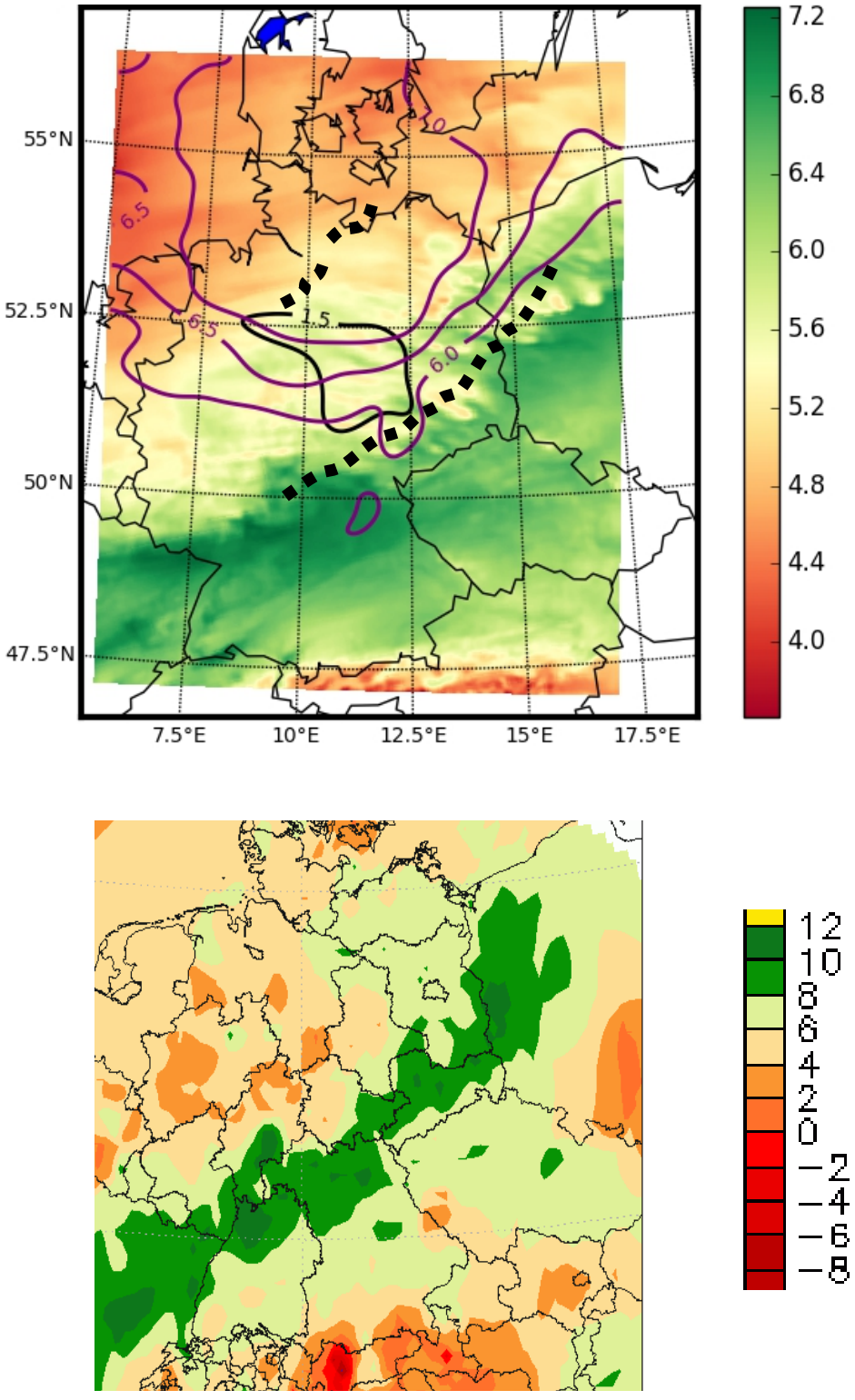

Figure 46: *28 January 2002, 15 UTC. Top: Derecho position, based on diagnostic data (dotted line), and simulated fields of low-level moisture (975 hPa, shaded, in g/kg), lapse rates (thin purple lines every 0.5 K/km, starting at 6 K/km) and PV (black lines every 1.5 PVU, starting at 1.5 PVU). Bottom: Interpolated surface dewpoint field derived from SYNOP data. Dewpoint is given in °C according to the color bar to the right. Data source: Deutscher Wetterdienst / Image courtesy: MeteoGroup.*

possible that the external forcing of the event, likely associated with the PV intrusion, moved differently in both events what affected also the derecho movement. Another difference is that there was very little lightning detected with the 2002 derecho. Unfortunately, proximity soundings are not available that might show warm equilibrium levels and less steep lapse rates in the 900 to 650 hPa layer. The COSMO model map confirms this suggestion as it indicates weak lapse rates of just 6 K/km overlapping with the band of rich moisture ahead of the derecho (Fig. 46, top). The little overlap is not resulting from model inaccuracies with respect to the position of the moisture field as can be seen from comparison with the dewpoint chart (Fig. 46, bottom). It can be suggested that the weak lightning is caused by the marginal overlap of lapse rates and low-level moisture as shown by the model map.

28 January 2002 (second derecho)

In the wake of the first derecho of 28 January 2002, another followed about three hours later. Following the wind measurements of this event, three narrow paths can be seen, of which the central path fulfilled derecho criteria with a path length of 430 km (Fig. 47, top). The intensity of this derecho could be classified as moderate since there are three wind measurement of more than 33 m/s separated by at least 64 km in the eastern part of the path. However, the easternmost of these measurements is at least a little questionable since this measurement site reported an hourly maximum gust of the same wind speed already 3 hours before with the passage of the first derecho. Therefore, the derecho is classified as low-end intensity. Corresponding to the wind paths, the radar display at 16 UTC shows three clusters of convective storms that party evolved into single bow echoes rather than cold-frontal rain bands with embedded bows (Fig. 47, bottom).

The second derecho obviously evolved in limited low-level moisture as can be seen in the model map as well as on the dewpoint chart (Fig. 46). The surface dewpoint is around 6°C what is much less compared to 10°C ahead of the first derecho. Steeper lapse rates compensate the effect of weak humidity in this case. To the south of the convective storms, the lapse rate decreases rapidly. This can explain why the southern storm cluster did not produce lightning at 16 UTC. Here, the equilibrium level temperature may have been too warm. Overlaid to the horizontal lapse rate gradient, a PV intrusion is visible on the model maps.

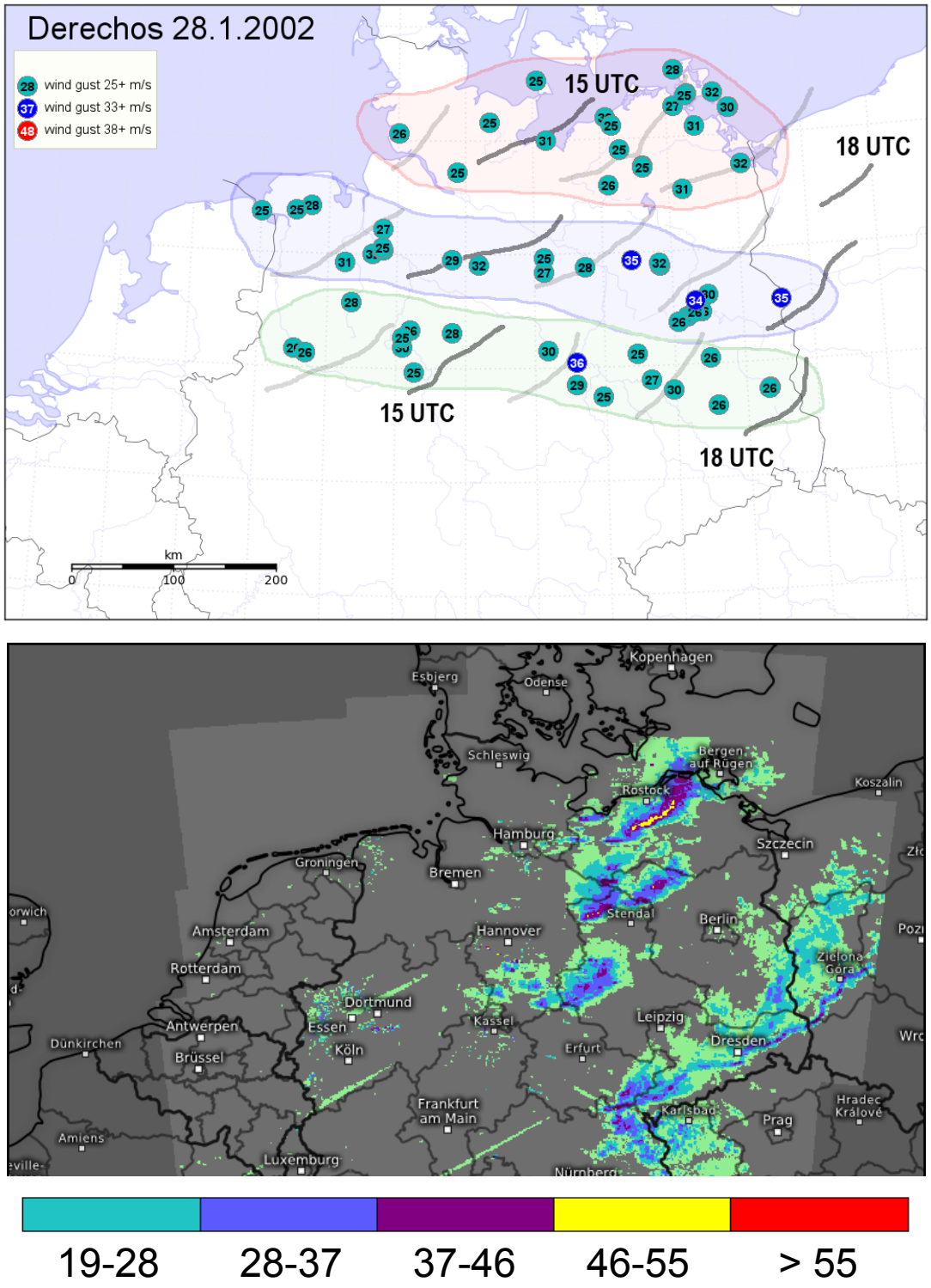

Figure 47: *Top: Wind measurements (dots, in m/s) and hourly derecho position (thick lines, labeled every third line) of the second derecho on 28 January 2002. The affected area is highlighted in blue. Bottom: Radar composite image of 28 January 2002, 16 UTC. Radar reflectivity is given in dBZ by the color bar below the radar image. Data source: Deutscher Wetterdienst / Image courtesy: Kachelmann GmbH (bottom).*

18 January 2007 ("Kyrill derecho")

The derecho that formed along the cold front of the severe winter storm "Kyrill" was difficult to classify due to high non-convective wind gusts in the pre-storm environment. Due to the methodology to classify convective wind gusts (section 3.1), many measurements were sorted out since they did not indicate a significant intensity increase. This is visible over western Saxony near the center of the gust front between 18 and 20 UTC (Fig. 48, top). Here, severe downslope wind gusts were typically as intense as the derecho wind gusts. At some locations, the derecho was even associated with a wind decrease. The derecho was of moderate intensity with numerous stations reporting wind gusts between 33 and more than 40 m/s. After the derecho formed along a narrow cold-frontal rain band, it evolved a few larger, persistent bow echoes. A pronounced bow echo formed close to the center line of the derecho at 17 UTC and could be followed well into southern Poland where it dissipated at 0 UTC. It was accompanied by frequent lightning (Fig. 48, bottom) and caused tornadoes along its path. Ahead of the cold-frontal rain band, thunderstorms formed over eastern Germany indicating that CAPE and cold equilibrium levels were present in the pre-derecho air mass.

The COSMO simulation reproduced the location of the pre-frontal moisture field quite well (Fig. 49). The simulation indicates a PV intrusion across western Germany, located at the south-western end of the derecho. Steep lapse rates are situated over northern Germany in the wake of the cold front. Lapse rates exceeding 6 K/km can also be seen in the moist, pre-frontal air mass. Both areas are separated by a zone of stable lapse rates that reflects the stable frontal zone or the convective cold pool. A proximity sounding from Lindenberg indicates a nearly moist adiabatic profile ahead of the derecho and it can be expected that the ascent is inside of clouds (Fig. 50). Though, the lapse rate between 900 and 650 hPa is close to 7 K/km, since the boundary layer is turbulently mixed what might be not reproduced by the COSMO model. Assuming a moist adiabatic lapse rate below 850 hPa, the lapse rate between 900 and 650 hPa would be 6.1 K/km. In the sounding, there is also weak CAPE at low levels between 850 and 700 hPa. Finally, the sounding indicates very strong vertical wind shear at low levels.

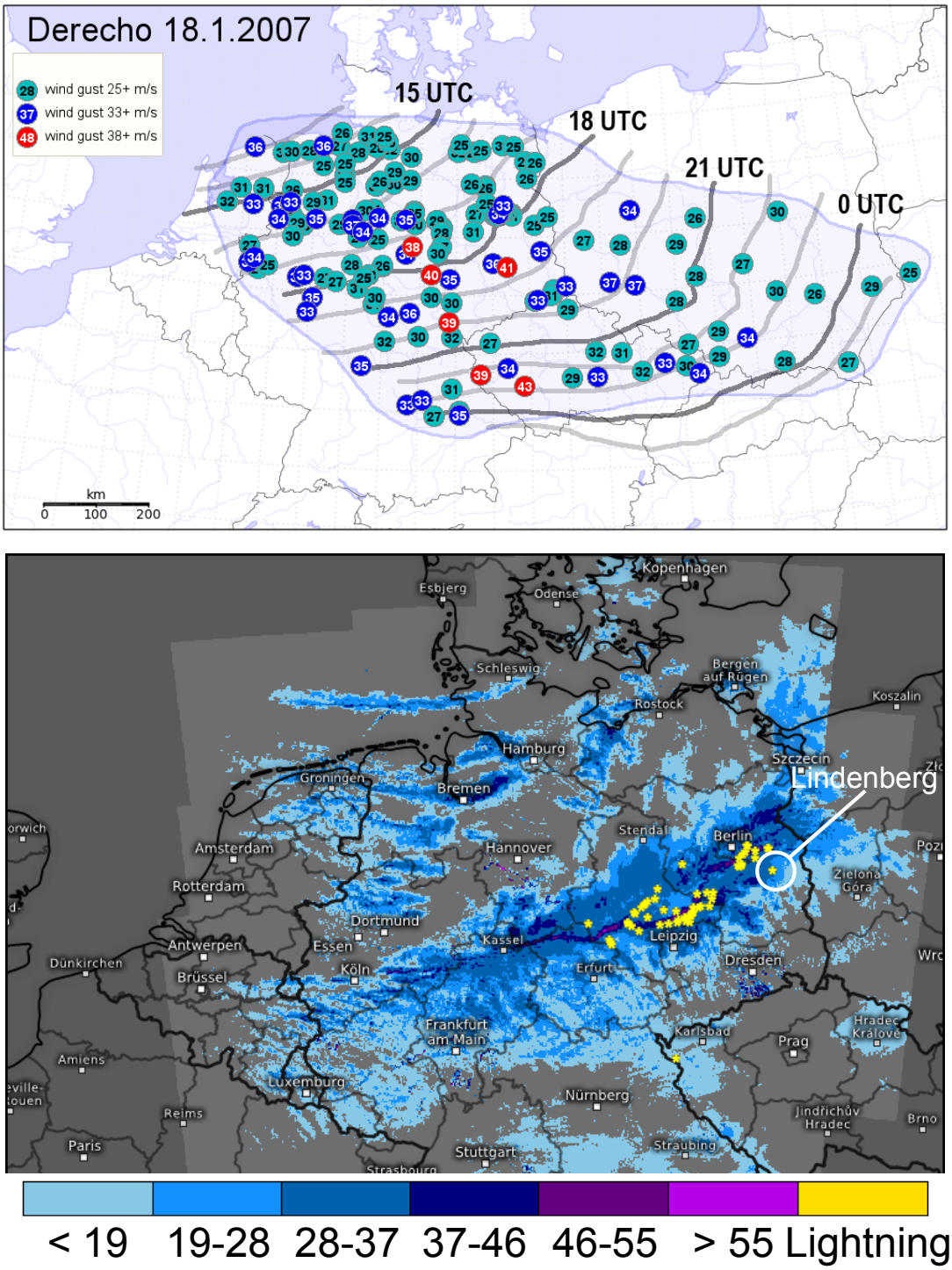

Figure 48: *Top: Wind measurements (dots, in m/s) and hourly derecho position (thick lines, labeled every third line) on 18 January 2007. The affected area is highlighted in blue. Bottom: Radar composite image of 18 January 2007, 18 UTC and lightning detection between 17:45 and 18 UTC. The location of a proximity soundings is indicated by a white circle. Radar reflectivity is given in dBZ by the color bar below the radar image. Lightning detection is given by yellow stars. Data source: Deutscher Wetterdienst / Image courtesy: Kachelmann GmbH (bottom).*

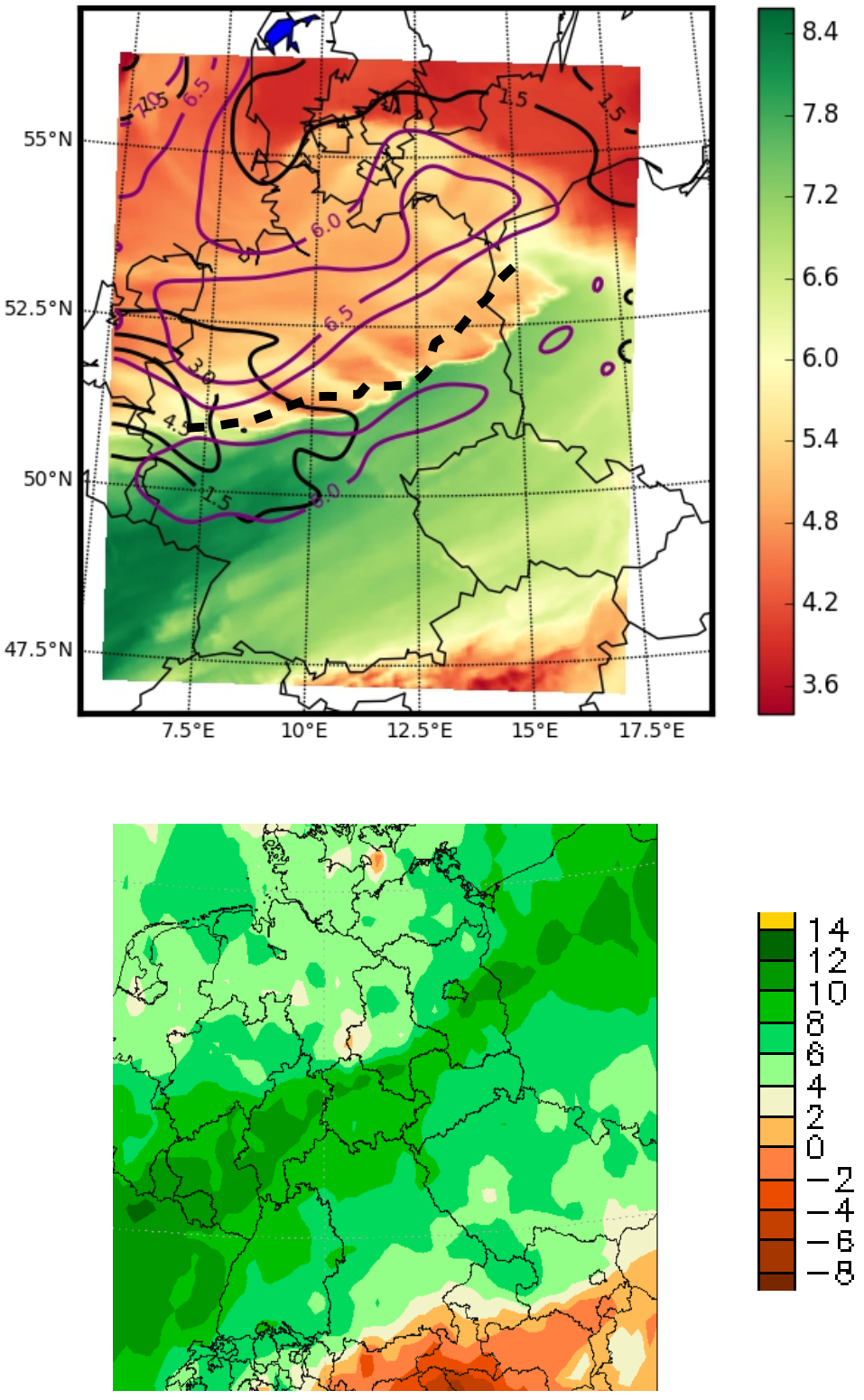

Figure 49: *18 January 2007, 18 UTC. Top: Derecho position, based on diagnostic data (dotted line), and simulated fields of low-level moisture (975 hPa, shaded, in g/kg), lapse rates (thin purple lines every 0.5 K/km, starting at 6 K/km) and PV (black lines every 1.5 PVU, starting at 1.5 PVU). Bottom: Interpolated surface dewpoint field derived from SYNOP data. Dewpoint is given in °C according to the color bar to the right. Data source: Deutscher Wetterdienst / Image courtesy: MeteoGroup.*

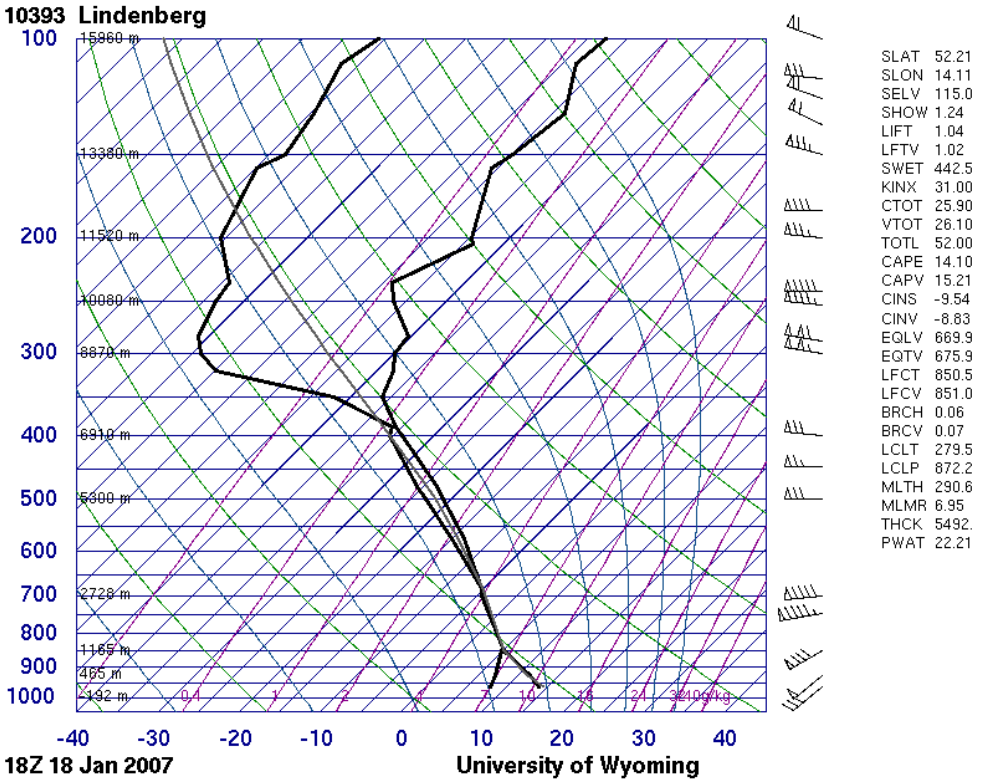

Figure 50: *Skew-T/log p diagram at Lindenberg on 18 January 2007, 18 UTC. Image courtesy: University of Wyoming.*

22 February 2008

Another narrow cold-frontal rain band crossed the north-east of Germany on late 22 February. It produced high wind gusts of more than 33 m/s at numerous places, in particular at the coasts where also gusts of more than 40 m/s were measured (Fig. 51, top). The path of severe wind gusts extends towards Berlin and farther into Poland, where only limited data was available. The rain band showed only small bowing segments (Fig. 51, bottom) while a period with no lightning detection is displayed. Lightning was detected before and later, e.g. 30 minutes later at 21:30 UTC. To the west of the derecho path, a rain band is visible. This rain band produced mostly sub-severe wind gusts. The derecho of 22 February 2008 was not associated with a broad overlap of rich low-level moisture and steep lapse rates as can be expected from the limited lightning detected. The COSMO simulation even looks like rich pre-frontal moisture was placed south of the PV intrusion and steep lapse rates (Fig. 52, top). However, the surface dewpoint chart differs significantly with respect to the area of rich moisture across north-eastern Germany. For example, the Baltic Sea coast east of 12.5°E is still ahead of the

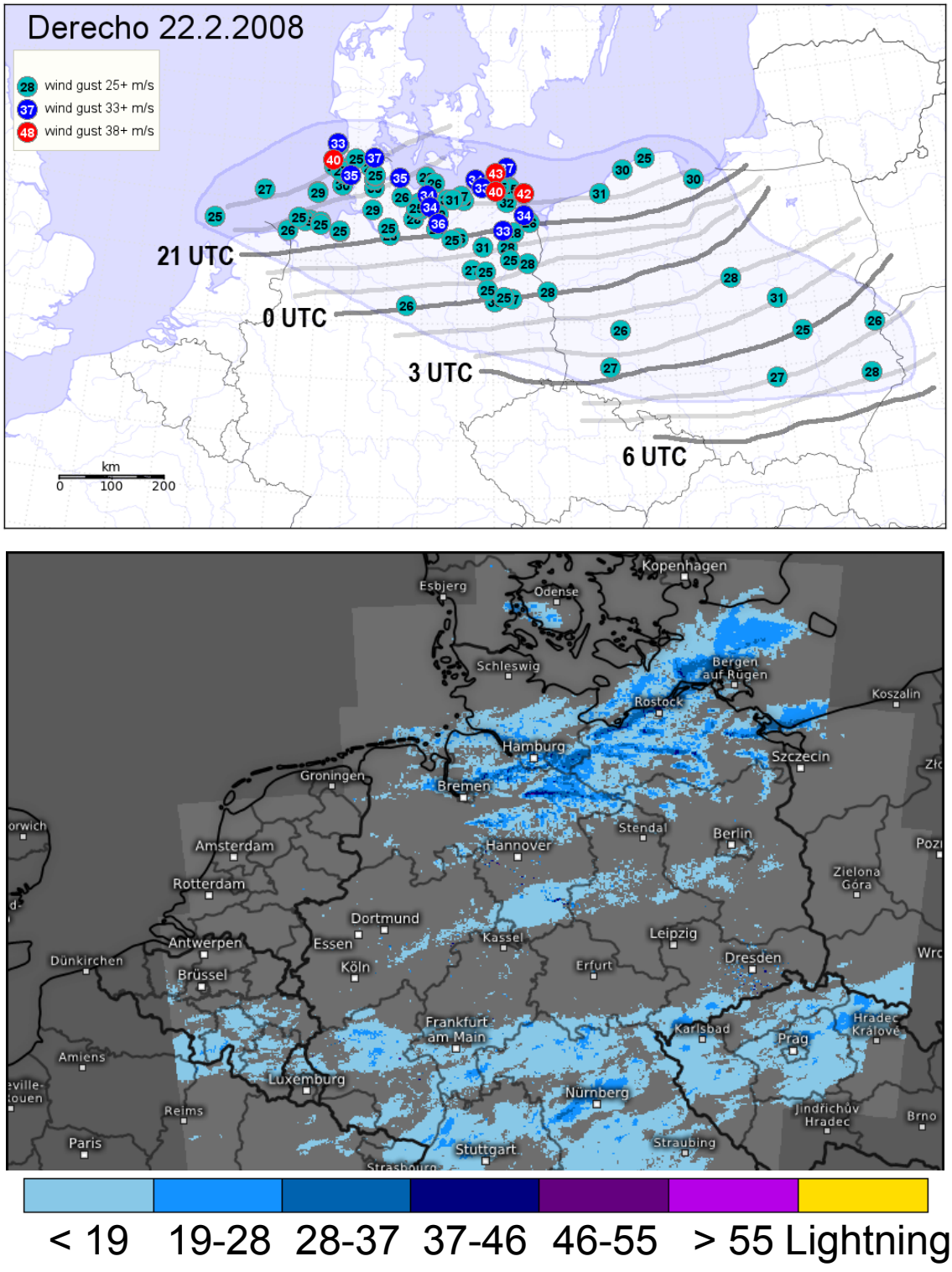

Figure 51: *Top: Wind measurements (dots, in m/s) and hourly derecho position (thick lines, labeled every third hour) on 22 February 2008. The affected area is highlighted in blue. Bottom: Radar composite image of 22 February 2008, 21 UTC and lightning detection between 20:45 and 21 UTC. Radar reflectivity is given in dBZ by the color bar, lightning detection by yellow stars. Data source: Deutscher Wetterdienst / Image courtesy: Kachelmann GmbH (bottom).*

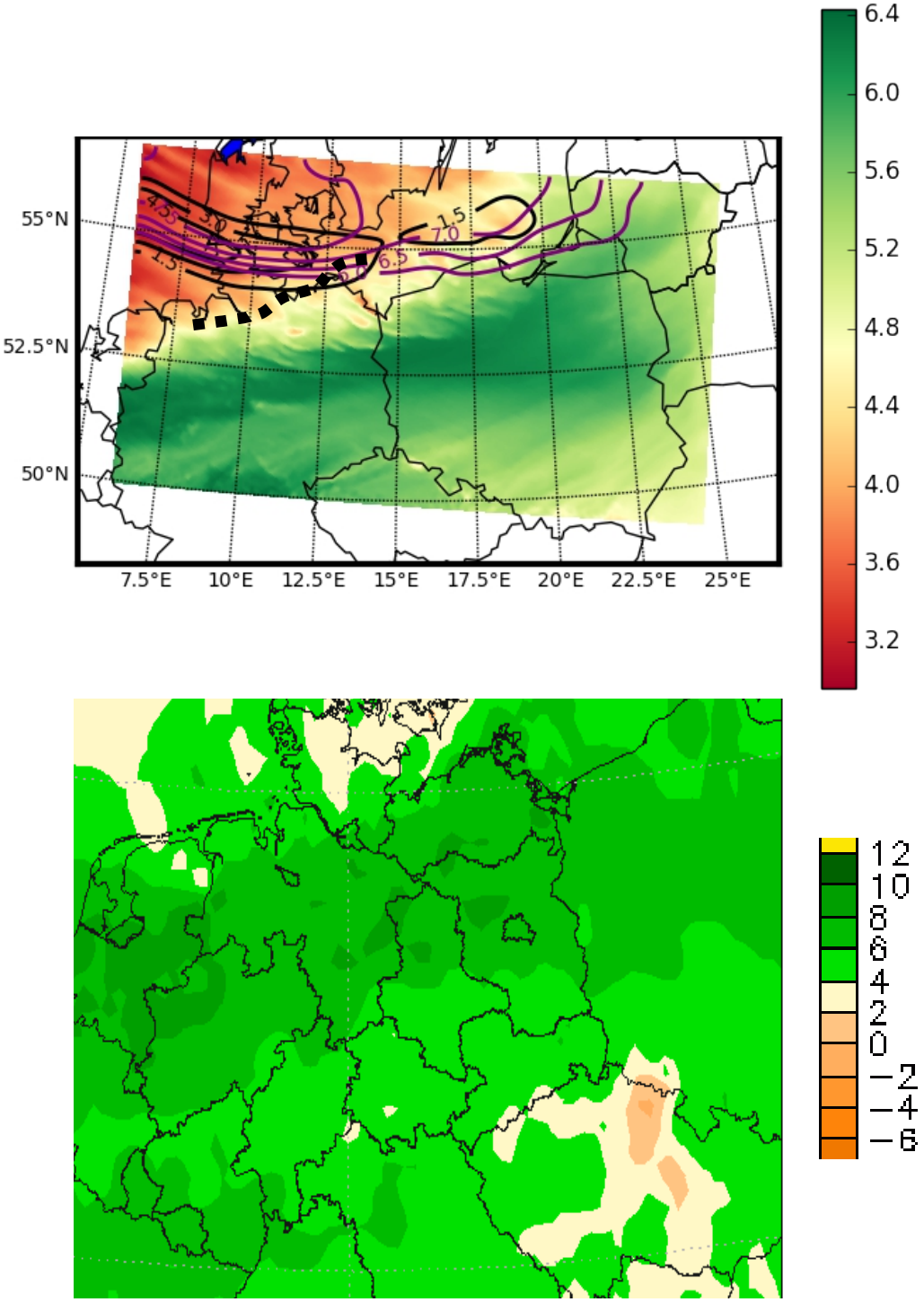

Figure 52: *22 February 2008, 21 UTC. Top: Derecho position, based on diagnostic data (dotted line), and simulated fields of low-level moisture (975 hPa, shaded, in g/kg), lapse rates (thin purple lines every 0.5 K/km, starting at 6 K/km) and PV (black lines every 1.5 PVU, starting at 1.5 PVU). Bottom: Interpolated surface dewpoint field derived from SYNOP data. Dewpoint is given in °C according to the color bar to the right. Data source: Deutscher Wetterdienst / Image courtesy: MeteoGroup.*

main low-level moisture gradient (Fig. 52, bottom). In the model, rich moisture has been already replaced and pushed south-east. As a consequence, steep lapse rates calculated from the model fields may overlap with the rich moisture near the coasts nevertheless. This overlap matches the area of lightning activity and highest wind gusts. In contrast to most low-instability derechos introduced in this section, the axis of the PV intrusion is nearly parallel to the cold-frontal rain band. At the same time, the rain band is located at the anticyclonically sheared flank of the PV intrusion (i.e. to the south in Fig. 52, top). Derechos can therefore develop at both flanks of PV intrusions, although most events are located close to the axis or at the cyclonically sheared flank. Gatzen (2011) found that narrow cold frontal rain bands were typically weak at the anticyclonically sheared flank of mid-level jet streaks. However, sometimes, they were quite intense as well and produced lightning. This was the case when the PV intrusion moved towards the area of the rain band.

1 March 2008 ("Emma derecho")

This derecho was the most intense event of the complete analysis period between 1997 and 2014. It produced a wide and 1500 km long path of very strong wind gusts exceeding 33 m/s and numerous wind gusts between 38 and more than 40 m/s (Fig. 53). Three large bowing lines formed over Germany in the early morning along a cold-frontal rain band. The southern persistent bow echo crossed eastern Austria in the late morning and caused extreme wind damage (Pistotnik et al., 2011). All three bow echoes are nicely displayed as separate areas of lightning occurrence between 5 and 6 UTC (Fig. 54). In between, the narrow cold-frontal rain band does not produce lightning. It can be speculated that convective cold pools formed in association with the most intense convection, and that these cold pools favored new initiation of intense storms. This would mean that there are internal factors in this low-instability derecho that contribute to the derecho. This can be deeper lift along the cold pool's gust front compared to that of the cold-frontal rain band. Additionally, the persistent bowing process could also indicate the development of persistent rear inflow jets. It can be argued that a clear distinction between externally and internally driven derechos is not possible for this and comparable events like the Kyrill event. To the north-east and west and the main bow echoes, the narrow cold-frontal rain band was weaker, but still, wind gusts exceeded 25 m/s at many locations.

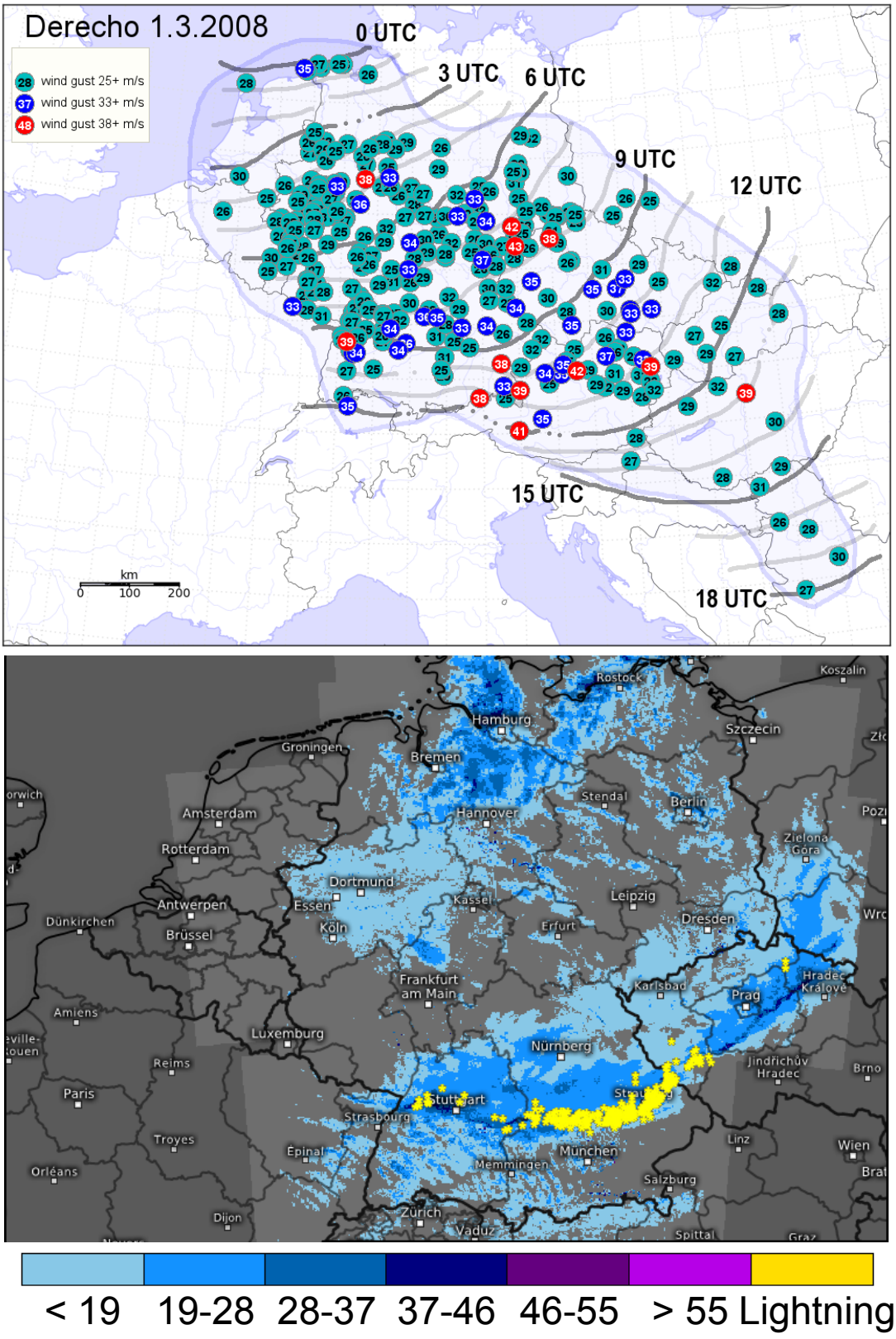

Figure 53: *Top: Wind measurements (dots, in m/s) and hourly derecho position (thick lines, labeled every third line) on 1 March 2008. The affected area is highlighted in blue. Bottom: Radar composite image of 1 March 2008, 09 UTC and lightning detection (yellow stars) between 08:45 and 09 UTC. Radar reflectivity is given in dBZ by the color bar. Data source: Deutscher Wetterdienst / Image courtesy: Kachelmann GmbH (bottom).*

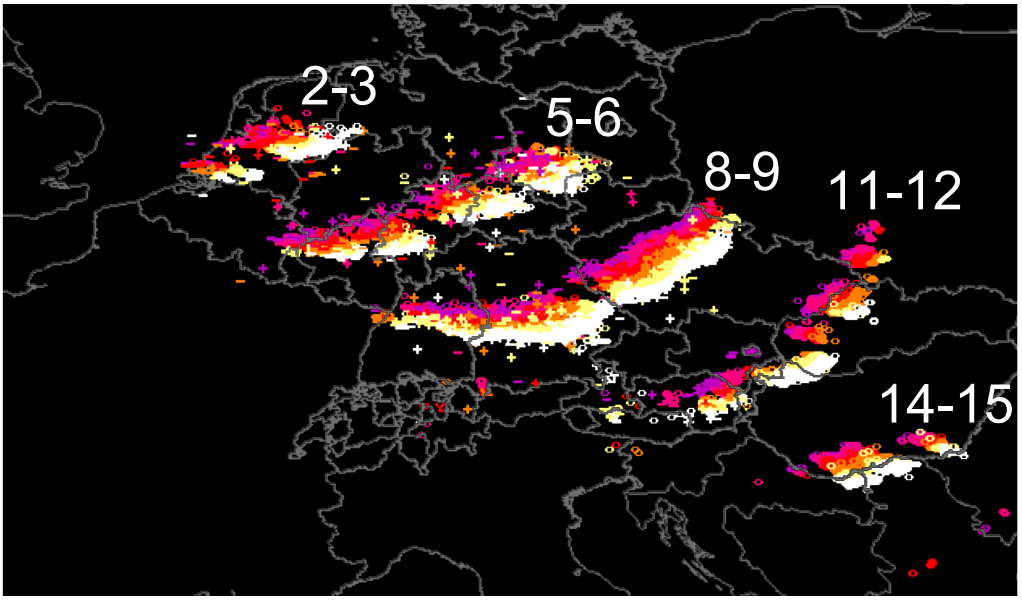

Figure 54: *1 March 2008: Hourly lightning data (displayed for 15 minutes intervals (symbols colored from white – purple backward in time). Data is given every three hours (in UTC as labeled in the figure). Data source: Deutscher Wetterdienst / Image courtesy: MeteoGroup.*

A sharp surface moisture gradient at the gust front of the derecho was reproduced by the COSMO simulation (Fig. 55, top). However, the observed derecho was significantly ahead of the modeled gust front across southern Germany and the Czech Republic (Fig. 55, bottom). This means that the derecho gust front moved faster in comparison to the model whereas the cold-front farther west across France and farther east across Poland was even slower compared to the model. Again, large gradients of the lapse rate occurred close to the derecho. In the simulation, the lapse rate in the pre-frontal moist air increases to more than 6.5 K/km ahead of the derecho across south-eastern Germany and the Czech Republic. Just north of the gust front, the lapse rate decreases to less than 6 K/km due to cold air masses near the ground. The overlap of moisture and lapse rates is relatively large in the model, however, given that the derecho was faster in reality, this overlap may have been quite limited. The PV intrusion of this case is aligned with a broad portion of the cold-frontal rain band. From southern Poland to south-eastern Germany, it is nearly parallel to it. Farther west, the derecho path is well south-west of the PV intrusion, i.e. at the anticyclonically sheared flank.

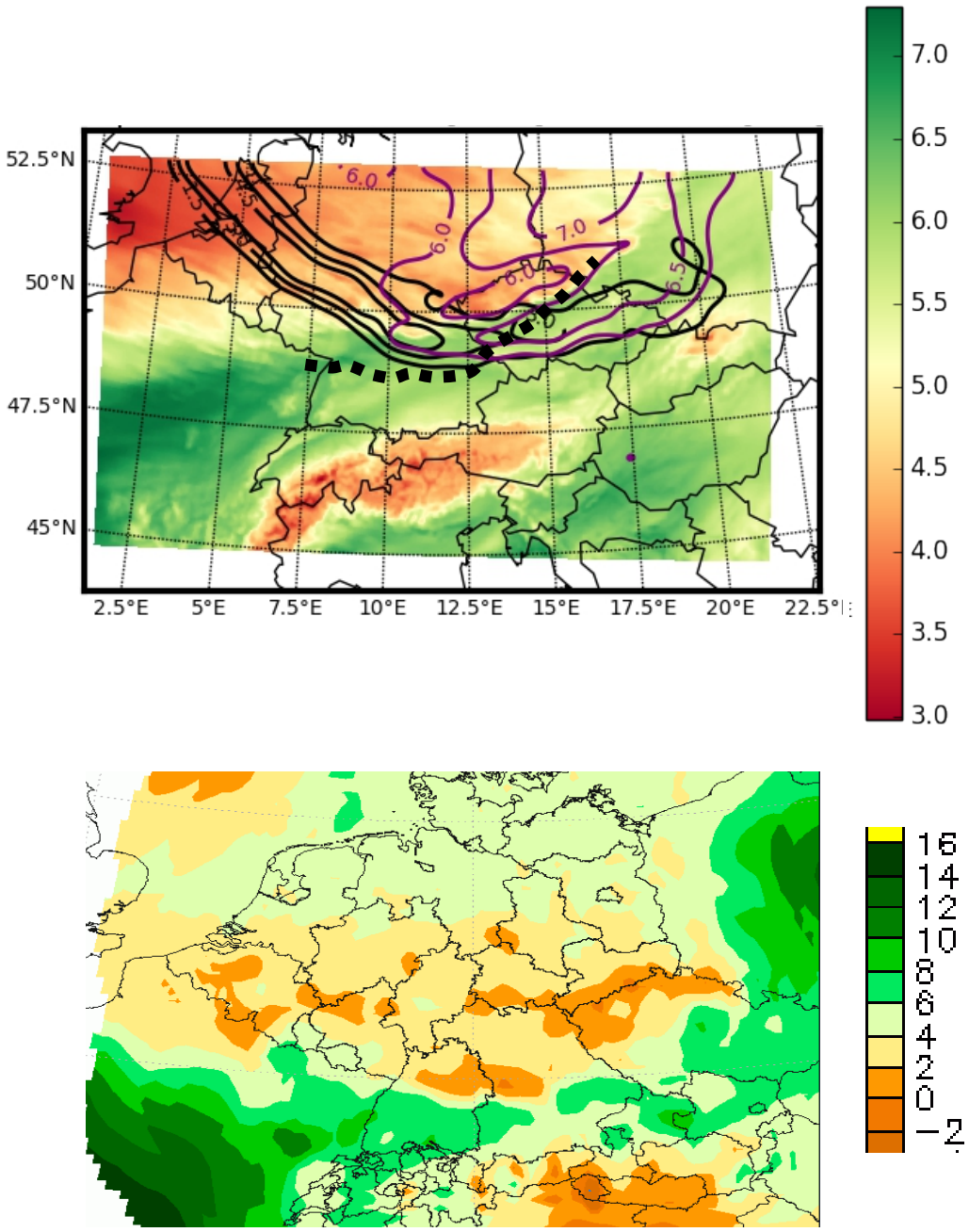

Figure 55: *01 March 2008, 09 UTC. Top: Derecho position, based on diagnostic data (dotted line), and simulated fields of low-level moisture (975 hPa, shaded, in g/kg), lapse rates (thin purple lines every 0.5 K/km, starting at 6 K/km) and PV (black lines every 1.5 PVU, starting at 1.5 PVU). Bottom: Interpolated surface dewpoint field derived from SYNOP data. Dewpoint is given in °C according to the color bar to the right. Data source: Deutscher Wetterdienst / Image courtesy: MeteoGroup.*

3 January 2014

The derecho of 3 January 2014 did not form at a narrow cold-frontal rain band. As in the second event of 28 January 2002, it formed from clusters of storms. These initiated over north-western France and merged to storms that developed across southern England. A larger cluster of storms moved farther east where an embedded bow echo approached over western Germany in the evening. Most wind gusts were marginally severe with about 25 m/s, but from a few locations, more than 33 m/s were reported (Fig. 56, top). Since the high winds over France and England are measured at exposed locations, the derecho was classified as a low-end intensity event. The bow echo was associated with frequent lightning (Fig. 56, bottom). As a side note, large hail up to 3 cm in diameter was observed according to reports in the ESWD. Large hail was also reported with the initial storm cluster over southern England that produced damage and even injuries at around 10 UTC.

As for the other events, a PV intrusion was observed close to the derecho that formed to the east at the anticyclonically sheared flank (Fig. 57, top). Aligned with the axis of the PV intrusion was a large lapse rate gradient, and lapse rates exceeded 7.5 K/km over southern England and northern France at 18 UTC. A band of rich low-level moisture extends from southern and eastern France to the Benelux countries and western Germany. The location of this moisture field is well simulated by the model, although the western edge over the Netherlands is too far to the west. This means that the derecho gust front moved faster in reality compared to the model. The rather large overlap of rich moisture and steep lapse rates indicated over the Benelux countries may have been smaller based on the surface dewpoint field (Fig. 57, bottom).

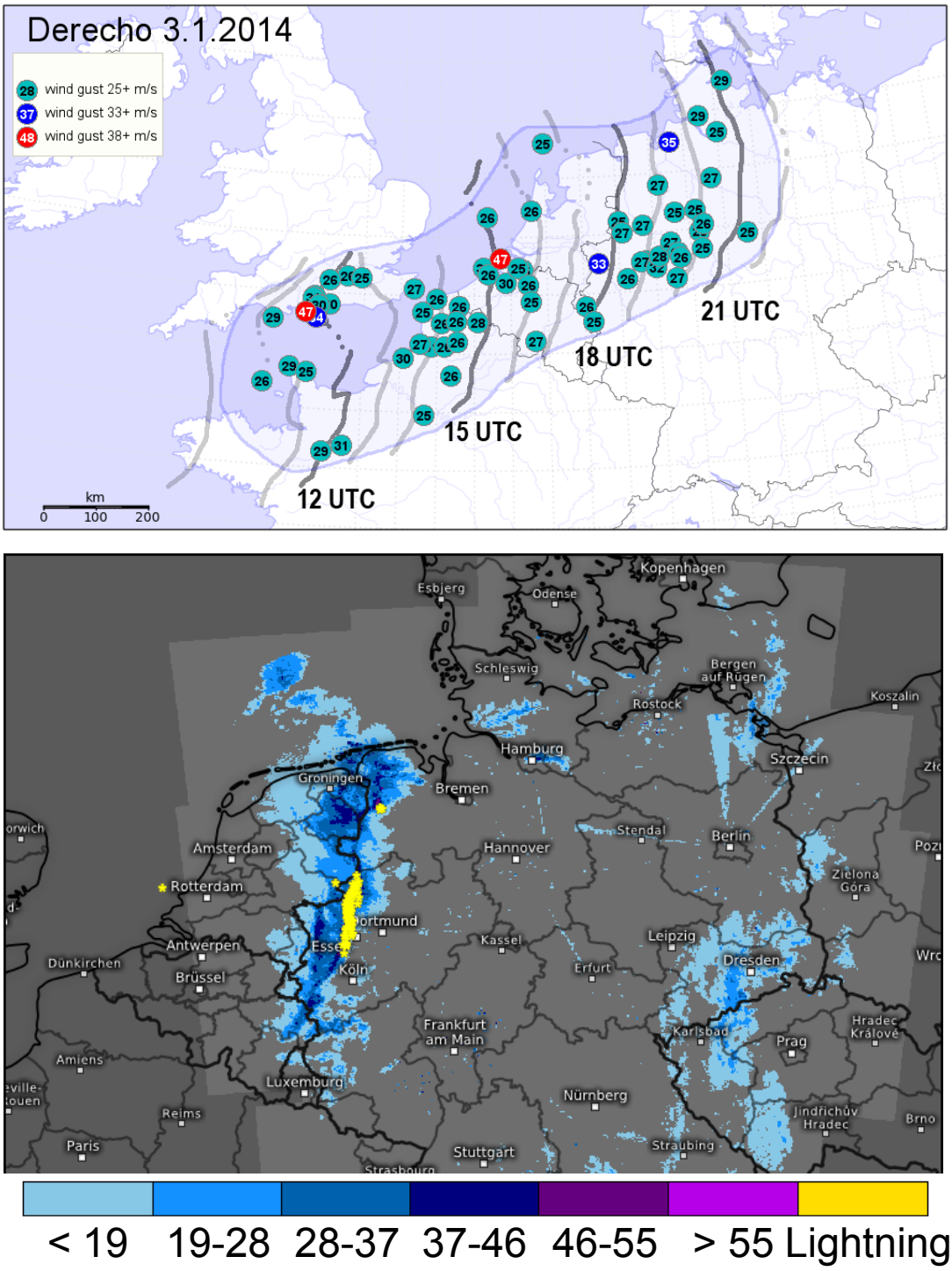

Figure 56: *Top: Wind measurements (dots) and hourly derecho position (thick lines) on 3 January 2014. UTC time is labeled at the end of every third line. Wind speeds are given in m/s, the affected area is highlighted in blue. Bottom: Radar composite image of 3 January 2014, 18 UTC and lightning detection between 17:45 and 18 UTC. Radar reflectivity is given in dBZ by the color bar below the radar image. Lightning detection is given by yellow stars. Data source: Deutscher Wetterdienst / Image courtesy: Kachelmann GmbH (bottom).*

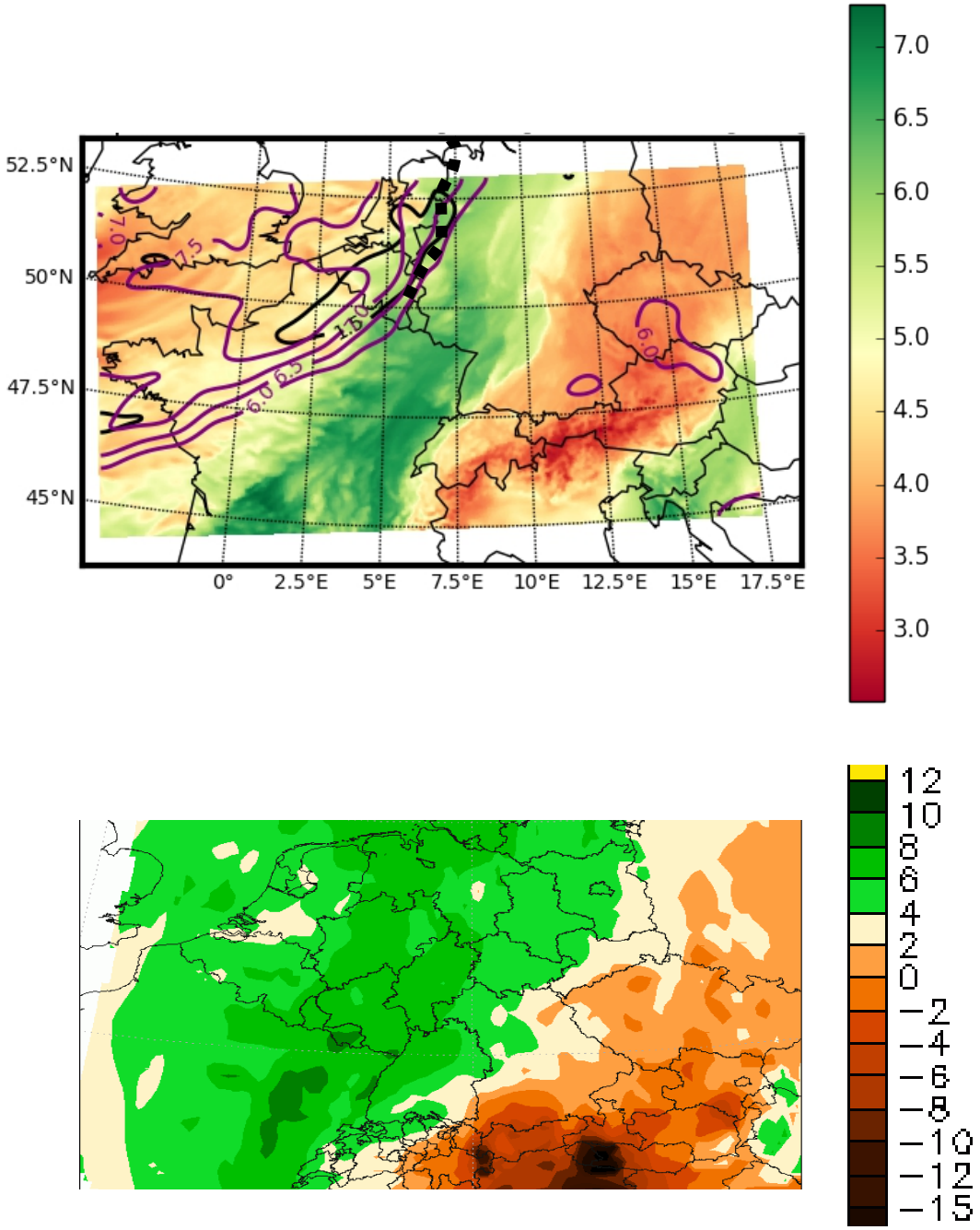

Figure 57: *3 January 2014, 18 UTC. Top: Derecho position, based on diagnostic data (dotted line), and simulated fields of low-level moisture (975 hPa, shaded, in g/kg), lapse rates (thin purple lines every 0.5 K/km, starting at 6 K/km) and PV (black lines every 1.5 PVU, starting at 1.5 PVU). Bottom: Interpolated surface dewpoint field derived from SYNOP data. Dewpoint is given in °C according to the color bar to the right. Data source: Deutscher Wetterdienst / Image courtesy: MeteoGroup.*

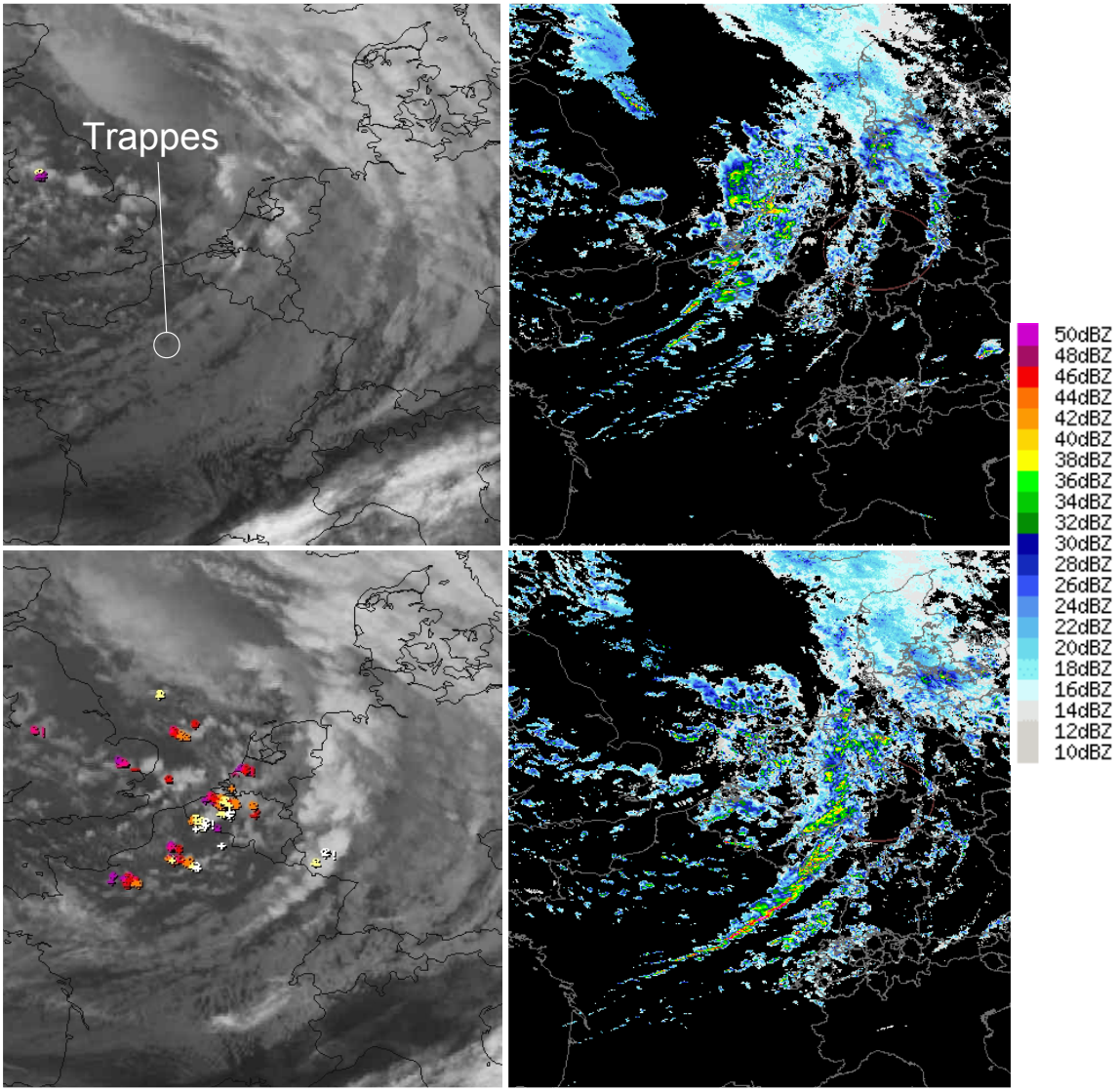

Figure 58: *21 October 2014. Infrared channel satellite image and radar display at 12 (top) and 15 UTC (bottom). The location of a proximity sounding is indicated by the white circle. Image courtesy: MeteoGroup.*

21 October 2014

Finally, we include a derecho in the fall of 2014 to the model analysis. This event was not a clear low-instability derecho as it moved into more unstable air masses close to the Mediterranean Sea (800 J/kg CAPE for the 23 October 2014, 0 UTC Udine sounding, not shown). However, north of the Alps, instability was weak. The derecho formed at noon over eastern France from the central of initially three rain bands (Fig. 58). In the afternoon, the derecho intensified close to the German border where it also started to produce lightning. At 17 UTC a period with

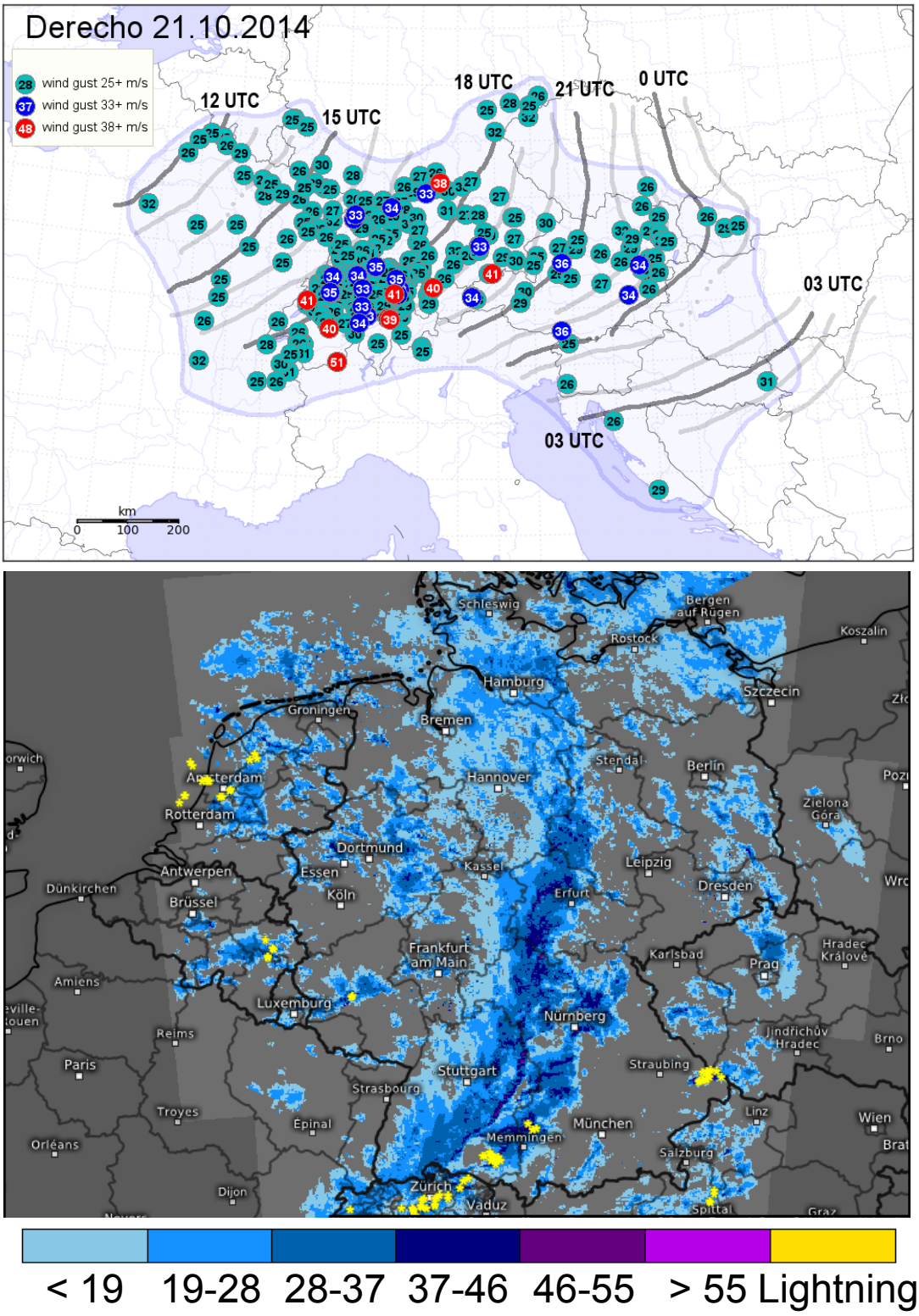

Figure 59: *Top: Wind measurements (dots, in m/s) and hourly derecho position (thick lines, labeled every third line) on 21 October 2014. The affected area is highlighted in blue. Bottom: Radar composite image of 21 October 2014, 15 UTC and lightning detection (yellow stars) between 14:45 and 15 UTC. Radar reflectivity is given in dBZ by the color bar below the radar image. Data source: Deutscher Wetterdienst / Image courtesy: Kachelmann GmbH (bottom).*

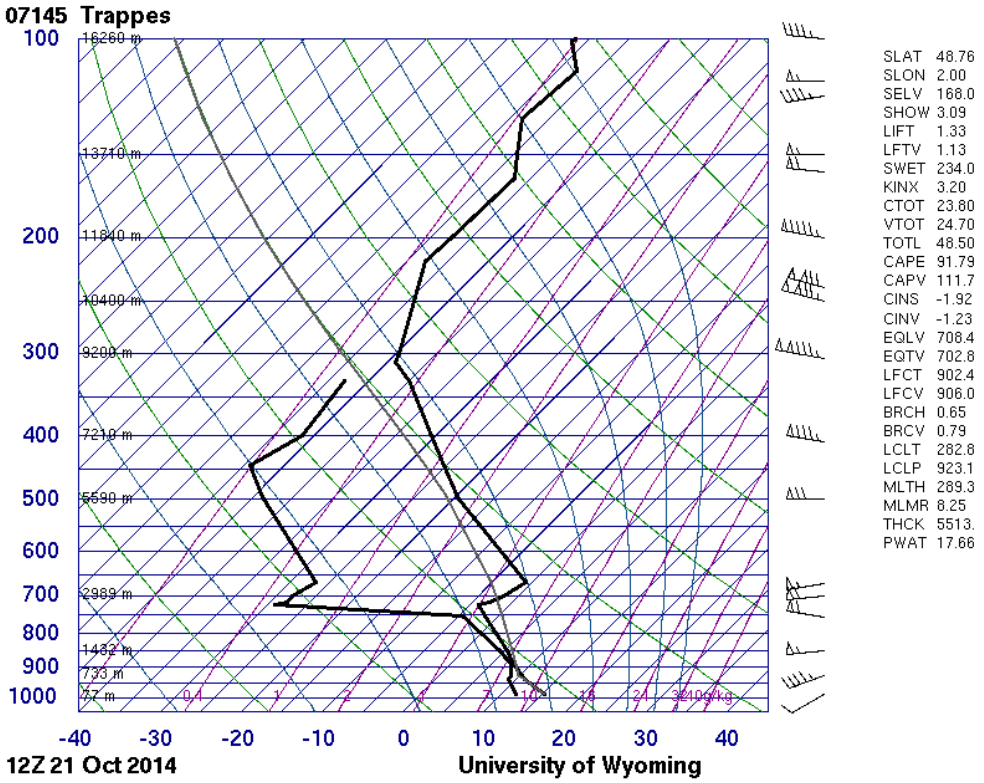

Figure 60: *Skew-T/log p diagram at Trappes on 21 October 2014, 12 UTC. Image courtesy: University of Wyoming.*

very high winds started while the derecho moved across Switzerland, southern Germany, and Austria (Fig. 59, top). As for the "Kyrill" derecho, thunderstorms formed ahead of the derecho that merged to the narrow cold-frontal rain band (Fig. 59, bottom). A well developed bow echo was visible on the radar displays in the evening when the derecho moved over south-eastern Germany into Austria (not shown).

A proximity sounding was available from Trappes close to the genesis region of the derecho (Fig. 60). At mid levels, dry air masses are present that could be attributed to the PV intrusion. At 700 hPa, it looks like the bottom of the dry air is lifted so that the cooler air below becomes deeper. At low levels, rich moisture is present and overlaps with steep lapse rates between 900 and 720 hPa. Relatively large CAPE is calculated in this layer. At the same time, very strong low-level vertical wind shear is present.

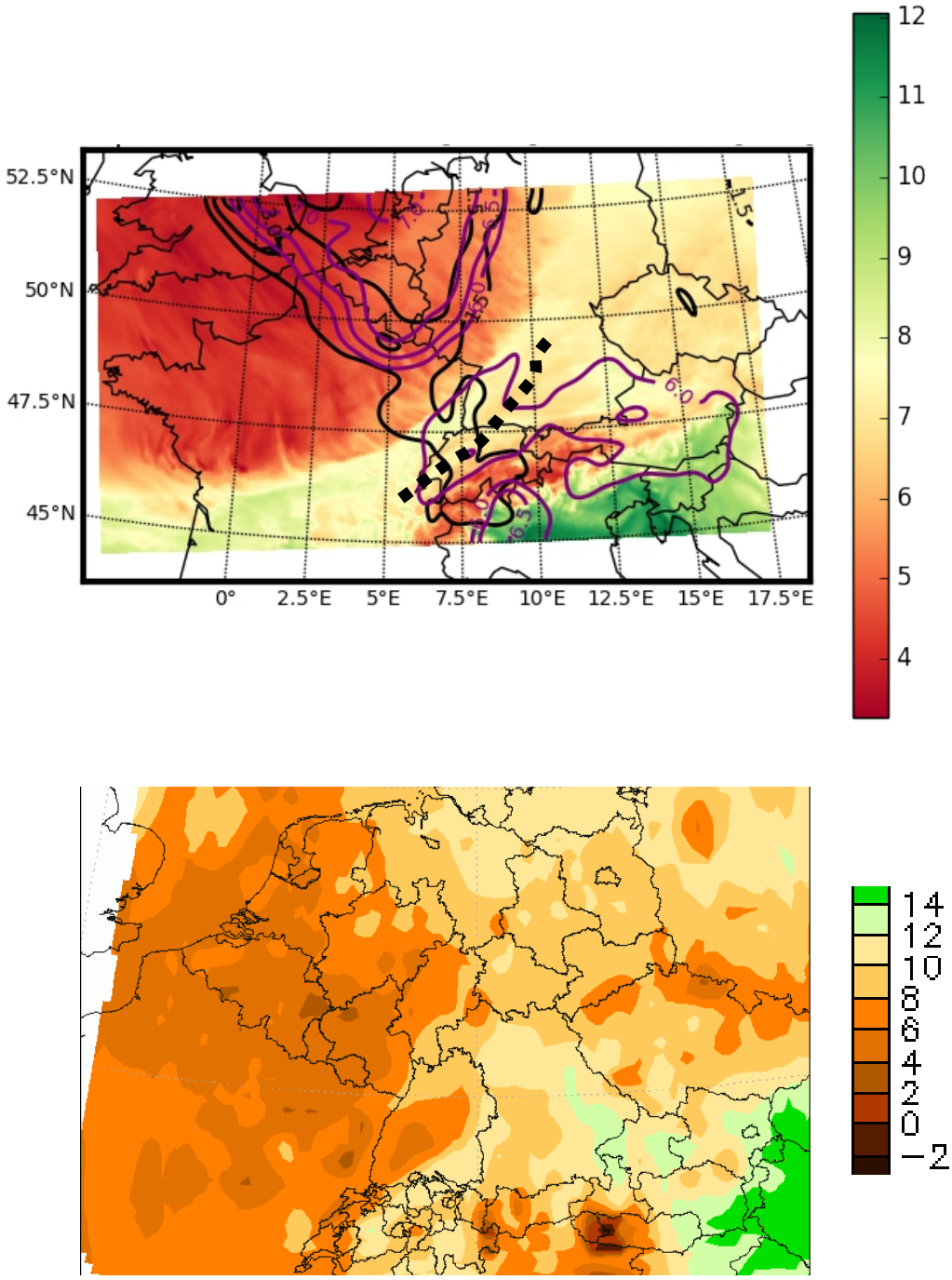

Figure 61: *21 October 2014, 18 UTC. Top: Derecho position, based on diagnostic data (dotted line), and simulated fields of low-level moisture (975 hPa, shaded, in g/kg), lapse rates (thin purple lines every 0.5 K/km, starting at 6 K/km) and PV (black lines every 1.5 PVU, starting at 1.5 PVU). Bottom: Interpolated surface dewpoint field derived from SYNOP data. Dewpoint is given in °C according to the color bar to the right. Data source: Deutscher Wetterdienst / Image courtesy: MeteoGroup.*

The PV distribution at 600 hPa as derived from the COSMO simulation is relatively complex (Fig. 61, top). There is a curved PV intrusion extending from eastern England to north-eastern France and farther into western Germany. Steep lapse rates are located at its cyclonically sheared flank. However, a region of high PV values can be also followed from eastern France to Switzerland. Lapse rates that exceed 6 K/km are present to the east of this feature as well. Only this second area overlaps with the moist pre-frontal air mass in the model simulation. As indicated by the radar image and the surface dewpoint chart (Fig. 61, bottom) the derecho gust front has moved farther into south-western Germany compared to the COSMO simulation.

Summary

In this group of low-instability derechos, there are four events of low-end intensity, three of moderate intensity (18 January 2007, 22. February 2008, and 21 October 2014), and one of high-end intensity (1 March 2008). The spatial density of severe wind measurements is variable. For example, the second half of the path of the 22 February 2008 derecho shows relatively large gaps with no wind reports over Poland compared to events like 18 January 2007 with a higher concentration of severe wind gusts. The track lengths of the derechos varies between 430 km (second derecho of 28 January 2002) and 1600 km (21 October 2014), the path width between less than 100 km (second derecho of 28 January 2002) and more than 800 km (derecho of 1 March 2008). One path is towards the north-east (3 January 2014) whereas all others are to the south-east.

Most events evolved along cold fronts and associated narrow cold-frontal rain bands as indicated on plan-view radar displays that were frequently embedded in stratiform precipitation. Within the derecho paths, relatively high radar reflectivity, lightning, graupel (not shown), and increasing cold pools (not shown) occurred. Two events did not form along narrow cold-frontal rain bands but were rather associated with groups of thunderstorms that merged to bow echoes later on. One is the derecho of 28 January 2002. On this day, groups of storms produced three paths of severe wind gusts. There were two bow echoes of which one was associated with a severe wind path that was more than 400 km long. On 3 January 2014, two groups of storms on both sides of The Channel merged to a linear mesoscale convective system with an embedded bow echo. Both events

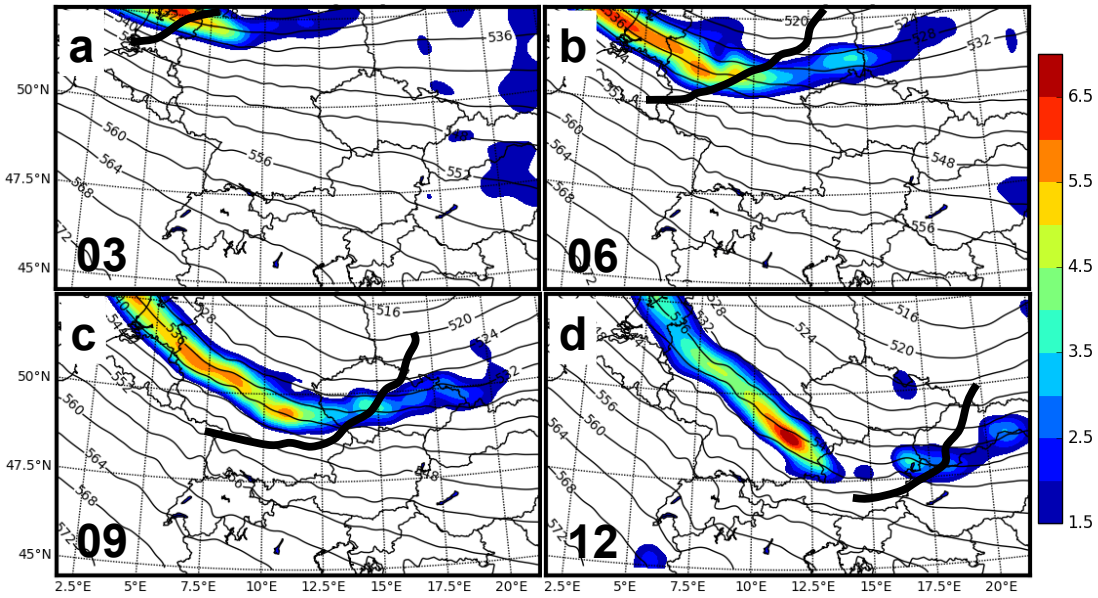

Figure 62: *PV at 600 hPa (in PV units given by the color bar to the right) and derecho position, based on diagnostic data (black line) of 1 March 2008, displayed in 3-hourly time steps (a – d). Data source: ERA-Interim, ECMWF / Image courtesy: MeteoGroup.*

formed behind a cold front in the cold sector of a cyclone; the event of 28 January 2002 even in the wake of a cold-frontal derecho.

The COSMO model was run in order to analyze the derecho environment in higher resolution. The position of the derecho gust fronts in the model simulation were compared to reality. Compared to the location of the gust front as indicated by ground observations and radar images, there were only small differences. The largest deviations was found for the event of 22 February 2008 when the simulated gust front was about 100 km ahead of the observed derecho. On 1 March 2008 and 21 October 2014, the simulated gust fronts are about 50 km behind the observed derecho position.

The close relationship of low-instability derechos and PV intrusions as summarized from the literature review (section 2.7) is confirmed for the investigated events. The charts of potential vorticity at 600 hPa indicate PV intrusions with PV exceeding 1.5 PVU. These PV intrusions were close to the derecho gust fronts during the derecho lifetime. This was especially evident from the temporal evo-

lution of derecho gust front and PV intrusion, e.g. on 1 March 2008 (Fig. 62). The orientation of the axis of PV intrusions at 600 hPa relative to the derecho gust front is quite variable. In some situations, the axis of the PV intrusions cross the central parts (28 December 2001 and 28 January 2002) or the right flank (18 January 2007, 3 January 2014, 21 October 2014) of the derecho gust front at a large angle. Here, the right flank is on the right hand side when looking with the derecho motion vector. However, the derecho gust front can also be nearly parallel to the axis of the PV intrusion (22 February 2008), or the relative orientation of both features change along the gust front, as in the case of the curved PV intrusion on 3 March 2008. In relation to the derecho gust front it can be followed that wide derecho paths occur when the axis of PV intrusions is more aligned with the low-level gust front. Larger angles are associated with narrower derecho paths. This can be seen as an indication of a close relation between PV intrusions and derechos.

The presence of PV intrusions close to derechos may help to explain how intense, persistent convective storms needed for derecho formation (section 2.6) are initiated even though proximity soundings sometimes indicate zero CAPE (section 4.3). CAPE is a combination of two necessary ingredients for deep moist convection, i.e. moisture and lapse rates. One or both of these could be affected by the PV intrusion so that CAPE builds. Consequently, the analysis focuses on gradients of moisture and lapse rates close to PV intrusions that would explain rapid local changes of these ingredients. The fields of low-level moisture presented in the charts frequently show an elongated band of relatively high mixing ratio. These tongues of moisture extend ahead of a large moisture decrease that marks surface cold fronts. Although most derechos formed at these cold fronts, they also formed in the wake of it.

In many situations, the forward flank of the moisture tongue also displays a large moisture gradient. This moisture gradient causes an increase in local low-level humidity. However, this increase is sometimes far away from the PV intrusion (e.g. over eastern Poland on 22 February 2008, Fig. 52). In some cases, a moisture gradient that would cause a rapid increase of local humidity is missing (28 January 2002, second derecho and 21 October 2014). It follows that close to PV intrusions a large increase of low-level moisture is not always indicated in the COSMO charts. Compared to data presented by Sherburn et al. (2016) from the south-eastern United States that indicated low-level moisture advection to be re-

sponsible for CAPE development, the presented events do not indicate a strong moisture increase. Moisture advection can be expected to be relatively strong across the south-eastern United States due to the Gulf of Mexico as a source of rich boundary layer moisture nearby. It can be assumed that moisture advection is typically weaker in Central Europe due to the large distance of potential sources like the Bay of Biscay. But moreover, the absence of a local low-level moisture increase may reflect that moisture advection is not needed for the development of CAPE. A complete calculation of moisture advection and its effect on conditional instability evolution is not given in this study, though, so that this factor cannot be ruled out. Instead, cases like the event of 28 December 2001 that do not show a local moisture increase at proximity sounding sites are used to justify a closer look at lapse rate changes to explain the observed development of conditional instability.

A correlation can be seen between steep lapse rates and PV intrusions. In all charts, lapse rates are generally weaker on the anticyclonically sheared flank of PV intrusions, whereas lapse rates increase to more than 6 K/km at the cyclonically sheared flank. The lapse rate gradient is largest along the PV intrusion and oriented perpendicular to the axis of highest PV. This correlation can be observed over time similar to the example in figure 63, so that the lapse rate gradient moves with the PV intrusion: For locations where PV increases with time, there is also a tendency for local lapse rate increase with time. It follows that in the presented cases PV intrusions are especially associated with local lapse rate changes. These could explain that derecho proximity soundings sometimes do not indicate CAPE: In the time after the sounding launch, changes of the local lapse rate can lead to positive CAPE until the derecho approach. On the other hand, the calculated lapse rates between 900 and 650 hPa are close to the moist adiabatic lapse rate and may just reflect the presence of moist adiabatic ascent, possibly due to forced lift, e.g. at a front, or due to deep moist convection. Cross sections that cut through the PV intrusion will be presented in the next section to discuss if conditional instability evolves.

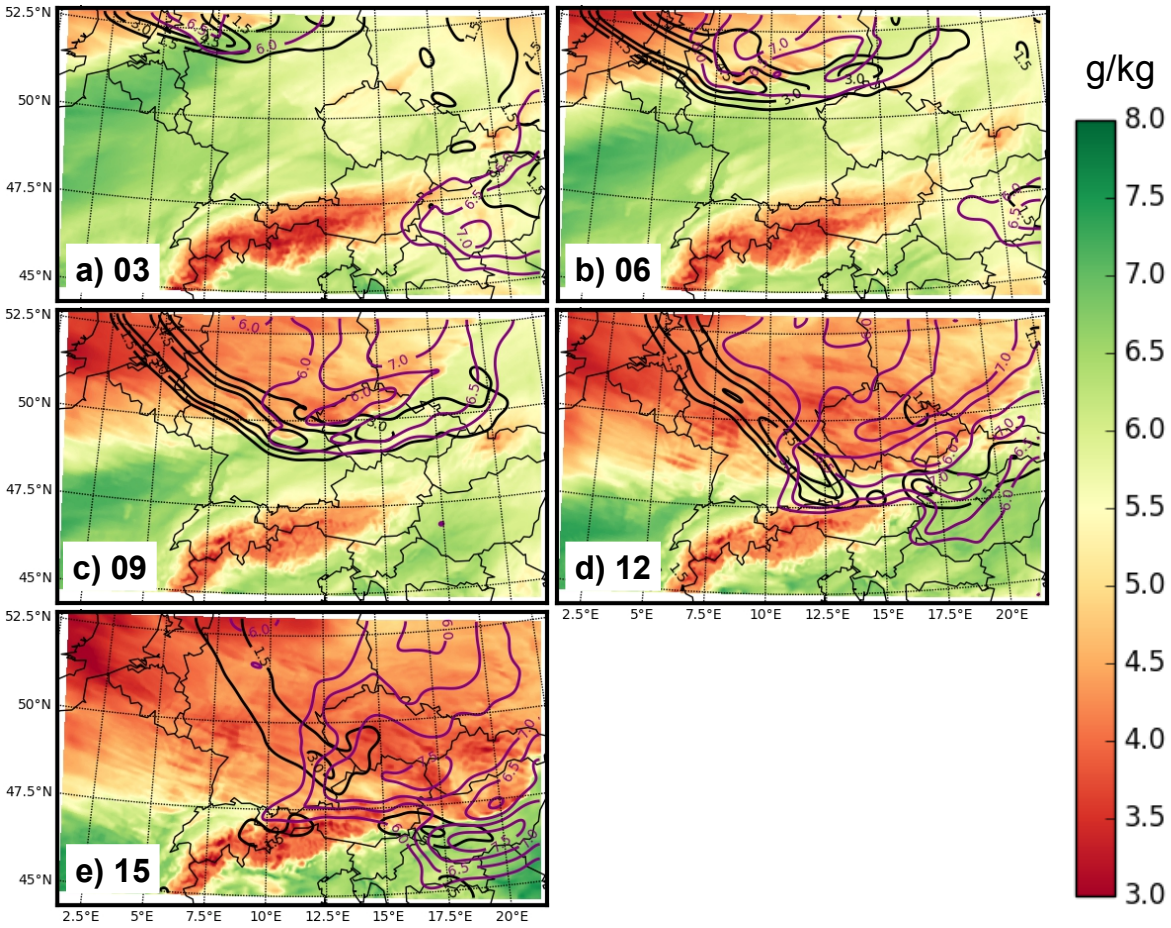

Figure 63: *COSMO simulation of 1 March 2001 at 03 – 15 UTC (a – e). Mixing ratio at 975 hPa (in g/kg, shaded as given by the color bar to the right), PV at 600 hPa (black lines, labels in PVU), and 900 – 650 hPa lapse rate (purple lines, labels in K/km).*

4.4 Cross sections of PV, lapse rate, and low-level moisture

The relation of steep lapse rates and PV intrusions is additionally visible in vertical cross sections. The PV intrusion is indicated by a wedge of high PV values extending from the tropopause level down to mid levels (Fig. 64). For some of the examined strongly-forced situations, PV intrusions descended well below 600 hPa. The intrusion of upper-level air masses is also indicated by low mixing ratios compared to the area south or west of the PV intrusions.

The lapse rate between 900 hPa and any level above starting at 850 hPa exceeds 6 K/km and locally even 7.5 K/km below the PV intrusions (Fig. 64, right, purple

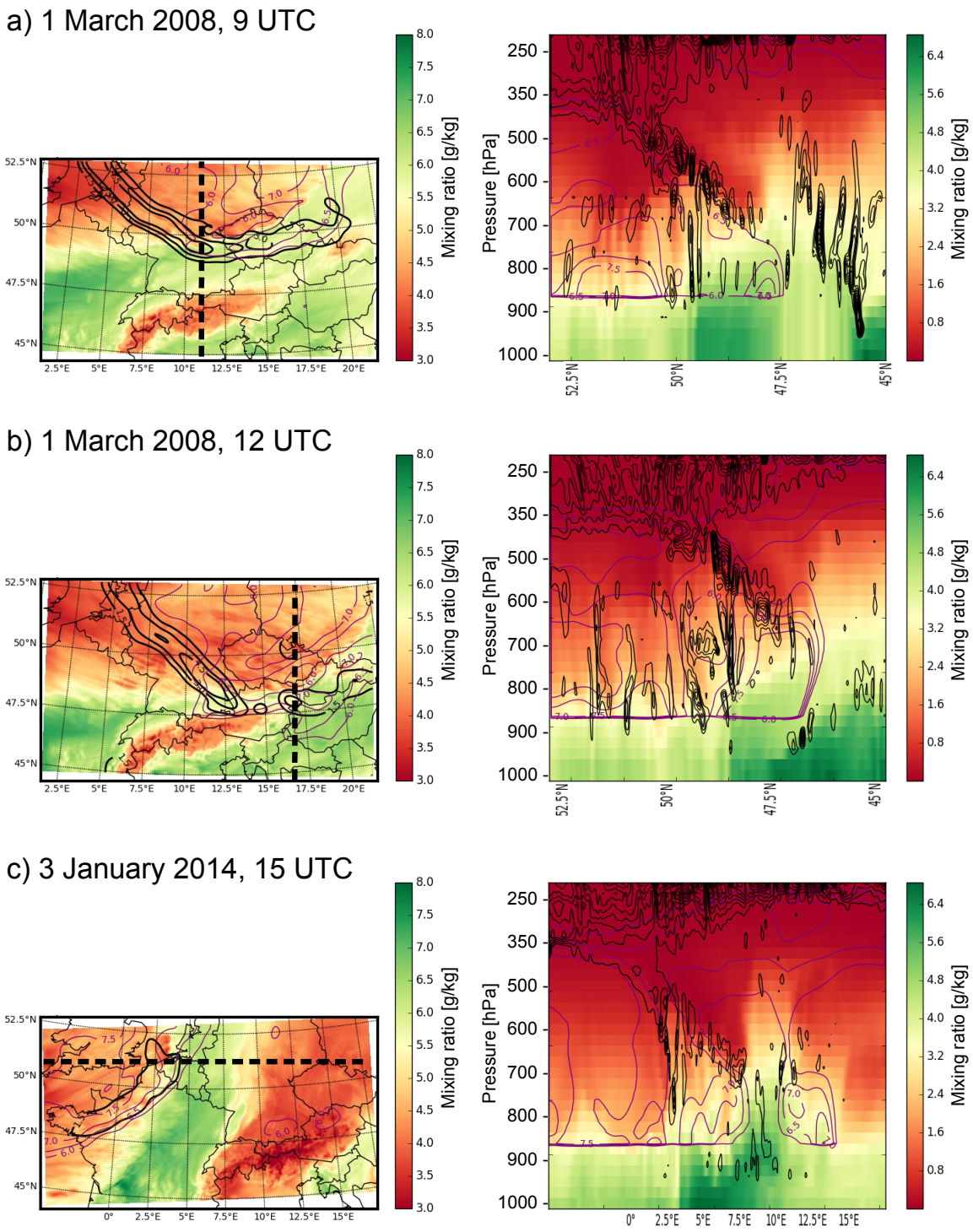

Figure 64: *Model cross sections on 1 March, 2008, 09 (a) and 12 UTC (b) and 3 January, 2014, 15 UTC (c). Right: Cross sections. Mixing ratio (shaded), lapse rate between 900 hPa and any model output level starting at 850 hPa (purple thin lines every 0.5 K/km, starting at 6 K/km), and PV (thick black lines every 1.5 PVU, starting at 1.5 PVU). Left: Low-level moisture at 975 hPa (shaded), lapse rates (900 to 650 hPa; thin purple lines every 0.5 K/km, starting at 6 K/km) and PV (600 hPa; black lines every 1.5 PVU, starting at 1.5 PVU). Positions of the cross sections displayed on the right are given by the dotted black lines (left).*

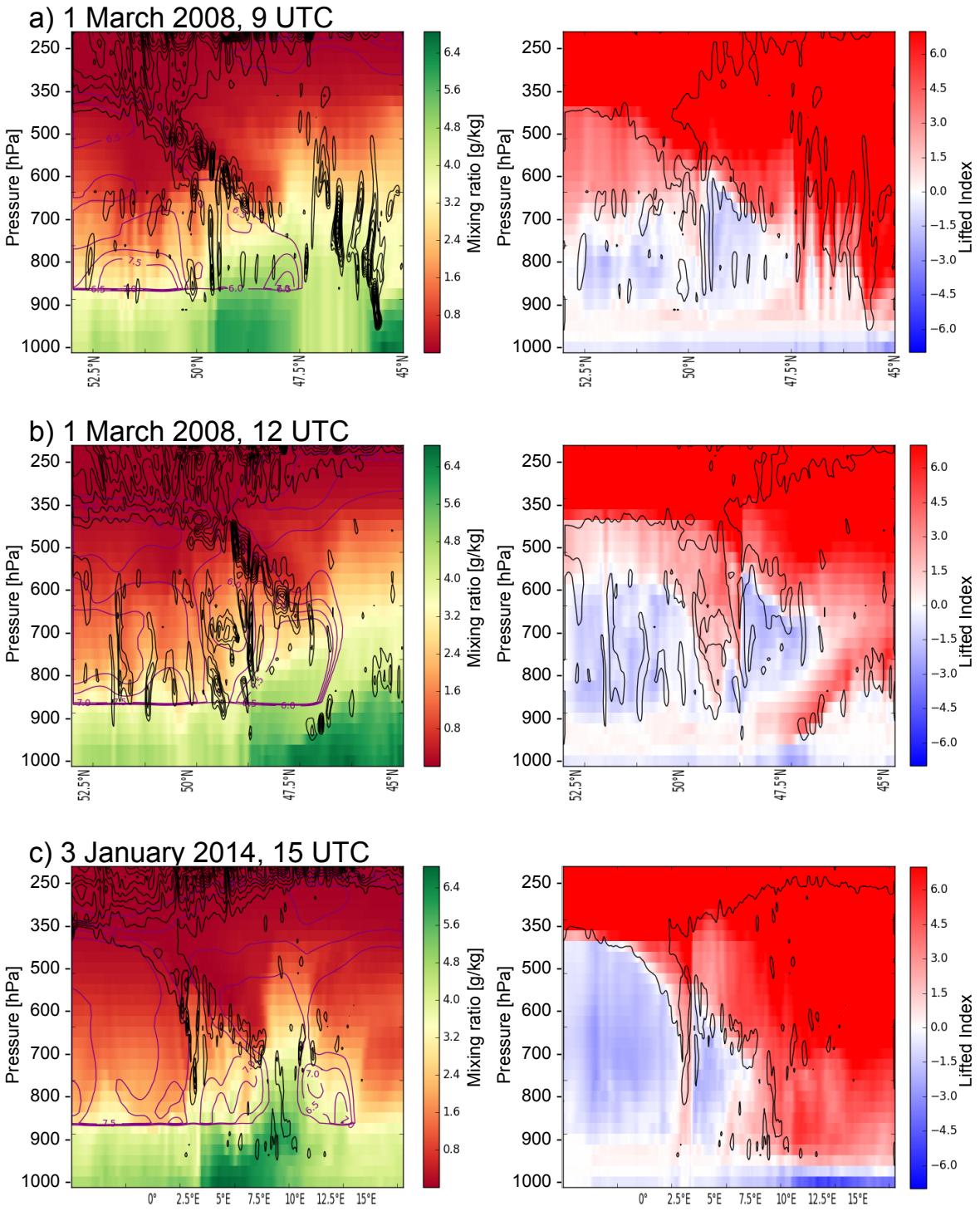

Figure 65: *Cross sections on 1 March, 2008, 09 (a) and 12 UTC (b) and 3 January, 2014, 15 UTC (c). Left: Mixing ratio (shaded), lapse rate between 900 hPa and any model output level starting at 850 hPa (purple thin lines every 0.5 K/km, starting at 6 K/km), and PV (thick black lines every 1.5 PVU, starting at 1.5 PVU). Right: Lowest 100 hPa mixed layer Lifted Index for every model output level (shaded), and 1.5 PVU isoline (black). Approximated positions of the cross sections are given in Fig. 64*

.

contours). Steep lapse rates are also located close to the ground, in particular where the noses of the PV intrusions reach their lowest position, and the layer of steep lapse rates becomes deeper where the PV intrusions are higher. Eventually, steep lapse rates can be found up to the tropopause where the PV intrusion starts.

Horizontal gradients of low-level mixing ratio can be also seen in the vertical cross sections, for example on 3 January 2014 between 2.5 and 5°E (Fig. 64c). Comparing these moisture gradients to the horizontal cross sections indicates that PV intrusions and associated steep lapse rates frequently cross low-level cold fronts. As a consequence, there are locations where steep lapse rates overlap with rich pre-frontal low-level moisture.

The overlap of steep lapse rates and rich low-level moisture results in conditional instability that can be detected by cross sections of the Lifted Index. The values of the Lifted Index as well as of CAPE are sensitive to the choice of the lifted air parcel. Here, a mixed layer parcel is used that typically has less chances to become positively buoyant compared to the most unstable parcel. Plotting the Lifted Index at every model output level using the lowest 100 hPa (between 1000 and 900 hPa) mixed parcel indicates negative values, i.e. conditional instability typically below the PV intrusion (Fig. 65, negative Lifted Index shaded in blue). The level of free convection is remarkably close to the ground as can be seen by a negative Lifted Index ahead of the gust front that is indicated by the sharp gradient of low-level mixing ratio (Fig. 65, left, shaded): This unstable zone goes down to 900 hPa, corresponding to a few hundred meters above ground level. Proximity soundings confirm low-based conditional instability (e.g. Fig. 42, bottom).

Together with strong low-level flow, CAPE close to the ground and a low level of free convection can be suggested to support low-instability derechos. A possibility would be that a low level of free convection results in upward acceleration of near-ground air parcels and hence stretching of the low-level air column below a buoyant updraft. In other words, weak CAPE close to the ground may cause the same magnitude of stretching as large CAPE with a level of free convection farther away from the ground. The combination of strong vertical wind shear and stretching close to the ground could effectively support mesovortex development in low-instability derechos. High-resolution trajectory simulations could help to calculate if updrafts in low-instability situations are indeed effective in stretching of low-level vorticity.

The unstable layer increases in depth where the PV intrusion is situated at higher levels. It can be assumed that deep moist convection increases in depth along this direction. This result would explain why cold-season narrow cold-frontal rain bands tend to produce thunder and severe weather mainly below the cyclonically sheared flank of mid-level jets as observed by Gatzen (2011), i.e. where the PV intrusion reaches up to mid levels. Furthermore, a zone of positive Lifted Index can be seen just in the wake of the low-level moisture gradient, approximately at 50°N in Fig. 65a, 49°N in Fig. 65b, and 2.5°E in Fig. 65c. This is likely the result of cold, stable air masses behind the gust front. Another zone of positive Lifted Index is frequently present ahead of the gust front, e.g. at 47.5°N in Fig. 65b: This is a low-level zone with convective inhibition that has to be overcome by sufficient lift. Such lift could be provided by the circulation at the gust front or the cold front.

Above the stable layer, steep lapse rates (Fig. 65b, left) result in a rapidly decreasing Lifted Index with height. The upper level of negative Lifted Index remains below the PV intrusion, so that positive buoyancy in the given examples is limited to the air below 600 to 550 hPa. However, deep moist convection likely penetrates the PV intrusion as can be seen by a relatively low Lifted Index ahead of the gust front (up to 300 hPa at 4–5°E in Fig. 65c). Note that the negative Lifted Index at the lowest model levels is an artifact as these pressure levels are below the ground. It does not indicate positive buoyancy for this reason.

4.5 The local lapse rate tendency in model cross sections

Based on model cross sections presented in the previous sections 4.3 and 4.4, local lapse rate changes close to PV intrusions are considered to cause rapid changes of CAPE. This would explain why proximity soundings sometimes do not indicate CAPE close to low-instability derechos, although thunderstorms are observed shortly after the sounding launch. In this section, the local lapse rate tendency is presented for some model cross sections (Fig. 66). Here, the local lapse rate tendency between 900 and 650 hPa is plotted for the same dates and the same cross sections as in Fig. 64.

For all simulated events, a region with positive lapse rate tendency that causes local lapse rate increase can be found ahead, i.e. downstream of PV intrusions (red areas in Fig. 66, right). This region of destabilization at least partly overlaps with the tongue to relatively rich low-level moisture. Close to the derecho, there is an area with a negative lapse rate tendency (blue areas in Fig. 66, right). This can be related to the cold front or the derecho cold pool that leads to low-level cooling and hence stabilization in the regarded layer. This region of stabilization is again followed by positive lapse rate tendency in the wake of the low-level cold air advection regime.

There is another region where sometimes a negative lapse rate tendency was observed. At the anticyclonically sheared flank of some PV intrusions, the local lapse rate decreases (e.g. Fig. 66 a, left, dashed purple contours). From the movement of the PV intrusions, it can be seen that these areas are located at their upstream flank (not shown). A moving PV intrusion was therefore associated with decreasing lapse rates at the upstream flank and increasing lapse rates at the downstream flank as can be expected from theory (section 2.7).

In vertical cross sections that cut through the PV intrusion and the region farther downstream, local lapse rate increase is related to high PV values: At low levels close to the ground, strong lapse rate increase of about 1 to more than 2 $\mathrm{K\,km^{-1}h^{-1}}$ occurs to the south and east of the lowest position of high PV values, corresponding to the bottom nose of the PV intrusion (Fig. 66, right). In the vertical, this area of positive local lapse rate tendency is situated at the lower flank of the PV intrusion and can be followed up to the dynamic tropopause. This correlation was found for all eight analyzed low-instability derechos. In this respect, lapse rate increase was observed downstream of PV intrusions.

4.6 Origin of local lapse rate increase

A large increase of the local lapse rate tendency occurs downstream of PV intrusions according to the model charts given in the previous section. In this section, the local lapse rate tendency equation terms (section 2.8) are analyzed separately in order to investigate which atmospheric processes cause this lapse rate increase.

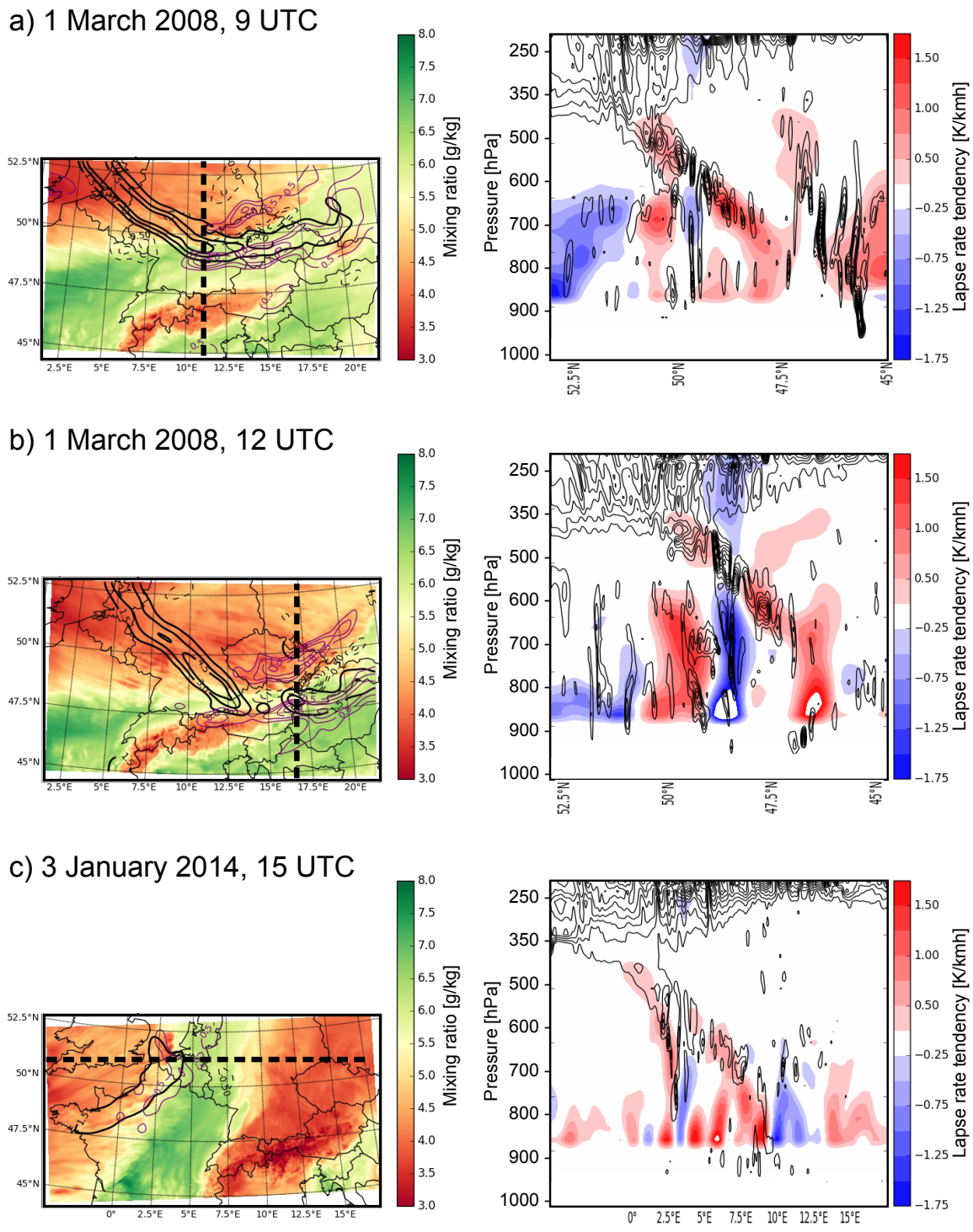

Figure 66: *Model cross sections on 1 March, 2008, 09 (a) and 12 UTC (b) and 3 January, 2014, 15 UTC (c). Right: Cross sections of lapse rate tendency between 900 hPa and any given level (in $K\,km^{-1}h^{-1}$; shaded), and PV (black lines every 1.5 PVU, starting at 1.5 PVU). Left: Low-level moisture at 975 hPa (shaded), lapse rate tendency (900 to 650 hPa; thin purple lines every 0.25 $K\,km^{-1}\,h^{-1}$ for absolute values greater than 0.5 $K\,km^{-1}h^{-1}$) and PV (600 hPa; black lines every 1.5 PVU, starting at 1.5 PVU). Positions of the cross sections displayed on the right are given by the dotted black lines (left).*

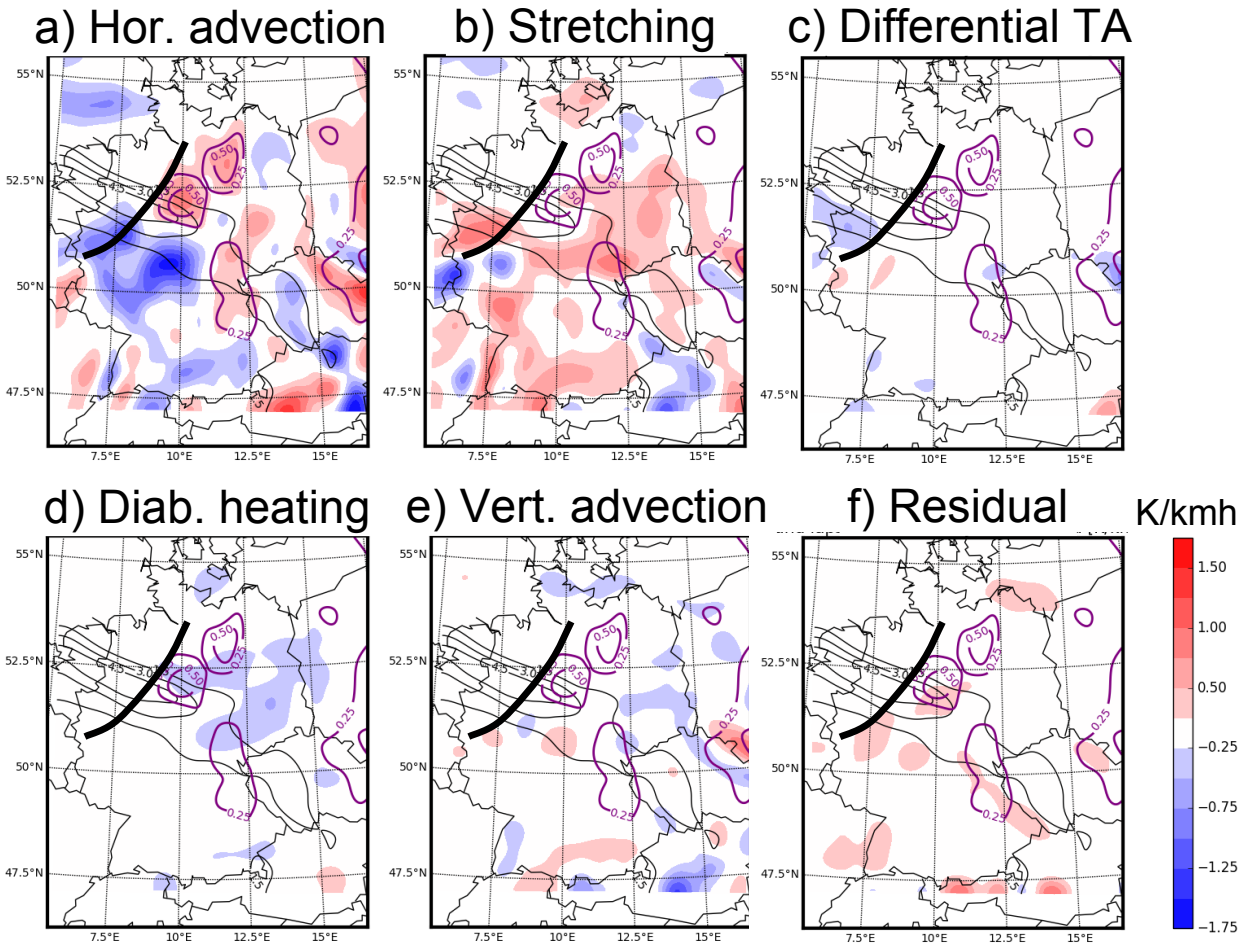

Figure 67: *Terms of the 900 – 650 hPa local lapse rate tendency equation for 28 December 2001, 12 UTC: a) horizontal lapse rate advection term, b) stretching term, c) differential temperature advection term, d) diabatic heating term, e) vertical lapse rate advection term, f) residual term. Values of each term are shaded according to the color bar to the right. The local lapse rate tendency is given by purple lines for values greater than 0.25 $K\,km^{-1}h^{-1}$. PV at 600 hPa is given by thin black lines every 1.5 PVU for values greater than 1.5 PVU. The thick black line gives the observed position of the derecho gust front for reference.*

As expected from the literature review (section 2.8), horizontal lapse rate advection is the dominant term for the 900 – 650 hPa lapse rate increase in COSMO charts (e.g. on 28 December 2001, 9 UTC, Fig. 67). This is especially true for regions with large local lapse rate tendency where the fields of local lapse rate tendency and horizontal lapse rate advection look quite similar (e.g. near 52.5°N / 10°E in Fig. 67 a). However, also other terms can become large on the mesoscale (e.g. Markowski and Richardson, 2011). For the 900 – 650 hPa layer of presented derecho cases, this is especially true for the stretching term (Fig. 67 b).

While both stretching and horizontal advection terms are relatively large in many areas, these terms also tend to cancel each other. This occurs for example where mountains are overflowed (Fig. 68). Over the mountain tops, stability is typically relatively large and isentropic surfaces are close to each other. In the wake of mountains, the distance between isentropes typically increases, corresponding to destabilization. The horizontal lapse rate advection term is then positive over the mountain top and negative in the valleys. At the same time, there is shrinking over the mountains (stretching term is then negative) and stretching in the valleys (stretching term positive). Both terms can cancel each other completely, so that the local lapse rate tendency is zero in total. In the presented example, this can be seen over the Upper Rhine Rift between the Vosges Mountains to the west and the Black Forest to the east (near 47.5° N / 7.5° E in Fig. 67 a) and b): Over the Rhine valley, the horizontal lapse rate advection term is negative, whereas the stretching term is positive. Over the mountains, both terms have opposite signs.

Close to PV intrusions, we see that areas of positive stretching and horizontal advection terms do partly overlap. Similar for all events is that the region with positive stretching is located farther ahead of PV intrusions compared to the horizontal advection. This displacement could be attributed to different processes that influence these terms. Stretching follows the movement of the PV intrusion, horizontal lapse rate advection is determined by the average flow within the considered layer. Since this is at lower levels where the flow is typically weaker compared to the level of the PV intrusion, lapse rate advection and stretching can move differently. This can explain the observed displacement of the stretching term to the downstream region of the strongest advection (Fig. 67 gives an example). The overlap of both terms may vary in space and time and therefore likely contributes to the development of the derecho. A positive overlap for both terms moving in phase would allow for the strongest lapse rate increase for a given PV intrusion.

The magnitude of the other terms of the lapse rate tendency equation were found to be smaller in the 900 – 650 hPa layer (e.g. Fig. 67 c – e). To study the contributions of the individual terms of the lapse rate tendency equation, three-hourly horizontal fields of each term were studied for each event, giving 30 fields altogether. Thereby we found that the horizontal advection and the stretching terms were always prevalent with respect to regions of relatively large lapse rate increase

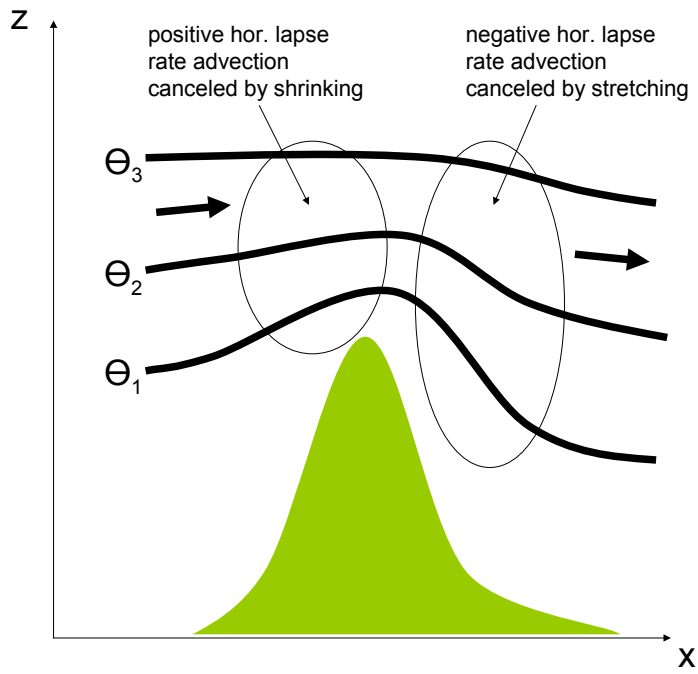

Figure 68: *Illustrated x,z cross section of isentropes (Θ_1 – Θ_3) in a flow over complex terrain where the local lapse rate tendency is zero. The direction of the flow is given by arrows. Regions where horizontal advection is canceled by stretching or shrinking are highlighted.*

in the vicinity of PV intrusions. In most cases (18 out of 30 fields) all other terms had a magnitude of less than 0.25 $\mathrm{K\,km^{-1}h^{-1}}$ and hence were not evident. Only in some fields (10 out of 30) also the differential thermal advection term exceeded 0.25 $\mathrm{K\,km^{-1}h^{-1}}$ in regions of lapse rate increase close to PV intrusions, for the vertical lapse rate advection this was the case for just 2 out of 30 maps. Finally, the residual term was relatively small with a magnitude of 0.25 $\mathrm{K\,km^{-1}h^{-1}}$ (for example near 52°N / 10°E in Fig. 67 f). The residual was also mostly positive. This means that the sum of the calculated individual terms does not completely give the local lapse rate tendency. All terms were frequently found to be also negative in regions with relatively large lapse rate increase close to PV intrusions.

An exception was the stretching term that was typically positive in regions with relatively large lapse rate increase close to PV intrusions. Based on this result it can be argued that stretching is the most important factor that explains the large lapse rate increase in low-instability derechos. Although not commonly used in conceptual models for low-instability deep moist convection, stretching is known to have an impact on storm initiation, e.g. due to its effect on capping inversions

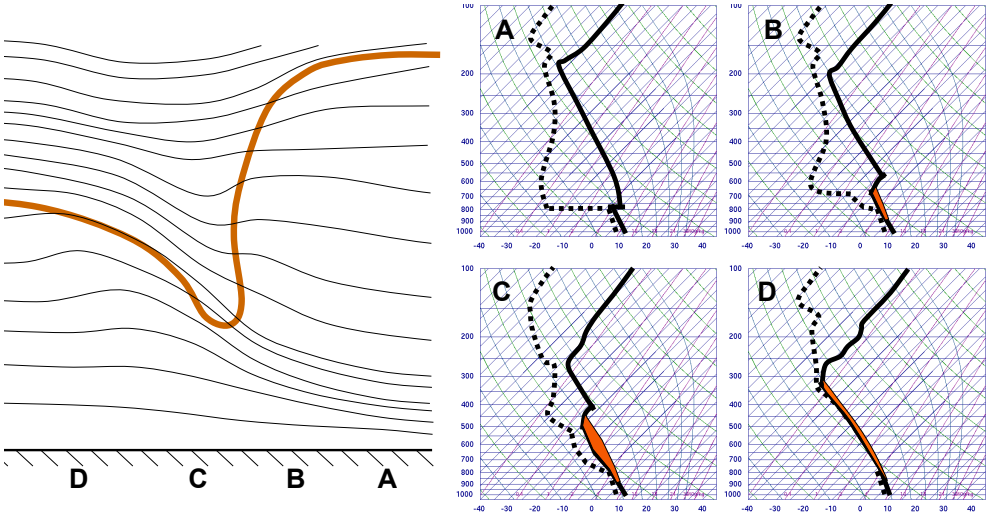

Figure 69: *Left: Illustrated x,z cross section of isentropes (black lines) close to a PV intrusion (orange line corresponds to the position of the dynamic tropopause). Right: Illustrated vertical profiles at the locations marked by letters A–D in the cross section. The dewpoint profile is given by a dashed, the temperature profile by a solid line. The orange areas illustrate CAPE for ascending low-level air parcels. The skew-T/log p - diagram in the background was taken from the University Wyoming (2015).*

that suppress initiation (e.g. for tropical convection Sun and Fang, 2013; Funatsu and Waugh, 2008).

In summary, we suppose that PV intrusions can lead to favorable thermodynamic environments for low-instability derechos. If these intrusions reach low levels, the associated lift causes stretching near the ground what results in rapidly increasing lapse rates. This process moves with the speed of the PV intrusion. If sufficient low-level moisture in present, CAPE evolves (Fig. 69). Initiation of storms does likely not need well-developed surface fronts as indicated by presented examples.

4.7 Statistical analysis of the lapse rate tendency equation

To complement the subjective analysis discussed in the previous sections, we include objective results for the region downstream of PV intrusions. As described in section 3.6, areas of large PV changes were identified by large PV advection on pressure levels. These areas were analyzed with respect to the average lapse rate tendency in comparison to that of the remaining model field. The same method was used to analyze the lapse rate tendency also for regions with PV changes at

later time steps up to $t + 75$ minutes (hereafter "time shift"). For the analysis, we looked at PV at 600 hPa and the lapse rate tendency between 900 and 650 hPa as discussed in section 3.3. Averaged for all model simulations, we found that the lapse rate increased with a rate of 0.315 $\mathrm{K\,km^{-1}h^{-1}}$ in regions with large PV increase in the next 15 minutes (Fig. 70). In areas that experience large PV increase for larger time shifts, the lapse rate increase becomes smaller but is still 0.179 $\mathrm{K\,km^{-1}h^{-1}}$ for a time shift of $t + 75$ minutes. In contrast, in the remaining model field with a PV increase below 2 PVU/h, the lapse rate tendency is only 0.003 $\mathrm{K\,km^{-1}h^{-1}}$ for $t + 15$ minutes (1 % of the average for large PV increase) and even negative when larger time shifts are used (up to -0.011 $\mathrm{K\,km^{-1}h^{-1}}$ for a time shift of 75 minutes).

Breaking the data down to the individual dates gives comparable results for the area-averaged values of the lapse rate tendency (Fig. 71). In general, for large PV increase the local lapse rate tendency is clearly larger as of the remaining model area. In this remaining area, the average lapse rate tendency is often negative (for the events of 28 December 2001, 28 January 2002, 22 February 2008, 1 March

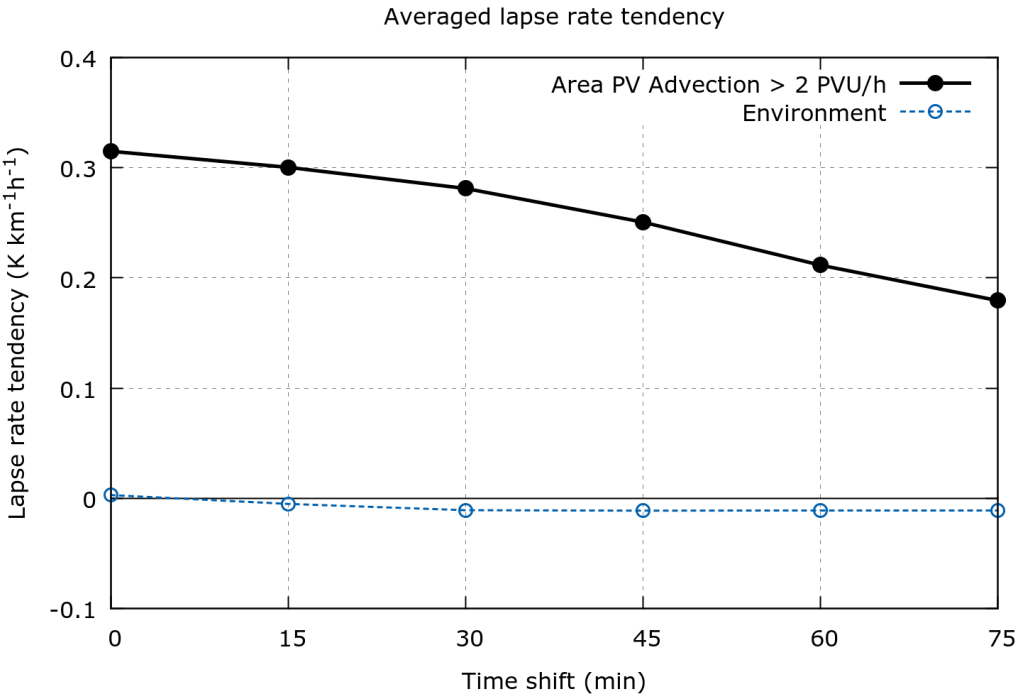

Figure 70: *Local lapse rate tendency (900 to 650 hPa) averaged over all simulated dates for all model grid points having PV advection greater than 2 PVU/h (solid lines) and less than 2 PVU/h (dotted line). Time shift at the x-axis corresponds to the time period PV advection is based on.*

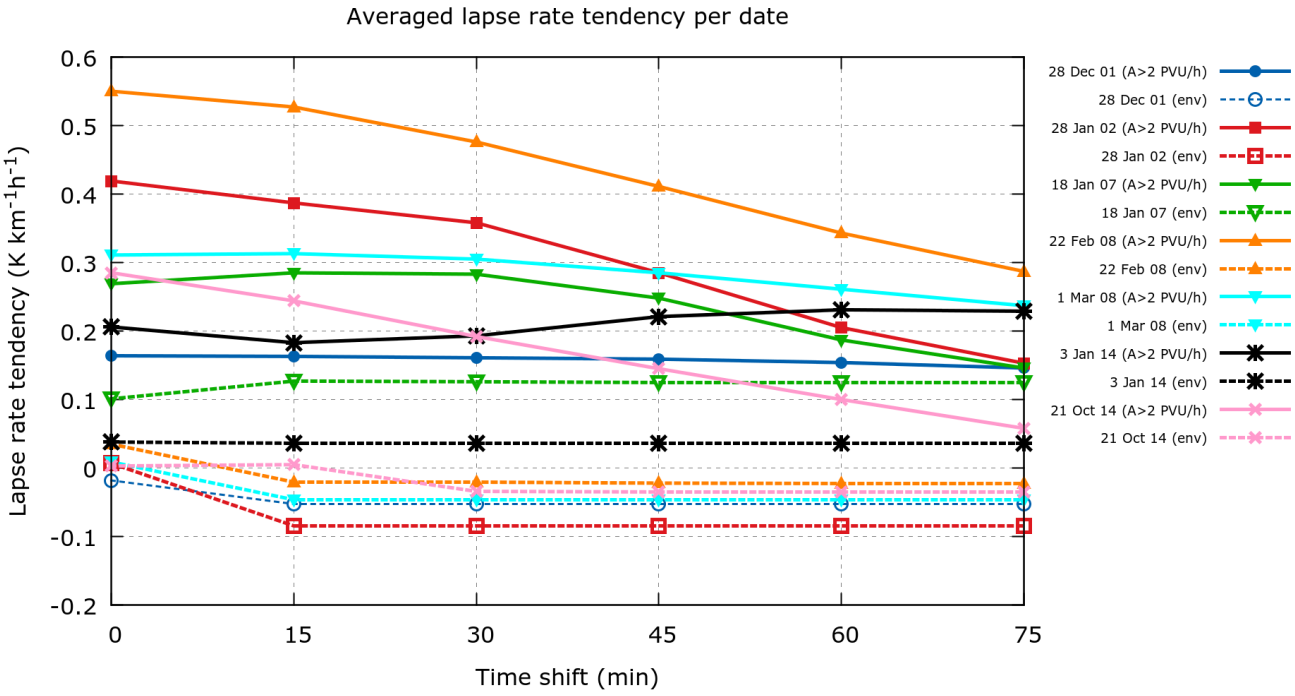

Figure 71: *Local lapse rate tendency (900 to 650 hPa) averaged over all model grid points (or areas A) having PV advection greater than 2 PVU/h (colored solid lines for different dates as given to the right) and less than 2 PVU/h (denoted by "(env)", dotted lines; same color for the same date). Time shift at the x-axis corresponds to the time period PV advection is based on.*

2008, and 21 October 2014), hence corresponding to stabilization, whereas it is positive within the area of strong PV increase. For longer time shifts, i.e. typically farther downstream of the PV intrusion, some events are characterized by a further increase of the lapse rate tendency (3 January 2014, 18 January 2007, and slightly for 1 March 2008). The differences between the environment and the area of strong PV increase can be followed up to the time shift of 75 minutes.

The computed values of the lapse rate tendency at each grid point have been used to plot box-and-whisker diagrams to compare the distributions for strong PV advection and the environment. The diagram in Fig. 72 shows that the upper quartile for most events is greater than 0.5 $\mathrm{K\,km^{-1}h^{-1}}$, peaking as high as 0.87 $\mathrm{K\,km^{-1}h^{-1}}$ for the event of 28 January 2002. This corresponds to a theoretical hourly temperature difference increase of more than 2 K in the respective layer assuming a height difference of 2.5 km what is the average for the digging trough pattern proximity soundings given in Table 3. The upper 5 % of the distributions frequently exceed 1 $\mathrm{K\,km^{-1}h^{-1}}$ lapse rate increase with a maximum of 1.38

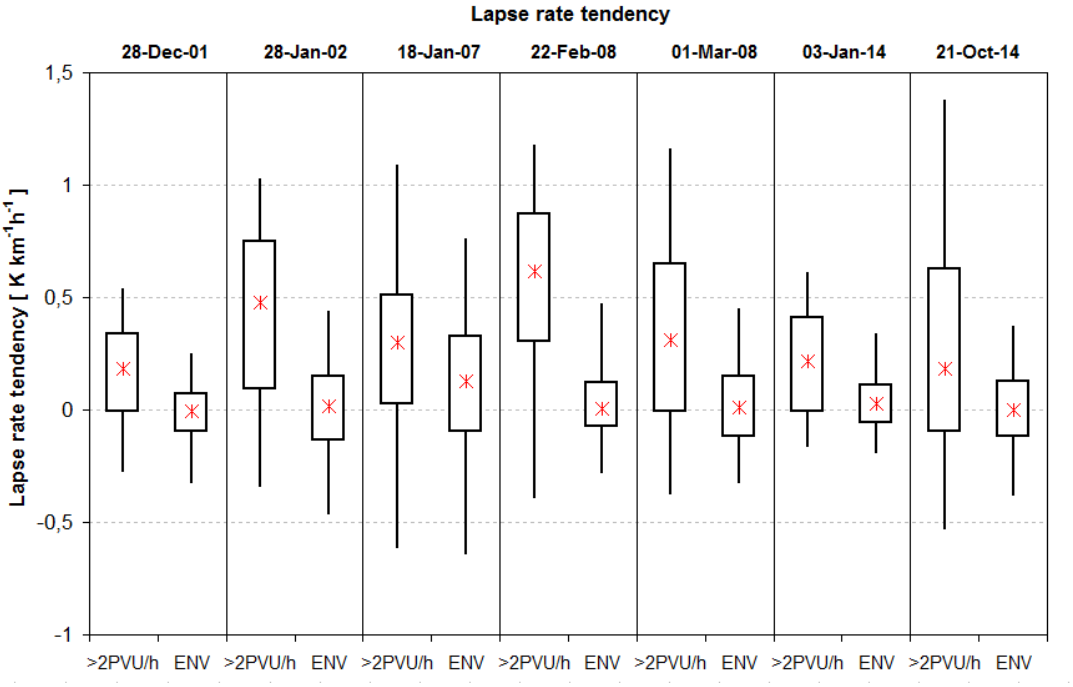

Figure 72: *Distribution of the local lapse rate tendency (900 to 650 hPa) for all model grid points having PV advection greater than 2 PVU/h (left bars) and less than 2 PVU/h (right bars). The crosses mark the median, boxes are plotted for the 25 and 75 percentile, and thin lines for the 5 and 95 percentile, respectively.*

$\mathrm{K\,km^{-1}h^{-1}}$ for the 21 October 2014, corresponding to a theoretical temperature difference increase of 3.45 K in one hour.

Fig. 72 also shows a clear difference between model points with high lapse rate changes and the environment, especially on 28 January 2002 and 22 February 2008, where the belonging distributions hardly overlap. These two dates represent three of eight derechos analyzed with COSMO for this work. For the other events, at least the median of the local lapse rate tendency for the area with large PV changes is located outside the inner quartiles of the distributions of the environment. An exception is the simulation of 18 January 2007. Here is a large overlap for both distributions, indicating that they differ not significantly. In summary, the plots indicate that areas with PV advection larger than 2 PVU/h at 600 hPa are also regions with lapse rate increase between 900 and 650 hPa. In the environment, lapse rates do not change much on average. Moreover, the environmental distribution and that for large PV increase are significantly different in most of the simulations.

An analysis of the terms in the local lapse rate tendency equation gives an estimation of the importance of processes that yield the lapse rate increase in regions

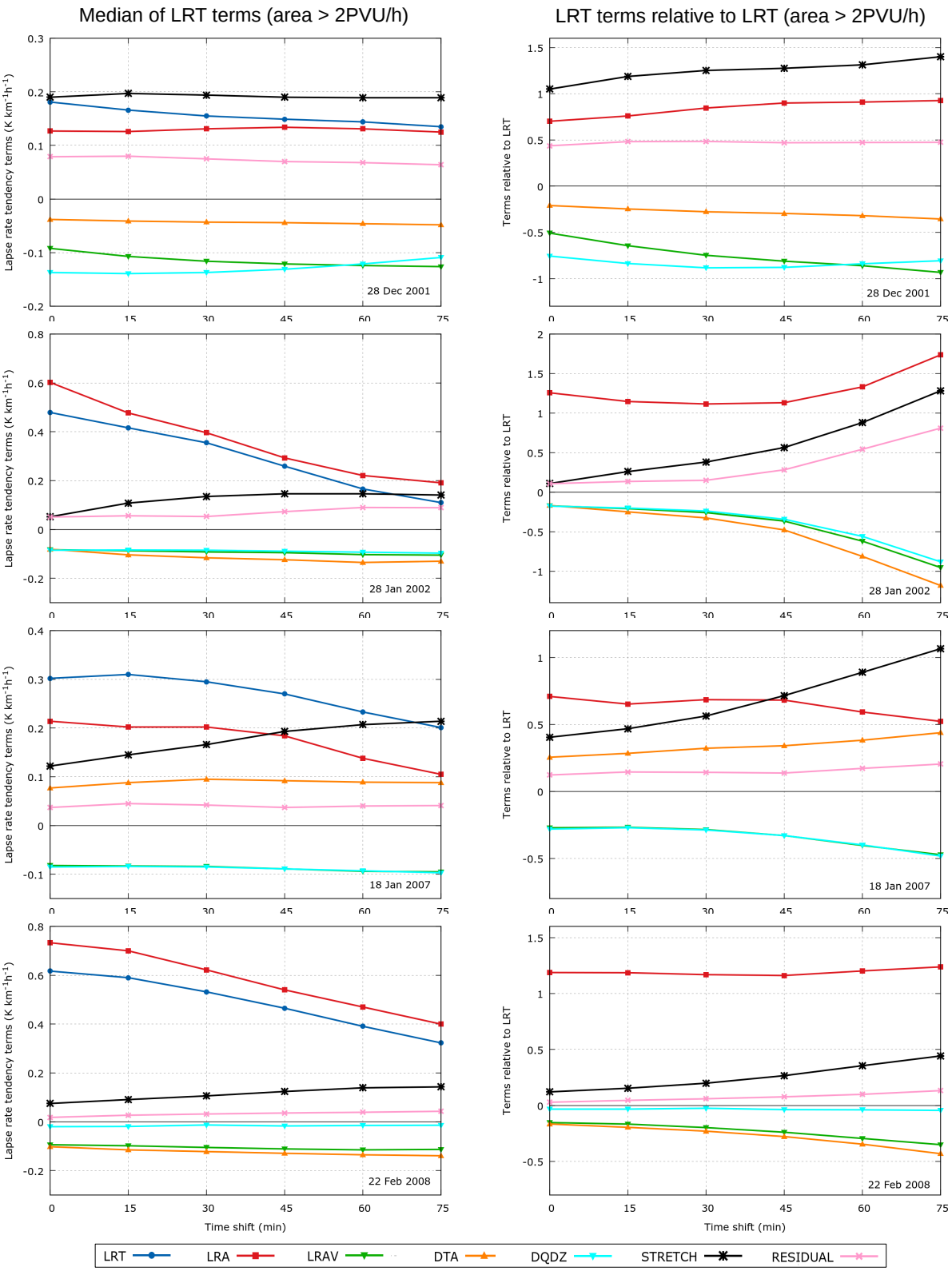

Figure 73: *900 to 650 hPa values of lapse rate tendency (abbreviated by LRT), LRT terms (horizontal advection LRA, vertical advection LRAV, differential thermal advection DTA, differential diabatic heating DQDZ, and stretching STRETCH) and residual (RES), averaged for the area of 600 hPa PV advection > 2 PVU/h. (Left) Median of all terms and residual; (right) LRT terms and residual relative to local lapse rate tendency (value of LRT=1).*

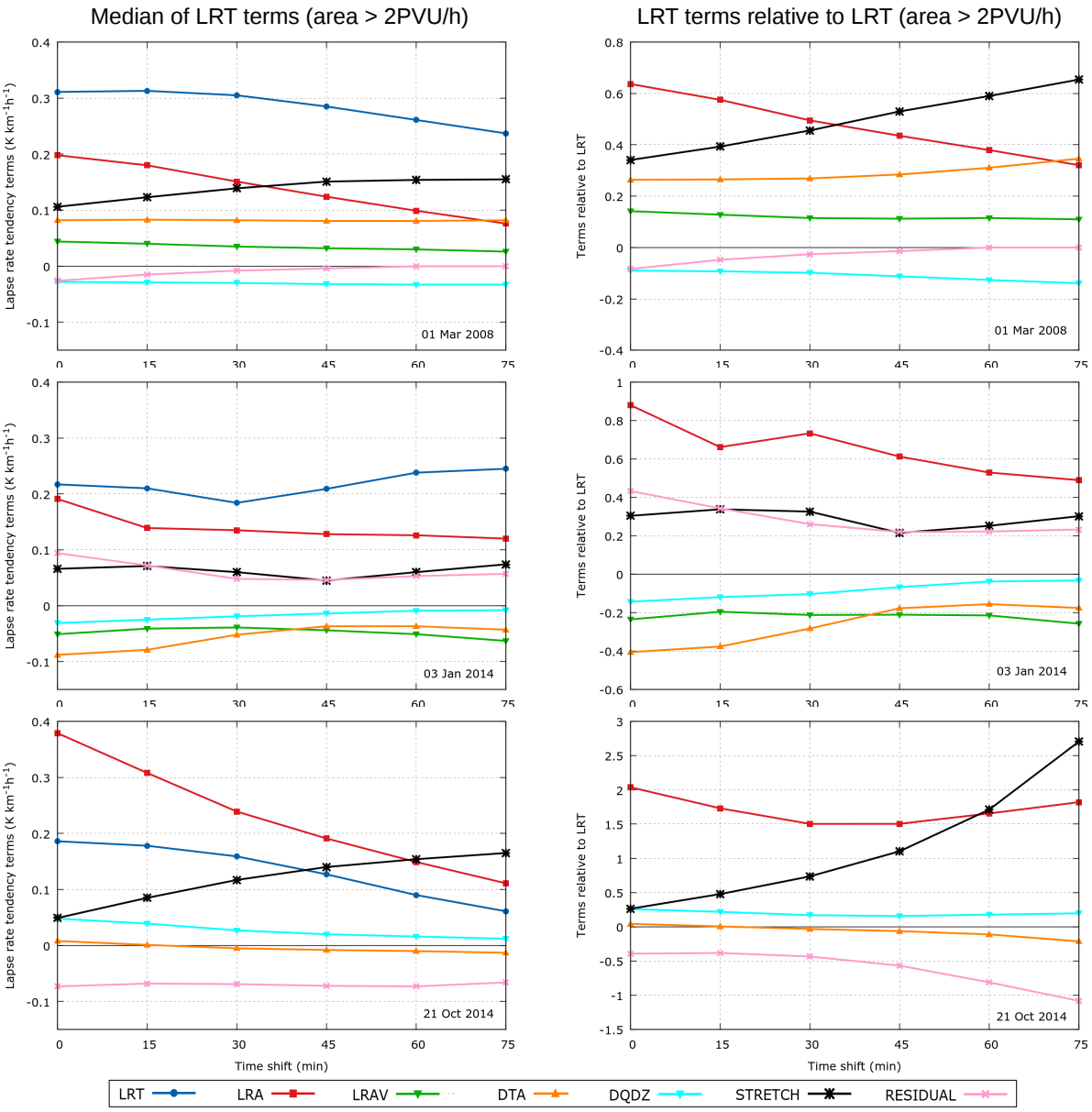

Figure 74: *900 to 650 hPa values of lapse rate tendency (abbreviated by LRT), LRT terms (horizontal advection LRA, vertical advection LRAV, differential thermal advection DTA, differential diabatic heating DQDZ, and stretching STRETCH) and residual (RES), averaged for the area of 600 hPa PV advection > 2 PVU/h. (Left) Median of all terms and residual; (right) LRT terms and residual relative to local lapse rate tendency (value of LRT=1).*

with strong PV advection. Figs. 73 and 74 show the average values of the different terms of the lapse rate tendency equation and the residual term. The residual term is calculated by the difference of the lapse rate tendency and the individual terms (Eq. 24). The absolute value (Figs. 73 and 74, left) of the horizontal lapse rate advection typically determines the lapse rate tendency. This is evident since both corresponding lines have a comparable shape and magnitude. The second average term that is always positive is that of the stretching process. However, the corresponding lines show an opposed slope for increasing time shifts of PV advection compared to lapse rate tendency and horizontal advection, and stretching increases for longer time shifts whereas the other two terms typically decrease. Due to this fact, the value of the stretching term increases strongly for longer time shifts and can even exceed the horizontal lapse rate advection for 28 December 2001, 18 January 2007, 1 March 2008, and 21 October 2014. This indicates that stretching starts far ahead of PV intrusions. The average of the other terms of the lapse rate tendency equation can be both positive and negative. Typically, they are also small in magnitude compared to horizontal advection and stretching. The residual is mostly positive indicating that the calculated lapse rate tendency terms are too small to explain the lapse rate tendency completely. An exception is 21 October 2014 with a negative residual and likely too large values of one or several of the calculated terms.

The relative values of the different terms have been combined to get an average overview of the simulated cases in Figs. 75. The horizontal lapse rate advection term is most important and generally has the same magnitude of the lapse rate tendency. However, for longer time shifts, stretching becomes more important and exceeds the advection for a time shift of 75 minutes. The residual term has a value of about 10 percent of the lapse rate tendency. The other terms are all negative on average and decrease further for larger time shifts. For example, the differential diabatic heating term is leading to stabilization, likely attributed to the low-level diabatic cooling of the maritime air mass over the continental land mass. Therefore, horizontal advection and stretching can be said to cause the increasing lapse rate in the simulated events rather than the vertical lapse rate advection term, differential thermal advection term, and differential diabatic heating term.

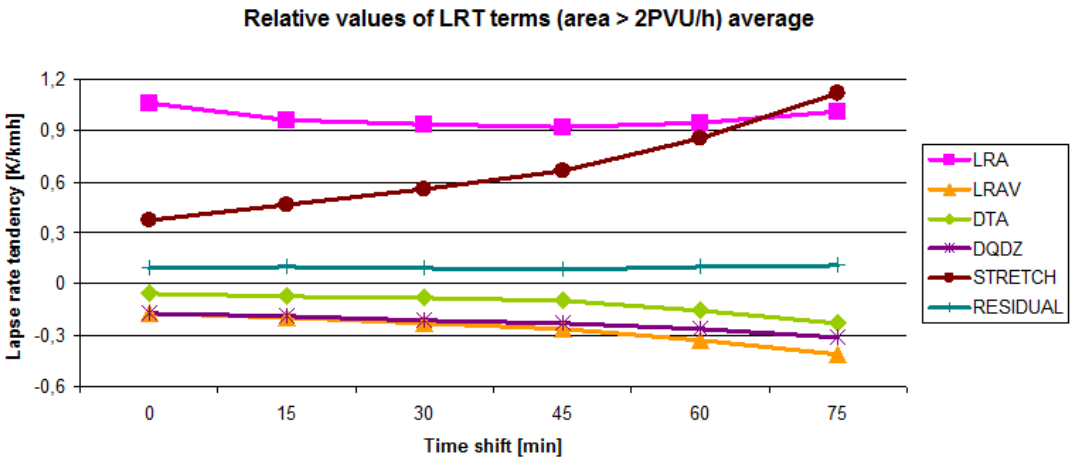

Figure 75: *900 to 650 hPa relative values (value of lapse rate tendency = 1) of lapse rate tendency terms (horizontal advection LRA, vertical advection LRAV, differential thermal advection DTA, differential diabatic heating DQDZ, and stretching STRETCH) and residual (RES), averaged for the area of 600 hPa PV advection > 2 PVU/h and for all simulated events.*

5 Summary, conclusion and outlook

This thesis deals with widespread, convectively-induced severe wind events in Germany. These are called derechos when their damage path exceeds a major length axis of 400 km. Derechos can cause numerous fatalities and high losses to the economy and infrastructure. Although derecho research has been initiated in the United States more than 30 years ago, the research on European derechos is still in the beginning. The work is divided into two parts: In the first part, we compiled a German derecho climatology of 18 years in the period from 1997 to 2014. This exceeds former research of single case studies (e.g. Gatzen, 2004; Gatzen et al., 2011). In the second part of this work, we analyzed eight low-instability derechos with the help of high-resolution COSMO model simulations in more detail.

The derecho climatology reveals an annual average frequency of more than two derechos of low, moderate or high intensity per year in Germany (40 events in 18 years). This is relatively frequent since most of the derechos affected large parts of Germany (Figs. 30 and 31). Limiting the number to only moderate and high intensity events still yields more than one event per year. In comparison to the United States climatology (e.g. Coniglio and Stensrud, 2004), we found differences that we attributed to the limited instability in Germany:

- Compared to United States, there are less derechos. Relative to the southern parts where the derecho frequency is highest across German, the spatial derecho density of the most affected regions of the United States is about twice as large according to Coniglio and Stensrud (2004).
- German derechos almost always form in strongly-forced synoptic situations. These are characterized by high-amplitude, progressive troughs and are associated with intense low pressure systems. Weakly-forced derechos are more common in the United States.
- German derechos form on average in weaker instability.
- The seasonal derecho distribution indicates a main warm-season and a secondary cold-season peak in the United States and in Germany. However, the German cold season peak is more pronounced when compared to the United States.

German cold-season derechos typically develop in different large-scale weather patterns compared to the warm season. The thermodynamic environment of cold-

season derechos is characterized by very low CAPE, but very strong low-level flow. Such derecho environments have been described in the United States as well and are named "high-shear, low-CAPE environments" (e.g. Evans, 2010; King and Parker, 2014).

Based on our novel German derecho climatology, we identified 16 of such low-instability events. Eight out of the 16 events were chosen for further analysis with the high-resolution, convection-permitting COSMO model. The main aim was to identify the processes that lead to destabilization forcing the convective developments along the derecho paths. Therefore, we analyzed the eight cases using the ingredients-based methodology. After Doswell et al. (1996), necessary ingredients for convection are instability, moisture, and lift. Our main results will be summarized in the following.

Regarding instability, we found sufficiently cold equilibrium levels to support thunderstorms in the vicinity of the derechos. We studied the local lapse rate tendency and each of its contributing terms separately in the simulated fields. In particular, we observed a rapid lapse rate increase close to the ground downstream of intense PV intrusions. This lapse rate increase can be attributed mainly to two terms of the lapse rate tendency equation: While the advection term is known to be the main factor to cause local lapse rate changes (Banacos and Ekster, 2010), the considerable contribution of the stretching term was rather surprising. In consequence, the ingredients-based methodology has to be used with care in low-instability events. In these highly ageostrophic situations the local lapse rate tendency can not be approximated by horizontal advection alone. It is therefore not possible to anticipate the overlap of low-level moisture and steep lapse rates by pure linear interpolation based on the analyzed lapse rate field and the horizontal flow. Further analysis showed that the stretching term was especially large downstream of PV intrusions which is in accordance with conceptual models in the potential vorticity framework (e.g. Fig. 19). However, this finding is new in association with low-instability derechos and it can complement existing conceptual models of convective initiation close to PV intrusions.

As third contribution to the local lapse rate tendency, the differential thermal advection term was rather large in some events. In combination with the horizontal advection term, this represents the influence of differential temperature advection on the local lapse rate. Although this process can be expected to influence

Table 4: *Contribution of the individual terms in the local lapse rate tendency equation relative to the local lapse rate tendency. The terms are calculated in the 900 – 650 hPa layer for areas with PV advection > 2PVU/h.*

Lapse rate tendency term	Frequency of importance	Average magnitude relative to lapse rate tendency	Tendency
Horizontal lapse rate advection	all events	1	positive
Stretching	all events	0.6	positive
Differential thermal advection	2 of 8 events	−0.1	2 positive, 6 negative
Vertical lapse rate advection	1 of 8 events	−0.2	2 positive, 6 negative
Differential diabatic heating	0 of 8 events	−0.2	negative
Residual	0 of 8 events	0.1	6 positive, 2 negative

the development of some derechos, we found it was also negative for some of our simulations. Therefore, its general contribution is not clear so far and needs to be addressed in the future. The differential diabatic heating term was typically small. This means that differential latent heat release is not important for the observed lapse rate increase. This is in some disagreement with the conceptual model of potential instability release in association with PV intrusions (Browning and Roberts, 1996). However, potential instability is needed before stretching can result in steep lapse rates. This would mean that potential instability provided by PV intrusions is not directly released but converted to conditional instability by the stretching process before deep moist convection initiates. The presented results do only represent the chosen layer, i.e. 900 – 650 hPa and are averaged over a large area for PV advection greater than 2 PVU/h at 600 hPa. A summary of all terms and their contribution to the local lapse rate tendency is given in Table 4.

Besides the lapse rate, low-level moisture was analyzed in the model fields and in observations. We found moisture changes relatively far ahead of derechos and PV intrusions. For proximity soundings with zero CAPE, we found no indications of a low-level moisture increase until the approach of a derecho. From the com-

bined maps of low-level moisture and lapse rates as well as from cross sections we argue that lapse rate changes are more important than moisture changes in German low-instability derechos. This is in some disagreement with studies from the United States that emphasize the importance of low-level moisture increase ahead of low-instability derechos (King et al., 2017; Sherburn et al., 2016). Based on our findings concerning the analysis of the lapse rate tendency terms, we propose to take also rapid lapse rate changes into account to forecast derechos for United States low-instability situations.

The overlap of rich low-level moisture and steep lapse rates can result in conditional instability. We found conditional instability indicated by negative values of the Lifted Index in all modeled low-instability events. Conditional instability formed where steep lapse rates overlapped with the pre-derecho moisture tongue, i.e. ahead and below the PV intrusion as well as ahead of the derecho gust front. Conditional instability formed close to the ground and extended upwards to the PV intrusion where the equilibrium level is cold enough to explain thunderstorms. The observed overlap of moisture and lapse rates was limited in space and time. Typically, only a very narrow band of conditional instability formed. We argue that proximity soundings are not always representative for this reason in accordance to other authors (e.g. Apsley et al., 2016).

Lift is needed to initiate storms according to the ingredients-based methodology. Indeed most of the German low-instability derechos form along cold fronts that provide mesoscale circulations that can lift parcels to their LFC. A PV intrusion that "overruns" a cold front to form a "split front" is an established conceptual model for such situations (Browning and Roberts, 1996). However, we have found that derechos can form in the absence of a well-developed frontal boundary as well. Consequently, we would propose to modify the split-front concept: Intense PV intrusions cause strong large-scale forcing that leads to sufficient mesoscale lift even in the absence of a cold front. Low-instability derechos form where PV intrusions overlap with rich low-level moisture. The PV intrusion would be associated with lapse rate increase and lift at the same time making it in particular prone for initiation. However, a convective system would be only maintained as long as it moves with the PV intrusion. If the PV intrusion moves away from the convective storm, it may weaken when lapse rates decrease in response to less large-scale forcing. In such situations, PV intrusions may cause periodic initiation along their paths instead of a single long-lived event.

The idea that low-instability derechos are mostly determined by PV intrusions can be regarded as a large-scale, external forcing. In contrast, internally driven derechos form in response to persistent, intense deep moist convection that forms a cold pool, rear inflow jet, and bow echo. Since low-instability convection is typically associated with colder air, the latent heat release will be weaker as for high-instability convective storms. It may be also possible that low-instability derecho cold pools are less deep and of weaker intensity. This would limit the perturbation pressure between cold pool and gust front resulting in less pronounced bow echoes compared to high-instability derechos. In this respect, the distinction into internally driven derechos for high-instability situations and externally driven derechos for those associated with low instability, strong synoptic forcing, and serial bowing lines (Corfidi et al., 2016) is supported by our results.

Strong low-level flow and associated vertical wind shear is likely an important factor of low-instability derechos. We hypothesize that strong vertical wind shear in combination with a level of free convection just a few hundred meters above the ground can effectively support mesovortices. Mesovortices are known from high-instability derechos but have also been documented in association with low-instability convection (Clark, 2009). Both high- and low-instability derechos may produce extreme wind gusts by the same phenomenon:

- In high-instability situations, intense convective storms can stretch low-level air masses to produce mesovortices. At the same time, they lead to the development of rear inflow jets that descend towards the low perturbation pressure in the center of mesovortices what results in high winds at the ground. This can be attributed to internally-driven processes.

- In low-instability situations, PV intrusions increase the low-level lapse rates due to the stretching term. This can lead to convective storms with low levels of free convection. These could stretch low-level air masses to produce mesovortices. Strong environmental flow will descend when entering mesovortices and hence cause severe winds at the ground. PV intrusions and strong environmental flow can be regarded as external processes.

In future work, more high-resolution simulations of derecho cases can help to understand regional characteristics of derechos. This includes the regional and seasonal frequency and intensity of mesovortices and the associated wind hazard.

On the large-scale, the availability of favorable thermodynamic conditions like strong low-level flow or high CAPE can support to estimate the derecho risk, for example for climate predictions.

Regardless of their different formation processes, we have documented that high- and low-instability derechos can be of similar intensity and track length. From an impact-based point of view, there are no reasons to distinguish between both types of storms: Their sudden appearance, high intensity, and large size result in a comparable impact. Furthermore, the damage patterns will be likely quite similar as they can be attributed to mesovortices. The most obvious difference is their seasonal occurrence: Low-instability derechos tend to form in the cold season, when PV intrusions and strong low-level flow are more frequent compared to the warm season. We therefore propose to continue to call both phenomena *derecho* instead of using different terms as proposed by Corfidi et al. (2016). To emphasize the different origin of the two derecho types, they could be named "cold-season" and "warm-season" derechos.

Operational forecasters should be aware that the ingredients-based methodology (Doswell et al., 1996) has to be used with care in low-instability situations. On the other hand, our work shows that the classic tripod of necessary ingredients for convective initiation is still valid. High-resolution data can support forecasters in strongly-forced cold-season situations to detect developing lapse rates. Water vapor channel satellite images are already used to follow PV intrusions that typically appear as dark stripes. Here, forecasters should anticipate lapse rate increase at mid levels and close to the ground.

We expect that detection of PV intrusions on the water vapor satellite channel and looking for their overlap with rich low-level moisture can support forecasters best in cold-season derecho situations. An example is a PV intrusion that moves across a surface cold front where it may overlap with rich pre-frontal moisture, so that convective storms can initiate along the front. This conceptual model is already in use (Fig. 18). We want to emphasize that our proposed mechanism for derecho development does not include the need of a well-developed surface front, though: If sufficient low-level moisture is present, deep PV intrusions may support derechos even in the absence of well-developed fronts as in the example of 28 January 2002 (Fig. 46). The classic concept needs to be modified in order to cover such situations as well.

Furthermore, forecast displays needs to be adjusted to cold-season situations to optimize the facilities of numerical weather prediction. For example, lapse rates are present at relatively low levels compared to the warm season. As presented in section 4.3, lapse rates could be displayed in the 900 – 650 hPa layer or even at lower levels. Classic displays using 700 – 500 hPa lapse rates can be useless in cold-season situations as they do not represent the layer where CAPE evolves. The CAPE value is also not a good predictor of storm intensity as CAPE is typically weak in cold-season situations. On the other hand, the low-level wind speed or vertical wind shear can be used as predictor for derechos. Where strong low-level vertical wind shear overlaps with low-based CAPE, forecasters should be aware of mesovortices in association with convective storms.

Despite the tremendous work conducted in this thesis, the German derecho climatology has limitations in particular due to the small area of Germany in comparison to the long paths of derechos. This causes an underestimation of events especially near the borders. In the future, this study should be expanded to Europe. For this aim, archived wind gust measurements and radar displays have to be analyzed in a consistent way.

A first attempt has been presented at the 6th European Conference on Severe Storms. Wind gust data and radar archives for Estonia, Germany, France, and Serbia have been analyzed together with respect to their association with convective storms (Gatzen et al., 2017). Several derechos have been found that crossed the border between France and Germany. Until now scientists of ten further countries joined this collaboration, representing the Netherlands, Portugal, Switzerland, Austria, Poland, the Czech Republic, Romania, Hungary, Finland, and the United Kingdom. The analysis of derechos has already begun in some of these countries.

In future work, our results can be compared to the frequency, intensity, and impact of other storm events like non-convective winter storms or Föhn events to evaluate the relative contribution of derechos to the overall wind hazard in Germany and other European countries. Regional characteristics like favorable derecho paths and life cycles can support international collaboration in warning situations, e.g. when storms initiate over France that evolve into a derecho over Central Europe later on. A recent example of such pan-European research has

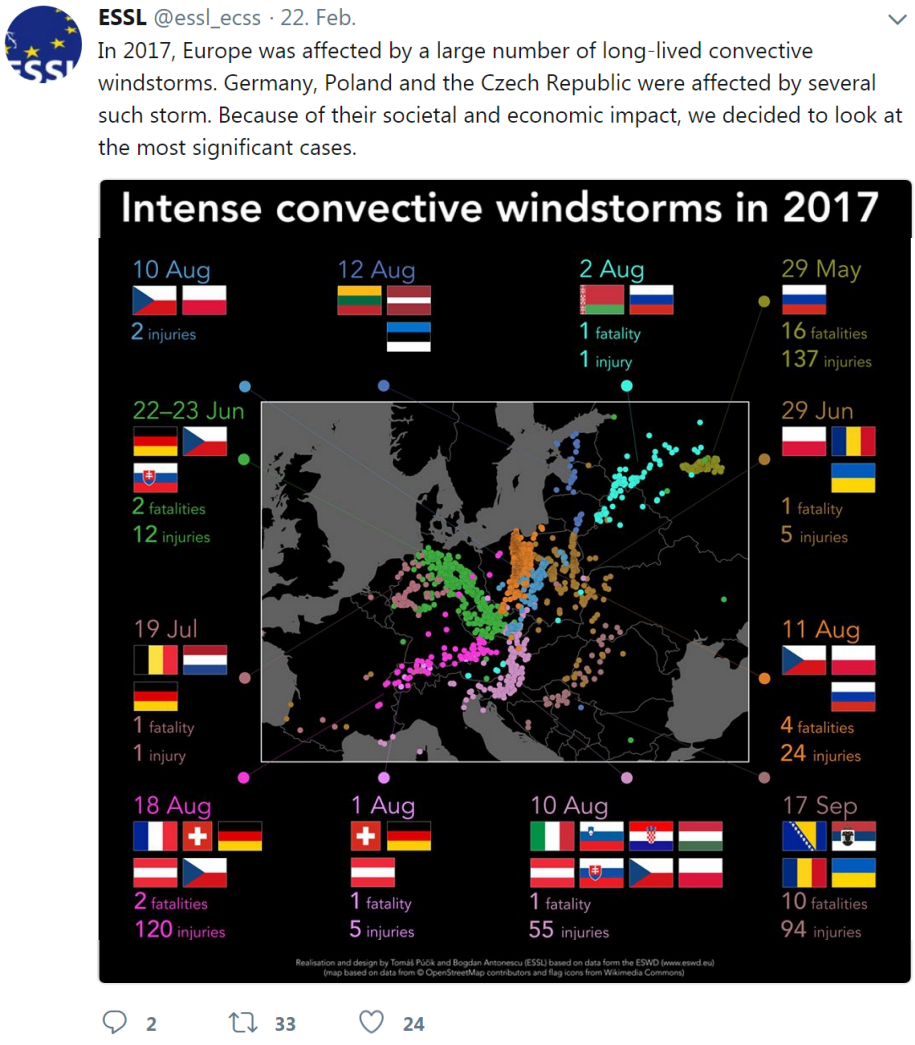

Figure 76: *Overview of widespread convective wind events in the warm season of 2017. Severe wind reports are displayed by colored dots according to the dates given at the borders. Image courtesy: Twitter / ESSL. Accessed: 2018-03-02*

been published by the European Severe Storm Laboratory. It shows an overview of several widespread convective windstorms that occurred in the warm season of 2017 (Fig. 76). This example documents the high impact these storms can have in Europe and that the research on European derechos is beneficial and should be continued.

Acknowledgments

I would like to thank Prof. Joaquim Pinto and Prof. Andreas Fink for giving me the opportunity to work on this thesis. I thank my supervisors Prof. Andreas Fink, Prof. Joaquim Pinto, and Prof. David Schultz for supporting me with helpful discussions and comments. I am grateful to Prog. Yaping Shao for agreeing to be the second referee of this thesis.

I am thankful to Dr. Patrick Ludwig for providing the COSMO simulations on which large parts of this thesis are based on. Furthermore, I would like to thank all who supported this work with insightful discussions, data, and help with the images: Dr. Lisa Schielicke, David Rỳva, Dr. Nikolai Dotzek, Dr. Ulrich Blahak, Dr. Pieter Groenemeijer, Prof. Johannes Dahl, Georg Pistotnik, Dr. Jan Hoffmann, Prof. Matthew Parker, Prof. Charles Doswell, Lars Lowinski, Dr. Peter Banacos, Paul Knightley, Dennis Schulze, Jörg Kachelmann.

I am grateful to my family, Lisa, Linus, Oskar, and Emil. Thank you for your support, understanding, the passion, distractions at the right time, and motivation you gave me in the last years. And I would like to thank Hannelore and Wolfgang, and Elke and Wolfgang, for the childcare during numerous conferences.

References

Adams-Selin, R. D. and Johnson, R. H. (2010). Mesoscale surface pressure and temperature features associated with bow echoes. *Monthly Weather Review*, 138(1):212–227.

Apsley, M. L., Mulder, K. J., and Schultz, D. M. (2016). Reexamining the United Kingdom's greatest tornado outbreak: Forecasting the limited extent of tornadoes along a cold front. *Weather and Forecasting*, 31(3):853–875.

Ashley, W. S., Mote, T., and Bentley, M. (2004). Derecho families. In *Preprints, 22d Conf. on Severe Local Storms, Hyannis, MA, Amer. Meteor. Soc., CD-ROM P*, volume 4.

Ashley, W. S. and Mote, T. L. (2005). Derecho hazards in the United States. *Bulletin of the American Meteorological Society*, 86(11):1577–1592.

Atkins, N. T., Bouchard, C. S., Przybylinski, R. W., Trapp, R. J., and Schmocker, G. (2005). Damaging surface wind mechanisms within the 10 June 2003 Saint Louis bow echo during BAMEX. *Monthly Weather Review*, 133(8):2275–2296.

Atkins, N. T. and St. Laurent, M. (2009a). Bow echo mesovortices. Part I: Processes that influence their damaging potential. *Monthly Weather Review*, 137(5):1497–1513.

Atkins, N. T. and St. Laurent, M. (2009b). Bow echo mesovortices. Part II: Their genesis. *Monthly Weather Review*, 137(5):1514–1532.

Avherald (2010). Online Archive of The Aviation Herald. http://avherald.com/h?article=434c6b66&opt=0. Accessed: 2015-12-13.

Banacos, P. C. and Ekster, M. L. (2010). The association of the elevated mixed layer with significant severe weather events in the northeastern United States. *Weather and Forecasting*, 25(4):1082–1102.

Bentley, M. L. and Mote, T. L. (1998). A climatology of derecho-producing mesoscale convective systems in the central and eastern United States, 1986-95. Part I: Temporal and spatial distribution. *Bulletin of the American Meteorological Society*, 79(11):2527–2540.

Bentley, M. L. and Mote, T. L. (2000). A synoptic climatology of cool-season derecho events. *Physical Geography*, 21(1):21–37.

Bentley, M. L., Mote, T. L., and Byrd, S. F. (2000). A synoptic climatology of derecho producing mesoscale convective systems in the north-central Plains. *International Journal of Climatology*, 20(11):1329–1349.

Bentley, M. L. and Sparks, J. (2003). A 15-year climatology of derecho producing mesoscale convective systems over the Central and Eastern United States. *Climate Research*, 24:129–139.

Berliner Zeitung (2012). Online Archive Berliner Zeitung. http://www.berliner-zeitung.de/berlin/orkan-anita-kraenze-zum-gedenken-an-sturmopfer,10809148,16592962.html. Accessed: 2015-12-13 (in German).

Blanchard, D. O., Cotton, W. R., and Brown, J. M. (1998). Mesoscale circulation growth under conditions of weak inertial instability. *Monthly Weather Review*, 126(1):118–140.

Born, K., Ludwig, P., and Pinto, J. G. (2012). Wind gust estimation for Mid-European winter storms: towards a probabilistic view. *Tellus A*, 64.

Brooks, H. E. (2009). Proximity soundings for severe convection for Europe and the United States from reanalysis data. *Atmospheric Research*, 93(1):546–553.

Browning, K. and Reynolds, R. (1994). Diagnostic study of a narrow cold-frontal rainband and severe winds associated with a stratospheric intrusion. *Quarterly Journal of the Royal Meteorological Society*, 120(516):235–257.

Browning, K. and Roberts, N. (1996). Variation of frontal and precipitation structure along a cold front. *Quarterly Journal of the Royal Meteorological Society*, 122(536):1845–1872.

Bryan, G. H., Knievel, J. C., and Parker, M. D. (2006). A multimodel assessment of RKW theory's relevance to squall-line characteristics. *Monthly Weather Review*, 134(10):2772–2792.

Bundesstelle für Flugunfalluntersuchung (2010). Untersuchungsbericht AX002-0/02. http://www.webcitation.org/66oThRvtT?url=http://www.bfu-web.de/cln_030/nn_223970/EN/Publikationen/Untersuchungsberichte/2002/Bericht__02__AX002__Saab2000__Werneuchen,templateId=raw,property=publicationFile.pdf/Bericht_02_AX002_Saab2000_Werneuchen.pdf. Accessed: 2015-12-13 (in German).

Burke, P. C. and Schultz, D. M. (2004). A 4-yr climatology of cold-season bow echoes over the continental United States. *Weather and Forecasting*, 19(6):1061–1074.

Celiński-Mysław, D. and Matuszko, D. (2014). An analysis of selected cases of derecho in Poland. *Atmospheric Research*, 149:263–281.

Clark, M. (2013). A provisional climatology of cool-season convective lines in the UK. *Atmospheric Research*, 123:180–196.

Clark, M. R. (2009). The southern England tornadoes of 30 December 2006: Case study of a tornadic storm in a low CAPE, high shear environment. *Atmospheric Research*, 93(1):50–65.

Cohen, A. E., Coniglio, M. C., Corfidi, S. F., and Corfidi, S. J. (2007). Discrimination of mesoscale convective system environments using sounding observations. *Weather and Forecasting*, 22(5):1045–1062.

Colson, D. (1960). High level thunderstorms of July 31–August 1, 1959. *Monthly Weather Review*, 88:279–285.

Coniglio, M. C., Corfidi, S. F., and Kain, J. S. (2012). Views on applying RKW theory: An illustration using the 8 May 2009 derecho-producing convective system. *Monthly Weather Review*, 140(3):1023–1043.

Coniglio, M. C. and Stensrud, D. J. (2004). Interpreting the climatology of derechos. *Weather and Forecasting*, 19(3):595–605.

Coniglio, M. C., Stensrud, D. J., and Richman, M. B. (2004). An observational study of derecho-producing convective systems. *Weather and Forecasting*, 19(2):320–337.

Conzemius, R. J. and Montgomery, M. T. (2009). Clarification on the generation of absolute and potential vorticity in mesoscale convective vortices. Technical report, DTIC Document.

Corfidi, S., Meritt, J., and Fritsch, J. (1996). Predicting the movement of mesoscale convective complexes. *Weather and Forecasting*, 11(1):41–46.

Corfidi, S. F. (2003). Cold pools and MCS propagation: Forecasting the motion of downwind-developing MCSs. *Weather and Forecasting*, 18(6):997–1017.

Corfidi, S. F., Coniglio, M. C., Cohen, A. E., and Mead, C. M. (2016). A proposed revision to the definition of "derecho". *Bulletin of the American Meteorological Society*, 97(6):935–949.

Corfidi, S. F., Corfidi, S. J., Imy, D. A., and Logan, A. L. (2006). A preliminary study of severe wind-producing mcss in environments of limited moisture. *Weather and Forecasting*, 21(5):715–734.

Corfidi, S. F., Evans, J. S., and Johns, R. H. (2017). About derechos; Part of the NOAA-NWS-NCEP Storm Prediction Center web site. http://www.spc.noaa.gov/misc/AbtDerechos/derechofacts.htm. Accessed: 2017-11-21.

Dahl, J. M., Parker, M. D., and Wicker, L. J. (2014). Imported and storm-generated near-ground vertical vorticity in a simulated supercell. *Journal of the Atmospheric Sciences*, 71(8):3027–3051.

Davies-Jones, R. and Brooks, H. (1993). Mesocyclogenesis from a theoretical perspective. *The Tornado: Its Structure, Dynamics, Prediction, and Hazards*, pages 105–114.

Davis, C., Atkins, N., Bartels, D., Bosart, L., Coniglio, M., Bryan, G., Cotton, W., Dowell, D., Jewett, B., Johns, R., et al. (2004). The bow echo and MCV experiment: Observations and opportunities. *Bulletin of the American Meteorological Society*, 85(8):1075–1093.

Davis, C., Biggerstaff, M., Bryan, G., Dowell, D., Johns, R., Jorgensen, D., Klimowski, B., Knupp, K., Przybylinski, R., Schmocker, G., et al. (2001). Science overview of the bow echo and MCV experiment (BAMEX). Online available at https://ams.confex.com/ams/pdfpapers/57767.pdf. Accessed: 30-12-2017.

Doswell, C. A. (1987). The distinction between large-scale and mesoscale contribution to severe convection: A case study example. *Weather and Forecasting*, 2(1):3–16.

Doswell, C. A. (2001). Severe convective storms – An overview. In *Severe convective storms*, pages 1–26. Springer.

Doswell, C. A., Brooks, H. E., and Dotzek, N. (2009). On the implementation of the enhanced Fujita scale in the USA. *Atmospheric Research*, 93(1):554–563.

Doswell, C. A., Brooks, H. E., and Maddox, R. A. (1996). Flash flood forecasting: An ingredients-based methodology. *Weather and Forecasting*, 11(4):560–581.

Doswell, C. A. and Rasmussen, E. N. (1994). The effect of neglecting the virtual temperature correction on CAPE calculations. *Weather and Forecasting*, 9(4):625–629.

Dotzek, N. (2009). Derivation of physically motivated wind speed scales. *Atmospheric Research*, 93(1-3):564–574.

Dotzek, N. and Friedrich, K. (2009). Downburst-producing thunderstorms in southern Germany: Radar analysis and predictability. *Atmospheric Research*, 93(1-3):457–473.

Dotzek, N., Groenemeijer, P., Feuerstein, B., and Holzer, A. M. (2009). Overview of essl's severe convective storms research using the european severe weather database eswd. *Atmospheric Research*, 93(1):575–586.

DWD (1997). AKORD–Anwenderkoordinierte Organisation von Radar-Daten. Produktkatalog.

Emanuel, K. A. (1994). *Atmospheric convection*. Oxford University Press.

ESRL, Earth System Research Laboratory (2015). ESRL website. http://www.esrl.noaa.gov/psd/data/composites/nssl/day/. Accessed: 2016-01-10.

Evans, C., Weisman, M. L., and Bosart, L. F. (2014). Development of an intense, warm-core mesoscale vortex associated with the 8 May 2009 "super derecho" convective event. *Journal of the Atmospheric Sciences*, 71(3):1218–1240.

Evans, J. S. and Doswell, C. A. (2001). Examination of derecho environments using proximity soundings. *Weather and Forecasting*, 16(3):329–342.

Evans, M. (2010). An examination of low CAPE/high shear severe convective events in the Binghamton, New York county warning area. *Nat. Weather Digest*, 34(2):129–144.

Faust, H. (1948). Untersuchungen von forstschäden hinsichtlich der windstruktur bei einer böe. *Meteorol. Rdsch.*, 1:290–297.

Fink, A. H., Brücher, T., Ermert, V., Krüger, A., and Pinto, J. G. (2009). The European storm Kyrill in January 2007: synoptic evolution, meteorological impacts and some considerations with respect to climate change. *Natural Hazards and Earth System Science*, 9(2):405–423.

Fokus (2002). Online Archive Fokus. http://www.focus.de/politik/deutschland/unwetter-toedlicher-strassenfeger_aid_205043.html. Accessed: 2015-12-13 (in German).

Forbes, G. S. and Wakimoto, R. M. (1983). A concentrated outbreak of tornadoes, downbursts and microbursts, and implications regarding vortex classification. *Monthly Weather Review*, 111(1):220–236.

Frankfurter Allgemeine Zeitung (2002). Online Archive Frankfurter Allgemeine Zeitung. http://www.faz.net/aktuell/gesellschaft/ostdeutschland-sieben-tote-nach-sommerorkan-171403.html. Accessed: 2015-12-13 (in German).

Fujita, T. (1978). Manual of downburst identification for Project Nimrod. Satellite and Mesometeorology Research Paper No. 156, 104 pp.[Available from Department of Geophysical Sciences, University of Chicago, Chicago, IL 60637.], 1981: Tornadoes and downbursts in the context of generalized planetary scales. *Journal of the Atmospheric Sciences*, 38:1511–1534.

Fujita, T. T. and Wakimoto, R. M. (1981). Five scales of airflow associated with a series of downbursts on 16 July 1980. *Monthly Weather Review*, 109(7):1438–1456.

Funatsu, B. M. and Waugh, D. W. (2008). Connections between potential vorticity intrusions and convection in the eastern tropical Pacific. *Journal of the Atmospheric Sciences*, 65(3):987–1002.

Funk, T. W., Darmofal, K. E., Kirkpatrick, J. D., DeWald, V. L., Przybylinski, R. W., Schmocker, G. K., and Lin, Y.-J. (1999). Storm reflectivity and mesocyclone evolution associated with the 15 april 1994 squall line over kentucky and southern indiana. *Weather and Forecasting*, 14(6):976–993.

Galway, J. O. (1992). Early severe thunderstorm forecasting and research by the United States Weather Bureau. *Weather and Forecasting*, 7(4):564–587.

Gamache, J. F. and Houze Jr, R. A. (1982). Mesoscale air motions associated with a tropical squall line. *Monthly Weather Review*, 110(2):118–135.

Gatzen, C. (2004). A derecho in Europe: Berlin, 10 July 2002. *Weather and Forecasting*, 19(3):639–645.

Gatzen, C. (2011). A 10-year climatology of cold-season narrow cold-frontal rainbands in Germany. *Atmospheric Research*, 100(4):366–370.

Gatzen, C. (2013). Warm-season severe wind events in Germany. *Atmospheric Research*, 123:197–205.

Gatzen, C., Kreitz, M., Leprince, S., Schielicke, L., Rabrenovic, M., and Enno, S.-E. (2017). Combined analysis of severe convective wind gusts in European data sets. http://meetingorganizer.copernicus.org/ECSS2017/ECSS2017-156-3.pdf. Accessed: 2017-11-30.

Gatzen, C., Púčik, T., and Ryva, D. (2011). Two cold-season derechoes in Europe. *Atmospheric Research*, 100(4):740–748.

Gatzen, C., Tuschy, H., Groenemeijer, P., Van Der Velde, O., Hoffmann, J., and Dimitrov, A. (2007). A close look at a severe mesoscale convective system during the Kyrill-winter storm over Central Europe. http://www.estofex.org/files/ecss_gatzen.ppt. Accessed: 2015-10-15.

Gospodinov, I., Dimitrova, T., Bocheva, L., Simeonov, P., and Dimitrov, R. (2015). Derecho-like event in Bulgaria on 20 July 2011. *Atmospheric Research*, 158:254–273.

Groenemeijer, P., Púčik, T., Holzer, A. M., Antonescu, B., Riemann-Campe, K., Schultz, D. M., Kühne, T., Feuerstein, B., Brooks, H. E., Doswell III, C. A., et al. (2017). Severe convective storms in Europe: Ten years of research and education at the European Severe Storms Laboratory. *Bulletin of the American Meteorological Society*, 98(12):2641–2651.

Haase-Straub, S. P., Hagen, M., Hauf, T., Heimann, D., Peristeri, M., and Smith, R. K. (1997). The squall line of 21 July 1992 in Southern Germany: An observational case study. *Beitrage zur Physik der Atmosphäre - Contributions to Atmospheric Physics*, 70(2):147–166.

Hakim, G. J. and Uccellini, L. W. (1992). Diagnosing coupled jet-streak circulations for a Northern Plains snow band from the operational nested-grid model. *Weather and Forecasting*, 7(1):26–48.

Hamid, K. (2012). Investigation of the passage of a derecho in Belgium. *Atmospheric Research*, 107:86–105.

Hamilton, R. E. (1970). Use of detailed intensity radar data in mesoscale surface analysis of the 4 July 1969 storm in Ohio. In *Preprints, 14th Conf. on Radar Meteorology, Tucson, AZ, Amer. Meteor. Soc*, volume 339, page 342.

Hinrichs, G. (1888). Tornadoes and derechos. *Amer. Meteor. J.*, 5:306–317, 341–349.

Hobbs, P. V., Locatelli, J. D., and Martin, J. E. (1990). Cold fronts aloft and the forecasting of precipitation and severe weather east of the Rocky Mountains. *Weather and Forecasting*, 5(4):613–626.

Holton, J. R. (2004). *An introduction to dynamic meteorology*, volume 88. Elsevier Academic Press, USA, 4th edition.

Hoskins, B., Pedder, M., and Jones, D. W. (2003). The omega equation and potential vorticity. *Quarterly Journal of the Royal Meteorological Society*, 129(595):3277–3303.

Hoskins, B. J. and Bretherton, F. P. (1972). Atmospheric frontogenesis models: Mathematical formulation and solution. *Journal of the Atmospheric Sciences*, 29(1):11–37.

Hoskins, B. J., McIntyre, M., and Robertson, A. W. (1985). On the use and significance of isentropic potential vorticity maps. *Quarterly Journal of the Royal Meteorological Society*, 111(470):877–946.

House, D. (1958). Airmass modification and upper level divergence. *Bulletin of the American Meteorological Society*, 39:137–143.

James, R. P. and Markowski, P. M. (2010). A numerical investigation of the effects of dry air aloft on deep convection. *Monthly Weather Review*, 138:140–161.

James, R. P., Markowski, P. M., and Fritsch, J. M. (2006). Bow echo sensitivity to ambient moisture and cold pool strength. *Monthly Weather Review*, 134(3):950–964.

Johns, H. (2007). Origin and evolution of the term “derecho” as a severe weather event. http://submit.crh.noaa.gov/Image/dvn/hinrichs/JohnsDerecho Story.pdf. online available.

Johns, R., Howard, K., and Maddox, R. (1990). Conditions associated with long-lived derechos – An examination of the large-scale environment. In *Preprints, 16th Conf. on Severe Local Storms, Kananaskis Park, AB, Canada, Amer. Meteor. Soc*, pages 408–412.

Johns, R. H. (1982). A synoptic climatology of northwest flow severe weather outbreaks. Part I: Nature and significance. *Monthly Weather Review*, 110(11):1653–1663.

Johns, R. H. (1993). Meteorological conditions associated with bow echo development in convective storms. *Weather and Forecasting*, 8(2):294–299.

Johns, R. H. and Hirt, W. D. (1983). The derecho: A severe weather producing convective system. In *Preprints, 13th Conf. on Severe Local Storms, Tulsa, OK, Amer. Meteor. Soc*, pages 178–181.

Johns, R. H. and Hirt, W. D. (1987). Derechos: Widespread convectively induced windstorms. *Weather and Forecasting*, 2(1):32–49.

Jorgensen, D. P. and Smull, B. F. (1993). Mesovortex circulations seen by airborne Doppler radar within a bow-echo mesoscale convective system. *Bulletin of the American Meteorological Society*, 74(11):2146–2157.

Kalnay, E., Kanamitsu, M., Kistler, R., Collins, W., Deaven, D., Gandin, L., Iredell, M., Saha, S., White, G., Woollen, J., et al. (1996). The NCEP/NCAR 40-year reanalysis project. *Bulletin of the American Meteorological Society*, 77(3):437–470.

Kaltenböck, R. (2004). The outbreak of severe storms along convergence lines northeast of the Alps. Case study of the 3 August 2001 mesoscale convective system with a pronounced bow echo. *Atmospheric Research*, 70(1):55–75.

Keyser, D., Pecnick, M. J., and Shapiro, M. (1986). Diagnosis of the role of vertical deformation in a two-dimensional primitive equation model of upper-level frontogenesis. *Journal of the Atmospheric Sciences*, 43(8):839–850.

King, J. R. and Parker, M. D. (2014). Synoptic influence on high shear, low CAPE convective events. In *Preprints, 27th Conference on Severe Local Storms, Madison, WI*.

King, J. R., Parker, M. D., Sherburn, K. D., and Lackmann, G. M. (2017). Rapid evolution of cool season, low-CAPE severe thunderstorm environments. *Weather and Forecasting*, 32(2):763–779.

Klimowski, B. A., Bunkers, M. J., Hjelmfelt, M. R., and Covert, J. N. (2003). Severe convective windstorms over the northern high plains of the United States. *Weather and Forecasting*, 18(3):502–519.

Klimowski, B. A., Hjelmfelt, M. R., and Bunkers, M. J. (2004). Radar observations of the early evolution of bow echoes. *Weather and Forecasting*, 19(4):727–734.

Köppen, W. (1882). Der Gewittersturm vom 9. August 1881 (The thunderstorm squall of 9 August 1881). *Ann. Hydrogr. Marit. Meteor.*, 10:595–619, 714–737.

Köppen, W. (1896). Die Windhose vom 5. Juli 1890 bei Oldenburg und die Gewitterböe vom 10. Juli 1896 in Ostholstein (The tornado on 5 July 1890 near Oldenburg and the thundersquall of 10 July 1896 in east Holstein). *Ann. Hydrogr. Marit. Meteor.*, 24:445–458, 493–508, 546–556.

Kurz, M. (1993). Severe thunderstorms over western Germany: a case-study of the weather situation on 20 August 1992. *Meteorological Magazine*, 122(1453):177–188.

Lackmann, G. (2011). *Midlatitude synoptic meteorology*. American Meteorological Society.

Lane, J. D., Moore, P. D., and Greer, S. (2006). Observations of a non-supercell tornadic thunderstorm from a terminal doppler weather radar. In *Preprints, 23th Conf. on Severe Local Storms, St. Louis, MO, Amer. Meteor. Soc.*

Lang, A. A. and Martin, J. E. (2010). The influence of rotational frontogenesis and its associated shearwise vertical motions on the development of an upper-level front. *Quarterly Journal of the Royal Meteorological Society*, 136(646):239–252.

Lee, A. (1986). An experimental study of the remote location of lightning flashes using a VLF arrival time difference technique. *Quarterly Journal of the Royal Meteorological Society*, 112(471):203–229.

López, J. M. (2007). A Mediterranean derecho: Catalonia (Spain), 17th August 2003. *Atmospheric Research*, 83(2):272–283.

Ludwig, P., Pinto, J. G., Reyers, M., and Gray, S. L. (2014). The role of anomalous SST and surface fluxes over the southeastern North Atlantic in the explosive development of windstorm Xynthia. *Quarterly Journal of the Royal Meteorological Society*, 140(682):1729–1741.

Macdonald, N. J. (1976). On the apparent relationship between convective activity and the shape of 500 mb troughs. *Monthly Weather Review*, 104(12):1618–1622.

Mahoney, K. M., Lackmann, G. M., and Parker, M. D. (2009). The role of momentum transport in the motion of a quasi-idealized mesoscale convective system. *Monthly Weather Review*, 137(10):3316–3338.

Markowski, P. and Richardson, Y. (2011). *Mesoscale meteorology in midlatitudes*, volume 2. John Wiley & Sons.

McCaul Jr, E. W. and Weisman, M. L. (2001). The sensitivity of simulated supercell structure and intensity to variations in the shapes of environmental buoyancy and shear profiles. *Monthly Weather Review*, 129(4):664–687.

Meaden, G. T. (1976). Tornadoes in Britain: their intensities and distribution in space and time. *Journal of Meteorology*, 1(8):242–251.

Morris, R. (1986). The Spanish plume-testing the forecasters nerve. *Meteorological Magazine*, 115(1372):349–357.

MunichRe (2012). GeoRisikoForschung, NatCatSERVICE. http://natcatservice.munichre.com/.

MunichRe (2018). Windstorm - major global natural hazard. https://www.munichre.com/touch/naturalhazards/en/naturalhazards/meteorological-hazards/storm/index.html. Accessed: 2018-02-01.

n-tv (2002). http://www.n-tv.de/politik/Die-Ahnung-des-Feuerwehrchefs-article124998.html. Accessed: 2015-12-13 (in German).

Negrón-Juárez, R. I., Chambers, J. Q., Guimaraes, G., Zeng, H., Raupp, C. F., Marra, D. M., Ribeiro, G. H., Saatchi, S. S., Nelson, B. W., and Higuchi, N. (2010). Widespread Amazon forest tree mortality from a single cross-basin squall line event. *Geophysical Research Letters*, 37(16).

Pajek, M., Iwanski, R., Konig, M., and Struzik, P. (2007). Extreme convective cases – the use of satellite products for storm nowcasting and monitoring. In *EUMETSAT Conference, Darmstadt, Germany.*

Parker, M. D. and Dahl, J. M. (2015). Production of near-surface vertical vorticity by idealized downdrafts. *Monthly Weather Review*, 143(7):2795–2816.

Pistotnik, G., Holzer, A. M., Kaltenböck, R., and Tschannett, S. (2011). An F3 downburst in Austria–A case study with special focus on the importance of real-time site surveys. *Atmospheric Research*, 100(4):565–579.

Potvin, C. K., Elmore, K. L., and Weiss, S. J. (2010). Assessing the impacts of proximity sounding criteria on the climatology of significant tornado environments. *Weather and Forecasting*, 25(3):921–930.

Przybylinski, R. W. (1995). The bow echo: Observations, numerical simulations, and severe weather detection methods. *Weather and Forecasting*, 10(2):203–218.

Púčik, T., Francová, M., Rỳva, D., Kolář, M., and Ronge, L. (2011). Forecasting challenges during the severe weather outbreak in Central Europe on 25 June 2008. *Atmospheric Research*, 100(4):680–704.

Púčik, T., Groenemeijer, P., Rỳva, D., and Kolář, M. (2015). Proximity soundings of severe and nonsevere thunderstorms in Central Europe. *Monthly Weather Review*, 143(12):4805–4821.

Punkka, A.-J., Teittinen, J., and Johns, R. H. (2006). Synoptic and mesoscale analysis of a high-latitude derecho-severe thunderstorm outbreak in Finland on 5 July 2002. *Weather and Forecasting*, 21(5):752–763.

Rasmussen, E. N. and Rutledge, S. A. (1993). Evolution of quasi-two-dimensional squall lines. Part I: Kinematic and reflectivity structure. *Journal of the Atmospheric Sciences*, 50(16):2584–2606.

Rockel, B., Will, A., and Hense, A. (2008). The regional climate model COSMO-CLM (CCLM). *Meteorologische Zeitschrift*, 17(4):347–348.

Rotunno, R. and Klemp, J. (1985). On the rotation and propagation of simulated supercell thunderstorms. *Journal of the Atmospheric Sciences*, 42(3):271–292.

Rotunno, R., Klemp, J. B., and Weisman, M. L. (1988). A theory for strong, long-lived squall lines. *Journal of the Atmospheric Sciences*, 45(3):463–485.

Rotunno, R., Markowski, P. M., and Bryan, G. H. (2017). "near-ground" vertical vorticity in supercell thunderstorm models. *Journal of the Atmospheric Sciences*, 74(6):1757–1766.

Rotunno, R., Skamarock, W. C., and Snyder, C. (1994). An analysis of frontogenesis in numerical simulations of baroclinic waves. *Journal of the Atmospheric Sciences*, 51(23):3373–3398.

Saunders, C. (2008). Charge separation mechanisms in clouds. In *Planetary Atmospheric Electricity*, pages 335–353. Springer.

Schenkman, A. D. and Xue, M. (2016). Bow-echo mesovortices: A review. *Atmospheric Research*, 170:1–13.

Schenkman, A. D., Xue, M., and Shapiro, A. (2012). Tornadogenesis in a simulated mesovortex within a mesoscale convective system. *Journal of the Atmospheric Sciences*, 69(11):3372–3390.

Schreiber, K. (2000). Der Radarverbund; Informationen zum Wetterradar-Verbundsystem. *Printsache des DWD Geschätsbereich technische Infrastruktur*.

Schultz, D. M. (2013). Comments on "The influence of rotational frontogenesis and its associated shearwise vertical motions on the development of an upper-level front" by AA Lang and JE Martin (January A, 2010, 136: 239–252). *Quarterly Journal of the Royal Meteorological Society*, 139(670):269–272.

Schultz, D. M. and Doswell, C. A. (1999). Conceptual models of upper-level frontogenesis in south-westerly and north-westerly flow. *Quarterly Journal of the Royal Meteorological Society*, 125(559):2535–2562.

Shapiro, M. A. (1982). *Mesoscale weather systems of the central United States*. Cooperative Institute for Research in environmental Sciences (CIRES), National Oceanic and Atmospheric Administration (NOAA), University of Colorado.

Sherburn, K. D. and Parker, M. D. (2014). High-Shear, Low-CAPE environments: What we know and where to go next. In *Preprints, 27th Conf. on Severe Local Storms, Madison, WI, Amer. Meteor. Soc.*

Sherburn, K. D., Parker, M. D., King, J. R., and Lackmann, G. M. (2016). Composite environments of severe and nonsevere High-Shear, Low-CAPE convective events. *Weather and Forecasting*, 31(6):1899–1927.

Simmons, A., Uppala, S., Dee, D., and Kobayashi, S. (2007). ERA-Interim: New ECMWF reanalysis products from 1989 onwards. *ECMWF Newsletter*, 110(110):25–35.

Simon, A., Kaňák, J., Sokol, A., Putsay, M., Uhrínová, L., Csirmaz, K., Okon, L., and Habrovskỳ, R. (2011). Case study of a severe windstorm over Slovakia and Hungary on 25 June 2008. *Atmospheric Research*, 100(4):705–739.

Smull, B. F. and Houze Jr, R. A. (1987). Rear inflow in squall lines with trailing stratiform precipitation. *Monthly Weather Review*, 115(12):2869–2889.

Sun, Y. and Fang, J. (2013). Numerical study on the initiation of the severe convective weather in Chongqing on 6 may 2010. *Acta Meteorologica Sinica*, 27(3):364–378.

Thorpe, A. (1985). Diagnosis of balanced vortex structure using potential vorticity. *Journal of the atmospheric sciences*, 42(4):397–406.

Toll, V., Männik, A., Luhamaa, A., and Rõõm, R. (2015). Hindcast experiments of the derecho in Estonia on 08 August, 2010: Modelling derecho with NWP model HARMONIE. *Atmospheric Research*, 158:179–191.

Trapp, R. J. and Weisman, M. L. (2003). Low-level mesovortices within squall lines and bow echoes. Part II: Their genesis and implications. *Monthly Weather Review*, 131(11):2804–2823.

Uccellini, L. W. and Kocin, P. J. (1987). The interaction of jet streak circulations during heavy snow events along the east coast of the United States. *Weather and Forecasting*, 2(4):289–308.

Ulbrich, U., Fink, A., Klawa, M., and Pinto, J. G. (2001). Three extreme storms over Europe in December 1999. *Weather*, 56(3):70–80.

University Wyoming (2015). Sounding data. http://www.weather.uwyo.edu/ upperair/sounding.html. Accessed: 2015-10-15.

Van Den Broeke, M. S., Schultz, D. M., Johns, R. H., Evans, J. S., and Hales, J. E. (2005). Cloud-to-ground lightning production in strongly forced, low-instability convective lines associated with damaging wind. *Weather and Forecasting*, 20(4):517–530.

Wakimoto, R. M., Murphey, H. V., Davis, C. A., and Atkins, N. T. (2006a). High winds generated by bow echoes. Part II: The relationship between the mesovortices and damaging straight-line winds. *Monthly Weather Review*, 134(10):2813–2829.

Wakimoto, R. M., Murphey, H. V., Nester, A., Jorgensen, D. P., and Atkins, N. T. (2006b). High winds generated by bow echoes. Part I: Overview of the Omaha bow echo 5 July 2003 storm during BAMEX. *Monthly Weather Review*, 134(10):2793–2812.

Wakimoto, R. M., Stauffer, P., and Lee, W.-C. (2015). The vertical vorticity structure within a squall line observed during BAMEX: Banded vorticity features and the evolution of a bowing segment. *Monthly Weather Review*, 143(1):341–362.

Wasula, T. A., Stuart, N. A., and Wasula, A. C. (2008). The 17 February 2006 severe weather and high wind event across eastern New York and New England. In *Preprints, 24th Conf. on Severe Local Storms, Savannah, GA, Amer. Meteor. Soc.*, volume 13.

Weisman, M. L. (1993). The genesis of severe, long-lived bow echoes. *Journal of the Atmospheric Sciences*, 50(4):645–670.

Weisman, M. L. (2001). Bow echoes: A tribute to TT Fujita. *Bulletin of the American Meteorological Society*, 82(1):97–116.

Weisman, M. L. and Davis, C. A. (1998). Mechanisms for the generation of mesoscale vortices within quasi-linear convective systems. *Journal of the Atmospheric Sciences*, 55(16):2603–2622.

Weisman, M. L. and Rotunno, R. (2004). "a theory for strong long-lived squall lines" revisited. *Journal of the Atmospheric Sciences*, 61(4):361–382.

Weisman, M. L. and Trapp, R. J. (2003). Low-level mesovortices within squall lines and bow echoes. part i: Overview and dependence on environmental shear. *Monthly Weather Review*, 131(11):2779–2803.

wetterzentrale.de (2016). Lightning archive of Wetterzentrale. http://old.wetterzentrale.de/topkarten/fsbeobl.html. Accessed: 2016-09-01 (in German).

Wheatley, D. M., Trapp, R. J., and Atkins, N. T. (2006). Radar and damage analysis of severe bow echoes observed during BAMEX. *Monthly Weather Review*, 134(3):791–806.

Wikipedia (2015a). Blids. https://de.wikipedia.org/wiki/BLIDS. Accessed: 2015-12-13 (in German).

Wikipedia (2015b). Kyrill (storm). https://en.wikipedia.org/wiki/Kyrill_(storm). Accessed: 2016-08-31.

Wikipedia (2015c). Swiss air flight 850. https://en.wikipedia.org/wiki/Swiss_International_Airlines_Flight_850. Accessed: 2015-12-13.

Xu, X., Xue, M., and Wang, Y. (2015). Mesovortices within the 8 May 2009 Bow Echo over the Central United States: Analyses of the Characteristics and Evolution Based on Doppler Radar Observations and a High-Resolution Model Simulation. *Monthly Weather Review*, 143(6):2266–2290.

List of Figures

List of Tables

Erklärung zur Dissertation

Ich versichere, dass ich die von mir vorgelegte Disseration selbstständig angefertigt, die benutzten Quellen und Hilfsmittel vollständig angegeben und die Stellen der Arbeit – einschließlich Tabellen, Karten und Abbildungen –, die anderen Werken im Wortlaut oder dem Sinn nach entnommen sind, in jedem Einzelfall als Entlehnung kenntlich gemacht habe; dass diese Dissertation noch keiner anderen Fakultät oder Universität zur Prüfung vorgelegen hat; dass sie – abgesehen von unten angegebenen Teilpublikationen – noch nicht veröffentlicht worden ist sowie, dass ich eine solche Veröffentlichung vor Abschluss des Promotionsverfahrens nicht vornehmen werde.
Die Bestimmungen dieser Prüfungsordnung sind mir bekannt. Die von mir vorgelegte Dissertation ist von Prof. Joaquim Pinto und Prof. Andreas Fink betreut worden.

Teilpublikationen liegen nicht vor.

Promotionsbeginn (Beginn der praktischen Arbeit): September 2012

Ich versichere, dass ich alle Angaben wahrheitsgemäß nach bestem Wissen und Gewissen gemacht habe und verpflichte mich, jedmögliche, die obige Angaben betreffenden Veränderungen, dem Dekanat unverzüglich mitzuteilen.

Datum Unterschrift